Eph Receptor Clustering is the Central Integrator in Eliciting Graded Kinase-dependent Signaling Responses

Dissertation

Der Fakultät für Biologie der
Ludwig-Maximilians-Universität München

vorgelegt am 30. November 2011

von Andreas Schaupp

Erster Gutachter : Prof. Dr. Rüdiger Klein
Zweiter Gutachter : Prof. Dr. Rainer Uhl

Tag der mündlichen Prüfung: 13.02.2012

Work presented in this dissertation was performed in the laboratory of Prof. Dr. Rüdiger Klein at the Max-Planck-Institute of Neurobiology, Martinsried, Germany and in the laboratory of Philippe Bastiaens at the Max-Planck-Institute of Molecular Physiology, Dortmund, Germany.

Andreas Schaupp was affiliated to the
International Max-Planck Research School
for Molecular and Cellular Life Sciences, Munich, Germany.

Eidesstattliche Versicherung

Ich versichere hiermit an Eides statt, dass die vorgelegte Dissertation von mir selbständig und ohne unerlaubte Beihilfe angefertigt ist.

München, den ....
(Unterschrift)

Erklärung

Hiermit erkläre ich, dass ich mich anderweitig einer Doktorprüfung ohne Erfolg nicht unterzogen habe.

München, den ....
(Unterschrift)

Für Heidemarie, Reinhard und Hedwig

Denke nicht gedacht zu haben! Denn wenn du denkst: „ich denke“, bringt das Denken der Gedanken dich auf den Gedanken, dass das Denken der Gedanken ein gedankenloses Denken ist.

(unbekannter Autor)

CONTENTS

Supplementary videos are available on CD located on the inside of the back cover.

LIST OF FIGURES & TABLES

ABBREVIATIONS

&	and
‘	minute(s)
‘‘	second(s)
°C	degree Celsius
µF	micro Farad
µl	microliter
1/2d	1-/2-dimensional
a.u.	arbitrary units
aa	amino acid
Abl	Ableson
ADAM	A-Disintegrin-And-Metalloprotease
ADC	analog-to-digital converter
AF-6	acute myeloid leukemia-1/chromosome 6 fusion protein/afadin-6
Ala	alanine
AMPA	α-amino-3-hydroxy-5-methyl-4-isoxazolepropionic acid
ANOVA	analysis of variance between groups
Arg	Abl-related gene
BF	brightfield
bgcorr.	background correction/corrected
BHK	baby hamster kidney
bidest.	bidestilled
bit	binary digit
BSA	bovine serum albumin
c	concentration
CaP	calcium phosphate
Cdc42	cell division cycle 42
CHO	Chinese hamster ovary
CMV	Cytomegalovirus
CO_2	carbon dioxide
COS	CV-1 origin, SV-40
cp.	compare to
CS	conformational spread
C-terminus	carboxy terminus
CTF	C-terminal fragment
Cys-rich	cystein-rich
DIV	days *in vitro*
DMEM	Dulbecco’s modified Eagle’s medium
DNA	deoxyribonucleic acid
dNTPs	deoxyribonucleoside triphosphates
Dsh	disheveled
e.g.	*exempli gratia*
ECFP	enhanced cyan fluorescent protein
EDTA	ethylenediaminetetraacetic acid
EEA1	early endosome antigen 1

efn	ephrin
EGF	epidermal growth factor
EGFP	enhanced green fluorescent protein
EGFR	epidermal growth factor receptor
Eph receptor	erythropoietin-producing hepatocellular carcinoma cell receptor
ephexin	Eph interacting exchange protein
ephrin	Eph receptor interacting protein
epiFL	epifluorescence
ER	endoplasmatic reticulum
Erk	extracellular-signal-regulated kinase
EtOH	ethanol
exp.	experimental
EYFP	enhanced yellow fluorescent protein
FAK	focal adhesion kinase
Fc	human Fc-antibody fragment
FGF	fibroblast growth factor
FGFR	fibroblast growth factor receptor
Fig.	figure
FKBP	FK506 binding protein
FL	fluorescence
Flt3	vascular endothelial growth factor receptor 3
FNIII	type-III fibronectin repeats
FP	fluorescent protein
FRET	Förster resonance energy transfer
g	gram
GAP	GTPase-activating protein
gc	axon growth cone
GCC	growth cone collapse
GDNF	glial cell line-derived neurotrophic factor
GDP	guanosine diphosphate
GEF	guanine nucleotide exchange factor
GIT 1	G protein-coupled receptor kinase-interacting protein 1
Glu	glutamate
GPCR	G-Protein-coupled receptor
GPI	glycosylphosphatidylinositol
G-protein	GTP-binding protein
GRIP	glutamate receptor interacting protein
GST	glutathion - S- transferase
GTP	guanosine trisphosphate
HBSS	Hank's balanced salt solution
HEK	human embryonic kidney
HeLa	Henrietta Lacks
HEPES	N-2-hydroxyethylpiperanzine-N'-2-ethanesulfonic acid
hr(s)	hour(s)
HRMEC	human renal microvascular endothelial cells
hrp	horse radish peroxidase
i.e.	*id est*

IC_{50}	half maximal inhibitory concentration
ILK	integrin-linked kinase
IP	immunoprecipitation
JM	juxtamembrane
KCl	potassium chloride
kd	kinase- dead/deficient
K_d	dissociation constant
kDa	kilo dalton (1000 g/mol)
KIT	kinase receptor
KNF	Koshland-Néméthy-Filmer
kV	kilo Volt
l	liter
LB_0	lysogeny broth
LBD	ligand binding domain
LMC_L	lateral motor column
LMW-PTP	low-molecular-weight protein tyrosine phosphatase
LnLL	N-acetyl-l-leucinyl-l-leucinal-l-norleucinal
LTP	long-term potentiation
lut	look-up table
MAP	mitogen-activated protein
mg	milligram
min	minute(s)
ml	milliliter
MPI	Max-Planck-Institute
ms	millisecond(s)
MWC	Monod-Wyman-Changeux
n.d.	not determined
n.s.	not significantly different
NA	numerical aperture
NMDAR	N-Methyl-D-Aspartate receptor
NMR	Nuclear magnetic resonance
N-terminus	amino terminus
odc	optical density correction (polynomal)
orf	open reading frame
PAGE	poly-acrylamide gel electrophoresis
PAK3	alpha-p-21-activated kinase 3
PDGF	platelet-derived growth factor
PDZ	PSD95/Dlg/ZO1
PECAM-1	platelet endothelial cell adhesion molecule 1
pH	*potentium hydrogenii*
PI3-kinase	phosphatidylinositol 3-kinase
PICK1	protein interacting with PRKCA 1
proc.	procedures
psf	point spread function
PTP1B	protein tyrosine phosphatases 1B
PTPRO	protein-tyrosine phosphatase receptor type O
RAP	rapalog/ rapamycin and derivates

RBD	receptor binding domain
Rin1	Ras/ Rab interactor 1
RNA	ribonucleic acid
ROCK	RhoA kinase
RT	room temperature
RTK(s)	receptor tyrosine kinase(s)
s	second(s)
SAM	sterile-α-motif
SEM	standard error of mean
SH	src homology
SHEP	SH2 domain-containing Eph receptor-binding protein
SHIP2	Src homology 2 domain containing phosphoinositide 5-phosphatase 2
SOS	son-of sevenless
SPAR	spine-associated RapGAP
TCL	total cell lysate
TGF-β	transforming growth factor-β
TIFF	tagged image file format
TM	transmembrane
Tris	Tris[hydroxymethyl]aminomethane
TrkB	tropomyosin receptor kinase B
UNT	untransfected cell lysate sample
v	volume
VEGF	vascular endothelial growth factor
w	weight
wt	wildtype
x g	x gravitational acceleration (~9.81 m/s²)

Units were abbreviated using the International System of Units (SI). The triple and single letter codes were used for abbreviations of amino acids. Chemicals are abbreviated according to guidelines by the International Union of Pure and Applied Chemistry.

SUMMARY

Eph receptor tyrosine kinases (RTKs) and their membrane-bound ephrin ligands have essential functions in development and disease. They regulate cell movement and positioning in establishing and stabilizing patterns of cellular organization. They have been suggested as graded molecular markers that monitor the abundance or density of their binding partners on opposing cells and relay this information, eliciting correspondingly graded cellular responses. *Trans*-interactions of Ephs with ephrins generate higher-order clusters that are substantial for triggering responses, such as neuronal growth cone collapse. Recently, array-like signaling assemblies by Eph ectodomain-driven interactions *in cis* were suggested to drive a nucleation mechanism, which is thought to cause recruitment of a proportion of receptors into a signaling cluster. In this respect, studies on clustering of the bacterial chemotaxis system have highlighted important features such as a heightened sensitivity, increased responsiveness, and other functional implications for receptor clustering in signaling systems. By contrast, progress into the mechanism of Eph cluster formation and the functional link to downstream signaling has been slow. The results presented in this thesis bridge this gap by investigating the function of clustering in Eph-mediated cell responses.

Firstly, I have implemented a versatile system to induce clustering and Eph signaling at a receptor- and cell-autonomous level. With the use of small chemical dimerizers, which non-covalently crosslink between one and three FKBP (FK506 binding protein) domains inserted into the EphB2 intracellular domain, the system allows the generation of clusters of defined sizes, which physiologically form at cell-contact interfaces. Mechanistically, cluster sizes were characterized using blue-native PAGE and homo-FRET imaging. Functionally, I demonstrate that receptor activation and kinase-dependent signaling is solely triggered by Eph-Eph *cis*-interactions, suggesting that ephrin *trans*-interactions may be necessary to trigger clustering, but may not be required to form a highly ordered array.
Secondly, Eph receptor clustering correlates with subsequent signaling events, including receptor autophosphorylation, cellular collapse responses and growth cone collapse of primary neurons. Surprisingly, the composition of the EphB2 cluster sizes determined the strength of the cellular response. This is based on the finding that different oligomer sizes have distinct activation states. Furthermore, not only the cluster size distribution, but also the quality or stability of clusters influences the cumulative signaling response. Thus, clustering appears to convert analog signals in a uniform digital output. In this respect, I suggest clustering to be beneficial for a high fidelity of response and robustness of signaling.
Digitalization through clustering has to be reconverted into an analog signal of kinase activity for interpretation by the cell's signaling network. Here, I hypothesize that clustering may also serve as a mechanistic relay for shifting the conformational dynamics of the kinase domain to the catalytically-competent, kinase-active state, caused by a clustering-evoked macromolecular crowding effect.

Thirdly, my findings propose clustering to be an instance of higher-order control, which allows for integration of multiple determinants in the Eph signaling process. Cells that express predimerized EphB2 are more sensitive to ephrins, suggesting that intracellular and extracellular clustering determinants synergize to induce downstream cellular effects. Furthermore, inhibition of clustering by steric hindrance abrogates Eph kinase-dependent signaling responses and turns repulsion between cells into adhesion, suggesting that clustering is a key regulator in determining if kinase-dependent or kinase-independent signaling dominates cellular outcomes.

Finally, RTK signaling is, by no small means, also influenced by movement and processing. I addressed this issue with respect to Eph clustering using TIRF microscopy. Here I substantiate that clustering leads to the formation of static spatial signaling entities, which preferentially accumulate at the lateral cell edge.

Overall, my study contributes substantially to the understanding of Eph clustering and its importance for signaling. It may be of broad interest for the whole field of Eph/ephrin research ranging from developmental neurobiology to cancer.

1. INTRODUCTION

One of the tremendous challenges an animal cell, as an integrated unit of a multicellular organism, has to face every millisecond (during development or adulthood) is to establish, send and process information. It took 2.5 billion years for unicellular life forms to evolve to multicellular organisms. The lag of time may reflect the difficulty for inventing machinery which would allow cells to collaborate and coordinate their behavior and labor constantly. Even present-day unicellular organisms like bacteria or yeast possess simple strategies of cell-cell communication and information processing. Although these cells largely live independently, they can communicate and influence one another's behavior by responding to chemical signals, i.e. quorum sensing to measure their population density in suspension [1,2].
In highly complex multicellular organisms such as vertebrates, communication between cells is needed to temporally and spatially control signals for processes like developmental pattern formation, organogenesis or homeostasis in adult organisms [2].
Secreted extracellular signaling molecules are used to bridge information processing between single cells. Some of these operate over long distances e.g. as hormones in the blood stream (endocrine system); others signal only to immediate neighbors by releasing signals into the extracellular space (paracrine signaling) or in a contact-dependent manner. In the nervous system, neurons send their signals through their axons, covering sometimes long distances in the body. Electrical or chemical signals are transduced through synapses (synaptic signaling) to the postsynaptic region of the target cell [2,3].
In general, reception of the signals depends on receptor proteins, usually located at the cell surface, which bind the signal molecule and relay the information to the inside of the cell. Immediate cell responses can vary significantly - from a rearrangement of the cytoskeleton to altering the cell metabolism, the function of single proteins or the gene expression pattern.
The three largest classes of cell-surface receptor proteins are ion-channel-coupled, G-Protein-coupled (GPCRs), and enzyme-coupled receptors each activating intracellular events through different mechanisms [2].
Ion-channel-coupled receptors or transmitter-gated ion channels are regulated by the binding of their ligands. The ligand binding changes the open-or-closed state equilibrium, influencing the ion permeability of the plasma membrane and thus the excitability of the neuron (e.g. glutamate regulation of ionotropic glutamate receptors, AMPA-receptors (AMPA - α-amino-3-hydroxy-5-methyl-4-isoxazolepropionic acid) [4-6]. GPCRs possess seven transmembrane helices that span the membrane. When a ligand e.g. neurotransmitter or hormone binds, the induced conformational change in the receptor leads to activation of a trimeric G-protein (GTP-binding protein). Trimeric G-proteins have 3 subunits α, β and γ, and upon the exchange of GDP with GTP the α-subunit dissociates from the β and γ subunits, and both G_{α}-GTP and $G_{\beta\gamma}$ can start different signaling cascades [7,8]. Enzyme-coupled receptors function directly as enzymes or associate directly with enzymes that they activate. They are usually

single-pass transmembrane proteins with an extracellular ligand binding site and a cytoplasmic catalytic or enzyme binding site. The majority of the enzyme-coupled receptors are protein kinases that act through phosphorylation of intracellular signaling proteins [2]. The most prominent and diverse class is comprised by RTKs. It consists of 20 heterogeneous families each having important functions in cell signaling [9]. Eph receptors (from erythropoietin-producing hepatocellular carcinoma cell, the cell line from which their cDNAs were first isolated) together with their ligands, the ephrins (Eph receptor interacting protein) represent the biggest family with very unique features among the RTKs [9]. These receptors shall be of particular interest in this study.

1.1 Cell signaling by receptor tyrosine kinases

RTKs play an important role in fundamental cellular processes such as cell cycle, cell proliferation and differentiation, cell migration as well as cell metabolism and survival [10,11]. They share a conserved domain architecture with ligand-binding domains in the extracellular region, a single transmembrane helix and a cytoplasmic region which contains the important catalytic protein tyrosine kinase domain. Apart from this rather uniform domain composition they exhibit variations in structural components, which often contain unique features for receptor function and signaling, as e.g. the juxtamembrane region, which in some receptor families controls kinase activity. Other structural assets like the PSD95/Dlg/ZO1 (PDZ)-binding motif might also serve as docking site for downstream adaptor proteins. Although the overall topology, some paradigms of kinase activation and some key components of the downstream signaling pathways are highly conserved in vertebrates, the latest structural studies of RTKs have also revealed an unexpected diversity in the mechanisms of activation by their ligand [9]. Interestingly, Eph receptors - in comparison to other RTK families - are a remarkable example of diversification in activation and signaling.

Fig. 1.1 Diversification in ligand-induced dimerization and kinase activation strategies among receptor tyrosine kinases.
(A) EGF receptor dimerization is entirely receptor-mediated. EGF binds simultaneously to two domains (L1 and L2) within the same receptor molecule and drives conformational rearrangement in the extracellular region. This causes the interaction of regions CR1 between neighboring receptors [12].TrkB receptor dimerization is entirely ligand-mediated. A nerve growth factor dimer like BDNF crosslinks two TrkB molecules without any direct contact between the two receptors [13,14]. Receptor dimers phosphorylate each other *in trans* (indicated by P). CR1/2, cystein-rich domain; L1/2, ligand binding domain; C1/C2: C-terminal domain; I, leucine-rich domain; K, kinase domain; N, N-lobe/kinase domain; C, C-lobe/kinase domain. **(B)** Dimerization of the extracellular regions of RTKs activates the intracellular tyrosine kinase domains, which contain a C-lobe (labeled with C), N-lobe (labeled with N) and an activation loop (AL, in grey or green for the inactive and active state, respectively). While the crystal structures of the activated kinase domains are very similar, structures of inactive kinase domains differ substantially among the receptors [15]. In Tie2, for example, the C-terminal tail (in red)

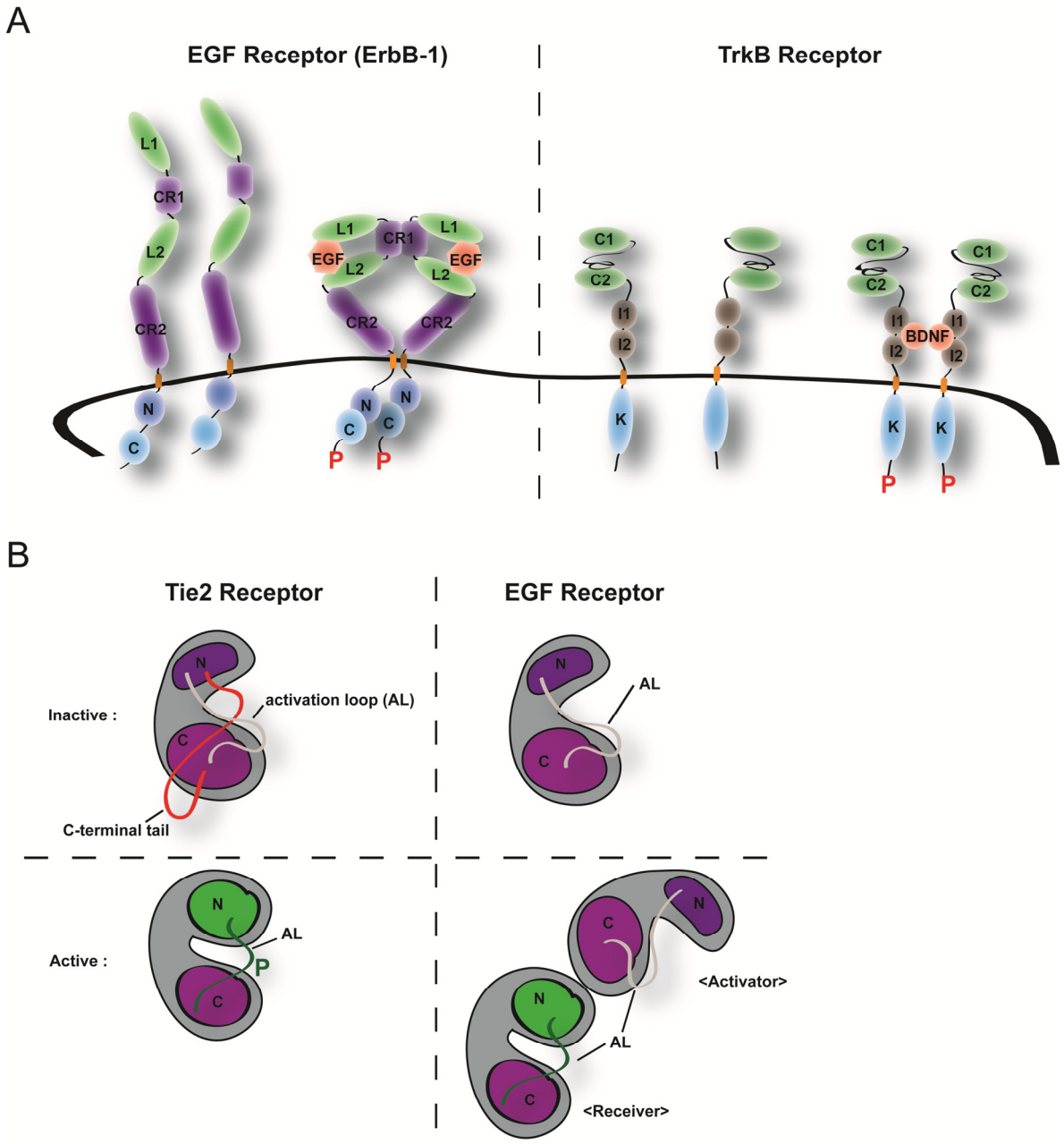

interacts with the active site of the kinase domain to stabilize an inactive conformation [16]. By contrast, in EGF receptor no such interaction is involved in inhibition of the kinase activity. However, for activation of EGF receptor a destabilization of the autoinhibitory *cis*-interactions is required by a direct contact between the C-lobe/kinase domain of one receptor, called the “activator” and the N-lobe/kinase domain of the neighboring receptor, called “receiver” [17-19]. (B) is adapted from [9].

Different modes of RTK dimerization. While the general mechanism of receptor activation was long thought to start out with ligand-induced receptor dimerization of monomeric receptors [20], recent studies for e.g. EGFR (epidermal growth factor receptor) and others, like the insulin receptor, made clear that a subset of RTKs forms oligomers even in the absence of their ligands [21-23]. Today, a more favorable view sees the general mechanism of RTK activation as stabilizing a specific relationship between individual receptor molecules in an active dimer or oligomer. The thereby provoked self-association of the extracellular region is thought to guide the intracellular domains into a dimeric conformation that activates their tyrosine kinase domains. One receptor in the dimer/oligomer phosphorylates one or more tyrosines on an adjacent RTK, a process called autophosphorylation, and the phosphorylated receptor then serves as a site for assembly of intracellular signaling proteins [20].
Early studies of ligand-induced dimerization of RTK extracellular regions suggested a conceptually straightforward mechanism with a bivalent ligand interacting simultaneously with two receptor molecules and thereby effectively crosslinking them non-covalently in a dimeric complex [24]. Recent structures of more complete extracellular regions of RTKs have provided important additional insight into the range of mechanisms used for ligand-induced dimerization, which can be categorized in two extremes: (1) dimerization is entirely "receptor mediated" and the ligand makes no direct contribution to the dimer interface, e.g EGFR [12,23]; (2) dimerization is entirely "ligand mediated" and the two receptors make no direct contact, e.g. TrkB (tropomyosin receptor kinase B) (Fig. 1.1A) [25]. Alternatively, dimerization can also involve a combination of ligand-mediated and receptor mediated components.

Diverse strategies in kinase activation mechanisms. The mechanisms which regulate kinase activation have been addressed in detail for several RTKs, including the stem cell factor receptor KIT (kinase receptor), FGFR (fibroblast growth factor receptor), the insulin receptor, EGFR and the angiopoietin receptor Tie2 and have turned out to be surprisingly diverse [9]. In their active conformation all tyrosine kinase domains share a great structural similarity [15]. The important structural elements are the "activation loop" and the αC helix in the kinase N-lobe, which reveal a specific conformation that is required for catalysis of phosphotransfer [26]. In their inactive conformation, by contrast, structural similarity among RTKs substantially vanishes, greatly reflecting the diversity in regulatory mechanisms. Autoinhibition of each tyrosine kinase domain is accomplished by a specific set of intramolecular *cis*-interactions. Upon ligand engagement and receptor dimerization, the release of structural constraints is the key event that triggers RTK activation [10] (Fig. 1.1B).

1.2 Eph receptors and ephrin ligands

Eph receptors and ephrin ligands are one of the key player families in contact-dependent cell signaling. They are found in a wide variety of cell types in tissues with reciprocal or overlapping expression patterns. When Eph receptors and ephrin ligands are expressed in a complementary pattern, the activation occurs at the interface of their expression domains [27,28].

Eph/ephrin interaction mediates cell-to-cell communication that has important roles in the establishment of neuronal, vascular and lymphatic networks during embryonic development, which involves diverse processes like (neuronal) cell migration, axon guidance, (neo-)angiogenesis and tissue patterning (e.g. topographic mapping, segmental patterning) [29,30]. Furthermore, Ephs/ephrins are implicated in an increasing number of physiological and pathological processes in many cell types and different organs of the adult organism summarized in Box 1 [28].

In distinction to other RTKs, Ephs/ephrins possess three unique features with respect to cell-contact dependence in signaling and mechanism of receptor activation. First, Ephs require membrane bound or preclustered ligands for activation [31]. Second, both receptor and ligand are membrane-anchored thereby requiring the actual cell-to-cell contact to initiate binding and signaling. In consequence, receptor and ligand can transduce signals bi-directionally into both the receptor-expressing cell (forward signaling) and the ligand-expressing cell (reverse signaling) [28,32,33]. And third, in contrast to other RTKs where dimerization is sufficient, multimeric Eph/ephrin complexes are necessary to induce robust Eph phosphorylation and biological responses [34].

Box 1. Overview of Eph/ephrin functions in physiology and disease.

Development	***Neuronal connections*** Ephs/ephrins have well-known roles in axon guidance and synaptogenesis. Ephs/ephrins are distributed in gradients or form boundaries and thereby influence the trajectories of axonal projections.	[30,35,36]
	Vascular & lymphatic system In cardiovascular development, Ephs/ephrins control the angiogenic remodeling of blood vessels and lymphatic vessels. They play essential roles in endothelial cells as well as in supporting pericytes and vascular smooth muscle cells.	[37-40]
Physiology & homeostasis	***Plasticity of neuronal circuits*** Eph/ephrin expression persists in the adult brain where neuronal circuits continue to be remodeled in response to environmental changes. Ephs/ephrins play a role in paradigms of acivity-dependent synaptic-plasticity that influence learning and memory.	[41-44]
	Immune system Ephs/ephrins are expressed in lymphoid organs and lymphocytes. Eph receptor function is implicated in development of thymocytes in mature T-cells, subsequent differentiation of activated T-cells into effector cells in the periphery, modulation of T-cell responses and various other processes of immune function including B-lymphocytes.	[45-47]
	Glucose homeostasis The β-cells of the pancreas communicate via EphA/ephrinA. EphA forward signaling (inhibits insulin secretion) and ephrinA reverse signaling (enhances insulin secretion) can be differentially regulated in pancreatic cells.	[48]
	Bone maintenance EphB/ephrinB bi-directional signaling between osteoblasts and osteoclasts has been shown to be important for the regulation of bone homeostasis in the adult.	[49,50]
	Intestinal homeostasis The intestinal epithelium undergoes continuous self- renewal throughout life. Newly born epithelial cells migrate while gradually losing EphB expression and acquiring ephrinB expression as they move away from mesenchymal cells which control Eph expression through Wnt secretion and stimulation of the canonical Wnt/β-catenin/Tcf signaling pathway.	[51-53]
Patho-physiology & disease	***Nervous system injury and repair*** Ephs/ephrins are upregulated in expression at sites of nervous system injuries. Ephs/ephrins may provide guidance cues enabling the re-wiring of neuronal projection patterns, but they may also hinder proper axon re-growth through repulsive signaling.	[54-57]
	Alzheimer disease A loss of EphB2 and EphA4 has been shown to precede memory decline in a murine model of Alzheimer's disease. Reversing EphB2 depletion rescues cognitive functions in Alzheimer model.	[58,59]
	Cancer Ephs and/or ephrins are present, and often upregulated, in essentially all types of cancer cells including pathologies of colorectal, breast and skin cancers. The Eph system is also operational in the tumor microenvironment through promoting tumor angiogenesis.	[28,60-63]
	Viral infections It was discovered that ephrinB2 and ephrinB3 serve as the cell entry receptors for Nipah and Hendra viruses, two emerging paramyxoviruses comprising the newly defined Henipavirus genus.	[64-67]

1.2.1 Eph/ephrin domain topology

In mammals, Ephs are subdivided based on sequence similarity and ligand-binding characteristics into an A-subclass (EphA1-EphA8, EphA10) and a B-subclass (EphB1-EphB4, EphB6) [33,68]. Their ligands, the ephrins, are also subdivided into an A-subclass (ephrinA1-A5) and B-subclass (ephrinB1-B3) according to their affinities for receptors, sequence conservation and the mode of membrane attachment [27,69].
EphAs bind to ephrinAs whereas EphBs bind to ephrinBs. Exceptions to this rule are EphB2, that can also bind to ephrinA5 [70] and EphA4 that can also bind to ephrinBs [33,71].

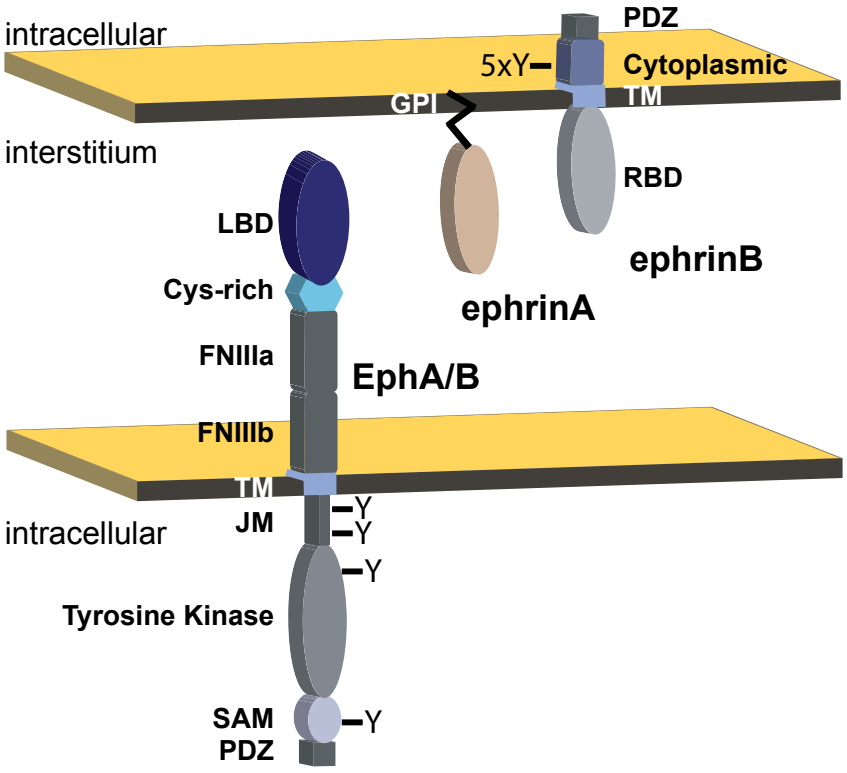

Fig. 1.2 Domain composition of Eph receptors and ephrin ligands.
Known tyrosine phosphorylation sites are indicated by Y. PDZ, PSD95/Dlg/ZO1 (PDZ)-binding motif; TM, transmembrane domain; RBD, receptor-binding domain; GPI, glycosylphosphatidylinositol-anchor; LBD, ligand-binding domain; Cys-rich, cystein-rich domain; FNIIIa/b, fibronectin type-III repeat a/b; JM, juxtamembrane segment; SAM, sterile-α-motif.

Ephs share a common domain organization throughout all subclasses (Fig. 1.2). They are characterized by their globular extracellular ligand-binding domain (LBD) followed by the cystein-rich (Cys-rich) domain segment and two type-III fibronectin repeats (FNIIIa/b). The previously uncharacterized Cys-rich domain is composed of a sushi domain and EGF-like domain [72]. A hydrophobic transmembrane (TM) α-helical domain spans the membrane. The

intracellular part of the receptor consists of a juxtamembrane (JM) segment containing two conserved tyrosines, the important catalytic kinase domain, the sterile-α-motif (SAM) and the PDZ-binding motif [28].
EphrinAs are tethered to the cell surface by a GPI-anchor (GPI - glycosylphosphatidyl–inositol), whereas ephrinBs are single pass transmembrane proteins (Fig. 1.2). They possess a short and highly conserved cytoplasmic region of ~80 amino acid (aa) residues with five conserved tyrosines, phosphorylated upon activation and a PDZ-binding motif. The extracellular part of both ephrin subclasses consists of a globular receptor-binding domain (RBD) distanced from the membrane by ~40 aa residues. Note, both subclasses lack an intrinsic catalytic activity [28].

1.2.2 Structural basis of Eph receptors and ephrin ligands

Extracellular Eph receptor structural architecture. Over the last couple of years, Ephs/ephrins have been studied intensively on a structural basis to better understand their molecular mechanisms of action. Their important role in oncogenesis has led to great interest in targeting Ephs/ephrins with small peptides or compounds [73], to generate specific anti-tumor drugs aside from broad-specificity kinase inhibitors binding in the enzyme's ATP/substrate pocket [74]. Indeed, small-molecule signaling inhibitors that bind to the EphA2 and EphA4 receptors were reported recently [75-77].
First structural studies led to detailed knowledge about the LBD of EphB2, which was shown to be a compact globular structure with a β-sandwich "jellyroll" folding topology consisting of a concave and convex β-sheet (Fig. 1.3A) [78]. Moreover two distinct ephrin-binding interfaces of different affinity were identified from a LBD-RBD x-ray crystallographic structure [79]. On one side of the globular LBD structure, the β-strands are connected by a loop of varying length, the so-called H-I loop, which packs against the concave β-sheet being part of the low-affinity tetramerization interface; on the other side, two other loops (D-E; J-K) protrude from the middle of the convex β-sheet, which forms the high-affinity dimerization interface. Interestingly, the length of the H-I loop differs significantly between subclasses but is conserved within [80]. A chimeric EphB2 LBD with an H-I loop from EphA3 adopted specificity for both A and B-subclass receptors prompting the loop to be entitled the "class-specificity-loop" [78].

Extracellular ephrin ligand structural architecture. The RBD of ephrinB2 shows a globular β-barrel structure with a Greek key folding topology [79,81]. Interestingly, in crystals of ephrinB2 not complexed with Eph receptors, hydrophobic regions of the RBD around a so-called G-I loop get buried in-between ephrin dimers indicating that ephrins undergo a significant rearrangement upon Eph binding. The 40 aa residues linker serves as disordered spacer to the membrane and does not seem to be involved in ligand-receptor binding [79,81].

NMR-studies of the complete cytoplasmic region of ephrinBs revealed a 33 aa residues long highly structured C-terminal tail forming a well-packed hairpin structure and a preceding 48 aa residues long random-coil structure prone to aggregation [82].

1.2.3 Eph/ephrin recognition and subclass specificity

EphBs/ephrinB recognition and subclass specificity. The recognition specificity of ephrinB2 and EphB2 is ensured by ligand induced receptor folding (induced fit mechanism). While binding, the dimerization interface centers on the long G-H loop of ephrinB2, which gets buried in a channel on the surface of EphB2. This process is thermodynamically driven by the hydrophobic effect. Loops lining the inside of the channel in EphB2 undergo a secondary-structure rearrangement from disordered to structured, thereby building an extensive interaction surface that is complementary to the ligand G-H loop. The conformational change in EphB2 is strictly localized to the interaction interface and most likely does not involve the intracellular part of the receptor [70,80]. The crystal structure from EphB2/ephrinB2 also gave insights into the molecular basis for subclass specificity [79]. The ligand-receptor high-affinity dimerization interface contains bulky and small polar and hydrophobic side chains on either side. In EphBs these residues are positioned in order to find an energetically favorable conformational state, whereas in EphAs, the side chains are shuffled in position, and therefore would produce an energetically unfavorable conformational state upon ephrinB-binding (e.g. polar residues to face hydrophobic ones). The H-I loop guarantees the formation of tetramers of receptor belonging to the same subclass. However, it is not sure, if a heterogeneous expression of different subclass members would cause heterogeneous clusters which contain more than one type of ligand and/or receptor.
Other structural studies of EphB4/ephrinB2 further suggested a single aa (Leu95) to be responsible for defining ligand selectivity of EphBs. This selectivity could be altered via protein engineering approaches [83]. On the ligand side, further structural studies of unbound ephrinB1 and ephrinA5 underlined the importance of the G-H loop for receptor recognition but also pointed out the uniqueness in the molecular mechanism for receptor-ligand specificity of each cognate pair [84,85].

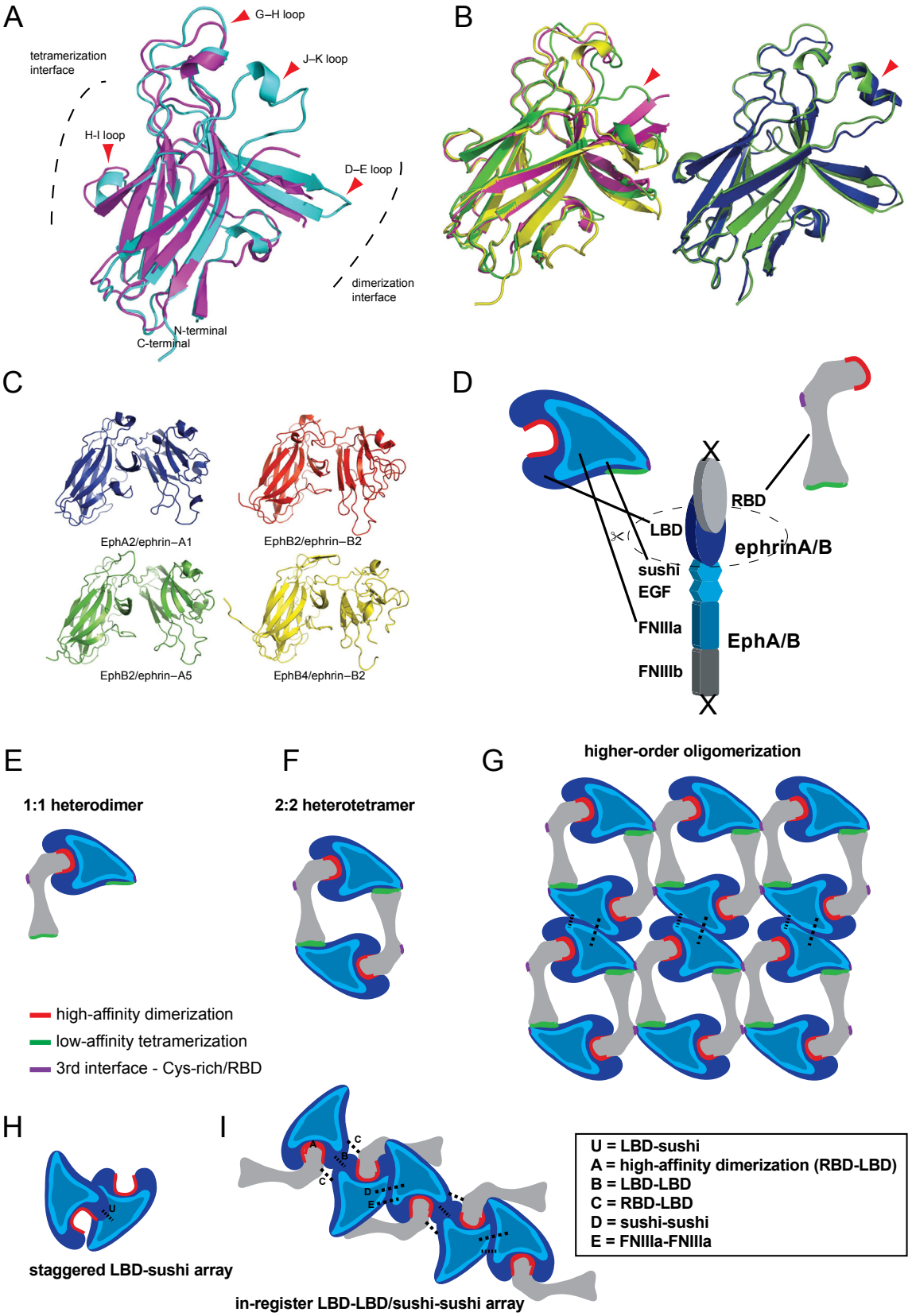
A
G–H loop
J–K loop
tetramerization interface
H-I loop
D–E loop
dimerization interface
N-terminal
C-terminal
B
C
EphA2/ephrin–A1
EphB2/ephrin–B2
EphB2/ephrin–A5
EphB4/ephrin–B2
D
X
RBD
LBD
ephrinA/B
sushi
EGF
FNIIIa
EphA/B
FNIIIb
X
E
1:1 heterodimer
F
2:2 heterotetramer
G
higher-order oligomerization
high-affinity dimerization
low-affinity tetramerization
3rd interface - Cys-rich/RBD
H
U
staggered LBD-sushi array
I
A
B
C
C
D
E
in-register LBD-LBD/sushi-sushi array
U = LBD-sushi
A = high-affinity dimerization (RBD-LBD)
B = LBD-LBD
C = RBD-LBD
D = sushi-sushi
E = FNIIIa-FNIIIa

Fig. 1.3 Eph/ephrin complex formation and cluster architecture.
(A) Comparison of the structures from the unligated EphA2 (cyan) and EphB2 (magenta) ligand-binding domain. Secondary structure elements are labeled on the ribbon diagram (arrows). Both the EphA2 and EphB2 structure are close to congruence. The main structural differences between EphA2 and the EphB receptors are the conformations of the D-E, J-K and H-I loops. The H-I loop length is the only clear feature that distinguishes the sequences of the A- and B-class molecules (with EphA receptors H-I loop four residues shorter in length). In the EphB2/ephrinB2 crystal structure, this H-I loop is involved in forming the low-affinity tetramerization interface [79]. The J-K and D-E loops are responsible for forming the ligand-binding cleft. Although in the unligated B-class receptors they adopt more open conformations [86], in EphA2 they form a compact ligand-binding channel - even in the absence of the ligand [87]. The tetramerization and dimerization interface is indicated by stippled lines [79]. **(B)** Conformational changes in A- and B-class Eph receptors upon ephrin binding. Left: comparison of the structures of unligated EphB2 (yellow), ephrin-bound EphB2 (green), and a 12-mer antagonistic peptide-bound EphB2 (magenta) [87,88]. Right: comparison of the structures of unligated (green) and ephrin-A1 bound (blue) EphA2. In contrast to EphA2, EphB2 undergoes significant structural rearrangements upon ligand/peptide binding (see arrows). **(C)** Comparison of the structures of the known A- and B-class Eph receptor/ephrin complexes except for EphA4/ephrinB2. EphB2: Val27-Arg207; ephrin-B2: Ile31–Gly168; ephrin-A5: Val28–Met165; EphB4: Glu17–Lys196. The EphA2/ephrin-A1 heterodimer is architecturally similar to the B-class complexes. **(D)** Schematic presentation of the 1:1 receptor - ligand contact of opposing cells. The circle indicates the cross-sectional view taken to depict receptor/ligand complex formation in panels (E) - (I). For simplification reasons, receptor and ligand are presented in a truncated form (indicated by X) only displaying the ectodomains. **(E)** Initial Eph/ephrin contact produces a high-affinity interaction of the receptor and ligand-binding domain. The G-H loop of ephrinB2 gets buried in a channel on the surface of EphB2-LBD leading to secondary structure rearrangements as shown in (B). **(F)** Formation of the tetrameric EphB2/ephrinB2 complex involving the class-specificity H-I loop and the surrounding surface as indicated in (A). This complex is thought to be the minimal functional unit to activate receptors [79]. **(G)** Hypothetical higher-order cluster formation model of Ephs/ephrins based on various structural and functional studies. Note, that a third interaction site is proposed between the ligand and receptor which belongs to neighboring tetrameric Eph/ephrin complexes [89] and interactions between the Cys-rich domains [90]. **(H,I)** Latest model to propose an extracellular steric seeding mechanism for the formation of array-like networks of EphA2 [72]. A switch from a parallel staggered array, produced by interactions of the LBD and sushi domain of adjacent unligated EphA2 receptors, to ephrin-bound in-register arrays, characterized by LBD-LBD/sushi-sushi and FNIIIa-FNIIIa interactions, is proposed. The Cys-rich and FNIII domain are highlighted to be required for higher-order cluster formation. Similar other results support this model [91]. Ribbon diagrams in (A,B,C) are adapted from [87].

EphAs/ephrinA recognition and subclass specificity. The first study to investigate the structural basis of EphAs/ephrinAs was done by Himanen and colleagues presenting the crystal structure of an EphA2/ephrinA1 complex [87]. Although these structures are overall similar to their B-class counterparts (Fig. 1.3B,C), they reveal important differences that define subclass specificity. EphAs/ephrinAs interactions involve smaller rearrangements in the interacting partners, better described by a "lock-and-key"- type binding mechanism, in contrast to the "induced fit" mechanism defining the B-class molecules (Fig. 1.3B). In retrospective, the fact that no small-molecule antagonists have been found for any EphBs so far highlights the biological relevance of their different binding modes.

Eph binding promiscuity. Cross-subclass interactions were revealed by the physiologically relevant receptor/ligand pair EphB2/ephrinA5 (Fig 1.3C) [70]. EphB2/ephrinA5 complex is a

heterodimer architecturally distinct from the tetrameric EphB2/ephrinB2 structure. The authors concluded that bi-directional signaling is the result of a combination of Eph/ephrin interactions - both intrasubclass and intersubclass. Thus, even interactions that are of lower affinity could significantly cause signaling responses depending on the number or density of interacting molecules. In this context, the authors also put up for debate that receptor activation might not require the precise positioning of nearby Eph receptors.
EphA4, one of the most studied Eph receptors, shows cross-subclass binding promiscuity. Published structures differ considerably from each other and strikingly different explanations for the exceptional cross-subclass specificity and affinity were proposed [71,77,92]. One report addressing these contradictory findings showed that the receptor has an unprecedented ability to adopt two distinct, well-ordered structures even in the unbound state. These results suggest that the ligand promiscuity of EphA4 is directly correlated with the structural flexibility of the ligand-binding surface of the receptor [93].

1.2.4 Eph/ephrin complex and higher-order cluster formation

Eph/ephrin complex formation. The first step in initiating signaling is a 1:1 heterodimer formation between Ephs and their cognate ephrin ligands (Fig. 1.3D,E) [94,95]. Subsequently, for EphB2/ephrinB2, heterodimers tetramerize into a ring-like structure with a much lower K_D into 2:2 complexes and eventually form higher-order oligomers (Fig. 1.3F,G) [79,96]. In the forward signaling direction, it is suspected that EphB2/ephrinB2 heterotrimers, consisting of one ligand in complex with two receptors form the minimal functional unit [80]. In order to signal bi-directionally, EphB2/ephrinB2 complexes have to adopt the tetrameric 2:2 stoichiometry [79].

Eph/ephrin higher-order cluster formation. Studies on EphA3/ephrinA5 using a random mutagenesis approach identified three distinct EphA3 surface areas that are essential for complex formation [89]. While two of these surfaces correspond to the dimerization and tetramerization interfaces of EphB2, the third falls outside the structurally characterized interaction domains. Further experimental work confirmed the existence of the third surface to be required for oligomerization and full activation of EphA3 [97]. Based on the EphB2/ephrinB2 x-ray crystallographic structure, the newly discovered third Eph-ephrin interface and the previously described EphA3-EphA3 interaction [79,89,90,97], the formerly introduced “tetramerization model” (Fig. 1.3F) was advanced to allow explanation of higher-order oligomerization into larger 2-dimensional Eph/ephrin signaling clusters (Fig. 1.3G) [89].
Lately, structural biologists have also crystallized the whole ectodomain of Eph receptors to get a deeper insight in the molecular basis of Eph/ephrin higher-order oligomerization. Homotypic interactions between the LBDs of EphA2 receptors as well as homotypic Cys-rich domain and FNIIIa interactions were confirmed and identified to be responsible for the

assembly of higher-order clusters [72,90,91]. Interestingly, unliganded EphA2 ectodomains form array-like networks with staggered, parallel interactions between the LBD and sushi domain which are relevant to the cell-surface signaling, as shown by functional experiments (Fig.1.3H) [72].
Upon ephrinA5 binding, arrays shift to in-register arrays involving LBD-LBD and sushi-sushi contact interfaces in addition to the previously described RBD-dependent contact interfaces (Fig. 1.3I) [72,80,87]. A similar ectodomain structure was obtained for the EphA2/ephrinA1 complexes [91], which also emphasized the receptor-mediated nature of the oligomerization process when looking beyond the size of tetrameric complexes.
Other Eph receptor domains such as the transmembrane segment [98], and the intracellular SAM domain [99-102] are also implicated in the constitution, stabilization and maturation of Eph signaling arrays but were so far not shown to be functionally relevant. FNIII repeats of EphA3 were also reported to interact with the RBD of ephrinA5. Yet, this interaction was shown to occur *in cis* with co-expressed ephrinA5 thereby inhibiting Eph complex formation and signaling [103].
Taken together, structures of whole ectodomains of EphAs/ephrinAs show an arrangement somewhat reminiscent of the tetramerization model observed in the initial EphB2/ephrinB2 structure (personal communication with E. Seiradake & [72,79,89,91]). However, structures of other Eph/ephrin complexes have not revealed explicit tetrameric arrangements [70,87,88,93], which may indicate an overgeneralization of the tetramerization model. Furthermore, the array-like model for higher-order cluster formation seems more consistent between crystal structures and mutagenesis analysis [72,89,91]. Thus at present, no consistent clustering model can be described. Future studies will show, if a general clustering model emerges or if structural arrangements remain at least unique to the level of A- or B-subclass receptors. It might even be possible that structural arrangements are defined by subtype-specific receptor/ligand combinations.

Eph/ephrin extracellular steric seeding mechanism. An extracellular steric seeding mechanism is suggested for the formation of Eph/ephrin signaling hubs. In analogy to previous work the Eph Cys-rich domain may function as a unique protein-interaction/dimerization module, which cooperates with ligand-dependent clustering to mediate the assembly of continuous oligomers also independent of ligand contact [72,90,91,104]. In such a scenario, ephrin binding at “nucleation” points may trigger a more widespread recruitment of EphAs into in-register arrays containing unbound receptor, thus facilitating, in a cooperative manner, additional ephrin binding [72]. However, it has to be shown in future studies, whether this nucleation mechanism is a general feature of Eph/ephrin cluster formation or if it is specific for EphAs/ephrinAs.

1.3 Mechanism of Eph receptor activation

The activation of all RTKs follows some general rules. Ligand binding brings at least two catalytically repressed kinase-domains together [9,105], which phosphorylate each other *in trans*. Phosphorylation of the kinase activation loop leads to the exposure of the kinase-active site, which is usually blocked. In some RTKs like Eph, KIT, Flt3 (vascular endothelial growth factor receptor 3), PDGFβ (platelet derived growth factor β) and TrkB, the juxtamembrane region is also involved in regulation of the kinase activity [106,107]. In Ephs, catalytic activation correlates with phosphorylation of two tyrosines (Tyr604 and Tyr610, for murine EphB2) within the JM segment [108-110], and possibly the phosphorylation of a third tyrosine in the kinase activation segment (referred to as $Tyr_{Act}788$, for murine EphB2; $Tyr_{Act}779$ for EphA4). *In vivo* phosphorylation sites were reported to be Tyr667, Tyr744 and Tyr750 [111], however, their role for Eph receptor regulation is so far unknown.

Fig. 1.4 Molecular mechanism of Eph receptor kinase activation.
Schematic presentation of the proposed activation mechanism by means of EphB2/EphA4 structural studies [107,112]. For better understanding of the structural features in relation to EphB2 sequence alignment, an illustration is shown on the bottom. **(A)** Unphosphorylated, autoinhibited state: the N-terminal lobe elements implicated in nucleotide binding are well ordered and adopt a prototypical protein kinase arrangement except for obvious distortions in helix αC and the G-loop. The G-loop plays an important role in coupling the β-strand movements to produce an altered twist to that of helix αC (indicated tachometer symbol). This overall structural scenario results from interactions with the JM segment (black arrows). In the C-lobe of the kinase domain, the activation segment, which is also located in the large catalytic lobe (not depicted here), is disordered (indicated by intensely scribbled light-blue line) and produces a steric contact with Tyr750 (indicated by red scribbled line), which adopts an alternate conformation impeding the activation segment from adopting a stabilizing path. The preceding JM segment is highly ordered forming αA' and αB' helices with intimate contact to αC helix of the N-terminal kinase lobe (black arrows) and limited interactions of the C-terminal lobe (black stippled arrow). This leads to an imposed kink on helix αC. The distortion couples to distortions of the N-terminal lobe elements, which appear to impinge on catalytic function by adversely affecting the coordination of the sugar and phosphate groups of the bound nucleotide (not depicted here). **(B)** Phosphorylated, active state: phosphorylation of Tyr604 and Tyr610 serves to destabilize the JM structure through electrostatic repulsion exerted by negatively charged phosphate groups. This abrogates the intimate contact to helix αC and the C-terminal lobe to cause overall enhanced interlobe dynamics comprising helix αC and the activation segment. Tyr750 adopts a conformation that no longer impedes the productive ordering of the activation loop. The dynamic conformational equilibrium is shifted from a kinked to a straight αC helix allowing the return of the N-terminal lobe to an undistorted active conformation. Conformational rearrangements are mediated via the G-loop to produce an altered twist in β-strand secondary structures (indicated by arrow in circle). The current idea is that catalysis is followed by dynamic fluctuations from a more stable conformation favoring a rather dynamic picture of Eph receptor kinase activation over the transition to a static active state. Red arrows indicate structural interactions.

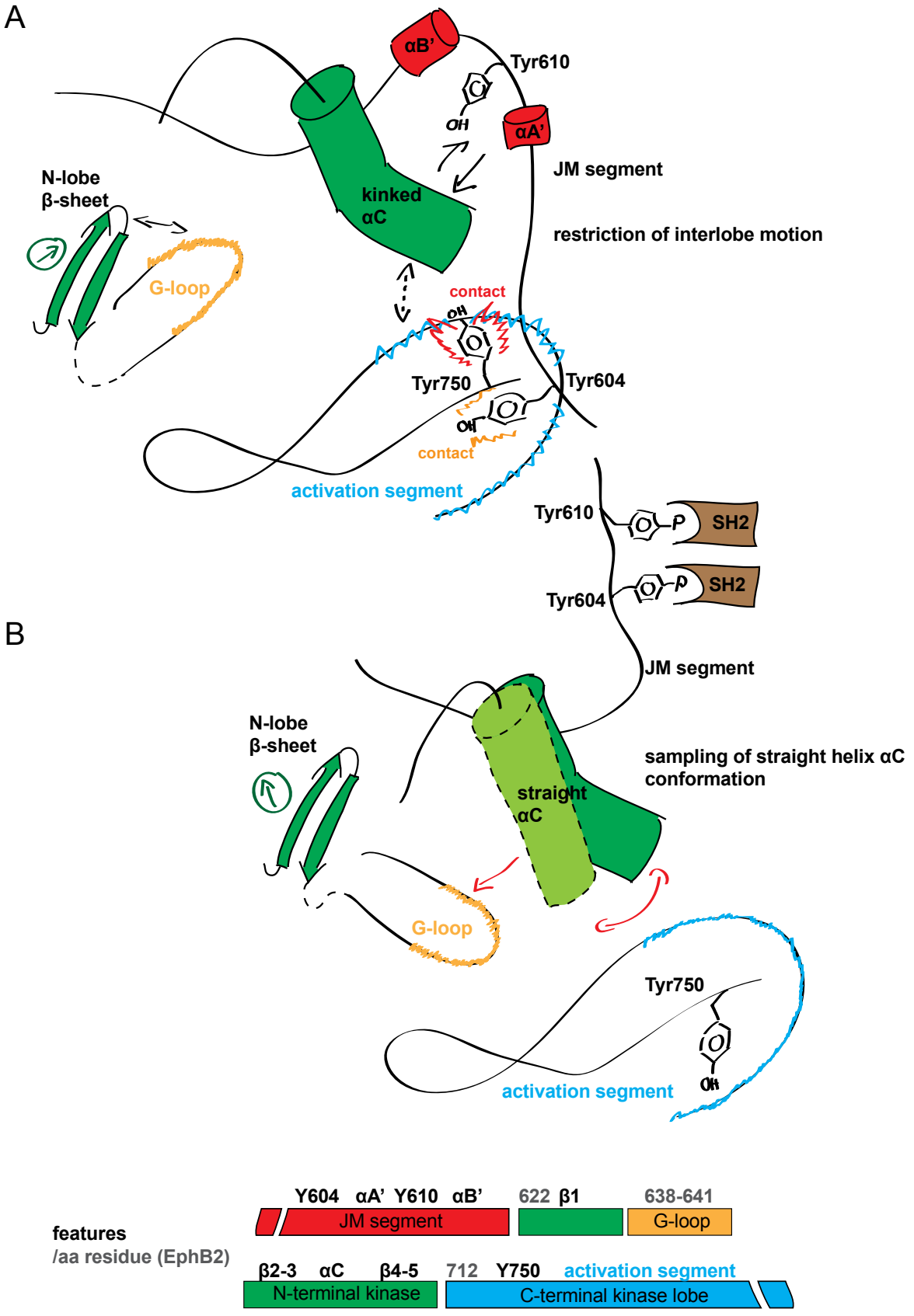
A
αB'
Tyr610
OH
αA'
JM segment
N-lobe
β-sheet
kinked
αC
restriction of interlobe motion
G-loop
contact
OH
Tyr750
Tyr604
OH
contact
activation segment
Tyr610
P
SH2
Tyr604
P
SH2
B
JM segment
N-lobe
β-sheet
sampling of straight helix αC
conformation
straight
αC
G-loop
Tyr750
activation segment
features
/aa residue (EphB2)
Y604 αA' Y610 αB'
622 β1
638-641
JM segment
G-loop
β2-3 αC β4-5
712 Y750 activation segment
N-terminal kinase
C-terminal kinase lobe

X-ray crystallography of the juxtamembrane and kinase domains of EphB2 indicate a dual inhibition mechanism involving the kinase activation loop and the two conserved juxtamembrane tyrosine residues [107]. In its non-phosphorylated form, the JM segment folds back to form a well-ordered structure, interacting with the N-terminal lobe of the kinase, presumably causing the distortion of the key α-helix C leading to repression of the kinase activity (Fig. 1.4A). Interestingly, α-helix C possesses a kink not previously observed in active state protein kinase structures. In addition, limiting the JM segment contacts with the kinase domain C-lobe appear to prevent the activation segment from adopting an ordered active conformation. The JM segment bridges the N- and C-lobes of the kinase and thereby restricts inter-lobe flexibility. Together, these disruptive features are suggested to account for the repression of kinase activity of Eph receptors in their autoinhibited states. Upon phosphorylation of the JM tyrosines electrostatic repulsion would then lead to a relief of the structural constrains controlling kinase activity [107]. Mutation of these JM tyrosines to negatively charged glutamate (eeEph) in EphA4 leads to a constitutively kinase-active EphA4 receptor, which remains sensitive to receptor ligation *in vivo* [113]. Exchange for uncharged phenylalanine (ffEph), in contrast, leads to a receptor frozen in its autoinhibited state [107]. Moreover, phosphorylation of the JM tyrosines enables docking of SH2-binding adaptor proteins (SH2 - Src homology domain 2) inducing further downstream signaling events [114].
Recently, the Sicheri lab performed a much more detailed study of Eph kinase activation utilizing a combination of mutational and structural analyses, also including NMR spectroscopy, to draw a more dynamic picture of autoinhibited and active forms of EphB2 and EphA4 [112]. They provided direct evidence that phosphorylation of the JM segment residues Tyr604 and Tyr610 and a gain-of-function point mutation of Tyr750 to alanine in the C-lobe of the kinase domain induces disorder of the JM segment and its dissociation from the kinase domain (Fig. 1.4B).
Interestingly, these induced disorders in the JM segment occur without major conformational changes to the kinase domain and with only partial ordering of the kinase domain activation segment. All these results suggest that rather a change in interlobe dynamics of the JM segment and kinase domain, than a transition to a static active conformation forms the mechanistic basis for Eph RTK activation [112].
While the importance of JM tyrosine phosphorylation for Eph receptor activation is well established, phosphorylation of other residues, such as Tyr788, Tyr667, Tyr744 and Tyr750 also seem to influence the stability of the autoinhibited structure and hence Eph receptor activity. [107,112].

1.4 Bi-directional signaling of Eph/ephrin complexes

Interactions between Eph receptors and ephrins activate a bi-directional signaling network transducing the signal in the Eph-receptor-expressing cell as well as in the ephrin-expressing cell. Signals into both cells are transferred along horizontal and vertical signaling cascades composed of various mediators, adaptors and effector proteins to eventually meet their intended cellular response tasks. Over the last years, a number of studies have been carried out to unravel the complex signaling networks configured by Eph/ephrin signaling (Fig. 1.5) (reviewed in [28,30,33]).

1.4.1 Eph forward signaling mechanisms

Eph-mediated signaling upon ligand binding *in trans* is by far the most heavily studied pathway of Eph/ephrin signaling. Eph receptors are activated through ligand binding, complex formation and subsequent higher-order cluster formation to activate the catalytic propensity of the kinase domain [33]. Phosphorylation of tyrosine residues leads to the emergence of signaling hubs for adaptor proteins on the JM segment, kinase and possibly the SAM and PDZ domain. Most of these adaptor proteins intrinsically lack catalytic function and bind through SH2/SH3 domains to phosphorylated tyrosines. Association of Src to Eph also assists in activation of many pathways by phosphorylation of downstream signaling components.

Regulation of Rho GTPases - effects on the cytoskeleton. A key component in this signaling context is the Rho family of small GTPases including RhoA, Cdc42 (cell division cycle 42) and Rac [61]. GTPases function by cycling between an active GTP-bound form and an inactive GDP-bound form thereby constituting a bistable switch in activating specific downstream effectors. Rho proteins are key regulators of actin cytoskeleton dynamics in cells, in addition to regulating a variety of other important cellular processes [115-117]. In neuronal cell lines, RhoA regulates stress fiber and focal adhesion formation and cell contractility, whereas Rac1 and Cdc42 activation results in the formation of protrusive structures such as lamellipodia and filopodia, respectively [118]. RhoA acts through ROCK (RhoA kinase) and LIM kinase on Cofilin, which effectively reorganizes the actin cytoskeleton through acto-myosin contractility [119]. In the case of mature neurons, activation of this pathway results in axon growth cone collapse [120-122].
Rho GTPases are tightly regulated by guanine nucleotide exchange factors (GEFs), which stimulate the exchange of bound GDP for GTP, thus activating Rho GTPases and GTPase-activating proteins (GAPs) like α2-chimaerin [123-126]. Upon Eph receptor activation, α2-chimaerin binds through its SH2 domain and undergoes tyrosine phosphorylation, which enhances its GTPase-activating protein activity towards Rac1. Ephs recruit the GEFs of the ephexin family (Eph interacting exchange protein; specific for EphA4) with its most prominent member ephexin1, directly and in a constitutive manner regardless of the activation

state of the receptor [122,127]. Bound on inactive Eph, ephexin1 is not tyrosine phosphorylated and moderately activates RhoA, Rac1 and Cdc42 with the consequence that the balance of GTPase activity is maintained to promote axon outgrowth. Eph activation then leads to ephexin phosphorylation, most likely by Src [128] and a shift to strong stimulation of RhoA GDP/GTP exchange by ephexin. In ephexin1 knockout mice, growth cone collapse from retinal ganglion cells (RGCs) was significantly reduced in response to ephrinA1 stimulation in comparison to controls [127].

Cdc42 is also activated by Eph receptor signaling mediated by ephexin1. It is, however, rather than being linked to contractility, proposed to regulate actin polymerization during dendritic spine morphogenesis [129]. EphB receptors, expressed in hippocampal neurons associate with other GEFs of the intersectin and kalirin family, which are exchange factors for Cdc42 and Rac [129,130]. Unlike the constitutive binding of ephexins and intersectins, kalirin only binds to activated Eph receptors. In endothelial cells it was shown that cell retraction and subsequent membrane respreading triggered by ephrinB2 is entirely dependent on myosin-II ATPase activity. In line with previous studies, it is only partially dependent on Rho-ROCK signaling but also to a significant degree on Cdc42 signaling [131-133].

The Rho GEF Vav2, which has no preferences for either EphAs or EphBs, acts in the same fashion as ephexin1, and it plays an important role in Eph receptor endocytosis.

Additionally Eph can regulate the organization of the actin cytoskeleton through the Ableson (Abl) family tyrosine kinases and Abl-related gene (Arg). Several protein interactions between Abl/Arg and EphA4/EphB2 were found in a yeast two-hybrid screen [134]. Abl/Arg have actin binding motifs in their carboxy-terminal tails and Abl and Ephs are localized in neuronal growth cones, which supports a role for Abl in regulating the actin cytoskeleton during Eph-mediated axon pathfinding. For instance, Abl plays a role in EphA-mediated axon guidance of retinal ganglion cells [135].

Overall, independent but also partially inter-connected pathways seem to exist to mediate the important Eph forward signaling response of cellular retraction via cytoskeletal rearrangements.

Fig. 1.5 Eph/ephrin bi-directional signaling pathways.
Schematic presentation of Eph/ephrin-induced signaling pathways as described in the main text. Arrows (→) denote a positive, (T)-indicators a negative regulation on downstream targets. Red arrows indicate the evenly balanced Rac/RhoA/Cdc42 activation prior to Eph receptor activation, which then shifts to stronger RhoA activation and weaker Rac/Cdc42 activation (stippled arrows). The location of the signaling proteins does not imply the involvement of a particular Eph/ephrin domain. (?) indicate signaling connections that have not been conclusively assessed in Eph/ephrin signaling. The relative activation of different pathways and their effects on cell behavior may depend on the Eph/ephrin levels, degree of ligand/receptor clustering and cellular context.

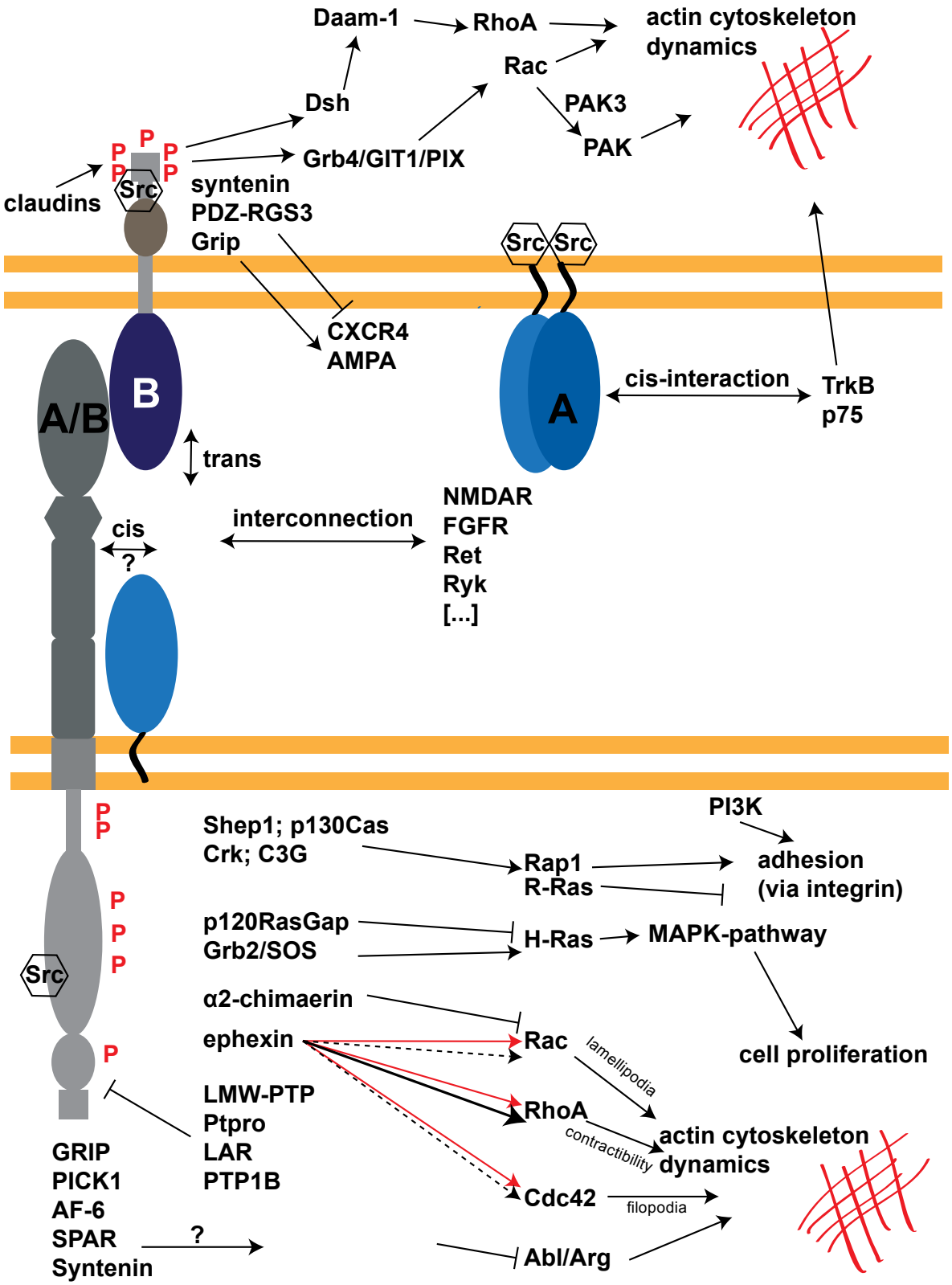
Daam-1
RhoA
actin cytoskeleton dynamics
Rac
Dsh
PAK3
PAK
P
Grb4/GIT1/PIX
claudins
Src
syntenin
PDZ-RGS3
Grip
Src Src
CXCR4
AMPA
A/B
B
A
cis-interaction
TrkB
p75
trans
cis
?
interconnection
NMDAR
FGFR
Ret
Ryk
[...]
PI3K
Shep1; p130Cas
Crk; C3G
Rap1
R-Ras
adhesion
(via integrin)
p120RasGap
Grb2/SOS
H-Ras
MAPK-pathway
α2-chimaerin
ephexin
Rac
lamellipodia
cell proliferation
RhoA
contractibility
actin cytoskeleton
dynamics
LMW-PTP
Ptpro
LAR
PTP1B
GRIP
PICK1
AF-6
SPAR
Syntenin
?
Cdc42
filopodia
Abl/Arg

Regulation of Ras GTPases - effects on mitogenesis. Aside from the regulation of Rho GTPases Eph receptors also have an impact on the activity of Ras family proteins. H-Ras binds and activates a row of serine/threonine kinases, amongst those are the MAP (mitogen-activated protein) kinases Erk1 (extracellular-signal-regulated kinase 1) and Erk2 [136,137]. The Ras/MAPK pathway is a key regulator of cell proliferation and transformation but was also implicated in influencing axon guidance and cell adhesion [138-140]. While most RTKs positively regulate H-Ras to cause increased MAP kinase activity, both EphAs and EphBs do the opposite [141-145], which may explain how the Eph receptors inhibit cell proliferation. H-Ras signaling is regulated by an intricate balance of H-Ras activators and inhibitors such as p120RasGap or Grb2/SOS (son-of sevenless) [142,146-148], and may under certain circumstances even override neurite collapse inducing Rho/ROCK signaling to mediate neurite outgrowth [138,149].

Implications for SAM/PDZ domain mediated signaling. A significant part of Eph signaling obviously relies on tyrosine phosphorylation of the JM region and the catalytic activity of the kinase domain. The functional relevance of the SAM or PDZ binding domains is not clear to date, and while cytosolic ligands for Eph PDZ-binding motifs were reported [150-152], truncation of the SAM or PDZ domain did not show a significant impact on EphA4 function *in vivo* or *in vitro* at the first glance [153,154]. Heterotypic interactions between the Eph receptor's SAM domain and the SAM domain of the cytosolic ILK (integrin-linked kinase) was shown to inhibit cell spreading and migration by altering Rac1 and RhoA activity [155]. Heterotypic interactions to SHIP2 (Src homology 2 domain containing phosphoinositide 5-phosphatase 2) maintain active Eph receptors on the cell surface by regulating endocytosis and subsequent receptor degradation [156]. Interestingly, Ephs are the only family of RTKs dependent on oligomerization for biological activity [31,34], and at the same time the only family to contain a SAM domain [105]. This peculiarity raises the possibility that homotypic SAM-SAM interactions between adjacent Eph receptors may serve to stabilize and participate in receptor clustering [99,100,102]. In fact, SAM domains were shown to mediate protein-protein interactions and homodimerization when present at high *in vitro* concentrations [101].
The PDZ-binding motifs at the C-terminal end of Eph receptors may also serve as phosphorylation independent adaptor sites for PDZ domain-containing proteins, including Syntenin, PICK1 (protein interacting with PRKCA 1), GRIP (glutamate receptor interacting protein), AF-6 (afadin), and SPAR (spine-associated RapGAP) [151,152,157,158]. Depending on the number of incorporated PDZ domains, adaptors could even interact with more than one Eph receptor simultaneously and thus serve as scaffolding proteins and alter Eph clustering and signaling as observed for ephrinBs [159,160]. This possibility was implicated in a study measuring mossy fiber LTP (long-term potentiation) upon infusion of soluble peptides interfering with binding of PDZ-adaptor proteins. Thus impaired Eph signaling causes the reduction of mossy fiber LTP implying that postsynaptic intracellular components may act on Eph signaling via PDZ-binding motif-mediated scaffolding of Eph receptors.

In conclusion, although the majority of proximal Eph receptor-induced signaling events appear to be phosphotyrosine-dependent, the SAM domain and PDZ-binding motif may have a modulating role on Eph clustering thereby altering Eph-specific signaling responses.

Link to integrin function - effects on cell-substrate interactions. Eph receptors have been linked to the integrin signaling pathway via R-Ras [161], and Rap1 proteins [162], through mediators like SHEP1, p130Cas, Crk and the Rap1 exchange factor C3G [163], via FAK (focal adhesion kinase) [164,165] and via the recruitment of LMW-PTP (low-molecular-weight protein tyrosine phosphatase) or SH2/SH3 adaptor protein Nck [166,167]. Moreover, PI3-kinase (phosphatidylinositol 3-kinase) activation is regulated by EphA8 kinase signaling through recruitment of the p110γ regulatory subunit to the plasma membrane acting on integrin function [168].

Kinase-deficient signaling. In some physiological scenarios Eph receptor function does not require forward signaling. EphB6 and EphA10 are known for their lack of kinase activity, which thereby does not allow kinase-dependent forward signaling responses [169]. However, kinase-independent signaling pathways emerging from kinase-null Ephs are implicated, e.g. the phosphorylation of EphB6 by the Src family kinase Fyn [170]. Another source for catalytically deficient Eph receptors is alternative splicing, which was shown to occur for EphA7 [171]. C-terminally truncated, spliced isoforms can intermingle with Eph signaling clusters and thereby impair signaling from full length receptors.
The silencing of the forward signaling branch in bi-directional Eph/ephrin signaling does, however, not prevent reverse signaling by ephrins initiated by Eph/ephrin ectodomain complex formation. It was shown that in some cases the ectodomain of the receptor is sufficient to activate ephrin-mediated reverse signaling in neighboring cells [153,172,173].

Negative regulation of Eph forward signaling. Cleavage and endocytosis will eventually lead to reduced Eph forward signaling [174]. However, these mechanisms of action are characterized by relocation and degradation and do not show per se how Eph signaling is inactivated. Increasing Eph surface densities lead to an increase in basal autoactivation of the Eph kinase activity of the receptor indicating a dynamic equilibrium between active and autoinhibited receptors which has to permanently be maintained by de-activation mechanisms [90,175]. De-activation mechanisms to convert Eph receptors into the autoinhibited, inactive state requires dephosphorylation of their juxtamembrane tyrosine residues. Recent work identified the phosphotyrosine-specific protein-tyrosine phosphatase receptor type O (PTPRO), LMW-PTP, PTP1B (protein tyrosine phosphatases 1B) and PTPs in general to efficiently dephosphorylate EphAs and EphBs, which results in negatively regulating the ephrin-mediated downstream responses such as receptor internalization, axon growth cone collapse or insulin secretion from β-cells [48,176-178]. The phosphatase LAR was shown to

reduce its dephosphorylation activity on EphB2 receptor after activation of FGFR1 signaling [179].
These results suggest phosphatases to be negative regulators of Eph forward signaling, which retain the fragile equilibrium between active and inactive Eph species prior to stimulation of ephrin. But they also have the capacity to alter ephrin-induced Eph activation and secondary processes.

1.4.2 Eph receptor signaling crosstalk

Eph signaling may incorporate crosstalk to signaling pathways from other receptor/ligand signaling systems by a direct physical interaction, also known as heterotypic Eph clustering, by directly affecting the interconnected receptor's signaling capacity or by intersecting on common downstream signaling pathways (Fig. 1.5). Eph receptors may also signal in a cooperative manner without intersecting on downstream signaling pathways to mediate the same or opposite cellular responses. Inversely, Eph receptors may also be targeted by other receptor/ligand signaling systems affecting their signaling capacity.

Direct biochemical crosstalk. An example of direct Eph receptor crosstalk through a signaling mediator like the PI3-kinase and others exists for the integrin receptor to mediate cell adhesion (cp. section 1.4.1) [168,180-183].

Indirect biochemical crosstalk. Eph receptors are also known to crosstalk with other growth factor receptors, which leads to either attenuation or integration of signals. Activation of several Eph receptors by ephrins can attenuate the stimulation of the Ras/MAP kinase pathway induced by PDGF, VEGF (vascular endothelial growth factor), EGF (epidermal growth factor) and others suggesting crosstalk of the signals downstream of Eph receptors [141,146]. FGF (fibroblast growth factor) was shown to antagonize EphB2 receptor signaling by blocking a positive MAP kinase feedback loop in EphB2 signaling via the transcriptional target Sprouty by FGFR1 [179].

Physical interaction. An important mutual inter-connection exists between Eph receptors and NMDARs (N-Methyl-D-Aspartate receptor). Active EphB2 receptors physically interact with NMDARs and promote clustering of these neurotransmitter receptors at synapses [42,184,185]. NMDARs get phosphorylated by EphB2, which increases NMDA-dependent calcium influx. Eph receptor signaling is in turn counter-regulated by intracellular mechanisms that cause degradation of EphB2 in response to increased calcium levels. This degradation process was shown to be solely triggered by calcium influx independent of ephrin binding [186]. NMDAR function is strongly related to Alzheimer's disease [187]. In fact, reversing EphB2 depletion, which precedes memory decline in a murine Alzheimer model, rescues cognitive functions [58,59].

Other physical associations with Eph receptors were shown for the kinase inactive Ryk receptor, which binds Wnt3 and acts in brain areas of retinotectal topographic mapping to counterbalance an ephrinB provided guidance signal [188-192]. Wnt3, which is expressed in an inverse pattern to ephrinB expression leads to avoidance by navigating retinal ganglion cell axons, which express EphBs. Here Wnt and ephrins work together to reinforce the same guidance trajectory in a cooperative manner [193,194].

Cooperative signaling. Other studies involving GDNF (glial cell line-derived neurotrophic factor) and its cognate receptor Ret also show a cooperation of this signaling system with EphA4 in axon guidance decision at the sciatic plexus [195,196]. In the first study motor neurons belonging to the LMC_L (lateral motor column) population were shown to require the cooperation of EphA4 and Ret signaling to project to the dorsal hindlimb [195]. In the second study, EphA4 and Ret signaling were shown to evoke opposite effects within the same growth cone to reinforce the same guidance decision. Indeed, EphA4/ephrinAs repel the LMC_L axons from the ventral mesenchyme whereas Ret/GDNF attract them to the dorsal mesenchyme [197].

1.4.3 *Cis*- versus *trans*-interactions in Eph/ephrin signaling

While binding of Ephs and ephrins expressed on opposing cells (*in trans*) represent the most common mechanism of interaction, growing evidence supports the importance of Eph/ephrin interactions *in cis*. In many regions of the developing brain, Ephs and ephrins are co-expressed in the same cell raising the questions whether or not Ephs can interact with ephrins *in cis* and whether *cis*-interactions change the responsiveness to ephrins presented *in trans* [32]. In order to interact *in cis* Ephs and ephrins have to share the same membrane microdomains [198]. *In vivo* Eph/ephrin *cis*-interactions are implicated in retinotopic mapping of axons and spinal motor axon guidance, where highest EphA to ephrinA ratio densities lead to less responsiveness to ephrin presented *in trans*, i.e. *cis*-attenuation of Eph receptor signaling [199-201]. *Cis*-interactions can be divided in LBD-dependent and non-LBD-dependent interactions [103]. Irrespective of the type of interaction, tyrosine phosphorylation and therefore forward signaling is greatly reduced for EphA, leaving retinal axons less sensitive to bath applied ephrinA5 *in trans*. The mechanism of how ephrins reduce Eph signaling through a *cis*-interaction is currently unknown. However, there is reason to speculate based on my work (see below) that Eph receptor clustering might be antagonized by steric interference with ephrins. Another possibility is the sequestration of Ephs into other membrane microdomains thereby preventing access to essential downstream signaling molecules [32]. Unlike the retinal system, co-expressed EphA4 and ephrinAs in chick motor neurons were observed to segregate into separate membrane microdomains. In that case, segregated Ephs and ephrins do not interact *in cis* and function as independent guidance receptors producing opposite effects on the growth cone [202]. The simultaneous existence of

cis and *trans* configurations highlights the importance of the cellular context for Eph/ephrin signaling.

1.4.4 Ephrin reverse signaling mechanisms

While EphAs and EphBs share a great homology, differences in the domain organization of ephrinAs and ephrinBs are responsible for their divergent downstream signaling mechanisms.

EphrinB reverse signaling. EphrinBs in contrast to ephrinAs possess a cytoplasmic domain with five conserved tyrosines, which are phosphorylated by recruited Src family kinases upon receptor binding and clustering [33,203,204]. The phosphorylated tyrosines and possibly a serine then serve as docking sites for SH2/SH3-domain containing proteins such as Grb4, which then in turn activate downstream signaling pathways targeting actin cytoskeleton rearrangements [205,206]. In neurons, ephrinB signaling is linked to dendritic spine morphogenesis through a molecular mechanism involving Grb4 and GIT 1 (G protein-coupled receptor kinase-interacting protein 1) and the exchange factor for Rac GTPase, PIX [207,208]. PIX in complex with GIT1 and PAK3 (α-p-21-activated kinase 3) regulates Rac activation acting on downstream PAK, which promotes formation of spine and dendritic protrusions [207]. By contrast, Grb4, Dock180 and PAK were shown to activate Rac-signaling regulating actin dynamics to cause growth cone collapse of murine hippocampal mossy fiber axons [209].
Src kinase is activated by Eph-induced metalloproteinase cleavage of ephrinB2 producing a C-terminal fragment (CTF) that is further processed by PS1/γ-secretase to produce the intracellular peptide ephrinB2/CTF2. This peptide then binds Src and inhibits its association with inhibitory kinase Csk allowing autophosphorylation of Src at residue Tyr418 [210].
Involvement of Src kinases has also been implicated downstream of ephrinB2 in reducing motility and reorganizing focal adhesions of smooth muscle cells [211].
EphrinB1 reverse signaling may also be induced by Dsh (disheveled), which binds either directly to the cytoplasmic tail of ephrinB1 or indirectly through association with Grb4, and acts through Daam-1 on the planar cell polarity pathway in *Xenopus* [212-214].
EphrinBs can also activate downstream molecular targets independently of tyrosine phosphorylation by docking of PDZ-domain containing proteins to the PDZ-binding motif at the C-terminal end of the ligand. Transgenic mice lacking a functional ephrinB2 PDZ-binding motif exhibit major lymphatic defects as compared to mice with impairment of the five tyrosine phosphorylation sites [215].
Enzymatically inert adaptor proteins, which could possibly mediate phosphotyrosine-independent responses, are known to be GRIPs, Syntenin and PDZ-RGS3 [216-218]. Binding of these adaptor proteins cannot only trigger ephrin-dependent signaling cascades but also modulate signaling cascades from other receptors representing ligand to receptor crosstalk. For example, ephrinB1 activation inhibits G-protein-coupled receptor CXCR4 signaling via

recruitment of PDZ-RGS3. PDZ-RGS3 acts as a GAP for the subunit of trimeric G proteins thereby inactivating signaling mediators downstream of CXCR4 [218].
EphrinB2 function also impacts on AMPA receptor trafficking through a PDZ-domain-mediated interaction [206]. GRIP adaptor proteins scaffold ephrinB ligands and AMPA receptors to lower the constitutive internalization of AMPA receptors thereby maintaining synaptic transmission. GRIP1 over-expression was also sufficient to rescue an ephrinB3 knockdown phenotype by restoring shaft synapse density [159]. In their model, the authors proposed GRIP to engage other subtype ephrinBs in reverse signaling by their scaffolding ability.
Crosstalk to other membrane bound molecules is e.g. observed in the regulation of cell adhesion and inter-cellular permeability through claudins. They are components of epithelial tight junctions between cells and presumably potent in causing ephrinB1 tyrosine phosphorylation independent of Eph receptor engagement [192].

EphrinA reverse signaling. In contrast to ephrinBs, ephrinAs present a GPI-anchor at their C-terminal tail tethering them to the outside of the plasma membrane. They are known to participate in reverse signaling events [219], genetically evidenced by important functions including axon guidance [220-222], cell migration [223], neurogenesis [224], insulin secretion [48] and cell adhesion [225-227]. Two different strategies have been proposed to address the intriguing question of how ephrinA activation gets relayed into the cell to trigger an ephrin-specific signaling cascade of biological importance.
GPI-anchored proteins including ephrinAs are often compartmentalized into cell membrane microdomains also known as lipid rafts, which are rich in cholesterol and sphingolipids [228-230]. Eph-induced clustering of GPI-anchored proteins like ephrin may trigger the constitution of larger raft domains, which would recruit intracellular signaling mediators like Src [225,228].
The other strategy suggests a signaling mechanism of ephrinAs interacting with either co-receptor TrkB or p75 *in cis* thereby modulating their intrinsic activity in a way similar to GDNF receptors [221,231-233]. Association with the respective co-receptor, either p75 or TrkB, was reported to produce differential cellular responses, either axon repulsion or axon branching, respectively [232].

1.4.5 Eph bi-directional signaling networks and cell response promiscuity

Signaling networks emerging from activated Eph receptors have become continuously more complex with more and more studies being carried out. While some signaling pathways like the RhoA/ROCK are shared by all Ephs, others seem to be much more subtype-specific. Similarly, mediators and adaptors also display mutuality and specificity among Eph receptors. This leads to confusion in allocating Eph induced signaling pathways and thereby connected mediators to respective cellular responses. The growing complexity in Eph signaling gives

rise to the concept of network-based signaling, which involves vertically and horizontally interconnected signaling chains [234]. In addition to that, the signaling network is embedded in a dynamic cellular context, which strongly influences respective signaling outcomes. For Ephs/ephrins in particular, bi-directional signaling and cell-contact dependence complicate the calculation of a cumulative signaling response [30]. In general, picking on one thread of the bi-directional signaling network causes fluctuations in the dynamic cellular signaling pattern on either cell side, which might explain cellular response promiscuity underlying Eph/ephrin signaling.

1.5 Eph/Ephrin signaling complexes in trafficking and processing

RTK signaling in general, but also Eph signaling in particular, is influenced by trafficking and processing prior and posterior to receptor activation. Upon ligand engagement, the amplitude and kinetics of signaling may be determined by a highly regulated endocytic process, which sorts activated receptors to degradation in lysosomes eventually leading to complete attenuation and termination of the initial signaling response (Fig. 1.6) [10,235].

Regulation of Eph internalization. Eph/ephrin complexes undergo internalization by endocytosis upon cluster formation and activation [174]. During this process, Eph/ephrin complexes at cell-contact interfaces are rapidly removed from the cell surface by *trans*-endocytosis into both the Eph-expressing cell (forward endocytosis) and the ephrin-expressing cell (reverse endocytosis) to terminate adhesion and allowing for contact-mediated repulsion [236-239]. Interestingly, *trans*-endocytosed Eph/ephrin complexes are still associated to their original membrane domains leading to double-membrane-coated intracellular vesicle structures [237,240]. Furthermore, *trans*-endocytosed Eph/ephrin complexes persist in signaling suggesting that active signal transduction can be redirected into one or the other adjacent cell depending on the balance of endocytic processing [237,238]. To date, the underlying mechanism for this rather unusual process is not known.
Activity of the small GTPase Rac1 is required for local rearrangements of the actin cytoskeleton to cause membrane ruffling for initiation of endocytic processes [156,237].

Fig. 1.6 Eph/ephrin processing and endocytosis.
Schematic presentation of Eph/ephrin processing by proteases, Eph pre/post-activation trafficking and surrounding signaling pathways as described in the main text. Arrows (→) denote a positive, (T)-indicators a negative regulation on downstream targets. The location of the signaling proteins does not imply the involvement of a particular Eph/ephrin domain. The question marks indicate signaling connections that have not been conclusively assessed in Eph/ephrin signaling. Eph processing and trafficking may depend on the Eph/ephrin levels, degree of ligand/receptor clustering, and cellular context. Some of the mechanisms were derived from studies using soluble Fc fusion proteins and are not validated by cell-cell stimulation experiments.

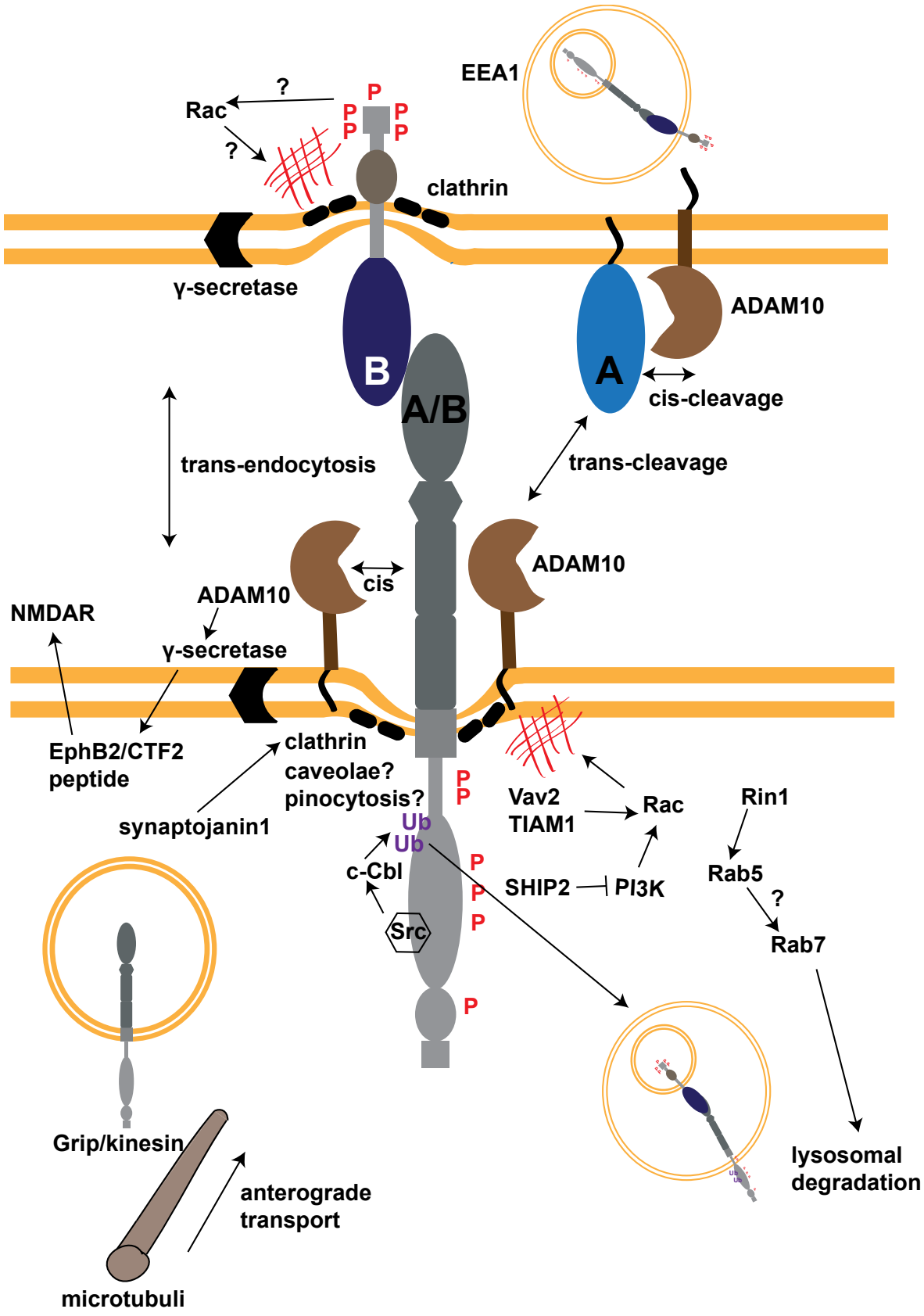
EEA1
?
Rac
?
P
P
P
P
P
clathrin
γ-secretase
ADAM10
B
A
A/B
cis-cleavage
trans-endocytosis
trans-cleavage
ADAM10
cis
ADAM10
NMDAR
γ-secretase
EphB2/CTF2
peptide
clathrin
caveolae?
pinocytosis?
synaptojanin1
P
P
Vav2
TIAM1
Rac
Rin1
Ub
Ub
c-Cbl
P
P
P
SHIP2
PI3K
Rab5
?
Rab7
Src
P
Grip/kinesin
anterograde
transport
lysosomal
degradation
microtubuli

Recent work has implicated the Rac exchange factor Vav (Vav1-3) in Eph receptor forward endocytosis. In contrast to the related ephexin1, Vav2 has no preferences for EphA or EphB and binds through its single SH2 domain to activated, phosphorylated JM-tyrosines subsequently enhancing Rac activation and Eph endocytosis [241]. Vav2/3 double knockout mice develop axon guidance defects, presumably due to the absence of Eph-mediated axon growth cone collapse in response to ephrinA1 [241]. Similar to Vav2 for EphA4, other GEFs like TIAM1 play an important role for EphA8-dependent Rac1 activation and its internalization [242].
SHIP2 was discovered as a negative regulator of ligand-induced EphA2 endocytosis. It binds to EphA2 via a heterotypic SAM-SAM domain interaction [156]. SHIP2 dephosphorylates PIP3 (phosphatidylinositol 3,4,5-trisphosphate) thereby suppressing PI3K signaling, which in turn is required for enhancing Rac1 activation [243].

Eph endocytic pathways. While it appears that Rac1 signaling generally enhances Eph/ephrin internalization [156,237], the exact role of the clathrin endocytosis machinery remains unclear [174]. To date, the only two studies linking Eph receptor internalization to the clathrin-dependent pathway show involvement of TIAM1 and synaptojanin1 [242,244]. Importantly, stimulation of cells with soluble Eph or ephrin fused to the Fc portion of human immunoglobulin likely activates endocytic pathways, which significantly differ from the ones induced by physiological cell-cell interactions. Indeed, a phospho-proteomic study has reported a different selection of targets and adaptors to be activated when soluble ephrin-Fc was used for stimulation [245].
In contradiction to a strictly clathrin-dependent mode of internalization, Ephs were also discovered to be concentrated in caveolae, and the EphB1 receptor to be associated with the protein caveolin-1 [246]. These few reports indicate that further work is required to elucidate the full molecular mechanism of Eph/ephrin endocytosis or identify other modes of internalization like caveolae or pinocytosis.

Eph trafficking. Vesicles loaded with receptor cargo undergo extensive sorting and maturation to various endocytic compartments. The Rab GTPase proteins are highly compartmentalized in organelle membranes and together with their effectors coordinate these consecutive stages of transport, which comprise processes like vesicle formation, vesicle motility and tethering of vesicles to their target compartment [247]. Eph receptor trafficking prior to and post ligand-engagement and cluster formation has only been poorly addressed so far.
Rin1 (Ras/Rab interactor 1) is a GEF for Rab5, which is known to control the fusion of endocytic vesicles and early endosomes. Like Vav, it was found to bind to EphA4 via its SH2 domain and to become phosphorylated upon EphA4 activation, causing the EphA4-sorting in Rab5-positive compartments. *In vivo*, EphA4 and Rin1 control neuronal plasticity in opposite

ways, suggesting that Rin1 antagonizes EphA4 function through induction of an enhanced internalization response [248].
The Eph receptor's final fate upon ephrin engagement and internalization was speculated to be degradation in lysosomes as observed for other RTKs as a mechanism to shut down signaling [10]. In fact, ligand binding induces cbl-dependent ubiquitinylation and EphB1 degradation through the lysosomal pathway, also marked by the late endosomal marker Rab7 identified in a proteomics approach and co-localization studies with lysosomal compartments [104,249,250]. However, these studies rely on a strong stimulation with soluble ephrin-Fc, which might not reflect the physiological situation of Eph stimulation response *in vivo*. It may be speculated that a rather differential trafficking response comprising recycling components aside from the crude lysosomal fate may also apply for Eph receptors, which e.g. only undergo mild clustering.
Ephs, as all other transmembrane receptors, are secreted from Golgi compartments to the plasma membrane, after translation and glycosylation [2]. For EphB2, in hippocampal neuronal cultures, a kinesin1-dependent anterograde transport mechanism to dendrites was observed involving the PDZ-adaptor protein GRIP1 [251] (Fig. 1.6).

Ephrin reverse endocytosis. The clathrin-dependent pathway has also been implicated in reverse endocytosis. GFP-tagged ephrinB1 co-localizes in clathrin-coated vesicles, positive for the early endosome marker EEA1 (early endosome antigen 1) after stimulation with CHO (Chinese hamster ovary) cells expressing EphB1 [252] (Fig. 1.6). As small GTPases are also activated downstream of B-class ephrins [209,253,254], GEFs might be good candidates for the regulation of reverse endocytosis.
EphrinB2 seems to be destined for degradation through the proteasomal pathway after stimulation with soluble EphB2-Fc. In *Xenopus* retina cultures, ephrinB2 degradation was inhibited by proteasome-specific inhibitors LnLL (N-acetyl-l-leucinyl-l-leucinal-l-norleucinal) and lactacystin [236].

Eph/ephrin cleavage. Cleavage of Ephs and ephrins by ADAM (A-Disintegrin-And-Metalloprotease) family metalloproteases and γ-secretase proteases is an additional mechanism to terminate Eph/ephrin contact. EphrinA2 was identified to associate with ADAM10, which cleaves the ephrinA ectodomain thus facilitating contact-repulsion of axons [255].
In addition, ADAM10 was also proven to interact with EphA3 and cleave ephrinA2 *in trans* only after binding to EphA3 [256,257] (Fig. 1.6).
For ephrinBs, γ-secretase-dependent cleavage takes place *in cis* but not *in trans* [210,258].
Recently, EphB2 ectodomain release to the extracellular space was evidenced following cleavage after EphB2 residue 543 insensitive to metalloproteinase inhibitor GM6001 [186]. Here, EphB2 is in addition cleaved by a presenilin-dependent γ-secretase activity releasing an intracellular peptide that contains the cytoplasmic domain of EphB2. Interestingly, cytosolic

peptides produced by the combined metalloproteinase/γ-secretase processing of cell surface proteins can function in signal transduction and protein phosphorylation [186]. Inhibition of ephrinB2-induced EphB2 cleavage also reduces Eph-mediated axon growth cone collapse [259]. Moreover, the released EphB2 intracellular peptide was shown to be important for NMDAR-subunit phosphorylation in primary neuronal cultures [260]. In the case of EphA4, intracellular peptide enhances preferentially Rac signaling [261].

1.6 Mechanisms of receptor clustering

In biological sciences, "clustering" is the widely used terminology to describe processes or states when a group of the same or similar elements are gathered or occurring closely together. Examples exist both on the genetic level (gene clusters) and on the protein level in different variations from cytoplasmic protein assemblies like the ribosome to receptor complexes on the cell surface. Limiting ourselves to the topic of receptor assemblies in membranes, i.e. receptor clustering, we miss a clear and common understanding of the underlying mechanisms and functional importance involved.

1.6.1 Concepts and statistical mechanical models to describe receptor clustering

Equilibrium and non-equilibrium receptor clustering. Receptor clustering comes in different flavors in the way of the grouping of elements of the same kind. While many cluster formation processes result in non-equilibrium states of protein assemblies on the cell surface, others are the result of a shift in the very dynamic equilibrium between monomeric receptor species and higher-order receptor oligomers [262].
In complex systems like the immunological synapse, receptor clustering is most likely established and maintained by non-equilibrium processes involving, for example, the cytoskeleton to stabilize a conglomerate of membrane proteins [263,264]. Occasionally in this context, the terminology of "aggregation" fits much better because it points out the irreversible nature of the constitution of such complexes, which then exist semi-permanently in 2-dimensional arrays on the cell surface.
In simpler systems, equilibrium thermodynamic interactions between receptors, ligands and associated proteins may be sufficient to explain the phenomenon of clustering and to shed light on the advantages it provides for transmembrane signal transduction. Extracellular ligands can cause the dimerization or oligomerization of receptors within the cell membrane and this in turn can activate signaling pathways within the cell. It is this rather dynamic formation of clusters in response to activation by an extracellular ligand, which will be explored in the following paragraphs [262].

The basic statistical mechanical model of receptor clustering (Fig. 1.7A). A good starting point to best model receptor clustering is the description of freely diffusing single receptor molecules in the planar cell membrane. The simplest physical model to describe this process is the so-called "lattice gas" [265], which describes density fluctuations of single elements. In this system, the membrane is abstracted to represent a 2-dimensional lattice of *M* sites. Each lattice-position may either be occupied by a protein or vacant. The interactions between single molecules are described by a decrease in the free energy of the system, by an amount *J*. This decrease in energy only occurs when two adjacent sites are simultaneously occupied by interacting proteins. In the next step the lattice gas model may be mapped onto the well-known Ising model for statistical mechanics, which enables scientists to study phase transitions [266,267]. Respectively, the formation of clusters can be seen as a phase transition from single monomers to higher-order oligomers. The system energy *E* in receptor clustering gives:

$$E = -\frac{J}{4}\sum_{<i,j>} s_i s_j - \frac{1}{2}(\mu + zJ)\sum_i s_i - \frac{M}{2}(\mu + zJ)$$

with the variable transformation to account for the model's ferromagnetic spin *s* :

$$s_i = 2t_i - 1$$

[266,267], where *J* is the coupling energy, t_i = 1 (0) corresponds to an occupied (unoccupied) lattice site *i*, the sum over <*ij*> includes all nearest neighbors, *z* is the number of neighbors of a lattice site, *M* is the number of lattice sites.

The Ising model can be solved exactly in 2 dimensions revealing the striking feature that there exists a critical coupling parameter J_c at which the nature of the solution changes abruptly to make a phase transition [268]. The above model may be transformed into the Bragg-Williams model of binary alloys since transmembrane receptors are not readily exchanged between the membrane and the cytosol and it is therefore appropriate to solve the model with the constraint of a fixed total number *N* of receptors in the membrane or, equivalently, a fixed surface coverage $\phi = \frac{N}{M}$ [267,269,270]. It basically states, that for high coupling energies *J*> J_c and a sufficiently high surface coverage ϕ, phase separation occurs, i.e. results in the aggregation of receptors to a dense cluster. Again, the model reveals a critical parameter, this time for receptor surface coverage ϕ_c. For low ϕ clusters are smaller and more transient, whereas for larger ϕ clusters are more permanent, but continually exchange individual receptors or small aggregates of receptors.

Note, that dissociation constants (K_d) can also be used to characterize the strength of receptor-receptor *cis*-interactions in transmembrane receptor clustering systems. While the microscopic K_d of isolated receptor monomers in the dimerization process with other isolated receptor monomers can be considered as constant, the effective dissociation constant K_d^{eff} of a receptor located within a cluster is significantly decreased by several orders of magnitude.

A

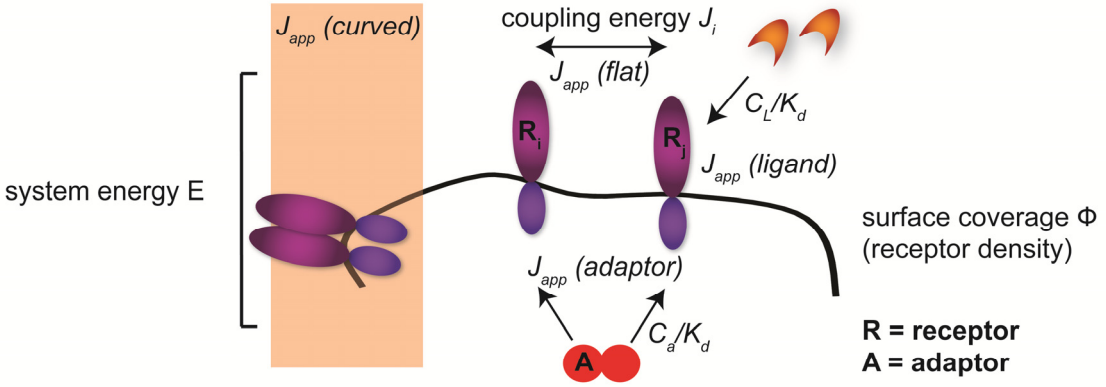
J_{app} (curved)
coupling energy J_i
J_{app} (flat)
C_L/K_d
R_i
R_j
J_{app} (ligand)
system energy E
surface coverage Φ
(receptor density)
J_{app} (adaptor)
C_a/K_d
A
R = receptor
A = adaptor

B

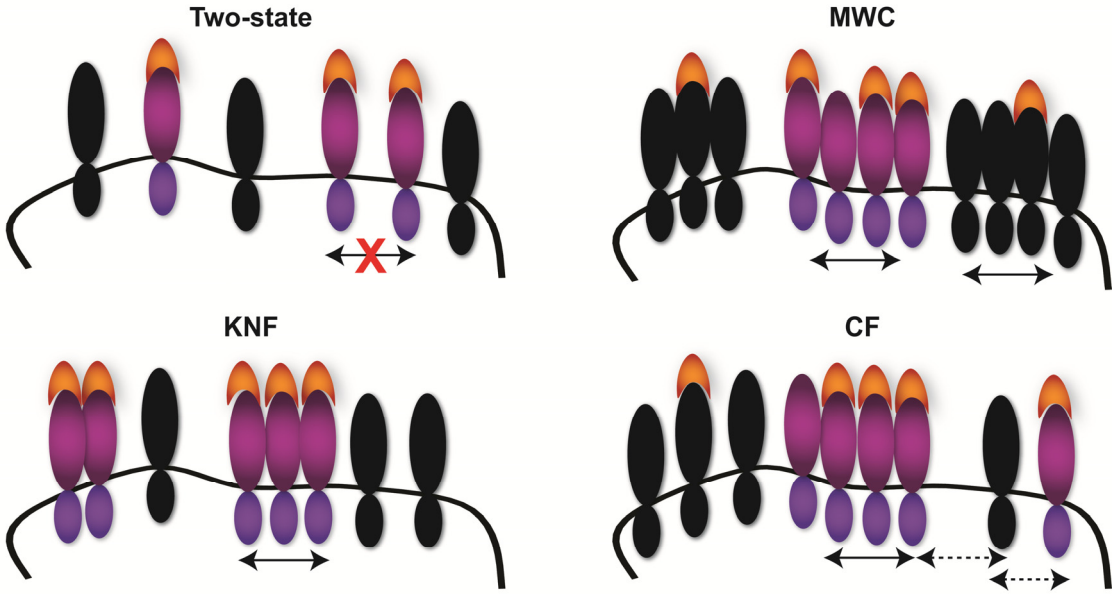
Two-state
MWC
KNF
CF

C

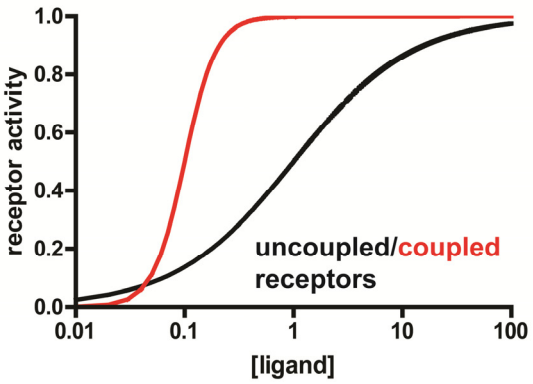
receptor activity
1.0
0.8
0.6
0.4
0.2
0.0
uncoupled/coupled
receptors
0.01
0.1
1
10
100
[ligand]

Fig. 1.7 Mechanisms of receptor clustering.
(A) Ising model to describe the allosteric behavior of receptor clustering. As outlined in the text, critical parameters are the coupling energies J ($J > J_c$) and receptor surface coverage ϕ ($\phi > \phi_c$) for phase transition, i.e. receptor clustering to occur. Clustering determinants like ligand or adaptor proteins act through their concentration c and dissociation constant on receptor coupling energies to give J_{app}. **(B)** Two-state and allosteric models of receptor regulation. The two-state model is based on conformational changes induced in receptors as a result of ligand binding. Changes in receptor activity directly reflect changes in ligand occupancy. The model does not reconsider coupling between receptors and thereby fails to explain features such as enhanced sensitivity and broader dynamic range in receptor cluster signaling systems. The MWC (Monod-Wyman-Changeux) model postulates independent receptor clusters to exist in all-or-none complexes fluctuating between active and inactive in concert. Ligand binding shifts the equilibrium to the active or inactive side. Whereas in the MWC model it only phenomenologically looks as if the ligand provokes the conformational transition, the KNF (Koshland-Néméthy-Filmer) model exactly incorporates this active role of the ligand to induce a conformational change in the receptor. The conformational change is then also seen to be the premise for receptor coupling *in cis*. The CS (conformational spread) model finally provides a natural integration of the MWC and KNF viewpoints. In addition to receptor-receptor interactions of receptors with bound ligand also receptors, which have not experienced ligand-induced conformational transition are incorporated into existing clusters. Arrows/red (X) indicate receptor coupling/no coupling. **(C)** Exemplary dose-response curve for receptor activity upon ligand engagement. For the case in which there is coupling between the receptors (red curve) overall sensitivity may be heightened by an order of magnitude (EC_{50} = 0.1 for coupled receptors as compared to EC_{50} = 1.0 for uncoupled receptors, red curve is shifted to the left). At the same time receptor clustering causes an increase in responsiveness to small variations in ligand concentration as represented by the slopes of the sigmoidal curves (Hill coefficient n for the activity increased from n= 0.8 to n= 3.0). Curves were generated with GraphPad Prism and parameters as indicated.

Two-state and allosteric models of receptor clustering (Fig. 1.7B). While in theory both a sufficiently high drop in the coupling energies J_i and critical receptor membrane density ϕ_c are sufficient to cause receptor-autonomous clustering, this is often not observed to be the trigger for receptor activation and/or clustering in a rather biological context of low receptor densities. However, transmembrane receptors are also influenced from the outside by the extracellular concentration of their cognate ligands. Often, the binding of a ligand molecule affects the equilibrium between two conformational states, favoring, for example the active state resulting in receptor signaling. In the two-state model of receptor regulation, receptors function autonomously without interaction to adjacent other receptors. Changes in receptor occupancy thereby directly relate to changes in receptor activity. The two-state model fails to reconsider receptor-receptor interactions and does not allow the study of receptor clustering processes. On the contrary, allosteric models of multi-receptor complexes can be seen as an extension of the two-state model, including interactions between receptors. In general, descriptions of allostery have been limited to changes within a single oligomeric molecule, usually a compact oligomeric protein such as hemoglobin. However, the concepts of allostery can be transferred to multimolecular arrays of proteins and stochastic patterns of conformational change [271].
Characteristic patterns of activity can be predicted by three models of allostery: i) the MWC (Monod-Wyman-Changeux) model, ii) the KNF (Koshland-Néméthy-Filmer) model and iii) the CS (conformational spread) model. According to the MWC model all receptors within an

array adopt the same conformation at the same time and the microscopic binding constant for the ligand depends only on the conformational state of the protein [272]. In the KNF model, ligand molecules force the receptor to adopt an active conformation [273]. In fact, for many receptor-ligand systems broad structural rearrangements are usually observed in change from one state to the other. The structural rearrangements may be relayed into a change for enhanced receptor clustering propensity represented by the apparent coupling energy J_{app}, which then exceeds the critical coupling energies J_c causing phase transition and receptor aggregation. For soluble ligand, both ligand concentration c_L and dissociation constant K_d determine the apparent coupling energies between receptors. The KNF model accounts for this effect by reconsidering a stronger propensity of ligand binding of neighboring subunits in a macromolecular complex. In the CS model, individual subunits have a certain probability of being active or inactive depending on whether they are bound to a ligand and on the conformational states of their two neighbors [274]. This model allows for a nucleation mechanism, in which ligand may induce an assembly of active receptors clustered together. At the same time, those receptors that have no ligand bound are very likely to be active as well. All models support the notion of cooperative signaling behavior and are able to explain enhanced sensitivity and increase in sensitivity in such allosteric signaling systems.
Popular mathematical models of allosteric behavior in receptor clustering are the CS model and the mean-field solution of the Ising-model as described in this study [274,275].

Clustering determinants. The statistical mechanical model for dynamic receptor clustering also allows for consideration of other clustering determinants apart from ligands, which may modulate the equilibrium thermodynamics of the cluster formation process (Fig 1.7A). A cell might dynamically control the formation of transmembrane receptors by the use of adaptor proteins that bind to the cytosolic domain of the receptors and modify receptor-receptor interactions. Adaptor protein binding to receptors can be controlled spatially and temporally in the cell by processes including synthesis, sequestration and buffering or enzymatic modifications like phosphorylation, methylation or cleavage of the adaptor protein. Either way, two parameters, c_A (cytosolic concentration of the adaptor protein) and the intrinsic K_d are able to characterize adaptor binding propensity to receptors by their quotient value c_A/K_d. Adaptor binding to receptors leads to a change in the coupling energies J between receptors. The formation of a cluster can be induced by raising the control parameter c_A/K_d above a critical value which then acts through J_{app} (J_{app} *adaptor*) on clustering propensity. A similar change in the coupling energies J between receptors may be obtained by geometric constraints provoked by the curvature of the cell membrane. Here, the intrinsic shape of the individual transmembrane receptor might for example favor a rather hemispherical shaped geometry for clustering as observed at the caps of many cylindrical shaped bacteria. A localization of receptor molecules in this geometric environment would therefore lead to higher apparent coupling energies (J_{app} *curved*) and a greater bias for clustering [267,276].

1.6.2 Functional significance of clustering for receptor signaling

Statistical mechanical models outlined above can most readily be discussed in the context of the bacterial chemotaxis system, for which extensive experimental investigation has provided enough knowledge about the composition of receptor clusters, their localization in the cell, and most important of all the role that clustering plays in signal transduction [277].
However, the phenomenon of cluster formation has emerged for various different receptor systems. The clustering feature of receptors ultimately raises the question for its common role in signaling. It has been postulated by modeling, and in specific cases experimentally confirmed that receptor clustering confers a wide range of advantages for signal transduction.
One of the more obvious significant functions of dynamic receptor clustering is augmentation of sensitivity and increase in responsiveness in response to a ligand stimulus with subsequent receptor signaling (Fig. 1.7C) [278-280]. But in addition, receptor clustering also promotes a broader dynamic signaling range and enhanced specificity in response to the stimulus [280,281]. The concerted arrangement of receptors in a signaling array also enhances the simultaneity of the response and enables an analog logical computation of a response to more than one ligand at a time [282,283]. It has also been suggested that the segregation of different types of transmembrane receptors into separate clusters might limit cross-talk between signaling systems [267,284]. Another important feature of clustering is its intrinsic property to cause spatial organization of receptors on the sub-cellular level in cell surface membranes. This might also assist the enzymatic adaption of individual receptors within a cluster [285]. In the case of conformational spread, clustering can also serve in signal amplification, or "gain". The most remarkable example in this context is the fact that individual *Escherichia coli* are able to detect the binding of just a few molecules of attractants, such as aspartate to their receptors [286]. Closely connected to the concept of signal amplification by clustering is robustness, i.e. toleration of the signaling system towards variations in protein concentrations, reaction rates and extrinsic and intrinsic noise of the signaling system [277,287]. Last but not least, inversely thought, clustering empowers the signaling system to return to the pre-stimulus pathway activity with high precision following a change in the strength of the input stimulus. This mechanism leads to perfect adaptive signaling in response to e.g. graded or changing ligand concentrations, which might differ in time and/or space throughout the course of ligand stimulation [277].

1.7 Role of Eph/ephrin clusters for cellular responses

Bi-directional signaling versus higher-order cluster formation. The Eph/ephrin signaling system displays distinct features, which may account for the range of cellular responses possible: i) Ephs are the only RTKs activated by membrane-bound ligands enabling bi-directional signaling [31,33]; ii) Ephs and ephrins oligomerize to produce higher-order cluster arrays. Both these processes may integrate *in vivo* to produce cumulative bi-directional

signaling responsible for a range of cellular responses possible [30]. However, for studying e.g. only the Eph signaling branch, soluble ephrin-Fc fusion proteins can be preclustered (with anti-Fc antibodies) into aggregates and be bath applied to stimulate the Eph-expressing cells [31]. This activates only Eph forward signaling and thereby associated cellular responses. But still, Eph signaling can lead to differential cellular readouts as observed for axon outgrowth or cell migration [288,289], which in part may rely on the remaining feature of Eph higher-order cluster formation. If one accepts ligand-densities as an obvious parameter in affecting Eph clustering, *in vitro* assays have demonstrated that low densities of ephrins promote outgrowth and integrin-mediated adhesion, whereas high densities trigger repulsion and de-adhesion [175,289]. Thus, the cell response appears to depend at least to some extent on the degree of receptor activation i.e. possibly Eph clustering and kinase activity to induce downstream signaling events. Interestingly, *in vitro*, in absence of ephrin stimulation an increase in Eph surface expression results in a concomitantly increase of Eph phosphorylation in a dose-dependent manner [90,166], while ephrin-induced cell adhesion follows a biphasic response pattern with strong adhesion for high and low ephrin densities [165,166,168].
Considering the fact that Ephs in addition to phosphorylation undergo higher-order oligomerization the question arises, if the oligomerization state from monomer to multimer could be considered as an overriding control governing biological responses [290].

Implications of Eph clustering for cellular responses. The ability of Ephs and ephrins to form ordered multimeric assemblies suggests a potential architectural role that could either be separated or linked to their direct signaling role [70,80]. Their paradoxical feature to produce opposite cellular responses ranging from adhesion to repulsion may at least in parts be linked to their uniqueness in forming higher-order cluster assemblies at cell contact interfaces. However, the regulation of Eph/ephrin clustering under physiological conditions and its impact on cellular responses is only poorly understood.
Recent x-ray crystallographic studies elucidate the structural basis of Eph/ephrin receptor clustering [72,91], but fail to establish a clear and direct link to functional signaling readouts. However, a few earlier studies addressed somehow indirectly the functional role of cluster formation for Eph signaling on a rather non-structural basis using soluble ephrinB2-Fc in its monomeric, dimeric or multimeric form to stimulate Eph-expressing cells. Since Ephs are the only RTKs activated by membrane-bound ligands, this presumably allows for Eph signaling to be regulated not only by receptor dimerization but also by the degree of ligand clustering. In fact, non-clustered ephrin-Fc can act as functional antagonist of Eph signaling [291]. Thus, in experiments by Stein and colleagues, preclustered, multimeric ephrinB1-Fc promotes endothelial capillary-like assembly in a two-dimensional *in vitro* assay using human renal microvascular endothelial cells (HRMEC) [292], whereas dimeric ephrin-B1/Fc does not [34]. In a P19 cell-based adhesion assay, preclustered ephrinB1-Fc multimers provoke P19 cell attachment to fibronectin. By contrast, applied in the same concentration, ephrin-B1/Fc dimers have a modest effect to decrease fibronectin attachment of a small subpopulation of

cells [34]. These functional effects correlate with LMW-PTP recruitment to EphB1 and EphB2 complexes upon stimulation with ephrinB1-Fc multimers and more specifically upon recruitment of ephrinB1-Fc tetramers to promote attachment. Growth cone collapse assays with ventral and dorsal retina neurons from *Xenopus* supported this finding by investigation of the bi-directional signaling mechanisms underlying stimulation with either pre- or unclustered EphB2 or ephrinB1 ectodomains [194]. Furthermore, in a kinetic analysis, the binding of monomeric, dimeric and multimeric ephrinB2s to EphB2 receptors expressed in neurons of rat hippocampal cultures show a dose-dependent growth cone collapse response, which correlates with an increase in apparent binding affinities measured *in vitro* by surface plasmon resonance [96].

Similarly, in an approach using a monoclonal antibody against the ectodomain of EphA3 to cause clustering, activation of the receptor and subsequent cellular responses like contraction of the cytoskeleton and cell rounding are observed [293]. Moreover, simultaneous ephrinA5 and antibody binding synergizes to activate the EphA3 receptor even stronger. The authors suggested that antibody binding triggers an EphA3 conformation, which is permissive for the assembly of EphA3/ephrinA5 signaling clusters.

In a rather biophysical approach using artificial membranes displaying ephrinA1, the effect of EphA2 cluster size and mobility was studied in breast cancer cells [294]. Lateral transport of ephrinA1 was blocked by physical barriers nanofabricated onto the underlying substrate [295,296]. Depending on how ephrinA1 transport was constrained, EphA2 receptor engagement produced different cell responses to ephrinA1, as observed by changes in cytoskeleton morphology and recruitment of metalloprotease ADAM10. The EphA2-expressing cell pulls the receptor laterally via an acto-myosin contractility process, and the outcome of the signaling process apparently depends on whether the ephrinA1 ligand in the apposed cell resists to this applied force. Thus, somewhere between receptor activation and the downstream signaling events, there is a signaling step that is sensitive to the large-scale spatial organization of the EphA2 receptors or possibly even the tensile forces acting on them. Intense cooperation between the cell membrane and cytoskeleton empowers this signaling system to respond to differences in the mechanical aspects of the microenvironment.

Taken together, Eph receptors can indeed discriminate specific ligand oligomers, antibody-induced Eph-ectodomain configurations or cluster sizes to determine alternative signaling complexes, attachment, assembly and trafficking responses, which most likely relies on their unique cluster formation properties. However, the mechanisms, which allow this discrimination of specific ligand oligomers or ectodomain configurations, are so far unknown and can only be speculated upon. Furthermore, these studies did not allow a direct and sensitive control of Eph clustering but clustering was provoked by external stimuli binding to the Eph ectodomain. Therefore, it will be extremely useful to design ways to gradually change clustering behavior of Ephs and ephrins in living cells [32].

Conformational spread mechanism for Eph receptors? Interestingly, experiments with ephrinA5 coated beads suggest that ephrins induce Eph clustering, but that cluster growth occurs independently of ephrin contacts and involves direct Eph-Eph interactions resembling an extracellular steric seeding or nucleation mechanism also confirmed by structural studies [72,91,104]. This rather uncontrolled clustering mechanism, which is somehow reminiscent of the conformational spread mechanism well characterized for bacterial chemotaxis receptors [274,297,298], is suited to recruit a proportion of receptors into a signaling cluster that would represent the overall receptor abundance of the cell and thereby control the strength of the signaling response (heightened sensitivity) (Fig. 1.7C). This concept allows for precisely adjusted cellular responses (heightened responsiveness) controlled by graded changes in ligand abundance and receptor/ligand occupancy, a characteristic feature of Eph-ephrin communication [104].

Implications of Eph clustering for *in vivo* scenarios. The only *in vivo* study to address the relative importance of kinase activation versus higher-order clustering genetically in the mouse was carried out by using the constitutively kinase-active receptor mutant eeEphA4 [113]. Receptor eeEphA4 mediates normal midline guidance of corticospinal tract and commissural interneuron axons in the spinal cord, where there is a localized source of repulsive ephrinB3 (midline). However, in circumstances where EphA4-positive axons have to react to a smooth gradient of ephrinA, eeEphA4 signaling is impaired. This suggests that eeEphA4 engaged ephrins normally at choice points, though, in situations where EphA4-positive axons have to react to a smooth gradient of ephrinA, eeEphA4 is unable to mediate the ephrin signal. Among other explanations, it was suggested that the ability to generate a graded response to ephrins might require a particularly tight regulation of Eph activation [113,299], presumably accomplished by graded clustering.
In fact, various scenarios *in vivo* describe situations where Ephs have to respond to gradients of ligand expression to establish fine patterns of innervation as e.g. observed in the topographic mapping of the visual system [300-302]. In ephrin-directed pathfinding, the current model suggests that migration of Eph-bearing cells into a gradient of ephrin expression is controlled by Eph receptor affinity and abundance and by competition for ephrin targets [303-305], which may produce a respective Eph clustered state and signaling response.

Heterotypic Eph/ephrin clustering. Another role for Eph/ephrin clustering at cell contact interfaces may be attributed to create stable membrane-associated platforms for the architectural organization of various cellular structures, e.g. in excitatory central nervous system synapses [306]. As already described (cp. section 1.4.2), EphB2 physically associates with NMDAR [184,307] to control both NMDAR density in postsynaptic clusters and the number of postsynaptic release sites [184].

2. SCOPE

The formation of higher-order signaling complexes is a unique feature of the Eph/ephrin family amongst all RTK families and is necessary to induce robust bi-directional signaling responses [31,33,34,113]. Structural work on Eph/ephrin complexes demonstrates an extracellular steric seeding or nucleation mechanism for Eph clustering [72,91,104]. However, clustering remains elusive when it comes down to establishing a clear link to kinase-dependent or -independent Eph signaling and cellular responses. Furthermore, current speculation about the role of cluster formation in producing graded cellular responses is based upon other receptor/ligand systems, implications from structural studies or mere intuition in the field of research. To date performed functional studies addressing the role of cluster formation fail to establish a clear and direct mechanistic link to clustering [34,113,293]. Instead, growing evidence points to a lack of consistency between Eph-induced signaling and thereby induced cellular responses. In this respect, I am convinced that clustering is a key element in determining adhesive versus repulsive Eph signaling responses.
This study investigates the function of clustering in Eph-mediated cell responses, thus seeking to answer the following central questions:

1) The formation of Eph clusters is a highly-ordered multistep process [80]. Is there a way to establish a system to artificially induce Eph/ephrin clusters independent of receptor/ligand-contact, in a cell-autonomous manner and with tight control over cluster size, stability and complexity and link them to functional signaling readouts?

2) Eph clustering is a prerequisite for robust kinase-dependent signaling [33]. Is there a direct correlation of Eph cluster sizes/stability to functional readouts? May clustering serve as a central control entity to elicit appropriate cellular responses?

3) Eph/ephrin signaling induced cellular responses range from adhesion to repulsion [36]. May adhesive versus repulsive cellular responses be linked to the oligomerization state of the receptor?

4) Eph receptors are subject to movement and processing [174]. What are the trafficking/processing effects upon transition from single receptor species to higher-order clusters?

3. RESULTS

3.1 Developing a strategy to control for Eph/ephrin cluster formation in living cells

3.1.1 Formation and processing of Eph/ephrin complexes at cell-contact interfaces

To establish a suitable strategy for studying Eph/ephrin clustering in detail, it is highly beneficial to gain a general insight in surrounding processes leading to, and governing the formation and processing of Eph/ephrin complexes. The most feasible and physiological way to sample cluster formation and surrounding processes is by performing a co-culture assay with two populations of cells, one expressing Eph receptors, the other expressing ephrin ligands [238,245]. HeLa cells were chosen because they show a high mobility on laminin substrate, morphological flexibility and responsiveness, and thereby nicely mimic the *in vivo* modality of Eph/ephrin signaling as observed in axon growth cone collapse or boundary formation processes.

Figure 3.1 depicts the formation and processing of Eph/ephrin complexes after cell contact. At the cell-contact interface, signals from fluorescence (FL) protein tagged Ephs/ephrins were formed as seen by the presence of entities, i.e. aggregates with higher FL intensity. As a control, co-expressed myr-mCherry FL remained diffuse at these sites (Fig. 3.1B-I) indicating that Ephs/ephrins were specifically clustered upon contact. These FL entities at cell edges were then rapidly processed into Eph^+ and $ephrin^+$ cells (Fig. 3.1B-IV/V,C,D). Entities emerging after cell-cell contact at the cell-edge were subsequently broken apart (Fig. 3.1C, D) over time with little fluorescent particles pinching off from the initial large complex. Entities, which were located in cut-off filopodia and/or not in direct contact to the cell's membrane surface did not undergo processing (Fig. 3.1 B-V-VII). In Eph^+ cells, the stimulation by ephrin ligand led to a signaling response resulting in retraction of the cell periphery (Fig. 3.1B, dotted black line, compare I with VI), similar to growth cone collapse in axons. In $ephrin^+$ cells, this cellular collapse response could not be observed. However, in contrast to the Eph^+ cell, due to the lack of cell retraction, the processing of FL particles away from the cell-edge became more evident (Fig. 1D). Little fluorescent particles were constitutively pinching off from a bigger surface-trapped FL entity and were moving towards the inner of the cell, presumably being internalized into endocytic vesicles for degradation. In Eph^+ cells, this process could not be so readily observed because of the simultaneous retraction of the cell periphery.

Taken together, I conclude that live-cell imaging based co-culture assays are a justifiable method to display physiological Eph/ephrin complex formation and functionality on the cellular level. However, this general insight into the processes surrounding Eph/ephrin cluster formation emphasizes two major aspects that severely complicate the investigation of the role

of cluster formation in Eph/ephrin signaling. This not only holds true for co-culture assays but also for other Eph/ephrin single cell assays in general:

1) Tangibility of the Eph/ephrin cluster. FL entities or aggregates are usually described as Eph/ephrin clusters based on their association to the experimentally proven structural feature of oligomerization. Yet the depiction of these FL entities as clusters is rather inaccurate and misleading since the limit of spatial resolution in epifluorescent imaging does not permit this degree of analysis. Upon formation, single FL entities could simultaneously be large, single clusters and assemblies of multiple Eph/ephrin complexes. Moreover, Eph/ephrin complexes are subject to rapid internalization processes, which in its initial steps, are accompanied by invagination processes of the membrane. These processes may very well lead to a crowding of multiple fluorescent complexes into one observed single FL entity. Presumably, FL entities observed at later stages after initiation of complex formation represent internalized Eph/ephrin in vesicles.
Since we do not know the exact composition and origin of these FL entities, it is not possible to extrapolate observed FL Eph/ephrin entities from a mechanistic to functional way. Therefore, an alternative experimental strategy implementing a direct clustering readout to specifically address Eph/ephrin complex formation is required.

Fig. 3.1 Formation and processing of Eph/Ephrin complexes at cell-contact interfaces.
(A) Co-culture situation of HeLa cell populations one transiently expressing YFP-wtephrinB2, the other wtEphB2-CFP in low resolution. The cartoon delineates the physiological event of receptor/ligand co-clustering at cell-contact interfaces. **(B)** Insets in higher resolution to outline the co-culture situation from (A) in time course. Co-culture of HeLa cell populations, one transiently expressing YFP-wtephrinB2, the other wtEphB2-CFP. Cell-contact events were imaged in time-lapse 35 min after seeding of ephrin expressing cells. Sequential time-lapse images show the processing of fluorescent (FL) entities over time. Dotted line serves as orientation for site of initial contact at start of imaging. During the time course of contact the Eph^+ cell gradually moved away from the $ephrin^+$ cell. (I) Arrows in blue indicate co-clustering of ligand and receptor but not myr-mCherry. (II) Arrows in green indicate an Eph/ephrin surface cluster on the Eph^+ cell. (III) Arrows in red indicate an Eph/ephrin surface cluster on the $ephrin^+$ cell. (IV) Arrows in green indicate an Eph/ephrin surface cluster beginning to be processed into the Eph^+ cell. (V) Arrows in red indicate an Eph/ephrin surface cluster beginning to be processed into the $ephrin^+$ cell. (V-VII) Red circles accentuate clusters at filopodia which are not subject to processing, presumably because they are not in contact to the active cell surface. **(C)** Image sequence starting from (B-II) outlines the processing of high-fluorescence entities into the Eph^+ cell. Graph highlights the size degradation of one FL entity (red) into multiple particles (entities X) **(D)** Image sequence starting from (B-III) outlines the processing of FL entities into Eph^+ cells. Image panels and graph (I) depict the size degradation of one FL entity (entity 1) into two particles (entities 2 + 3). Image panels and graph (II): pinched off FL particles were moving towards the center of the cell (displayed as distance [µm] to cell edge) whereas entity 1 remained stable at cell edge. Scale bar, 10 µm.

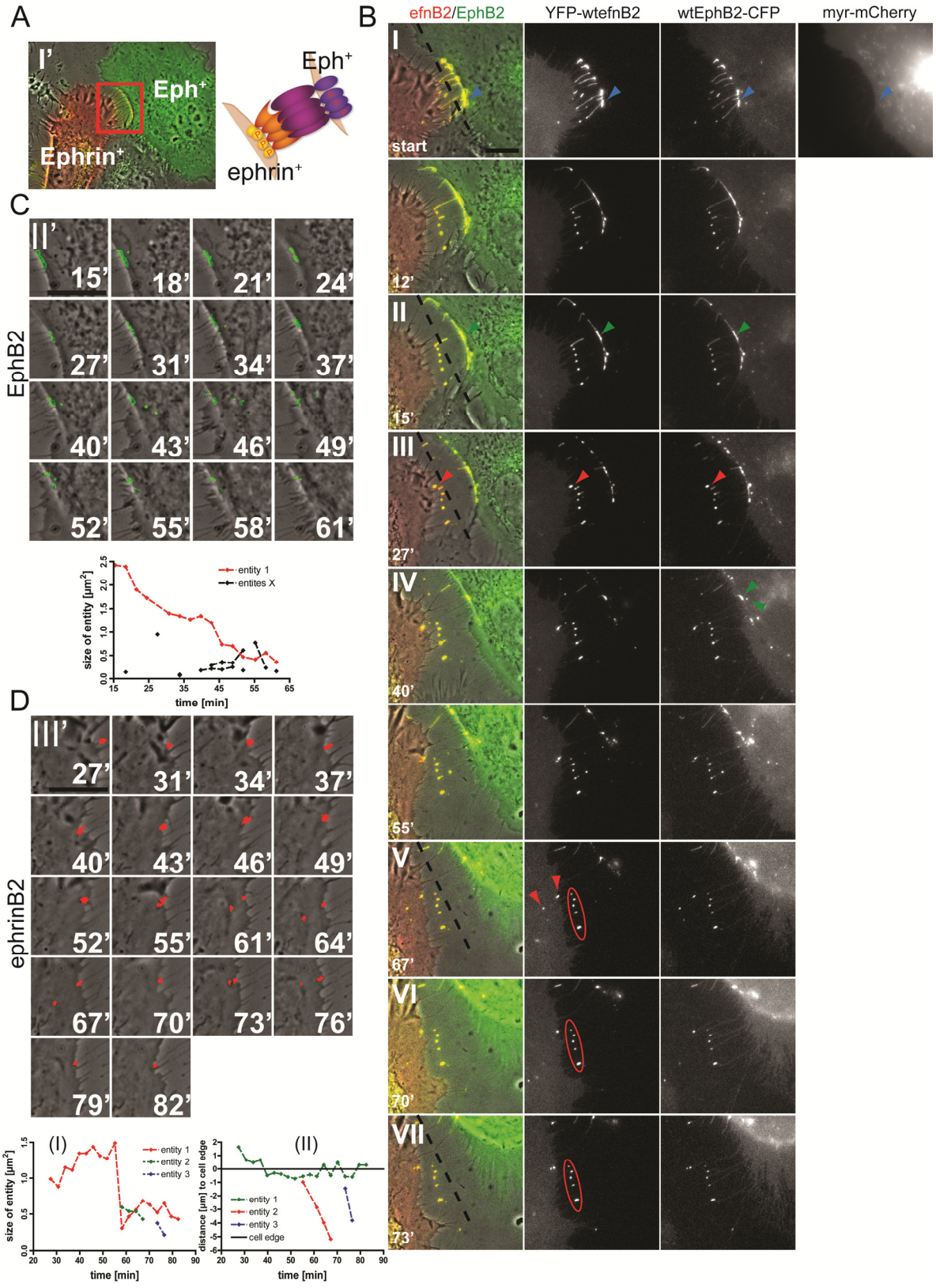
A
I'
Eph+
Ephrin+
Eph+
ephrin+
B
efnB2/EphB2
YFP-wtefnB2
wtEphB2-CFP
myr-mCherry
I
start
12'
II
15'
III
27'
IV
40'
55'
V
67'
VI
70'
VII
73'
C
II'
15'
18'
21'
24'
27'
31'
34'
37'
40'
43'
46'
49'
52'
55'
58'
61'
EphB2
size of entity [µm²]
entity 1
entites X
time [min]
D
III'
27'
31'
34'
37'
40'
43'
46'
49'
52'
55'
61'
64'
67'
70'
73'
76'
79'
82'
ephrinB2
(I)
size of entity [µm²]
entity 1
entity 2
entity 3
time [min]
(II)
distance [µm] to cell edge
entity 1
entity 2
entity 3
cell edge
time [min]

2) Multi-parameter impact on cluster formation, processing and signaling. Another big issue is the handling of multiple parameters, which have, at least in parts, a significant influence on cluster constitution and processing. In addition to the amount and significance of parameters governing other RTK signaling systems, Eph/ephrin signaling is also subject to additional controls due to their unique features, such as cell-contact dependent receptor/ligand engagement. Furthermore, in consideration of temporal aspects, only few parameters can be seen as static (related to the time frame of observation), such as receptor/ligand density. Most parameters are also strongly influenced by temporal aspects e.g. the cell-contact interface, which varies over time. Eventually the nature of Eph/ephrin signaling also comprises spatial control on the sub-cellular level. Overall, parameters could be grouped in Eph/ephrin-specific and cell-specific determinants. A list of possible parameters that may be involved in governing clustering, processing, and signaling of Ephs/ephrins is shown in Fig. 3.3A, without claim to be complete.

3.1.2 Generating an instant imaging-readout for Eph clustering in living cells

In awareness of the aspects stated above that complicate the study of Eph/ephrin clustering in a cellular and biochemical context, I tried to address certain issues step by step.

Homo-FRET imaging. First, in order to compensate for the lack of spatial resolution in conventional FL live-cell imaging approaches, I searched for an alternative imaging technique retaining the live-cell readout ability but giving me the power to resolve cluster size distributions. I therefore implemented homo-FRET imaging into the Eph/ephrin system, in collaboration with the MPI of Molecular Physiology in Dortmund, Germany (Ola Sabet, Philippe Bastiaens). Homo-FRET imaging was shown to be a reliable readout for the study of dynamic oligomerization processes of cytoplasmic proteins or other membrane-bound receptors in living cells. Homo-FRET can be detected as a decrease in steady-state fluorescence anisotropy that results from energy transfer between identical fluorophores (for theoretical background refer to Experimental Procedures) [308-310]. When using homo-FRET imaging one limitation is based on the fact that anisotropy values do not necessarily represent a homogeneous population of clusters. The anisotropy value of a single pixel is the additive result of FRET signals of the underlying cluster population. Since the use of homo-FRET imaging is not a real improvement in optical resolution, it is rather possible to interpret certain anisotropy values as relative cluster size distributions than absolute cluster sizes. However, with homo-FRET we were able to dynamically visualize and quantify the relative degree of clustering with high sensitivity.
For preparation of homo-FRET imaging, EphB2 receptor constructs were tagged with monomeric GFP (mGFP) (Fig. 3.4) carrying the A206K mutation (in addition to EGFP mutations) within the intracellular region [311]. In different experiments, expression

constructs were then transfected into COS-7 cells, which have a flat cell morphology and even membrane protein distribution ideal for imaging.

Cluster size distribution upon cell-cell contact. In order to validate homo-FRET imaging for visualization of cluster size distributions in living cells, we performed a cell co-culture assay, which also represented the cluster formation process under the best physiological conditions possible (Fig. 3.2). COS-7 cells expressing kinase-dead (kd) EphB2-mGFP receptors were seeded with Hek293T cells expressing wildtype (wt) ephrinB2 (tagged with mCherry), serving as stimulating donor cells. We chose the kd Eph receptor over the wt variant to avoid complications from rapid internalization of the Eph receptor and downstream signaling.

Low values of FL anisotropy were the result from an increased homo-FRET effect between aligned EphB2-receptor mGFP domains, which was caused by a higher degree of Eph oligomerization. By contrast, single monomeric receptor species did not enable homo-FRET transition between mGFPs, thereby leading to high values of FL anisotropy. Heterogeneous cluster size distributions were only observed at sites of cell contact, where pixel anisotropy values dropped dramatically. This effect is highlighted by the left-skewed anisotropy-histogram with the color-coded pixel distribution mapped to the co-culture image of anisotropy (Fig. 3.2,V/V').

First of all, these results indicate that clustering is spatially limited to sites of cell contact, and that at these sites rather than single cluster species, heterogeneous cluster size distributions are formed - as visualized by the anisotropy histogram. Secondly, these results also support the notion that clustering of Eph receptors becomes - in contrast to a mere FL readout (as displayed in Fig. 3.1 or Fig. 3.2-I, II, III) - more tangible using homo-FRET imaging in living cells. However, due to the overwhelming number of parameters in co-culture assays and the lack of parameter control, this experimental setup does not allow a direct mechanistic to functional readout from Eph/ephrin cluster formation. Beyond an improvement in directly and instantly visualizing clustering by homo-FRET imaging, I needed to exclude, control, or measure the multiple parameters governing Eph/ephrin cluster formation, processing, and signaling. In addition, the lack of an uniform spatial and temporal clustering response complicated correlation to functional readouts even more and called for strategies circumventing these problems.

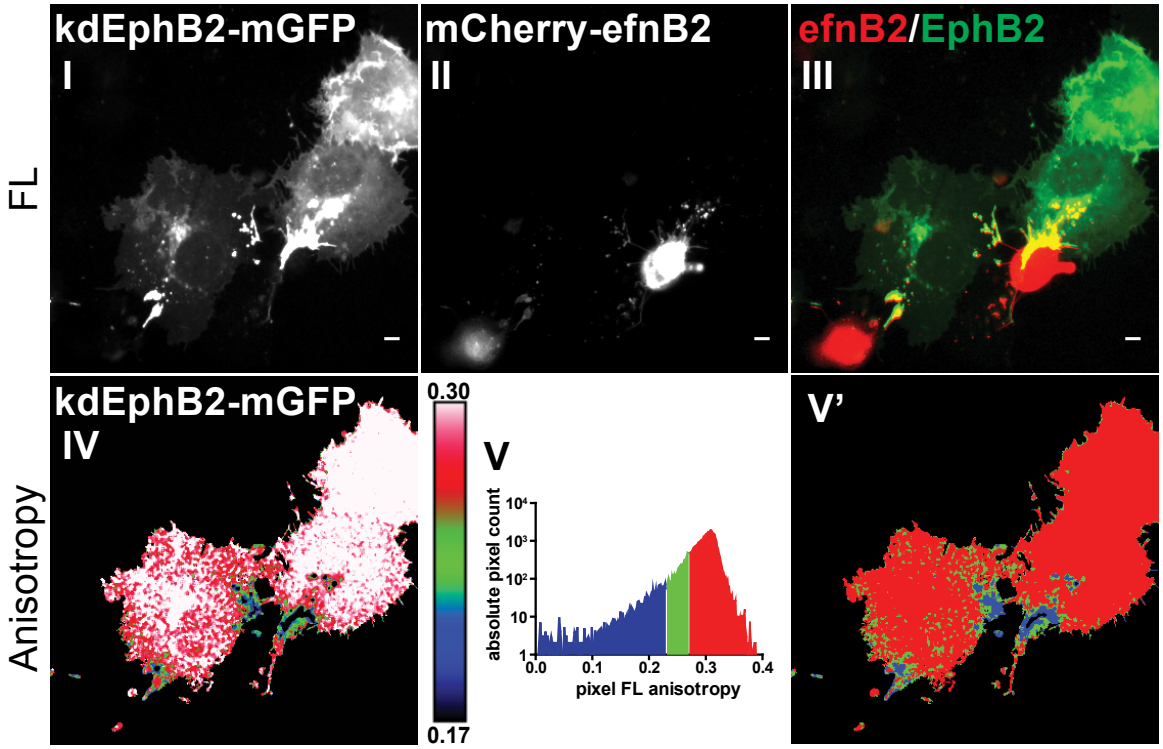

Fig. 3.2 Non-uniform clustering response of kdEphB2 upon contact with ephrinB2-expressing cells.
Non-uniform clustering response of kdEphB2 upon contact with ephrinB2-expressing cells. COS-7 cells, transiently transfected with kdEphB2-mGFP (I) and co-cultured with HEK293T cells transiently expressing wildtype mCherry-ephrinB2 (II) were imaged on a dish heated at 37 °C. Homo-FRET between kdEphB2-mGFP was determined by FL anisotropy (IV). (V) Anisotropy-histogram of whole image plane from co-culture image. Color-coded anisotropy-histogram pixel distribution is mapped to co-culture image to show for the spatial distribution of clustering, which is strictly limited to sites of cell-contact (V'). Zero-background pixel values were excluded from graphs. Higher power magnification is shown for region 2 (inset). Black pixels within areas of lower anisotropy are saturated in intensity and artifactual in anisotropy. Cells were imaged immediately upon contact after seeding of HeK293T cells. Representative experiment from a series of co-cultures (n= 20 cells analyzed). **Experiment and calculation of all anisotropy values was carried out by Ola Sabet, MPI Dortmund, Germany according to Squire *et al.*** [309]**.**

Fig. 3.3 Overview of Eph/ephrin signaling and a strategic approach for studying the receptor/ligand clustering.
(A) Table of possible parameters influencing Eph/ephrin clustering, processing and signaling scenarios. Parameters are classified as Eph/ephrin-specific and cell-specific. Table does not make a claim to be complete. **(B)** Strategic cell/receptor-autonomous approach deduced from the physiological cell-cell contact situation to study the mechanistic to functional effects of Eph/ephrin cluster formation in living cells. Schematic presentation of cell-cell contact highlighting important steps in the Eph/ephrin signaling cascade that qualify as stages for plausible readouts to study the functional side of clustering. Mechanistically, cluster formation can be controlled by the FKBP-system and visualized by homo-FRET imaging. Functionally, readouts are taken on a biochemical and cellular level. Abbreviations: N, cell nucleus; V, vesicle; P, Eph: auto/substrate-phosphorylation, ephrin: phosphorylation by Src-kinase.

A

Eph/ephrin- specific clustering determinants:	Cell- specific clustering determinants:
cell-cell contact interface cell-cell contact time Eph/ephrin cell surface density Eph/ephrin clustering propensity	membrane protein composition membrane lipid composition cell membrane curvature cell metabolism cell cycle state

B

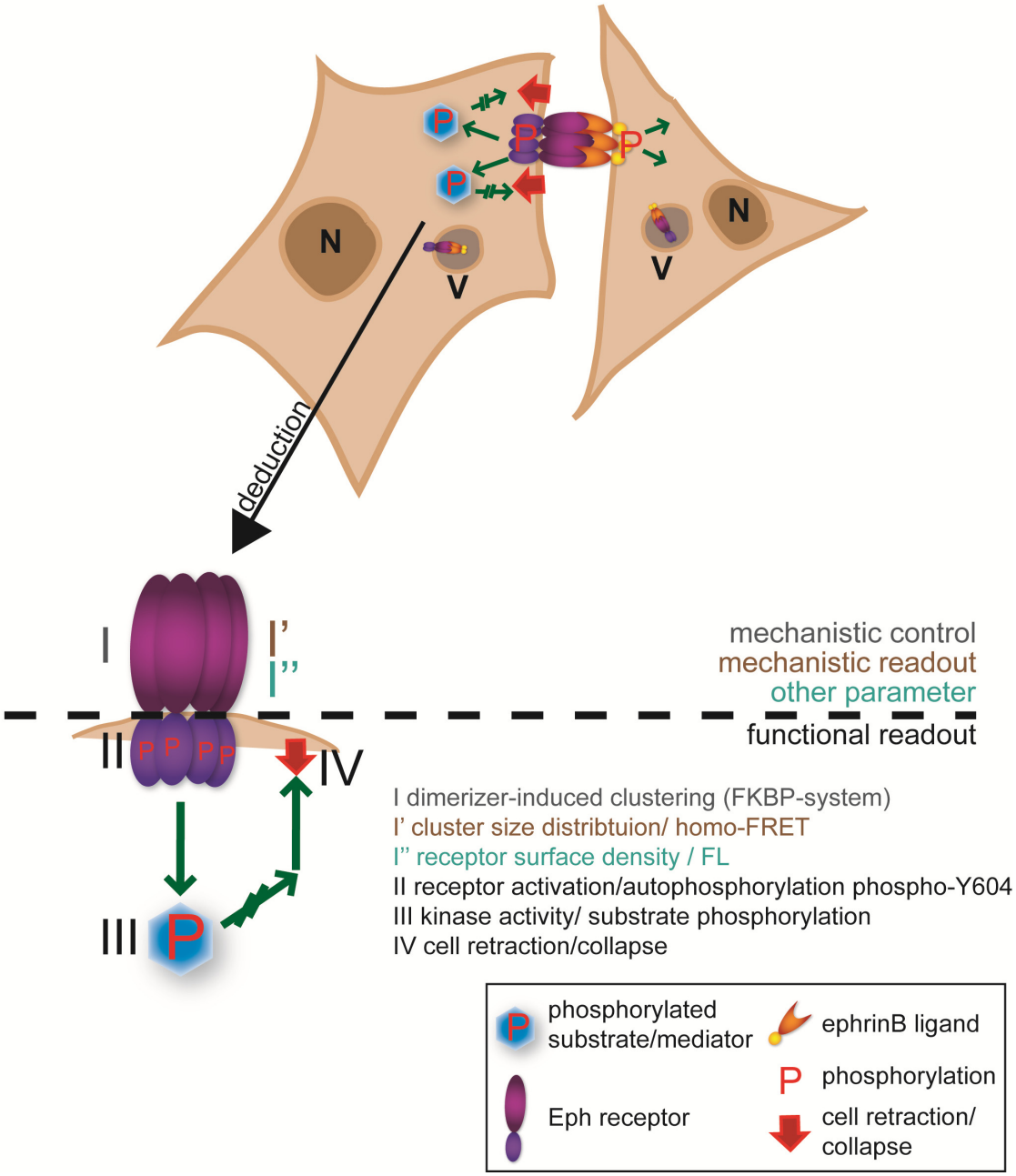

3.1.3 Generation of the dimerizer-induced system of Eph/ephrin clustering

Strategic approach. The need of parameter reduction for the study of the Eph/ephrin cluster formation process was highlighted in the previous paragraph. To achieve this goal, we designed a way to induce Eph/ephrin clustering independently of Ephs/ephrins and in a cell- and receptor-autonomous way. Most importantly, the experimental approach needed to fulfill certain criteria apart from enabling parameter reduction. Firstly, a mechanistic to functional experimental approach should preserve the functional integrity of the receptor while allowing for physiological readouts (Fig. 3.3B,C). Secondly, to be able to study Eph/ephrin clustering in detail, clustering should be highly controllable and temporally inducible on the mechanistic side - in respect to producing clusters of different sizes and quality. Ideally, the oligomerization state should be controllable ranging from total inhibition of clustering, thereby keeping Ephs/ephrins as monomers, to the presence of stable higher-order clusters at discrete sizes. Structural features underlying Eph/ephrin clustering suggest multiple domain interactions, which are to some extent all responsible for the initiation of the oligomerization process, maturation, and maintenance of the Eph/ephrin clustered state. A possible strategy to study clustering could be a loss-of-function approach by knocking down numerous sites responsible for cluster formation. However, such a broad overall mutagenesis approach could also impair the functional integrity of the Ephs/ephrins, resulting in signaling deficient or dead mutants. Additionally, this approach would not allow a positive control of oligomerization, i.e. clustering.

Implementation of the FKBP/FRB system. Thus, to assess the role of Eph/ephrin clustering cell-autonomously and in a mechanistic to functional way, a system to artificially produce Eph/ephrin clusters was introduced to meet all of the above mentioned requirements. The approach is based on the ARGENT® Regulated Homo(Hetero)dimerization kit from Ariad Pharmaceuticals (for details refer to Experimental Procedures).

Fig. 3.4 Conceptional approach for the generation of synthetic dimerizer-induced Eph/ephrin clustering in living cells.
(A) Domain and amino acid structure, and schematic model of Eph receptors showing sites of insertion for one to three FKBPs. Variants of fluorescent proteins (xFP) are in the cytoplasmic tail of EphB2 and EphA4. Model includes predicted homodimerizer-dependent receptor clustering of the different [1-3] FKBP isoforms. Homodimerizers AP20187 (IC_{50}= 1.8 nM) or AP1887 (IC_{50}= 40 nM) non-covalently crosslink FKBP domains of neighboring Eph receptors. **(B)** Domain structure with sites of insertion for one to three FKBPs and xFP in the cytoplasmic tail of ephrinB2. **(C)** Model of inhibition of EphB2 clustering by steric hindrance through heterodimerization with myristoylated FRB-mCherry using the heterodimerizer AP21967. Hypothetically, it is expected that the inducible, non-covalent fusion of myr-FRB-mCherry through AP21967 to the side of the receptors keeps them in their monomeric state. Abbreviations: JM, juxtamembrane segment; FKBP, FK506 binding protein; xFP, fluorescent protein variant; myr, myristoylation signal sequence; FRB, 93 aa portion of FRAP (RAFT, mTOR), sufficient for binding the FKBP-rapamycin complex [312].

A

[mut]EphB2-
xFKBP-xFP:

...IAIVCNRRGFERADSELATRYTDKLQGVQV...KLETSRDPPVATMVSK...ELYKGGGSIDYTDK...

[mut]EphA4-
xFKBP-xFP:

...AFVISRRSKASGSGVQV...KLETSRDPPVATMVSK...ELYKGSSGASYSKA

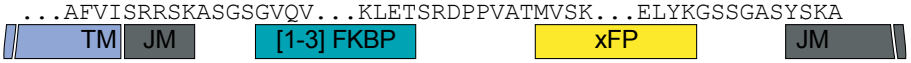

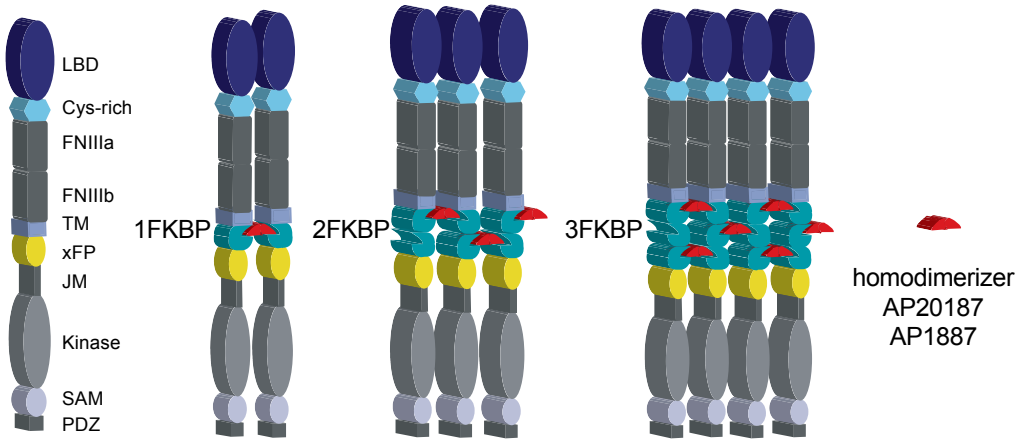

B

xFP-[mut]efnB2
-xFKBP:

...ELYKLAYPYDVPDYAISRSIV...VLLLKYRR...TTTTRGVQV...KLETSLSL...

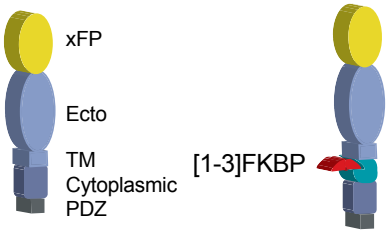

C

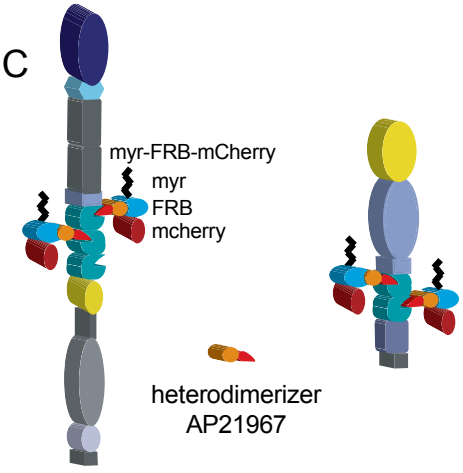

myr-FRB-mCherry:

MLCC...DQKIGSSGMASRIL...SKTSTGMVSK...ELYKKL-

Both dimerization kit components were used to establish a versatile dimerizer-induced system of Eph/ephrin cluster formation (Fig. 3.4). Previously constructed xFP-tagged wt and mutant EphB2/EphA4/ephrinB2 served as starting constructs for the insertion of one to three FKBP-F_v clustering domains [238,239,313]. Sites of FKBP insertion for both ephrinB2 ligand and EphB2/EphA4 receptor were chosen directly downstream of the TM domain on the intracellular side of the ligand/receptor. This strategy permitted both the possibility for physiological Eph/ephrin stimulation and intracellular clustering initiation with the high-affinity homodimerizer AP20187 and the low-affinity homodimerizer AP1887 while keeping the structural and functional integrity of the proteins unaffected. Theoretically, tagging the ligand/receptor with an increasing number of FKBP domains permits the constitution of clusters with increasing order, density and complexity; whereas, 1FKBP constructs only allow dimer-formation of tagged receptor/ligand molecules. However, it is likely that the dimerizer-induced system does not only produce a population of same sized cluster species, but rather a distribution of different cluster species.
In order to keep ligand/receptor molecules in their monomeric state in the membrane, FKBP constructs are co-expressed in combination with the inhibitory construct myr-FRB-mCherry, a myristoylated fusion of the FRB domain and mCherry (Fig 3.4C).

Optimizing expression conditions of FKBP-tagged receptor/ligand isoforms. FKBP-isoform expression was set under the control of the CMV-promoter in pcDNA3.1 backbone vectors (Invitrogen). Transfection into HeLa cells using the calcium phosphate transfection method resulted in an immediate strong over-expression of the ligand/receptor isoforms with intracellular protein inclusions in ER and Golgi (Fig 3.5A). I speculated, that in addition to the inherent strong protein expression from the CMV-promoter, fast expression kinetics with permanent protein translation overstrained the cell's ability to process protein through the Golgi and ER accordingly. Moreover, incorporated FKBP-domains may have a latent, unspecific affinity to each other despite the absence of the dimerizer agent. The high protein density in Golgi and ER due to spatial limitations may then contribute to this aggregation, i.e. unspecific clustering phenotype. As an unfavorable result, less protein was trafficked to the cell surface membrane. To fight this scenario of quantitative over-expression, unspecific clustering and fast expression kinetics, I followed up two approaches. Firstly, I blocked sites for unspecific clustering on FKBP-domains by infusion of monomeric FK506 agent, which would bind to single FKBP-domains, preventing the unspecific interaction to neighboring FKBP domains. In fact, the presence of FK506 after transfection improved the redistribution of FKBP-tagged ligand/receptor isoforms in mammalian cells (Fig 3.5A). Secondly, to slow down expression kinetics in HeLa, I optimized calcium phosphate transfection parameters (low amount of DNA, co-transfection with empty backbone vector) in combination with screening for HeLa cell populations, which produced favorable characteristics, such as a decreased growth rate, leading to modest quantitative protein expression (data not shown)

[314]. A beneficial side effect was a flattened cell morphology and better cellular responsiveness to Eph signaling (Fig. 3.5B).

While strategies for establishing correct expression patterns of FKBP-tagged receptor isoforms were rather straightforward for mammalian cell culture, primary hippocampal neurons obtained from rats at embryonic stage day 18.5 (E18.5) were more difficult to transfect and maintain after transfection. A popular way to obtain good transfection efficiencies in primary hippocampal neurons is by viral infection. I constituted Semliki Forest Virus FKBP-isoform expression variants and infected cultures overnight. Whereas infection of Hek293T cells showed a decent transfection efficiency and cell survival (Fig 3.5C), primary hippocampal neurons had difficulties in handling the virally induced strong expression of Eph receptor isoforms (Fig 3.5E). This led to inclusions and aggregation of receptor protein in somata despite the presence of FK506. Furthermore, neuronal cells were incapable of trafficking a significant amount of receptor protein to the neuronal periphery i.e. neurites and growth cones. Morphologically, cells had collapsed growth cones and rough somata. Immunoblotting from BHK-21 cells, which contain viral particles, was performed to verify for correct target size and domain integrity of target receptor isoforms (Fig. 3.5D). Some functionally relevant domains were tested for by immunoblotting to ensure the overall integrity of the receptor isoforms. A possible frame-shift in the open reading frame was thereby excluded, which might have been responsible for producing dysfunctional protein and causing the observed phenotype in neurons.

As a consequence of these results, I stopped using Semliki Forest Virus as carrier for FKBP receptor isoforms, supposing that the induced expression is quantitatively and kinetically too strong.

In exchange for a good transfection efficiency, I also transfected hippocampal neuronal cultures using the lipofectamin transfection method to obtain viable neurons that express receptor isoforms of interest. Transfection of receptors was only accomplished in a few cells, as seen by a correct protein receptor distribution without significant inclusions, and an intact growth cone (Fig 3.5F). Experimental possibilities were thereby greatly limited. In search for a compromise in obtaining a high transfection efficiency and morphologically intact neurons at the same time, I decided to truncate the FKBP-tagged Eph receptor isoforms at their N-terminus. This step now permitted the use of the AMAXA® electroporation method, known to be unsuccessful at transfecting full-length Eph receptor constructs [313]. The reduction in receptor size with removal of most of the ectodomain may have led to better transfection and distribution in hippocampal neurons but may also have abolished engagement with endogenously expressed ephrin in cultures. Indeed, the N-terminal truncation in combination with AMAXA® transfection actually allowed for expression of all FKBP-isoforms with a decent transfection efficiency, expression strength, and healthy cell morphology displaying proper neurite branching, a clear axonal polarity, intact growth cone structures and an even receptor distribution (Fig. 3.5G).

Fig. 3.5 Strategies for optimizing culture and expression conditions of FKBP-tagged Eph receptor and ephrin ligand isoforms in mammalian cells.
(A) Beneficial effect of the monomeric antagonist FK506 on expression conditions. HeLa cells were transfected with CFP-wtefnB2-2FKBP CMV-promoter controlled pcDNA3.1 expression constructs by calcium-phosphate transfection. Addition of FK506 (500 nM) improves the even expression and distribution of FKBP-tagged Eph/ephrin in the cell membrane. In absence of FK506, proteins get trapped and unspecifically clustered in the Golgi/ER of the cells (red arrows). **(B)** HeLa cell populations (population 2) selected for reduced expression kinetics and decreased total expression of target protein exhibit characteristics favorable for studying Eph/Ephrin clustering in living cells: a flattened cell morphology, decreased growth rate, better cellular responsiveness, reduced membrane ruffling (arrows) as compared to population 1. **(C)** Testing for Semliki-Forest-Virus mediated expression of wtEphB2-xFKBP-YFP constructs. Hek293T cells were infected overnight and imaged for expression the next day. BF/YFP FL overlay images show expression of FL protein (red arrows). Transfection efficiency is decreased for the 3FKBP receptor isoforms. **(D)** Receptor isoforms expressed from Semliki-Forest-Virus in BHK-21 cells have correct construct length and domain integrity for domains tested. 36 hrs after transfection with Semliki-Forest-Virus constructs, BHK-21 cells were lysed and lysates subjected to SDS-PAGE and Western blotting using anti-FLAG, anti-EphB2Sam and anti-FKBP antibodies. Western blot shows bands of predicted molecular weight (141.6 kDa/0FKBP; 175.6 kDa/3FKBP). When probing with anti-FKBP, no band was detected for lysates containing wtEphB2-0FKBP-YFP, as expected. **(E)** Semliki-Forest-Virus infected hippocampal cultures (rat E18, infection DIV 1, imaged DIV2) cause toxic over-expression of target EphB2 receptor protein, somal trapping with lack of membrane protein distribution to neuron periphery (arrows). **(F)** Lipofectamin-transfected hippocampal cultures (rat E18.5, DIV1, imaging DIV2) have proper receptor isoform distribution and a healthy cell morphology (arrows). **(G)** Rat hippocampal neurons (rat E18.5, fixation DIV1) transfected via electroporation (AMAXA®, Lonza, Basel, Switzerland) and immunostained using the axon specific marker anti-Tau1, neurite specific marker phalloidin and anti-YFP to visualize for expression of target proteins. Neurons are morphologically inconspicuous after transfection showing a clear neuronal polarity (anti-Tau1, arrows) and intact growth cones (phalloidin, lower arrow) with evenly distributed receptor protein (anti-FLAG, arrows). Scale bars, 10 µm. Image acquisition and processing: B,C,E,F, epifluorescent (epiFL) live-cell images, background corrected (bgcorr); A, epiFL fixed-cell images, bgcorr; G, 9x 0.5 µm z-stacked spinning-disc confocal FL images, maximum projected, bgcorr). Abbreviations: UNT, untransfected. **Preparation, transfection and immunostaining of rat hippocampal cultures in (G) was carried out by Irina Dudanova.**

3.2 Dimerizer-induced clustering is sufficient to produce Eph-specific physiological signaling responses

Establishment of a cell- and receptor-autonomous system for investigation of clustering requires the preservation of the physiological signaling functions of the receptor. This claim is not trivial, since it is well known, that such artificial modifications (total size insertion of ~64 kDa for 3FKBP + xFP) on the receptor's domain topology may very well lead to dysfunctional receptors. Moreover, clustering accomplished by the non-covalent crosslinking of FKBP domains does not necessarily activate receptors in a physiological way. It was therefore necessary to test for physiological signaling responses at the very beginning of this project (Fig. 3.3). To get a quick overview of the functionality of the FKBP system I selected receptor activation, i.e. autophosphorylation and cell collapse as Eph-specific readouts.

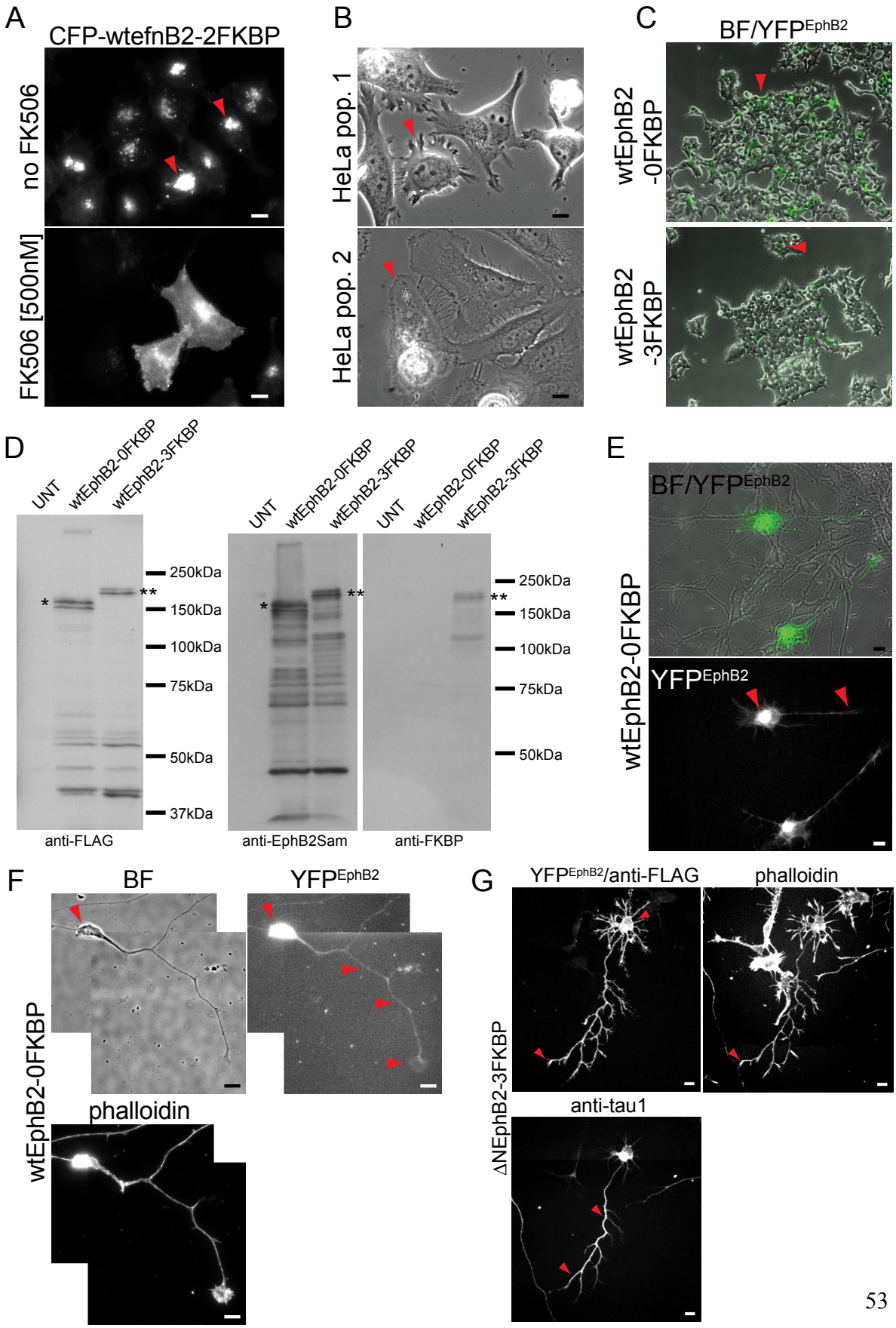
A
CFP-wtefnB2-2FKBP
no FK506
FK506 [500nM]
B
HeLa pop. 1
HeLa pop. 2
C
BF/YFPEphB2
wtEphB2 -0FKBP
wtEphB2 -3FKBP
D
UNT
wtEphB2-0FKBP
wtEphB2-3FKBP
250kDa
150kDa
100kDa
75kDa
50kDa
37kDa
anti-FLAG
anti-EphB2Sam
anti-FKBP
E
BF/YFPEphB2
wtEphB2-0FKBP
YFPEphB2
F
BF
YFPEphB2
wtEphB2-0FKBP
phalloidin
G
YFPEphB2/anti-FLAG
phalloidin
ΔNEphB2-3FKBP
anti-tau1

3.2.1 Dimerizer-induced clustering causes receptor autophosphorylation and an overall phospho-activated cell state

Immediately following ligand engagement, Eph receptors start signaling via their intrinsic kinase activity, which causes phosphorylation of other neighboring receptors (autophosphorylation) and effector proteins (transphosphorylation). The autophosphorylation response qualifies as immediate readout for receptor activation since the autoinhibition of the kinase domain is only completely removed by phosphorylation of the two JM tyrosines Tyr604 and Tyr610 (for EphB2). Thus, using a JM phosphotyrosine specific antibody I tested for receptor activation of FKBP-tagged EphB2 receptors. Eph receptors undergo maximal autophosphorylation upon stimulation for 20 min with 100 nM AP20187 or more (Fig. 3.6A). In another approach, using the heterodimerizer AP21967 as competitor against AP20187, mixtures of both agents were used for stimulation of wtEphB2-3FKBP-YFP-expressing HeLa (Fig 3.6B). With increasing concentrations of AP21967 added, a gradual decrease in autophosphorylation was observed. For the subsequent dimerizer applications I decided to work with excess concentrations of 250 nM, and 20 min stimulations as a standard condition, to exclude concentration-dependent, dose-response effects. Therefore, cluster size distributions (see next sections) will be determined by the number of inserted FKBP domains.

Fig. 3.6 Dimerizer-induced EphB2 clustering is sufficient to activate Eph receptors.
(A) Dose-response curve of dimerizer-induced Eph clustering using increasing concentrations of AP20187 (0.1 nM to 1000 nM) to stimulate (t= 20 min) HeLa cells expressing wtEphB2-3FKBP. After immunoprecipitation with anti-FLAG M2 resin and performance of a Western blot, EphB2 receptors were detected for phospho JM-Y604 using the anti-phospho-EphB antibody. After stripping, blots were probed for total receptor protein using anti-FLAG M2 antibody. Graph: the fraction of activated receptors for each condition tested was plotted on a logarithmic scale and fitted to a sigmoidal dose-response curve. Saturation of receptor activation was reached with 100 nM AP20187. **(B)** Competitive binding dose-response curve of dimerizer-induced Eph clustering using dimerizer mix of AP20187 (at 250 nM) and competitor AP21967 (2 nM to 200 nM) for stimulation (t= 20 min) on HeLa cells expressing wtEphB2-3FKBP. Immunoblotting for the fraction of activated receptors was performed on total cell lysates. Total receptor protein was probed for using the anti-FLAG M2 antibody. Graph: the fraction of activated receptors was plotted on a logarithmic scale and fitted to a sigmoidal dose-response curve. With increasing amounts of competitive dimerizer AP21967 added, the fraction of activated receptor decreases. **(C)** Immunostainings of wtEphB2-[0,3]FKBP-YFP transfected HeLa stimulated with control stimuli (Fc), ephrinB2-Fc (2 µg/ml) and AP20187 dimerizer (250 nM) for 40 min before fixation. Images show an increase of the cell's phosphorylation status visualized with phosphotyrosine specific antibody (clone 4G10) in ephrinB2-Fc and AP20187/3FKBP conditions. For AP20187/0FKBP no significant signal increase from 4G10 antibody binding can be observed. Image acquisition and processing: epiFL 8x 0.6 µm z-stacked images; optical densitiy correction (odc); adaptive-blind psf deconvolution; maximum projection. Graph: mean ratio ± SEM of total intensity (FL phospho^{4G10}/FL YFP^{EphB2}) from maximum projected images of n≥ 10 cells. Scale bars, 10 µm.

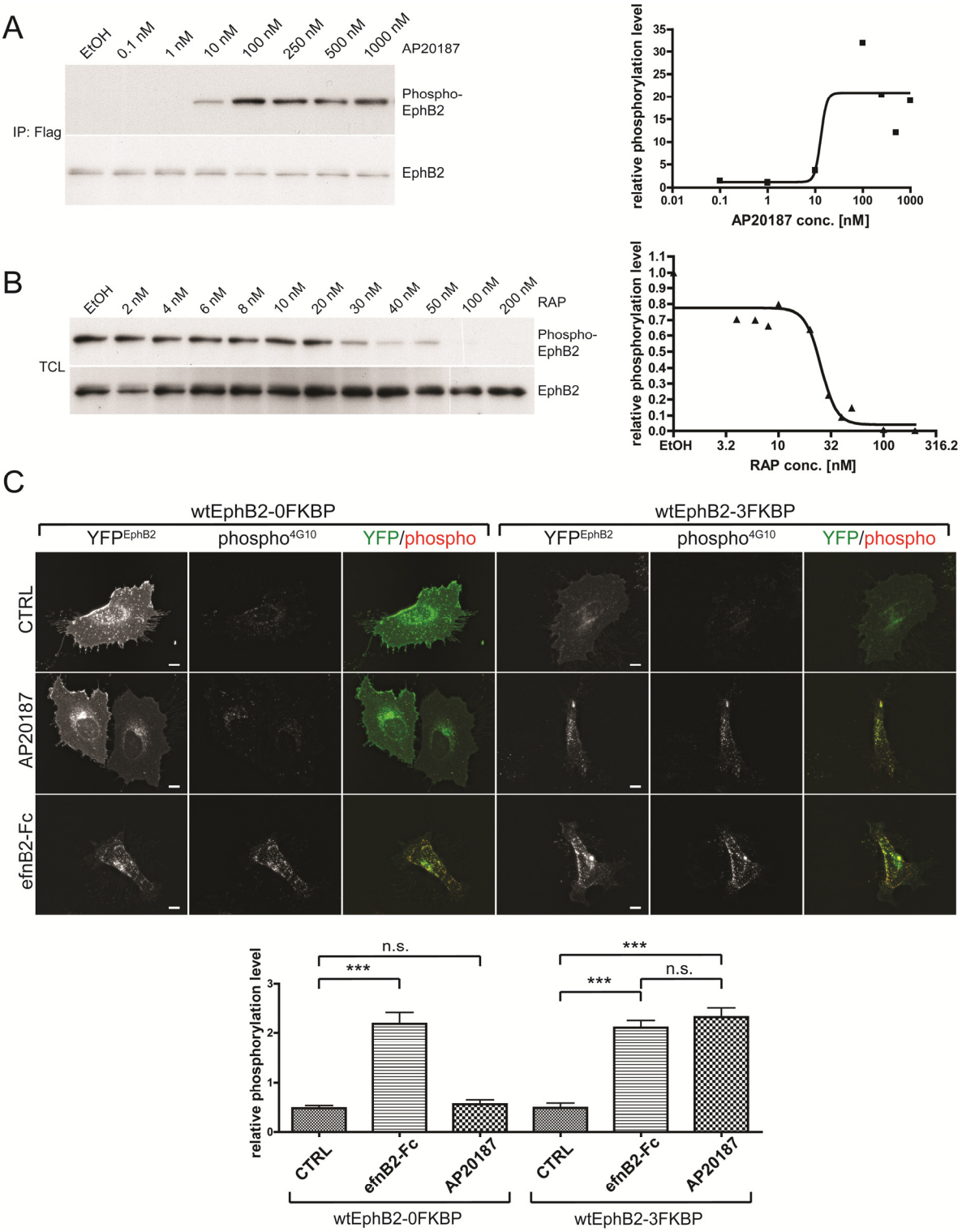
A
EtOH
0.1 nM
1 nM
10 nM
100 nM
250 nM
500 nM
1000 nM
AP20187
IP: Flag
Phospho-EphB2
EphB2
relative phosphorylation level
AP20187 conc. [nM]
B
EtOH
2 nM
4 nM
6 nM
8 nM
10 nM
20 nM
30 nM
40 nM
50 nM
100 nM
200 nM
RAP
TCL
Phospho-EphB2
EphB2
relative phosphorylation level
RAP conc. [nM]
C
wtEphB2-0FKBP
wtEphB2-3FKBP
YFPEphB2
phospho4G10
YFP/phospho
CTRL
AP20187
efnB2-Fc
relative phosphorylation level
n.s.
***
CTRL
efnB2-Fc
AP20187
wtEphB2-0FKBP
wtEphB2-3FKBP

Following activation by autophosphorylation, Eph receptors also phosphorylate effector proteins *in trans*, thereby increasing the overall phosphorylation state of the cell. To test whether dimerizer-induced clustering also causes this positive shift in the steady-state of the phospho-activated, Eph-expressing cell, I utilized a substrate-unspecific general anti-phosphotyrosine antibody (clone 4G10) in immunostainings (Fig. 3.6C). As expected, ephrin stimulation induces the Eph signaling response to elevate the cell's phosphorylation status. Wildtype EphB2-3FKBP-YFP receptor stimulated with AP20187 dimerizer caused a similar increase, indicating that the clusters produced are functional in activating the Eph receptor's *trans*-kinase activity leading to an elevated phospho-activated cell state.

3.2.2 Dimerizer-induced clustering causes a cellular collapse and recovery response

A decisive cellular response to activated Eph receptor signaling is actin de-polymerization leading to cellular rounding and/or retraction of the cell periphery, as seen in the collapse of axonal growth cones. To investigate if dimerizer-induced cluster formation would cause the same cell response, I set up a cell collapse assay using HeLa cells imaged in time-lapse after stimulation (Fig. 3.7A). For both stimulation with soluble, preclustered ephrin ligand and dimerizer AP20187, I observed a similarly characteristic cellular response pattern with initial strong cellular contraction of the cell body (Fig. 3.7B, phase I) that resulted in a maximal collapse amplitude (Fig. 3.7B, phase II and Fig. 3.7C), followed by a recovery phase of the cell's growth surface area (Fig. 3.7B, phase III). To verify that the cellular response pattern induced is indeed specific to Eph signaling caused by dimerizer AP20187, I impaired actin de-polymerization via the myosin-II inhibitor blebbistatin [133]. In presence of blebbistatin, cell collapse is significantly reduced at 30 min after stimulation with AP20187 (Fig. 3.7D).

Fig. 3.7 Ligand-independent, dimerizer-induced EphB2 clustering is sufficient to cause cell rounding responses similar to an ephrinB2-Fc stimulation.
(A) FL time-lapse imaging of HeLa cells transiently expressing wtEphB2-[0,3]FKBP receptors (carrying YFP) in the presence of ephrinB2-Fc or AP20187. Cell surface area was scored from BF and FL images (red circles around cells). Images for start (immediately after stimulation, 0 min), ~24 min and ~65 min are displayed in BF and FL channels. Co-expressed, myristoylated mCherry served for better visualization of the cell during time-lapse imaging. Scale bars, 10 µm. **(B)** Curve graph of the characteristic cell response pattern from cells in (A). Cell collapse started immediately after stimulation (phase I) and reached a maximal collapse amplitude (minimal cell surface area) after about 20 min (phase II), followed by a re-spreading response of the cell (phase III). **(C)** Bar graph: changes in collapse amplitude (minimal area in percent relative to start of experiment) of cells within 60 min after stimulation (mean cell area ± SEM from n= 8-12 cells for each condition tested; *** p< 0.001, n.s. not significant; one-way ANOVA with posthoc Tukey-Kramer test, asterisks in red represent significance level to control situation of each data set). Cellular response pattern and collapse amplitude resulting from dimerizer-induced Eph clustering are similar to an ephrinB2-Fc induced clustering response. FKBP-tagging does not significantly affect the ephrinB2-Fc induced cell collapse response (see bar 3FKBP/efnB2-Fc). **(D)** Cell-collapse assay using the myosin-II inhibitor blebbistatin. HeLa cells were

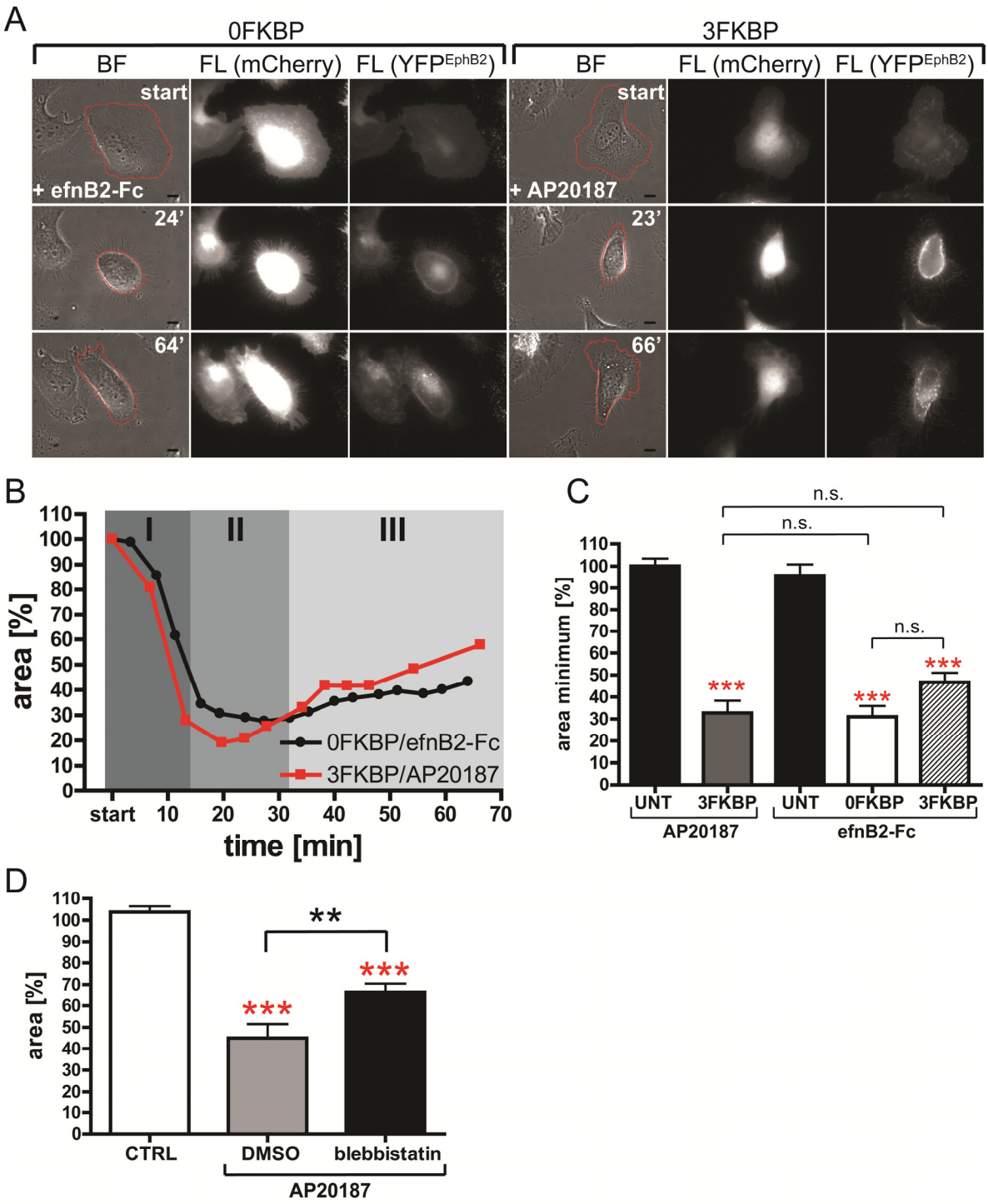

incubated in solvent DMSO or 10 µM blebbistatin/DMSO for 10 min. Following stimulation with AP20187 (250 nM) for 30 min, cell collapse was scored as described in (B). As control, collapse of untransfected HeLa cells was monitored both in presence of blebbistatin and AP20187. Bars represent mean cell surface ± SEM from n= 7-8 cells for each condition tested at time point 30 min post-stimulation; ** p< 0.01, *** p< 0.001, one-way ANOVA with posthoc Bonferroni test, asterisks in red represent significance level to control condition.

Overall, these functional assays demonstrate that dimerizer-induced cluster formation properly imitates an ephrin-Fc-induced clustering response. These important findings not only fulfill the premise for having an efficient tool to study cluster formation, but they also imply that ephrin-induced physiological effects can also be provoked in a ligand-independent way by artificially clustering the Eph receptor. This finding shifts the main focus of attention from ligand-mediated to receptor-mediated clustering as being the critical step in Eph receptor activation.

Fig. 3.8 Phenotypic effects of Eph clustering in mammalian cells.
(A) Upon AP20187 (250 nM) dimerizer-induced clustering, a ring-shaped FL intensity rise was observed for wtEphB2-3FKBP-YFP at cell edges emerging 5 min after stimulation (arrow) and lasting for several minutes (arrows in blowup) before disappearing (see also supplementary video 1). In the control co-transfected myr-mCherry FL channel this rise in FL intensity at the same site of the cell edge was not observed. Blowup images of both FL channels are shown from the region indicated by the red box. Image acquisition and processing: scanning-confocal time-lapse image acquisition, 1 frame/min, maximum projection of 5x 3.1 µm z-stacked images, bgcorr. **(B)** As with (A) but using the kinase-dead kdEphB2-3FKBP-YFP receptor isoform, transfected COS-7 cells were stimulated with AP20187 (250 nM, start) and imaged at RT over time using scanning confocal time-lapse microscopy (10x 0.5 µm; 1frame/5 min; maximum projection). A blowup image is shown from the region indicated by the red box. Again, a FL intensity rise at the cell edge is observed, which in contrast to (A) is persistent over time. **(C)** EphrinB2-Fc induced clustering on kdEphB2-3FKBP-YFP causes the same phenotypic effect of FL intensity rise in the cell edge. HeLa cells transfected and stimulated with preclustered and Alexa594 labeled ephrinB2-Fc (2 µg/ml) were imaged in time-lapse. At 15 min post stimulation a significant rise in FL intensity could be observed (linescans) at cell edges in both Eph FL and ephrin FL channels indicating a ligand/receptor accumulation at the cell edge. Linescans measuring the average FL intensity per increment were performed over the whole cell body as indicated by the white line (indicated by asterisk). Image acquisition and processing: adaptive-blind psf deconvolved epiFL images from 6x 0.2 µm z-stacks; odc; maximum-projected. **(D)** Cell-surface applied anti-Eph^{ecto} antibody (23 µg/ml, t= ~40 min) causes receptor accumulation equitable to an ephrinB2-Fc (2 µg/ml, preclustered, t= ~40 min) administration (arrows). Image acquisition and processing: epiFL time-lapse recording of 8x 0.2 µm z-stacks; odc; adaptive-blind psf deconvolution; sum-projection; images of same cell detail are scaled equally. **(E)** Immunostaining of fixed COS-7 for surface EphB2 after transfection with kdEphB2-3FKBP-YFP and stimulation with AP20187 (250 nM, t= 20 min). Surface kdEphB2-3FKBP-YFP was visualized by immunostaining with anti-FLAG antibody. Total protein was detected via YFP FL. Dimerizer-induced cluster formation causes a characteristic rise in FL intensity at cell edges of total and stained surface receptor, which persists over time without internalization of the kd receptor. Average intensity linescans from regions IV and V show a peak increase in FL intensity 20 min post-stimulation with AP20187 at cell edges for total and stained surface receptor (green/red line). In control-stimulated (EtOH) cells, fluorescence distribution in regions I and II remained diffuse. These results indicate a redistribution and accumulation of receptor protein to the lateral side (edge) of the cell. Image acquisition and processing: 10x 0.3 µm z-stacked scanning-confocal images, bgcorr., maximum-projected. Scale bars, 10 µm.

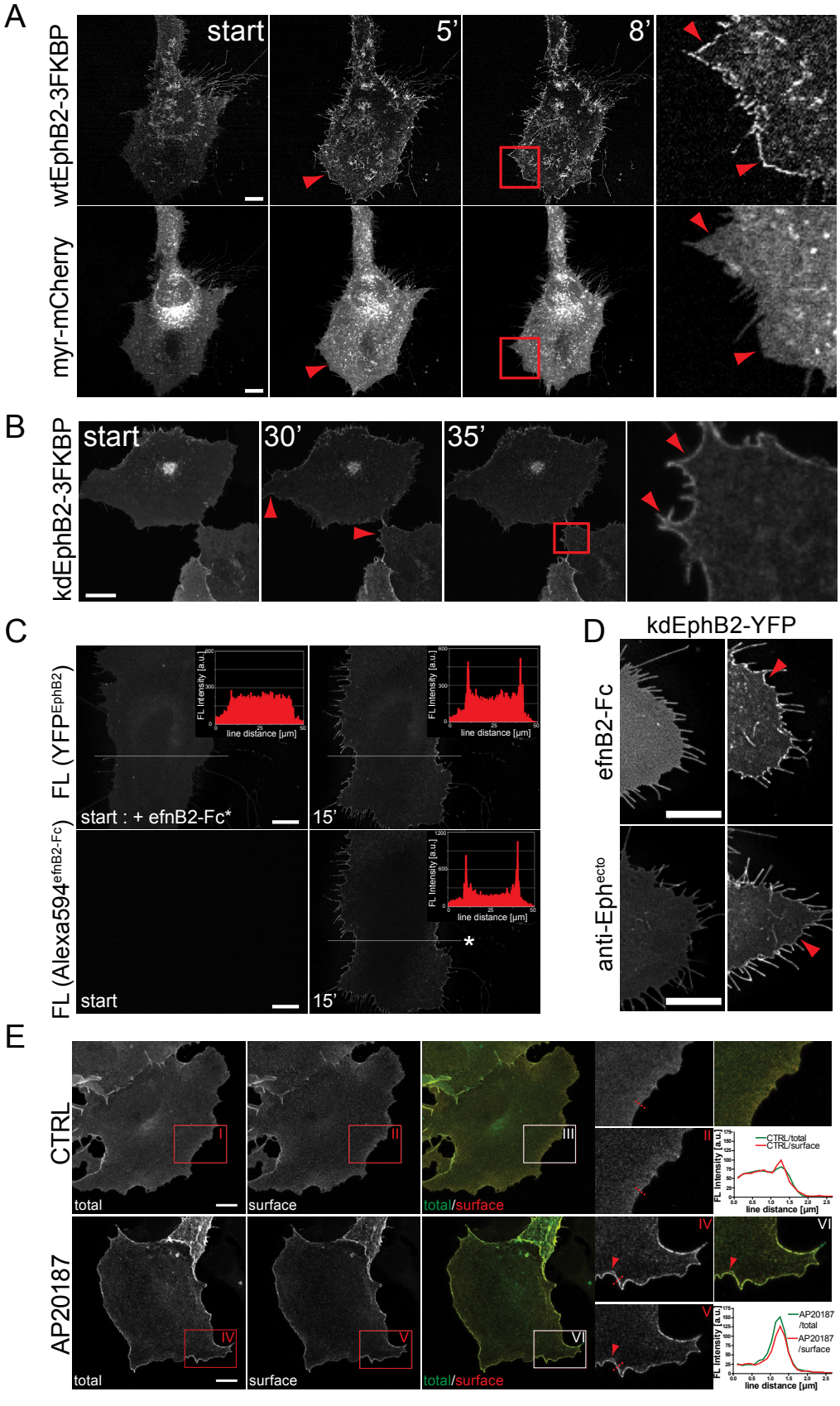
A
wtEphB2-3FKBP
myr-mCherry
start
5'
8'
B
kdEphB2-3FKBP
start
30'
35'
C
FL (YFPEphB2)
FL (Alexa594efnB2-Fc)
start : + efnB2-Fc*
15'
start
15'
FL intensity [a.u.]
line distance [µm]
D
kdEphB2-YFP
efnB2-Fc
anti-Ephecto
E
CTRL
AP20187
total
surface
total/surface
I
II
III
IV
V
VI
CTRL/total
CTRL/surface
AP20187 /total
AP20187 /surface

3.3 Dimerizer-induced clustering produces distinct Eph receptor cluster size distributions in living cells

Above I have shown that the dimerizer-inducible system is physiologically functional, and therefore a legitimate substitute for ephrin-Fc induced clustering. The design of the system suggests intrinsic properties that improve the system, such as tight controllability and inducibility, precision in clustering, and the possibility to implement available mechanistic readouts. Next I present experimental proof to corroborate the beneficial mechanistic assets and open up a detailed view on characteristic aspects of the dimerizer-inducible clustering system.

3.3.1 Eph clustering causes the accumulation of receptors in cell edges

I investigated the effects of dimerizer-induced clustering using both confocal and epiFL imaging. HeLa cells transfected with wtEphB2-3FKBP-YFP isoforms and clustered by the addition of AP20187 displayed a significant ring-shaped FL intensity rise at the cell edge that was specific to transfected Eph receptors (Fig. 3.8A). This phenotypic effect was only transient and disappeared within 10 min after stimulation upon the onset of secondary processes like internalization and cell collapse (supplementary video 1). In order to stabilize, and thereby clarify this phenomenon, I then utilized the kinase-dead variant of FKBP-receptor isoforms to exclude receptor activation-dependent secondary processes such as receptor internalization and cell collapse that most likely terminate the effect. Indeed, the AP20187 induced FL intensity rise of kinase-dead EphB2 persisted more than 35 min longer (Fig. 3.8B) than wildtype receptor (Fig 3.8A and supplementary video 1).
Next, I asked how this dimerizer-dependent phenotypic effect would compare to ephrin-induced clustering. The dimerizer stimulation corresponds well to a soluble, preclustered ephrinB2-Fc exposure, which in the end turns out to show almost identical phenotypic effects upon stimulation (Fig 3.8C). Alexa-dye labeled ephrinB2-Fc provoked the same ring-shaped FL intensity rise as AP20187 homodimerizer and was stable over time when used on kd receptor isoforms. Interestingly, the same effect was caused by an antibody specific to the Eph ectodomain (Fig. 3.8D) thereby denoting that the phenotypic effect is not stimulus-specific but rather receptor-specific.
Finally the question remained, if the phenotypic effect of increased FL intensity at cell edges is indeed a true accumulation or crowding of Eph receptors at the lateral side of the cell. Therefore, immunostainings for kd surface receptor proteins were performed. In correspondence to the increase of FL intensity signals from receptor proteins, the stoichiometric equivalent portion of antibodies is bound to receptors resulting in the same phenotypic FL intensity rise upon stimulation with AP20187 visualized by linescan measurements (Fig. 3.8E).

These results suggest that receptor proteins redistribute and accumulate upon clustering at the lateral side of the cell - irrespective of the kind of stimulus used.

3.3.2 Dimerizer-induced Eph clustering is self-contained

One reason for implementation of dimerizer-induced Eph clustering relies on the possibility to produce distinct Eph/ephrin cluster size distributions in living cells. A characteristic premise for this is the absence of a seeding (nucleation) mechanism, which would counteract the self-containment of the system. A seeding mechanism was shown to take place for Eph receptors [72,104]. Existing Eph clusters, bound by ephrin ligand, recruit adjacent Eph monomers independent of ligand-contact to form 1-dimensional signaling arrays.
I tested the dimerizer-inducible system as a priming mechanism for Eph activation, both mechanistically (using epiFL imaging), and functionally (in biochemical assays for receptor autophosphorylation to monitor receptor activation). For all experiments, in order to avoid secondary processes resulting from dimerizer-/ligand-induced clustering, only isoforms lacking kinase activity and internalization response were used (Fig. 3.9A). In the biochemical autophosphorylation assay, clustering was induced by application of dimerizer AP20187 on co-expressed full-length and C-terminally truncated EphB2-YFP receptor isoforms (Fig. 3.9B). Autophosphorylation was exclusively observed in the presence of preclustered ephrinB2-Fc, which binds to the globular domain of both co-expressed isoforms and served as a positive control for the assay. In the presence of AP20187, which only clusters the catalytically-inactive FKBP-domain containing isoform, no autophosphorylation was detected.
By performing epiFL imaging, AP20187-induced clustering of kdEphB2-3FKBP produced the same FL intensity rise at cell edges within 10 min after stimulation as described previously (Fig. 3.9C-I). The FL intensity distribution of co-transfected wtEphB2 lacking FKBP domains, however, remained unaffected (Fig. 3.9C-II), indicating that the two receptor variants do not interact under these conditions. In contrast, externally applied ephrinB2-Fc resulted in a co-localized increase in FL signals at cell edges (Fig. 3.9B-III,IV).
Taken together, these results indicate that dimerizer-induced EphB2 clusters do not serve as nucleation points to which additional Eph receptors are recruited by Eph-Eph interactions. The system of dimerizer-inducible clustering is therefore self-contained, enabling the generation of distinct cluster size distributions in living cells.

3.3.3 Dimerizer-induced Eph clustering does not co-precipitate an unidentified Eph interaction partner

Next, I searched for Eph interaction partners that may be able to specifically discriminate an cluster depending on whether it is ephrinB2-Fc-induced, i.e. forming via its extracellular receptor entity or dimerizer-induced, i.e. forming via its intracellular receptor entity. Eph

receptors have been described to specifically and physically interact with other (trans)membrane proteins and may possibly also incorporate alien (trans)membrane proteins into their clusters [32,184,192,256]. To test for such a clustering-dependent interaction partner for Ephs, HeLa cells expressing wtEphB2-3FKBP-YFP were stimulated with either AP20187 dimerizer or preclustered ephrinB2-Fc (1.5 hrs), in the presence or absence of the dynamin-dependent endocytosis inhibitor dynasore (Fig. 3.9D). Inhibition of endocytosis was meant to counteract a possible fast degradation of the internalized Eph/interaction partner complex. After cell surface biotinylation to detect for (trans)membrane bound protein, lysates were subjected to immunoprecipitation using anti-FLAG resin. Blots were probed for biotinylated protein using streptavidin-hrp (hrp - horse radish peroxidase) and anti-EphB2Sam antibodies (Fig. 3.9D). Interestingly, dimerizer-induced clustering did not co-precipitate a protein of ~50-55 kDa as compared to an ephrinB2-Fc stimulation.

Taken together, Eph receptor clusters differ in their ability to co-precipitate an unidentified interacting protein depending on whether they are induced by dimerizer or by ephrinB2-Fc. Although those clusters are indistinguishable in causing intracellular JM tyrosine phosphorylation and downstream cell collapse responses, distinct differences may exist in the configuration of the extracellular/intramembrane cluster entity.

Fig. 3.9 Dimerizer-induced Eph clustering is mechanistically distinct from ephrinB2-Fc-induced clustering.
(A) Cartoon depicting the experimental model to test whether AP20187-induced clusters of EphB2-FKBP isoforms laterally recruit neighboring, co-transfected EphB2 receptors lacking FKBP domains. **(B)** Western blots of immunoprecipitated wtEphB2 lacking FKBP (carrying a Flag epitope tag) using anti-phosphoEphB2 antibodies (upper panel), followed by anti-EphB2 antibodies (against C-terminal SAM domain which was deleted from ΔCEphB2-3FKBP) to monitor expression (middle panel). Anti-FLAG immunoprecipitates of co-transfected kdEphB2-3FKBP were probed with anti-FKBP antibodies (lower panel). Note that wtEphB2 lacking FKBP was autophosphorylated after ephrinB2-Fc stimulation, but not when ΔCEphB2-3FKBP was clustered with AP20187. **(C)** HeLa cells were co-transfected with kdEphB2-3FKBP (tagged with EYFP) and wtEphB2 lacking FKBP (tagged with mCherry). Before stimulation with AP20187 or ephrinB2-Fc, both receptor isoforms are evenly distributed in the cell (upper panels). Upon stimulation (t= 30 min) with 250 nM AP20187, only kdEphB2-3FKBP accumulated in the lateral edge of the cell (I, arrow), whereas EphB2 lacking FKBP remains evenly distributed (II). Upon stimulation with ephrinB2-Fc both receptor variants accumulate at the lateral edge of the cell (III, IV, arrow). BF images on far left are low power magnifications. Red boxes indicate areas of higher magnifications. Image acquisition and processing: 6x 0.2 µm z-stacked epiFL images; odc; adaptive-blind psf deconvolution; sum-projection. Scale bars, 10 µM. Results from (B) and (C) indicate that there is no lateral recruitment into AP20187-induced clusters, possibly because the ephrin-unbound EphB2 ectodomain does not favor Eph-Eph interactions. Dimerizer-induced Eph clustering is self-contained. **(D)** Western blot co-precipitation analysis of Eph clusters induced by dimerizer or ephrinB2-Fc in presence or absence of dynasore (80 µM). Cells were surface biotinylated after stimulation and lysates immunoprecipitated with anti-FLAG resin. Blot was probed with streptavidin-hrp to visualize for biotinylated membrane surface protein. Dimerizer-induced Eph clustering does not cause co-precipitation of a biotinylated 50-55 kDa protein. (*** anti-FLAG immunoprecipitated wtEphB2-3FKBP-YFP; ** co-precipitated ephrinB2-Fc; * IgG heavy chain; red* unidentified co-precipitated protein). The presence of dynasore (dyn) did not affect the co-precipitation analysis. The model depicts the possible co-clustering scenario of Eph receptors, ephrinB2-Fc and the unidentified (trans)membrane protein.

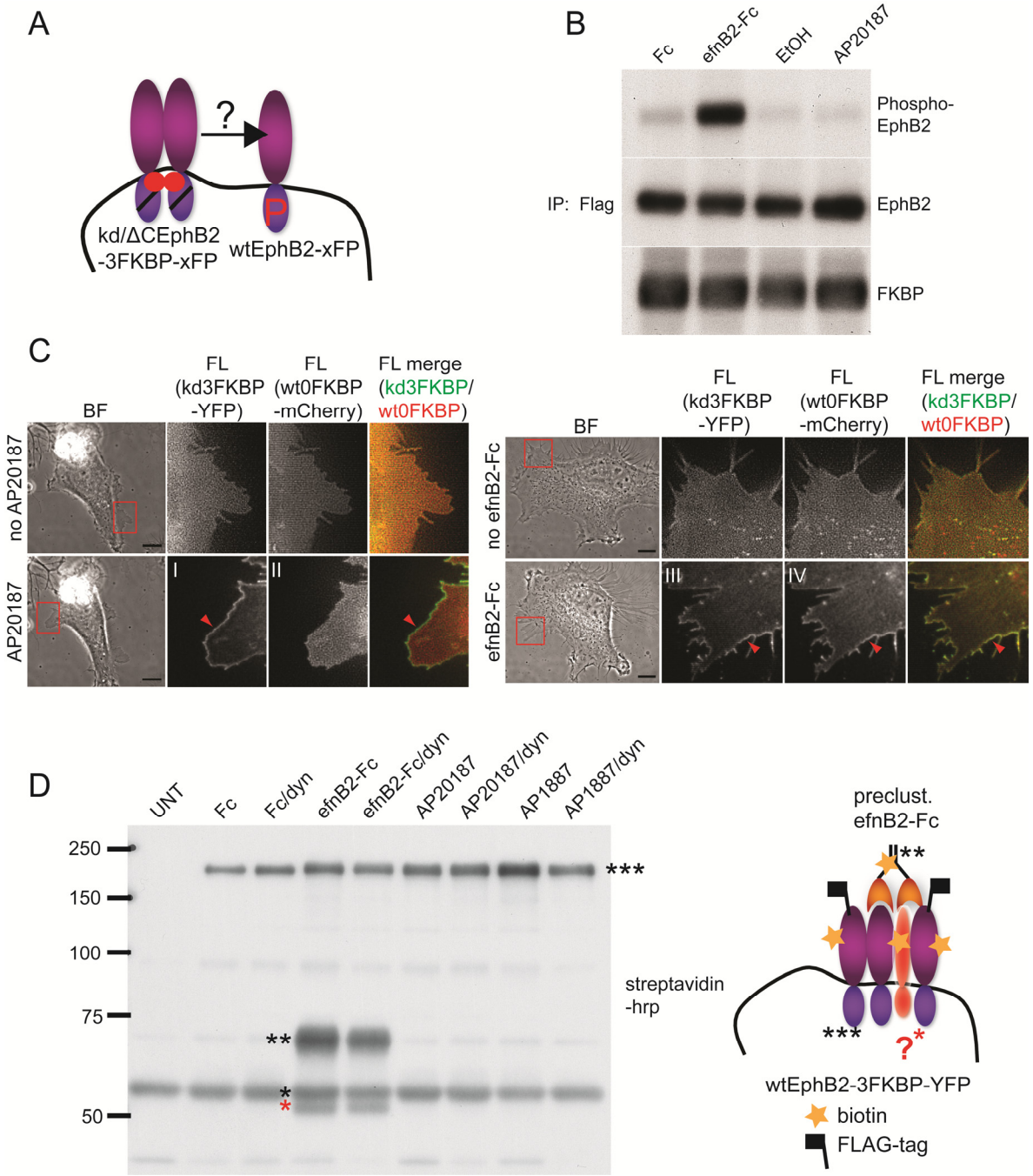
A
?
P
kd/ΔCEphB2
-3FKBP-xFP
wtEphB2-xFP
B
Fc
efnB2-Fc
EtOH
AP20187
Phospho-
EphB2
IP: Flag
EphB2
FKBP
C
BF
FL
(kd3FKBP
-YFP)
FL
(wt0FKBP
-mCherry)
FL merge
(kd3FKBP/
wt0FKBP)
no AP20187
AP20187
I
II
no efnB2-Fc
efnB2-Fc
III
IV
D
UNT
Fc
Fc/dyn
efnB2-Fc
efnB2-Fc/dyn
AP20187
AP20187/dyn
AP1887
AP1887/dyn
250
150
100
75
50
***
**
*
*
streptavidin
-hrp
preclust.
efnB2-Fc
**
***
?*
wtEphB2-3FKBP-YFP
biotin
FLAG-tag

3.3.4 Dimerizer-induced clustering produces distinct Eph cluster size distributions in living cells

By implementation of the dimerizer-inducible system of cluster formation, I aimed at controlling Eph cluster size distributions. We have seen that in a cell co-culture assay (cp. Fig. 3.2) homo-FRET is a suitable readout for Eph clustering to account for relative differences in cluster size distributions. However, absolute size distributions of Eph receptors remain elusive using such imaging techniques. A straightforward approach to resolve absolute cluster size distributions is blue-native polyacrylamide gel electrophoresis (PAGE) [315]. This approach allows for absolute quantification of single species from the total pool of varying cluster sizes.

Fig. 3.10 Dimerizer-induced EphB2 clustering causes distinct cluster sizes.
(A) AP20187 induced clusters of kdEphB2-FKBP-mGFP isoforms. Blue-native PAGE of unstimulated controls (CTRL) show only monomeric Eph receptor species with a shift in molecular weight in accordance to the number of FKBP domains inserted. Upon AP20187 stimulation (t= 20 min) 1FKBP isoforms produce mostly dimeric receptor species, whereas 2 and 3 FKBP isoforms lead to higher-order clusters. Overall, molecular weights from blue-native PAGE are higher than calculated values, most likely due to an extended native receptor conformation. Graph: an incremental average optical density linescan was performed to give the distribution patterns with peaks indicating single resolvable cluster species. Incremented average optical density was normalized to the sum over all increments. **(B)** Steady-state FL anisotropy of dimerizer-induced EphB2 clusters in living cells. COS-7 cells transiently expressing kdEphB2 carrying different numbers of FKBP domains (fused to mGFP) were stimulated with 250 nM AP20187 in a heated (37 °C) dish holder. Anisotropy values of representative cells pre and 20 min post stimulation with AP20187 are shown. Anisotropy values decrease with increasing numbers of FKBP domains indicating a higher degree of homo-FRET. Scale bars in upper panels: 10 µM. The color coding of images is shown to the right. The graph shows quantified anisotropy plots of pre and post stimulation of 0 to 3 FKBP isoforms. Data represent mean anisotropy ± SEM of n= 57, 28, 22 and 20 cells for 3FKBP, 2FKBP, 1FKBP and 0FKBP integrated over the whole image frame, respectively. Post-stimulation curves of 0-3FKBP are all significantly different to each other and to controls. (0/1FKBP, 0/2FKBP, 0/3FKBP, 1/3FKBP, 2/3FKBP: $p < 0.001$; 1/2FKBP: $p < 0.01$; Mann-Whitney Wilcoxon nonparametric *t*-test). **(C)** Dimerizer-induced EphB2 clustering kinetics visualized by time-lapse FL anisotropy imaging. Receptor kdEphB2-[0-3]FKBP isoforms were transiently transfected into COS-7 cells. FL anisotropy recordings show a sigmoid decrease after AP20187 stimulation over time, reaching steady-state after 20 min. The rate of decline in FL anisotropy directly correlates with the number of inserted FKBP domains. (FL anisotropy in percent relative to start prior stimulation, normalized to 0FKBP/AP20187 control, curves are representative examples of time-lapse anisotropy measurements from single cells). **(D)** EphrinB2-Fc-induced cluster formation readout using homo-FRET. EphB2-xFKBP-mGFP transfected COS-7 cells were stimulated with either unclustered ephrinB2-Fc or preclustered ephrinB2-Fc. Anisotropy values of representative cells prior (upper panels) and 20 min post stimulation with AP20187 (lower panels) are shown. Anisotropy values decrease with increasing amounts of unclustered ephrinB2-Fc added indicating a higher degree of homo-FRET. For preclustered ephrinB2-Fc stimulation conditions saturating low anisotropy values were reached with as little as 1 µg/ml ephrinB2-Fc. Scale bars, 10 µM. The color coding of the lut is shown to the right. Data represent mean anisotropy ± SEM of n≥ 20 cells for each condition. Post-stimulation curves are all significantly different to each other and to controls; significance level as indicated with ** $p < 0.01$; *** $p < 0.001$; n.s. not significant; Mann-Whitney Wilcoxon nonparametric test. **Calculation of all anisotropy values was carried out by Ola Sabet, MPI Dortmund, Germany according to Squire *et al.*** [309]**.**

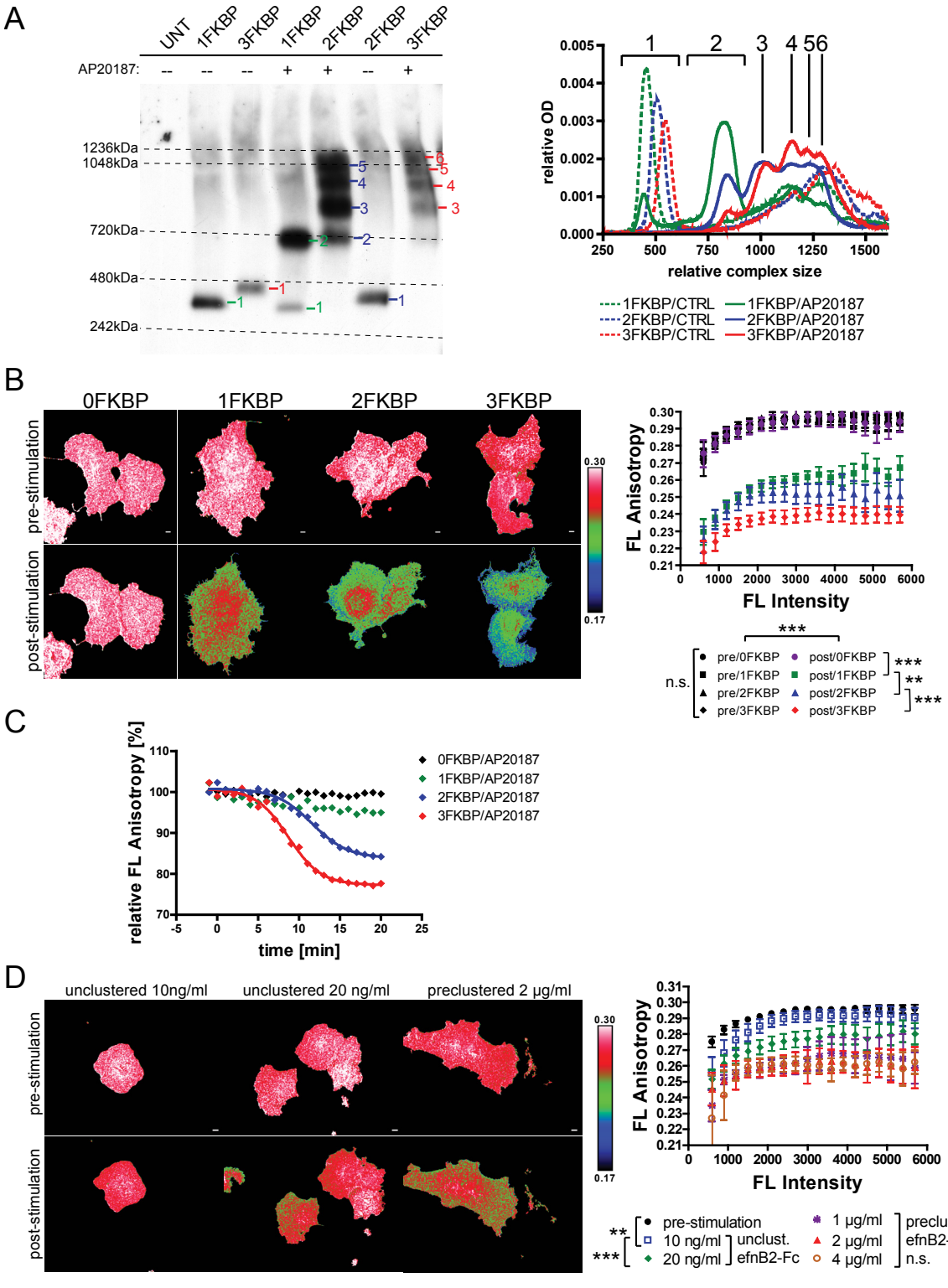
A
UNT
1FKBP
3FKBP
1FKBP
2FKBP
2FKBP
3FKBP
AP20187:
1236kDa
1048kDa
720kDa
480kDa
242kDa
relative OD
relative complex size
1FKBP/CTRL
2FKBP/CTRL
3FKBP/CTRL
1FKBP/AP20187
2FKBP/AP20187
3FKBP/AP20187
B
0FKBP
1FKBP
2FKBP
3FKBP
pre-stimulation
post-stimulation
FL Anisotropy
FL Intensity
pre/0FKBP
pre/1FKBP
pre/2FKBP
pre/3FKBP
post/0FKBP
post/1FKBP
post/2FKBP
post/3FKBP
n.s.
C
relative FL Anisotropy [%]
time [min]
0FKBP/AP20187
1FKBP/AP20187
2FKBP/AP20187
3FKBP/AP20187
D
unclustered 10ng/ml
unclustered 20 ng/ml
preclustered 2 µg/ml
pre-stimulation
post-stimulation
FL Anisotropy
FL Intensity
pre-stimulation
10 ng/ml
20 ng/ml
unclust.
efnB2-Fc
1 µg/ml
2 µg/ml
4 µg/ml
preclustered
efnB2-Fc
n.s.

Upon transient expression in COS-7 cells and stimulation with the high-affinity dimerizer AP20187, lysates were subjected to blue-native PAGE. In order to obtain an immediate snapshot of the cluster size distribution after stimulation, inert kinase-dead receptor isoforms (kdEphB2-[1-3]FKBP-mGFP) were used. In anti-EphB2 immunoblots, single cluster species can be resolved as peaks (Fig. 3.10A). In the absence of AP20187, all receptor isoforms are predominantly monomeric. AP20187 stimulation of cells expressing the 1FKBP isoform resulted in the formation of dimers, with a minor residual amount of monomers present. Binding of AP20187 to 2FKBP isoforms resulted in the formation of EphB2 oligomers. Although dimers were still present, trimers became the predominant form, and oligomers up to pentamers could be distinguished. The presence of three FKBP domains shifted the distribution pattern towards bigger oligomers. Dimeric species were no longer present, trimers were no longer the predominant species, and hexamers could be detected.

Next I asked if different EphB2 cluster size distributions would also cause graded changes in FL anisotropy in living cells (Fig. 3.10B). In control conditions all receptor isoforms displayed the same FL anisotropy across different FL intensities. Addition of AP20187 to transfected cells decreased FL anisotropy, with a large reduction observed when EphB2 was dimerized. Further significant reductions in FL anisotropy were detected in cells expressing the two and three FKBP domain isoforms, indicating that different EphB2 cluster size distributions were present in living cells. Cluster formation saturated within 20 min for all FKBP isoforms (supplementary video 2 & Fig. 3.10C). The rate of decline in FL anisotropy directly correlates with the number of inserted FKBP domains.

EphrinB2-Fc stimulations on kd EphB2 receptor-expressing COS-7 also caused a significant drop in FL anisotropy due to clustering of mGFP-tagged Eph receptors (Fig. 3.10D). While low amounts of unclustered ephrinB2-Fc provoked only a mild clustering response with a very subtle drop in FL anisotropy, doses of 1 to 4 µg/ml preclustered ephrinB2-Fc led to saturation in homo-FRET. Overall, the decrease in anisotropy from 3FKBP/AP20187 clustered receptors was stronger than from ephrinB2-Fc clustered receptors.

Fig. 3.11 Comparison of dimerizer-induced Eph clustering using AP1887 or AP20187.
(A) AP1887-induced clusters are less stable than AP20187-induced clusters. Blue-native PAGE of lysates from COS-7 cells transfected with wtEphB2-3FKBP and stimulated with either AP20187 or AP1887 for 20 min. After transfer, EphB2 receptor was blotted against anti-EphB2Sam. In contrast to the formation of multiple cluster sizes upon stimulation with AP20187 (cluster species dimer to tetramer and possibly of higher-order), application of AP1887 did not lead to the maturation of a stable cluster size distribution but solely monomers. Asterisks in blot indicate unspecific background smear.
(B) AP1887-induced clustering readout using homo-FRET. Kinase-dead EphB2-3FKBP-mGFP transfected COS-7 cells were stimulated with either AP20187 (250 nM) or AP1887 (250 nM). AP1887 does not cause a decrease in anisotropy values. Data represent mean anisotropy ± SEM of n≥ 20 cells for each condition; significance level as indicated with *** p< 0.001; n.s. not significant; Mann-Whitney Wilcoxon nonparametric test. **(C)** AP20187 dimerizer-induced Eph clustering can only be reversed by competition for binding with AP21967. HeLa cells expressing kdEphB2-3FKBP-YFP and inhibitor construct myr-FRB-mCherry were imaged live while being stimulated with AP20187, then

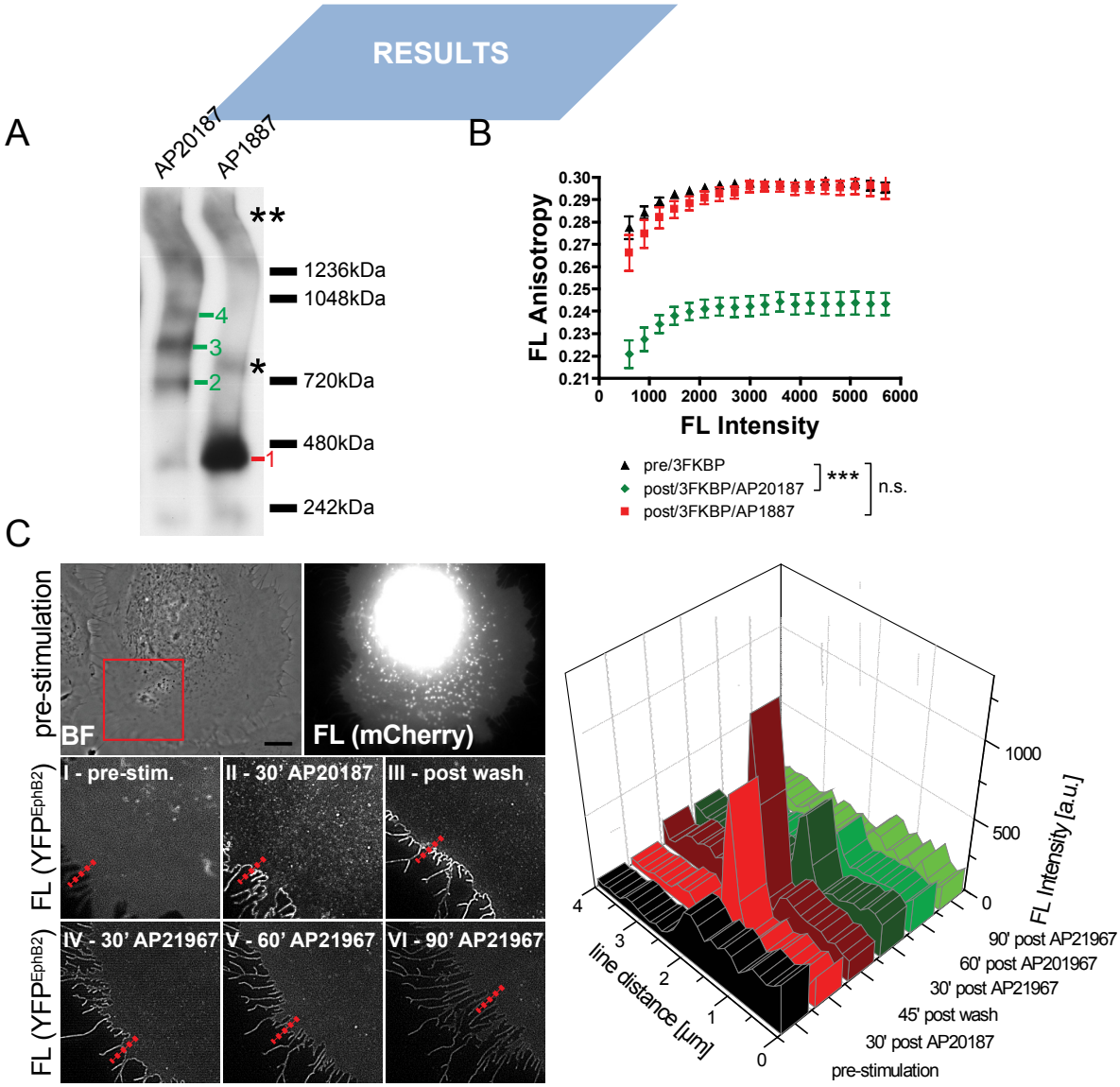

removing the stimulus, and finally incubating with dimerizer AP21967. Upon addition of AP20187, rapid and stable clustering was induced as shown before and visualized by the FL intensity rise at the cell edge (II). Removal of AP20187 by washing of the cells did not significantly reverse clustering (III), while addition of competitor AP21967 succeeded in reversing the clustering process gradually (IV,V,VI). Image acquisition and processing: 3x 0.2 µm z-stacked epiFL images; odc; adaptive-blind psf deconvolution; sum-projection. An average FL intensity linescan (dotted lines in panels I-IV) on cell edges was performed and values at different stages of the experiment were plotted in a 3-dimensional graph. **Calculation of all anisotropy values was carried out by Ola Sabet, MPI Dortmund, Germany according to Squire *et al.*** [309].

In summary, in excess of dimerizer, FKBP-induced clustering produces clusters of discrete size distributions depending on the number of FKBPs present. As expected, dimers are the highest order species possible for 1FKBP receptor isoforms, and the cluster formation process saturates within 20 min after stimulation for all FKBP isoforms. Homo-FRET imaging confirms the results obtained from blue-native PAGE on the single-cell level showing an inversely proportional decrease in FL anisotropy to cluster size distributions. For ephrinB2-Fc-induced clustering, the decrease in FL anisotropy reaches saturation at a higher level as for 3FKBP/AP20187-induced clustering.

3.3.5 Controlling the mechanical dynamics of dimerizer-induced cluster formation allows for production of clusters of different stability or quality

In the previous section, AP20187 was shown to produce cluster size distributions, which were stable enough to remain during the process of cell lysis or blue native-PAGE (cp. Fig. 3.10A). By contrast, the use of the alternative low-affinity dimerizer AP1887 did not result in higher-order cluster species (Fig. 3.11A). Furthermore, addition of AP1887 to kdEphB2-3FKBP-mGFP-expressing COS-7 did not result in a significant decrease of the steady-state anisotropy in homo-FRET imaging (Fig. 3.10B). In conclusion, the approximately 20 fold lower binding affinity of AP1887 in comparison to AP20187 [316], suggests the constitution of more transient clusters, which are less stable or cohesive, and thus cannot persist during the process of cell lysis or blue native-PAGE. It may, however, be assumed that cluster complexity is not affected by the dimerizer but by the number of inserted FKBP domains.
For a closer investigation of AP20187-induced clustering, I also tested for reversibility of the phenotypic effect caused in cell edges. Myristoylated FRB-mCherry was co-transfected with kdEphB2-3FKBP-YFP into HeLa cells. Clustering was induced by addition of AP20187 to produce the characteristic effect of receptor accumulation at cell edges (Fig. 3.11C-I,II). Exchange for fresh imaging medium containing no AP20187 was then performed as a washing step, but did not reverse the phenotypic effect (Fig. 3.11C,III) supporting the notion that the off-rate in binding of the high-affinity dimerizer AP20187 is basically negligible.The formation of diffusion-limited cavities could also contribute to the irreversibility of AP20187 mediated FKBP-FKBP binding, creating a state of strong cohesiveness between receptor molecules in AP20187-induced clusters. However, it is possible to abrogate AP20187 receptor accumulation at cell edges by addition of heterodimerizer AP21967. Phenotypically, addition of AP21967 reverses the effect of FL intensity rise at cell edges back to a rather diffuse distribution of EphB2 receptor FL signal (Fig 3.11C-IV,V,VI). On the molecular level, the formation of FKBP-FRB complexes is likely to cause a neutralization of the FKBP-FKBP cohesiveness in a proactive way, since in the absence of myr-FRB-mCherry, addition of AP21967 does not reverse the phenotypic clustering effect (data not shown).
Overall, these results give a deeper insight in mechanical aspects of the dimerizer-induced clustering system. They show that dimerizer-induced clustering can be reversed by competition with AP21967 in the presence of inhibitor construct myr-FRB-mCherry. Moreover, qualitative versatility of the system can be realized by use of the alternative low-affinity homodimerizer AP1887.

3.4 Movement and processing of Eph receptor clusters in mammalian cells

RTKs like EGFR that are embedded in the cell's surface membrane, undergo constant lateral movement (within the cell surface membrane) and vertical trafficking (between membrane compartments) [317-319]. Vertical trafficking is characterized as a dynamic steady-state turnover of receptor molecules between the cell's surface membrane and intracellular membrane compartments, such as the Golgi and ER, as well as exosomal and endosomal compartments. Receptor sequestration, i.e. internalization into degradative compartments like lysosomes, is also a well-known mechanism to shut down signaling responses after stimulation, a process that has also been studied for EphB2 [249]. All processes eventually leading to degradation, or change in the oligomerization state of Eph receptors following cluster formation will be termed "processing" below. Horizontal receptor movement is mostly based on passive diffusion, but also consists of active processes that lead to lateral transport within the membrane to different cell surfaces [294]. It is rather intuitive that higher-order entities such as clusters might behave differently in movement and processing as compared to monomeric or only dimeric species. I was therefore interested in characterizing the movement and processing of Eph receptors with respect to cluster entities induced by the FKBP-system or ephrinB2-Fc both prior and post stimulation.

3.4.1 Receptor accumulation correlates with dimerizer-induced cluster size distributions

Eph clustering causes a FL intensity rise either as a ring-shaped FL syncytium around the stimulated cell (cp. Fig. 3.8) or as distinct FL entities (cp. Fig. 3.1). This phenomenon may be interpreted as receptor accumulation at the lateral side of the cell. For a more detailed study of this phenotypic effect I employed FKBP-tagged, kd Eph receptor variants and produced different cluster size distributions in living cells. Interestingly, the strength of receptor accumulation correlated with the [0-3]FKBP derived cluster size distributions induced by AP20187 dimerizer (Fig 3.12). This result strengthens the already made assumption that receptor accumulation is the cause for the FL signal intensity rise in cell edges. As with AP20187, AP1887-induced clustering accumulation was present, but weak. Again, this result backs conclusions from the previous section stating that AP1887-induced clusters are less stable or cohesive.
Overall, the tight correlation between AP-dimerizer/FKBP-induced cluster size distributions and receptor accumulation at the lateral side of the cell highlights a direct link between the formation of clusters and - in a secondary process - their redistribution to the lateral side of the cell in a size-dependent manner.

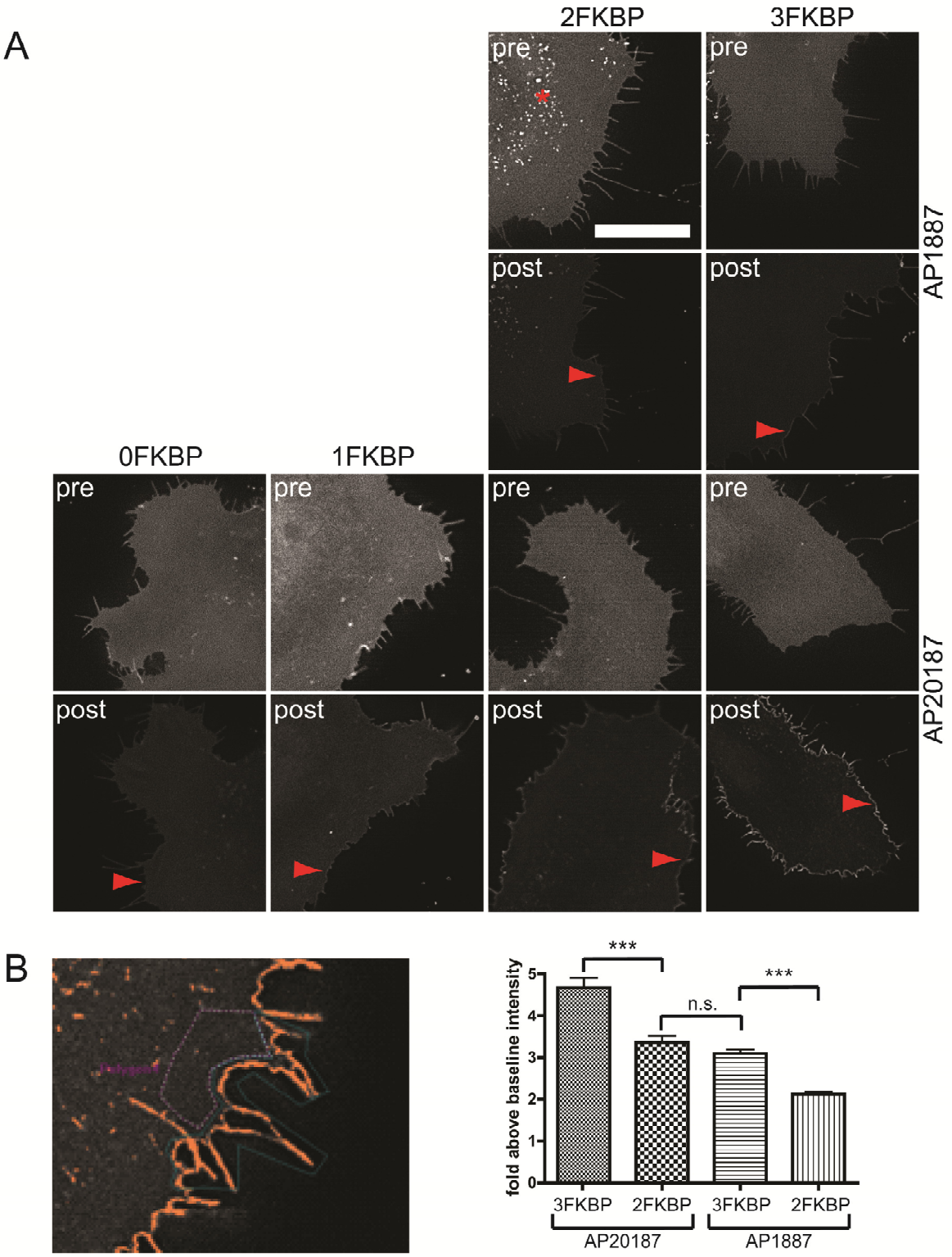
A
2FKBP
3FKBP
pre
pre
post
post
AP1887
0FKBP
1FKBP
pre
pre
pre
pre
post
post
post
post
AP20187
B
fold above baseline intensity
***
n.s.
***
5
4
3
2
1
0
3FKBP
2FKBP
3FKBP
2FKBP
AP20187
AP1887

Fig. 3.12 The strength of the phenotypic effect of receptor accumulation at cell edges correlates with the number of inserted FKBP-domains.
(A) HeLa cells expressing YFP-tagged kdEphB2-[0-3]FKBP were imaged in high resolution before (pre) and after stimulation (post, 10 min) with AP20187 and AP1887 dimerizer (each 250 nM). Arrows indicate sites of receptor/FL accumulation of different extent correlating to the number of FKBP domains and dimerizer agent used. Asterisk in uppermost left panel indicates membrane debris left behind from moving around HeLa cells. Pre and post images are equally scaled within the same group (pre/post). Representative cell samples were selected for alike receptor membrane density (60 < average intensity < 100 counts). Image acquisition and processing: epiFL 6x 0.2 µm z-stacks; odc; adaptive-blind psf deconvolution; sum-projection; bgcorr. Scale bar, 10 µm. **(B)** Quantification of cell edge receptor accumulation caused by clustering of FKBP isoforms. The approach is shown as screenshot from the analysis procedure in MetaMorph software (image: kdEphB2-2FKBP/AP20187). In FL-thresholded images two regions were defined, one to outline the cell edge where accumulation occurs, one to define a region close by to correct for receptor membrane density (baseline intensity). Images for analysis: maximum projection from 6x 0.2 µm z-stacks; bgcorr. Data represent mean fold above baseline intensity ± SEM of n= 15, 14, 15 and 17 region pairs from minimum 5 cells for 3FKBP/AP20187, 2FKBP/AP20187, 3FKBP/AP1887 and 2FKBP/AP2087; *** p< 0.001, n.s., not significant; one-way ANOVA with posthoc Bonferroni test.

3.4.2 Diffuse rapid receptor movement converts into distinct spatial signaling entities upon clustering

One suitable approach to study processes in the basal cell surface membrane and proximity is the use of TIRF (total internal reflection fluorescence) microscopy. In live-cell applications it also empowers the user to visualize dynamic events. In collaboration with the MPI Dortmund, Germany (Ola Sabet, Philippe Bastiaens), I carried out experiments to investigate Eph receptor clustering-dependent movement and processing in detail. Again, both TIRF and epiFL/confocal microscopy produce images below the optical resolution for small, single cluster species, and can therefore only resolve pools of clusters of varying sizes as shown earlier (cp. Fig. 3.12).

Static TIRF imaging of Eph receptor clustering. Thus, prior to generating a dynamic view of Eph clusters in the cell surface membrane, I assessed the phenotypic clustering effect from epiFL/confocal imaging at the lateral side of the cells, identified as receptor accumulation, in TIRF microscopy. COS-7 cells expressing myr-mCherry, and respective wt or kd Eph receptor isoforms were imaged in TIRF angle prior and post stimulation with either AP20187 or ephrinB2-Fc (Fig. 3.13A). While for myr-mCherry no significant FL accumulation could be seen, clustering via ephrinB2-Fc or AP20187 caused the rise of a few single FL dots in the TIRF field of imaging. Note that soluble ephrinB2-Fc can theoretically only access the apical-lateral side of the cell and not penetrate the basal membrane very well. Therefore, clusters form predominantly at the apical-lateral side of the cell outside the TIRF field of vision, and only to a small degree at basal side of the cell. In few cases, ephrinB2-Fc can access the membrane and cause clustering, which could be due to, for example, uneven basal membrane adhesion to the growth surface (often visible as dark patches and more common for HeLa cell

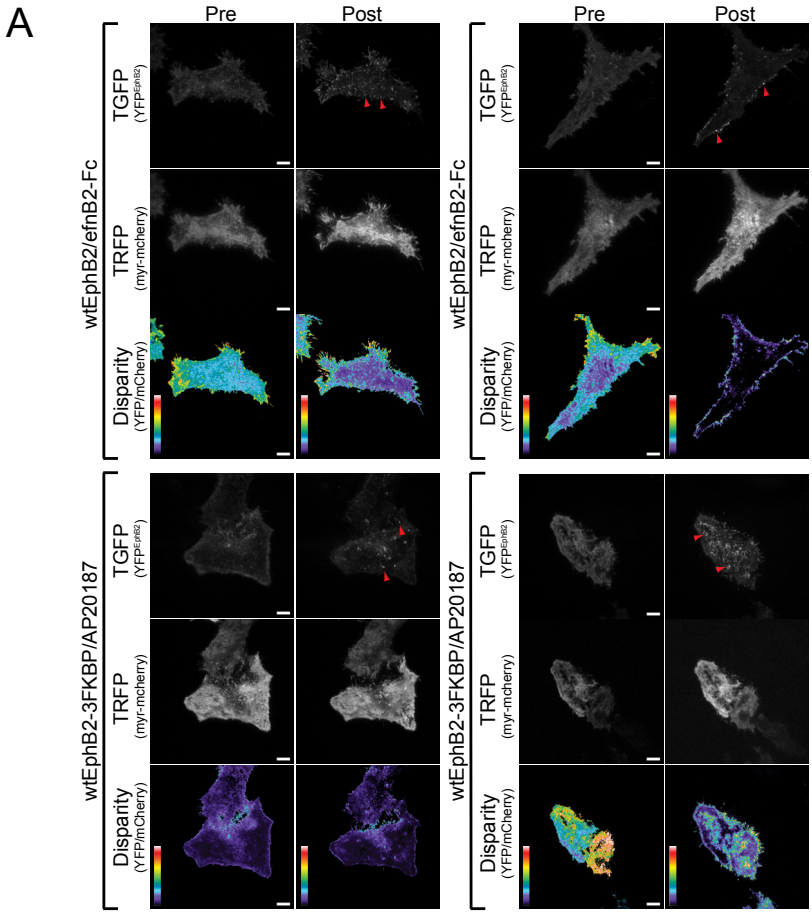
A
Pre
Post
Pre
Post
wtEphB2/efnB2-Fc
TGFP (YFPstrep)
TRFP (myr-mcherry)
Disparity (YFP/mCherry)
wtEphB2/efnB2-Fc
wtEphB2-3FKBP/AP20187
wtEphB2-3FKBP/AP20187

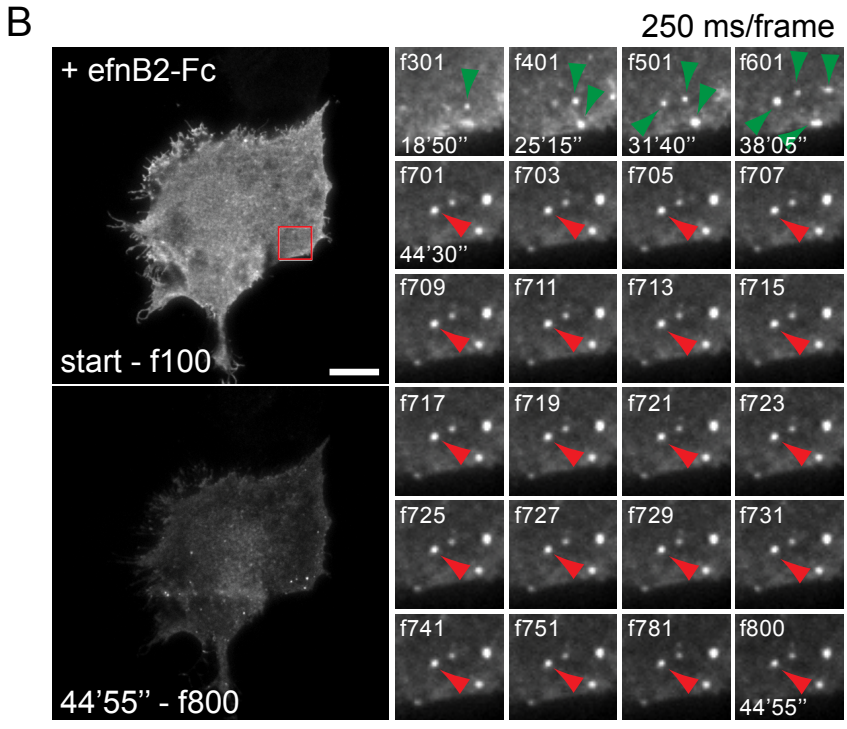
B
250 ms/frame
+ efnB2-Fc
start - f100
44'55'' - f800
f301
18'50''
f401
25'15''
f501
31'40''
f601
38'05''
f701
44'30''
f703
f705
f707
f709
f711
f713
f715
f717
f719
f721
f723
f725
f727
f729
f731
f741
f751
f781
f800
44'55''

Fig. 3.13 Stationary FL foci appear in the basal membrane upon stimulation with ephrinB2-Fc/AP20187 homodimerizer.
TIRF (total internal reflection fluorescence) microscopy was used to image the basal membrane and its proximity. **(A)** HeLa cells transfected with respective [0,3]FKBP receptor isoforms were imaged prior and post stimulation (~30 min) with preclustered ephrinB2-Fc (2 µg/ml) or AP20187 (250 nM) dimerizer. Receptor distribution changed from being diffuse to distinct foci (arrows) over the time course of stimulation. For comparison, co-transfected myr-mCherry was imaged in parallel, which retained its diffusive FL intensity pattern. The FL signals from EphB2 receptor protein were normalized to myr-mCherry to show the disparity in contrast, which reflects their plasma membrane localization. Color bar indicates normalized ratio (range 0-10) of pixel values. Single plane FL images, acquired in TIRF angle, were background corrected. Scale bars, 10 µm **(B)** EphrinB2-Fc induced clustering causes the constitution of high FL entities forming at the basolateral side of the wtEphB2-YFP transfected COS-7 cell. High power magnification image sequence (from region in red) shows the formation of high FL entities starting approximately 18 min after stimulation (green arrows; frames 301-601). A fast acquisition image sequence (red arrows; frames 701-800) points out the static nature of the clusters formed. Note that in TIRF microscopy, the most lateral side of cells is not visible due to membrane bending at cell edges.

TIRF imaging). In the case of homodimerizer stimulation, the compound can penetrate the whole cell, including the basal membrane. The formation of these FL foci is also very much limited in number and size and cannot be compared to the extensive phenotypic effect of FL intensity rise observed in epiFL/confocal imaging. In consequence, this result on the one hand indirectly supports the idea of clustering-dependent lateral receptor accumulation, while on the other hand proves that receptor accumulation is a secondary process following the initial cluster formation.

Dynamic TIRF imaging of Eph receptor clustering. Next, I wanted to generate a more dynamic view of Eph clusters in the cell surface membrane using TIRF imaging in fast acquisition mode (250 ms/frame) to obtain high temporal resolution. COS-7 cells, transiently expressing wildtype EphB2-YFP receptor isoforms, were imaged while stimulated with preclustered ephrinB2-Fc (2 µg/ml) (Fig. 3.13B). About 15 min after addition of the stimulus, first FL foci appeared at the basolateral side of the cell, increasing in number and size over time (Fig. 3.13B, f301-f601). In addition to the live visualization of cluster formation upon ephrinB2-Fc stimulation, I also addressed the question of lateral cluster movement within the membrane. Clusters, which have formed upon ephrinB2-Fc stimulation, remained surprisingly stationary over an extended period of time (Fig. 3.13A, f701-f800).
For proper validation of the finding that Eph receptor signaling entities, caused by clustering, are stationary in localization, I investigated Eph receptor movement and processing prior to clustering. To do so, HeLa cells were transfected with wt (Fig. 3.14A) or kd (Fig 3.14B) EphB2 receptors tagged with YFP and imaged in fast acquisition mode using live-cell TIRF imaging. High magnification images from sequential frames were then analyzed pixel by pixel over time, measuring the range of FL intensity fluctuations and standard deviation in FL intensity. For comparison, co-transfected myr-mCherry was also analyzed accordingly in parallel. Fluctuation curves indicating range and standard deviation of the FL intensity per

pixel over time describe a representative population of 100 pixels from all pixels averaged in bar graphs. Color coded FL intensity panels from the region of interest (red rectangle) reveal stable FL intensity patterns for myr-mCherry as compared to wtEphB2-YFP, highlighting increased dynamics in Eph receptor movement. Both for kd and wt Eph receptor isoforms, movement was significantly enhanced as compared to myr-mCherry, although wtEphB2-YFP receptors are significantly bigger in size (about 30 kDa as compared to 140 kDa, respectively).

Taken together, these results outline rapid lateral movement of Eph receptors prior to ligand engagement, which, upon ligand binding, is converted into the establishment of spatial Eph receptor signaling entities. Furthermore, these clusters seem to be rather static in localization at the lateral side of the cell surface plasma membrane.

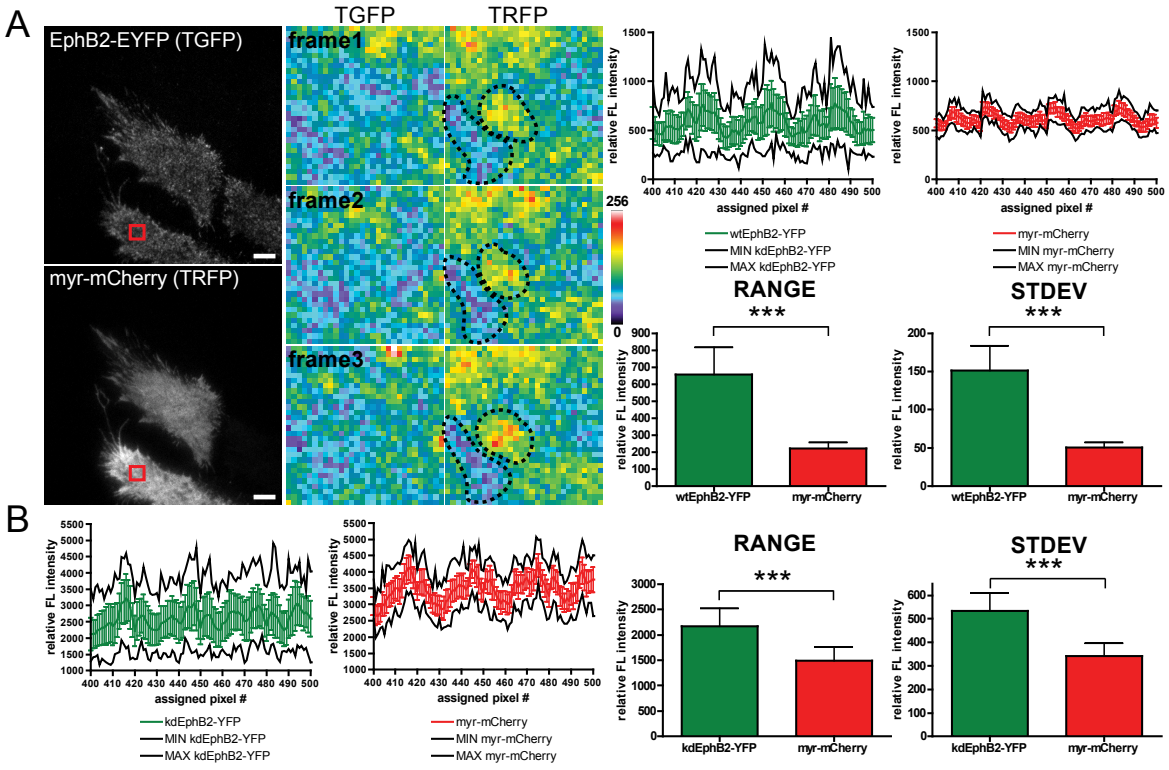

Fig. 3.14 High receptor density fluctuations in the cell membrane prior to clustering.
Receptor density fluctuation analysis using TIRF time-lapse microscopy in rapid acquisition mode from HeLa cells transfected with kd or wt EphB2-YFP. **(A)** Pixel intensity fluctuations from TRFP (myr-mCherry) and TGFP (wtEphB2-YFP) were analyzed over time (Δt= 2s/frame) from region (30x30 pixels) indicated by red boxes. The higher FL intensity level for myr-mCherry was corrected by normalization to the FL intensity from wtEphB2-YFP. The FL intensity standard deviation and the total range in FL intensity (min/max pixel intensities) were determined over time. A representative population of 100 pixels are plotted against the FL intensity standard deviation over time (green/red error bars) and range (min/max; lower/upper black line) of total FL intensity over time. Bar graphs: mean FL intensity range over time ± SEM of n= 900 pixels for each TGFP/TRFP channel; *** p<

0.001, student *t*-test. Small panels are representative blowups for 3 consecutive time frames of the indicated region for visualization purpose of density fluctuation (color code shown to the right). While for TRFP (mCherry) a constant FL intensity pattern over time can be observed (black dotted regions), TGFP (wtEphB2-YFP) undergoes enhanced fluctuations. **(B)** Pixel intensity fluctuations over time measured from kdEphB2-YFP in comparison to co-transfected myr-mCherry in the HeLa cell's basal membrane and proximity. Analysis and data presentation as described in (A) within a region of 30x30 pixels (Δt= 650ms/frame. Bar graphs: mean FL intensity range over time ± SEM of n= 900 pixels for each TGFP/TRFP channel; *** p< 0.001, student *t*-test. Scale bars, 10 µm.

3.4.3 Processing of spatial signaling entities

In studying vertical aspects of receptor movement, i.e. trafficking between membrane compartments, I conducted TIRF experiments to visualize dynamic events surrounding Eph clustering and subsequent processing. In presence of ephrinB2-Fc, kd Ephs form stationary receptor accumulations at the lateral side of the HeLa cell, visible in the TIRF field (Fig. 3.15A) and presented in detail for one FL entity in high power magnification sequential images (Fig. 3.15A'). While stationary accumulations from kd receptors persisted over time without further processing, newly synthesized receptor protein was delivered to the cell's surface membrane in vesicles: a FL entity appears in f1 (Fig. 3.15A') and travels along the trajectory outlined in green over a time of approximately 130 s until it disappears in f200. A kymograph (Fig. 3.15B) serves for determination of vesicle velocity, and for better visualization of the vesicles. Vesicle speed varied from almost a standstill to 0.57 µm/sec, suggesting a guided vesicle transport along microtubules as described by others [251]. At the end of the trajectory, the vesicle enlarged, increasing in FL intensity, and diffused out into the membrane periphery, a phenomenon that points to a membrane fusion event simultaneous with cargo delivery [320]. By contrast, stationary kd Eph receptor FL foci represent signaling entities on the cell surface plasma membrane (Fig. 3.15A', red arrow).
By contrast to kinase-dead EphB2 receptor, wildtype EphB2 receptor signaling entities at the cell surface were subsequently "processed" (Fig. 3.16). Following the formation of spatial signaling entities within 15 min after stimulation (data not shown), a proportion of clusters underwent decay over time until they disappeared totally (Fig 3.16, panel 37'20''continuing). Others remained stable and stationary (green arrow). Here, AP20187-induced clustering produced the same FL foci as seen for an ephrinB2-Fc stimulation (cp. Fig. 3.13A), visible in the TIRF field of imaging of COS-7 cells that were transfected with the 3FKBP-tagged wt receptor isoform.

Processing of clusters in neurons. While dynamics of movement and processing of Eph clusters may also encompass a cell-specific component, it is important to check for the same results in a different, and biologically more relevant cellular background, such as neurons. For this, hippocampal neurons obtained from rat embryos at embryonic stage 18.5 days were taken in culture and transfected with 3FKBP-tagged wt and kd Eph receptor isoforms using the lipofectamin transfection method (Fig. 3.17).

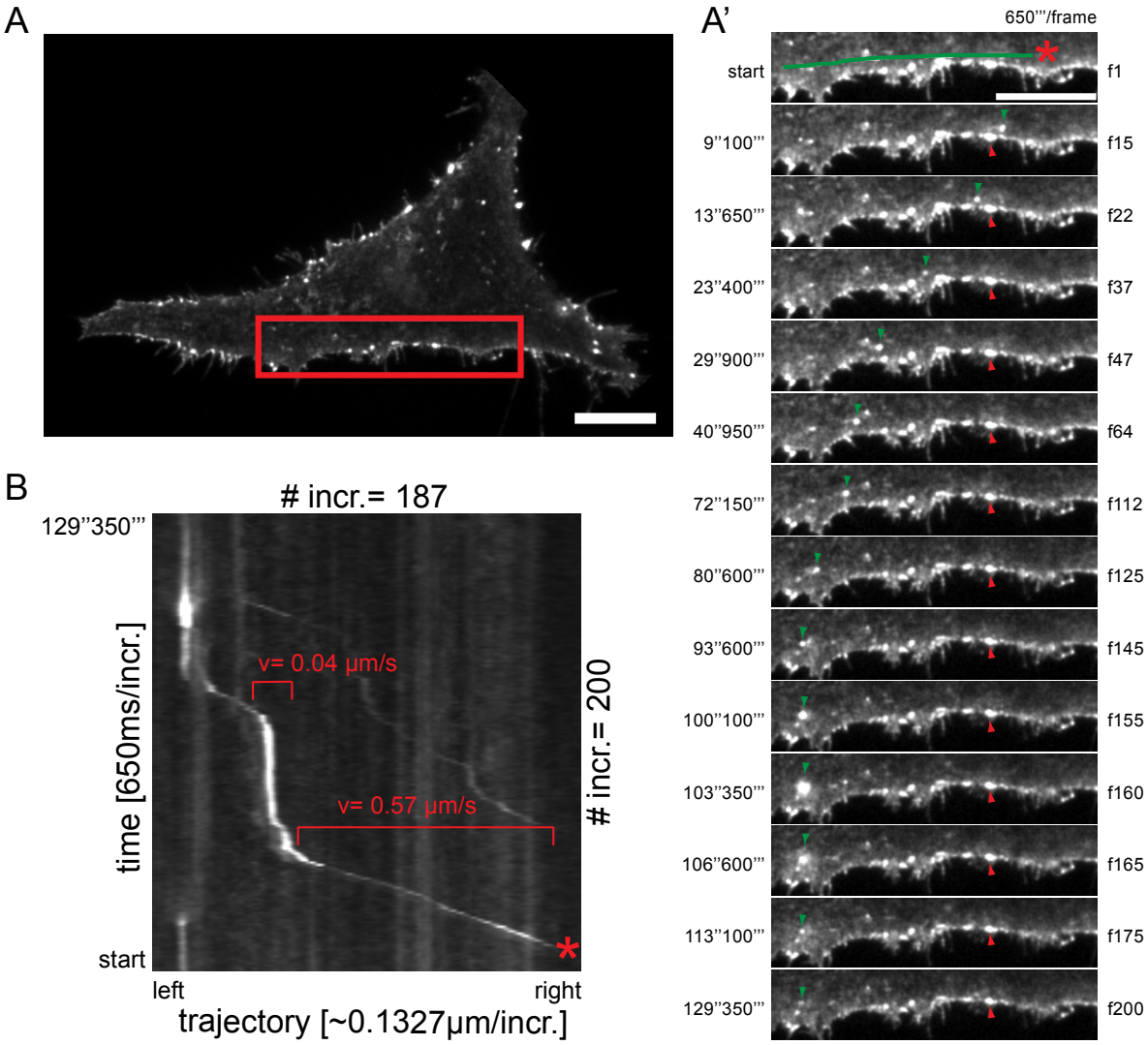

Fig. 3.15 Eph receptors are transported in vesicles to the cell surface where upon ephrin contact stationary clusters are formed.
TIRF time-lapse microscopy in fast acquisition mode (total ~130 s; ∆t= 650 ms/frame) was performed performed after stimulation of kdEphB2-YFP-expressing HeLa cells with preclustered ephrinB2-Fc (2 µg/ml). **(A)** After stimulation, high FL entities are visible in the TIRF field at the lateral side of the cell representing Eph clusters. **(A')** Sequential TIRF time-lapse (high power magnification) images from region in (A). The green line in the first panel outlines the trajectory, the high-FL particle (green arrow) is taking in the time period of observation (frame 1 to 200) until it starts to disappear in frame 175. The red arrow indicates a stationary cluster, typically present after an ephrinB2-Fc induced stimulation (cp. Fig. 13). Note, that kd EphB2 receptor clusters do not undergo immediate processing and degradation. **(B)** Kymograph of trajectory (outlined as green line in A') with its start point indicated by an red asterisk (corresponding to start point indicated by asterisk in A'). The velocity of the vesicle under observation ranges from 0.04 to 0.57 µm/s along its trajectory. Starting in frame 145 the vesicle comes to a complete stop, increases in size and FL intensity and subsequently vanishes to produce a diffuse FL intensity signal. This phenomenon is typical for a vesicle fusing with the outer cell membrane to deliver its cargo [320]. Single plane FL images, acquired in TIRF angle at high speed were background corrected. All images were scaled equally. Scale bars, 10 µm.

Upon stimulation (time point 0 min) with AP20187 dimerizer, both wt and kd receptors formed FL foci at the tips of axon growth cones. As with previous results, clusters remained rather stationary at the basis of the axon growth cone and along the axon when kd Eph receptor was present (red arrows). In contrast, wildtype receptor accumulations (green arrows) were less prominent and rapidly "processed" retrograde along the axon.
Overall, the presented results describe processes surrounding Eph receptor signaling entities that have formed upon clustering with AP20187 or ephrinB2-Fc. Irrespective to the stimulus used to induce clustering, wildtype receptors undergo decay and rapid anterograde processing in hippocampal neurons after a static retention period at the cell surface membrane. Moreover, receptor protein is delivered to the cell surface in vesicles which move along defined trajectories.

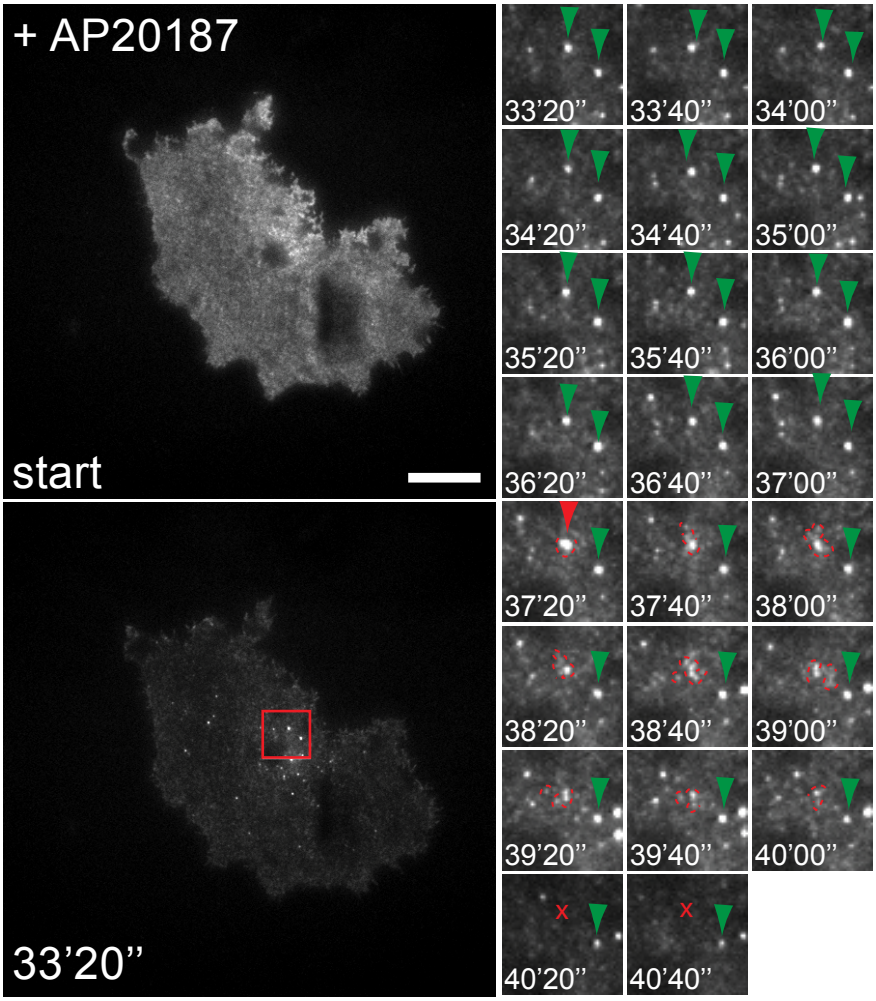

Fig. 3.16 Clusters are subject to decay.
COS-7 cells expressing wtEphB2-3FKBP-YFP and stimulated with dimerizer AP20187 (250 nM) were imaged in fast acquisition mode using TIRF microscopy starting at time point ~33 min after stimulation (sequential blowups from red region). One of the stationary clusters (green arrows) starts to decay over time (red arrows, dotted region) vanishing from the TIRF field of imaging (red x). All images were scaled equally. Scale bar, 10 µm.

Fig. 3.17 Processing of clusters in primary hippocampal neurons.
Hippocampal neuronal cultures (rat, E18.5) were transfected (DIV 1) with kdEphB2-3FKBP-YFP or wtEphB2-3FKBP-YFP and stimulated with AP20187 (DIV2, 250 nM) at timepoint 0 min while imaging in epiFL time-lapse microscopy (single focal plane). Immediately after addition of the compound, FL foci form at the tips of the axon growth cones. Whereas clusters in neurons expressing kinase-dead receptor remain rather stationary (purple and red arrows), clusters from wildtype receptor undergo rapid retrograde processing (green arrow). For better visualization, blowup images of wt axons are shown. Images were corrected for background FL. Scale bars, 10 µm.

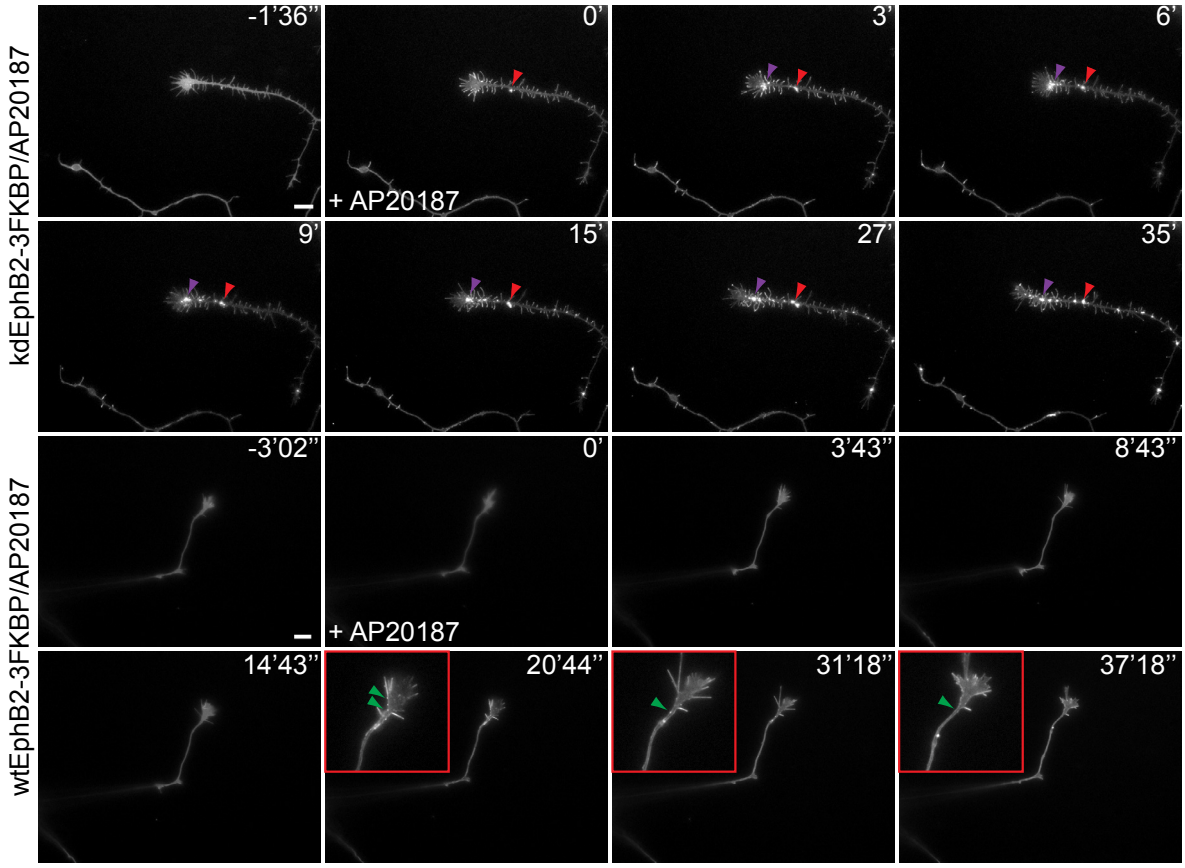

3.4.4 Dimerizer-induced Eph receptor signaling clusters are sequestered from the cell surface membrane

Clustering of Eph receptors causes activation and signaling from spatial entities, which are gradually removed from the cell's surface membrane by internalization processes. To investigate if dimerizer-induced clustering is also sufficient to produce spatial signaling entities prone for internalization, I conducted confocal time-lapse imaging experiments and immunocytochemistry to test for proper internalization into Eph transfected HeLa. AP20187 and ephrinB2-Fc stimulation caused both rapid clustering, collapse of the HeLa cell, and the formation of focal FL entities pinching off the cell's lateral side (Fig. 3.18A, supplementary video 1). In corroboration with these results, immunocytochemistry experiments were performed to determine the internalized fraction of protein, which is not stained by a surface-applied antibody (Fig. 3.18B). Clusters present in both the merge and total protein panels that do not co-stain with the surface signal are internalized Eph receptors. Quantifications of surface versus total receptor protein FL intensities confirm the visual results and reveal no significant difference between AP20187 and ephrinB2-Fc induced internalization under the given conditions (Fig. 3.18C).

As for wildtype receptor internalization, constitutively active eeEphB2 receptors internalized upon stimulation with either AP20187 or ephrinB2-Fc (Fig. 3.18B). Here, the exchange of residues Tyr604Glu and Tyr610Glu, which represent SH2 binding sites for downstream adaptor proteins, does not seem to affect AP20187-induced or soluble ephrinB2-Fc-induced receptor internalization.
In summary, it appears that the process of disintegration observed in TIRF imaging at the surface plasma membrane is accompanied by internalization of Eph receptor signaling entities upon clustering. Receptor-autonomous clustering is sufficient to cause internalization irrespective of ligand engagement.

3.5 Eph receptor clustering correlates with cellular responses

As shown previously, the dimerizer-inducible system provides a tight regulation of cluster size distributions in living cells. Next, I therefore asked if the degree of higher-order clustering would cause a graded signaling response. With the use of the low and high-affinity dimerizers AP1887 and AP20187, it was possible to study the signaling process in detail from receptor activation, kinase activity and cell collapse responses to gain detailed insights in clustering-related signaling dynamics.

3.5.1 EphB2 clustering correlates with the strength of cellular response

Correlation of cluster size distributions with Eph signaling was assessed at the ultimate response of cell contraction using the collapse assays as described before. Dimerizer-induced cluster size distribution patterns were translated into a corresponding cellular response both in terms of total collapse magnitude as well as a time-dependent response pattern (Fig. 3.19A). As expected, the formation of EphB2 dimers produced very mild responses. In contrast, cells expressing the 2FKBP isoform responded to AP20187 with pronounced cell collapse. Importantly, cells expressing the 3FKBP isoform showed a significantly stronger cell collapse response, both in terms of kinetics and degree of cell contraction. In an alternative approach using the 3FKBP isoform clustered with AP20187 in mix with competitor AP21967 the total collapse amplitude decreased significantly, whereas kinetics of collapse remained rather similar (Fig 3.19B).

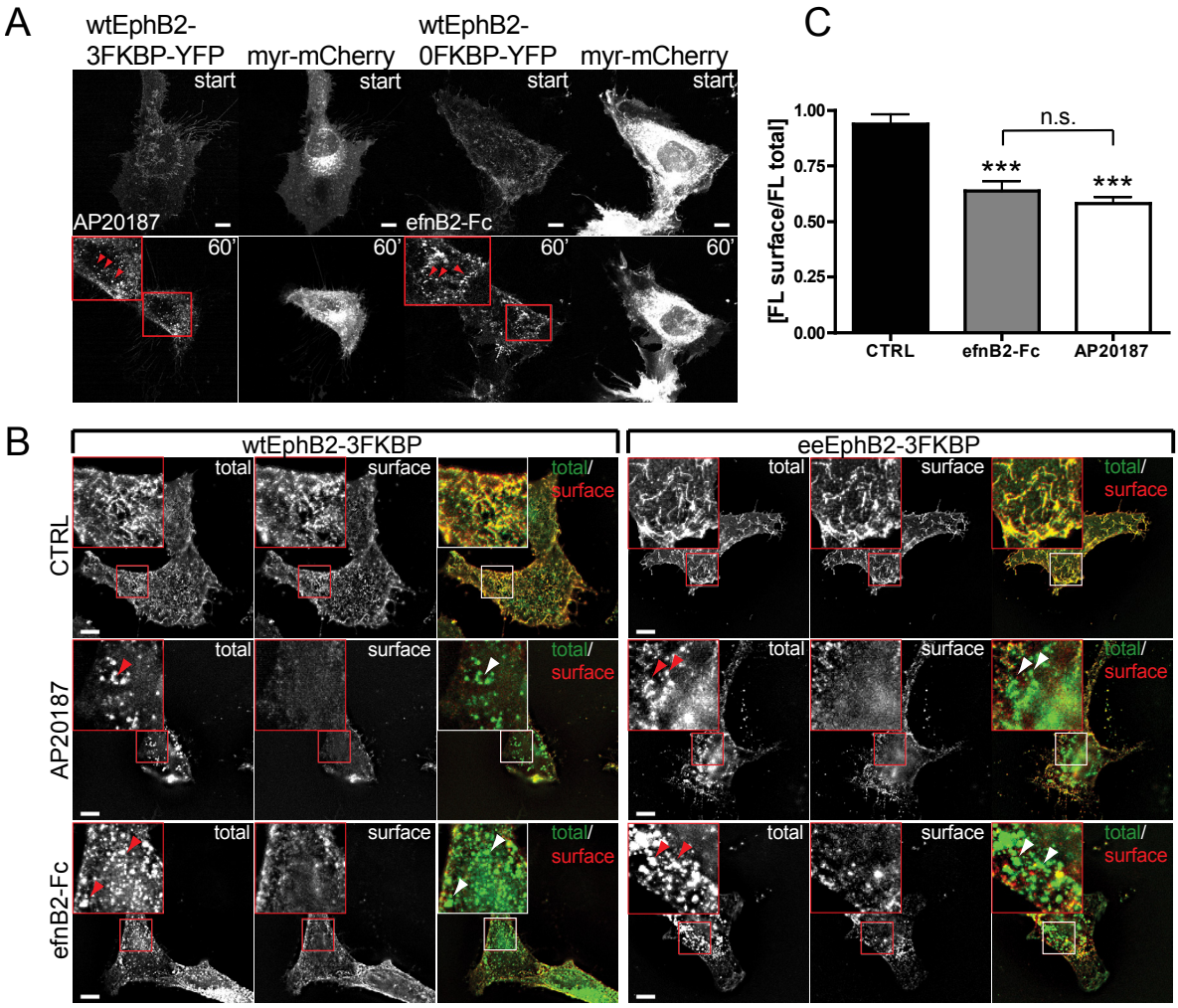

Fig. 3.18 Dimerizer-induced clustering is sufficient to induce receptor internalization.
(A) Confocal time-lapse to visualize for Eph receptor internalization upon stimulation with ephrinB2-Fc or AP20187 in transfected HeLa cells as indicated. Distinct FL foci appear 60 min after stimulation away from the cell edge (arrows in blowups), indicating internal vesicles loaded with EphB2 receptors. For better visualization and comparison, HeLa cells were co-transfected with myr-mCherry, which did not show the formation of FL foci (see also supplementary video 1). **(B)** Immunostaining to test for internalization upon stimulation with ephrinB2-Fc or AP20187. HeLa cells transiently expressing [wt/ee]EphB2-3FKBP receptors (carrying EYFP) were either mock stimulated (CTRL: Fc/EtOH), stimulated with 2 µg/ml preclustered ephrinB2-Fc or 250 nM AP20187 for 90 min, then fixed without permeabilization and stained for surface EphB2 with anti-FLAG antibodies. YFP clusters, which do not co-localize with anti-FLAG staining (green in the merge), represent intracellular clusters. Yellow or red clusters in the merge represent surface clusters. Qualitatively, there was no difference in the internalization response between wildtype and constitutively kinase-active Eph receptors. Image acquisition and processing: 7x 0.2 µm z-stacked epiFL images; odc; adaptive-blind psf deconvolution; maximum-projection). **(C)** Wildtype receptor internalization was quantified by the mean ratio of FL intensity (surface/total) ± SEM from clustered sub-cellular regions of n≥ 5 cells. (*** p< 0.001; n.s., not significant; one-way ANOVA with posthoc Bonferroni test).

Together these results indicate that i) a mix of clusters with predominantly EphB2 trimers (cp. Fig. 3.10) is physiologically active, (ii) there is a positive correlation between the degree of EphB2 clustering and the strength of the response.

I also analyzed the effects of the low-affinity dimerizer AP1887, which may lead to similarly complex, yet less stable clusters with decreased cohesiveness between the monomeric elements. Compared to AP20187, the AP1887-induced cell collapse response was slower, weaker and of different response quality with flattened response curves (Fig. 3.19C). They resemble the response curves elicited with the low-affinity ligand ephrinA5-Fc [70], which are also weaker than those triggered by ephrinB2-Fc, ephrinB3-Fc or an anti-EphB2 antibody (Fig. 3.19D). These externally binding stimuli differ in their respective affinities towards the Eph LBD [70,96]. As with AP1887-induced clustering, they may provoke the constitution of clusters of different stability, which directly translates into the respective cellular response pattern. These results suggest that the stability or turnover of EphB2 clusters also determine the strength of the cellular response.

Fig. 3.19 Correlation between EphB2 cluster size and strength of cellular response.
(A) Images of representative HeLa cells in BF and FL, expressing equal and moderate levels of wtEphB2 carrying 0 to 3 FKBP domains, before and after stimulation with 250 nM AP20187. Cell collapse was scored by measuring the cell's surface area (red circles around cells, see Methods). Curve graph: changes in mean cell area ± SEM from n= 10 cells for each isoform over time (in percent relative to the start of the experiment) induced by AP20187 ($p< 0.01$ for 0FKBP/1FKBP, $p< 0.001$ for all other curves, Mann-Whitney nonparametric *t*-test). Bar graph: changes in collapse amplitude (minimal surface area in percent relative to start of experiment) of cells within 40 min after stimulation (mean cell area ± SEM from n= 30 cells for each isoform; ** $p< 0.01$, Student's *t*-test). Scale bars, 10 µm. **(B)** Quantification of cell collapse responses of cells expressing wtEphB2-3FKBP-YFP induced simultaneously by equal concentrations of AP20187 (250 nM) and AP21967 in concentrations as indicated. As a control, cell collapse from untransfected cells (UNT) was measured upon AP20187 (250 nM) addition. (mean cell area ± SEM from n= 8 cells for condition 5 nM AP21967, n= 10 for conditions UNT, 10 nM AP21967, no AP21967; * $p< 0.05$, *** $p< 0.001$; Mann-Whitney nonparametric *t*-test; asterisks in red indicate significance level to UNT control). **(C)** Quantification of cell collapse responses of cells expressing the wtEphB2-3FKBP or eeEphB2-3FKBP isoform induced by the low-affinity dimerizer AP1887 compared to AP20187 (each 250 nM; mean cell area ± SEM from n= 17, 16, 12 cells for conditions AP20187, AP1887, CTRL; $p< 0.001$ for all curves, Mann-Whitney nonparametric *t*-test). Note that the response induced by AP1887 is slower, weaker and more flattened. The constitutively kinase-active ee mutant exhibits a smaller total collapse amplitude. **(D)** Quantification of cell collapse responses of cells expressing wtEphB2 induced by equal concentrations (2 µg/ml) of preclustered ephrinB2-Fc and ephrinB3-Fc compared to the low-affinity ligand ephrinA5-Fc and ectodomain-specific anti-EphB2 antibody (11.1 µg/ml). As a control, cell collapse from untransfected cells (UNT) was measured upon efnB2-Fc stimulation. (mean cell area ± SEM from n= 13, 14, 15, 11, 8 cells for conditions efnB2-Fc, efnB3-Fc, efnA5-Fc, anti-EphB2, UNT/efnB2-Fc; significance level for time period 0-40 min, * $p< 0.05$, ** $p< 0.01$; Mann-Whitney nonparametric *t*-test).

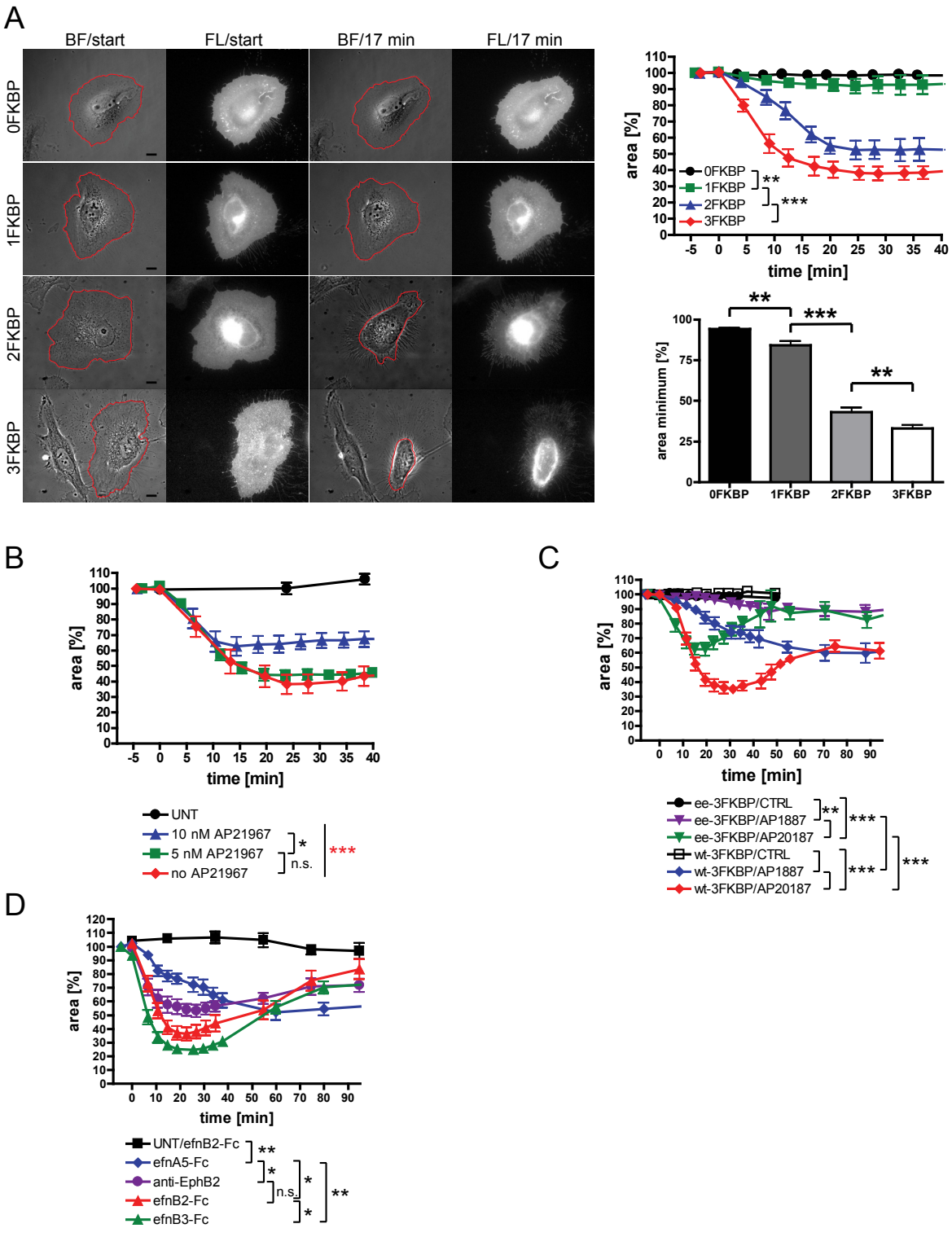
A
BF/start
FL/start
BF/17 min
FL/17 min
0FKBP
1FKBP
2FKBP
3FKBP
area [%]
time [min]
0FKBP
1FKBP
2FKBP
3FKBP
**
***
area minimum [%]
B
UNT
10 nM AP21967
5 nM AP21967
no AP21967
n.s.
C
ee-3FKBP/CTRL
ee-3FKBP/AP1887
ee-3FKBP/AP20187
wt-3FKBP/CTRL
wt-3FKBP/AP1887
wt-3FKBP/AP20187
D
UNT/efnB2-Fc
efnA5-Fc
anti-EphB2
efnB2-Fc
efnB3-Fc

In parallel, constitutively kinase-active eeEph receptors were tested for their propensity to cause cell collapse upon clustering with dimerizer agents (Fig. 3.19C). Surprisingly, for eeEphB2, AP1887 or AP20187, stimulation still produced a marked collapse response with similar kinetics, yet decreased absolute collapse magnitude as compared to wtEphB2. These results support the notion that Eph clustering is a critical parameter in Eph signaling, even for receptor mutants with an enhanced kinase-active state.

Taken together, these results indicate that clustering not only seems to be a mere signaling step for Ephs but even more a sensitive determinant in eliciting graded cellular responses as seen for [0-3]FKBP/AP20187-induced and 3FKBP/AP20187/AP21967-induced clustering. Moreover, the quality, i.e. stability of clusters plays a crucial role in provoking unique cell collapse response patterns as observed for dimerizer AP1887 or external stimuli like ephrinA5-Fc.

Fig. 3.20 Eph clustering correlates with receptor activation in single cells.
(A) Representative FL images from immunostainings of HeLa cells expressing YFP-tagged wtEphB2-[0-3]FKBP isoforms used for quantification in (B). Cells were stimulated with control stimuli (CTRL) and dimerizer AP20187 (250 nM), AP1887 (250 nM) or preclustered ephrinB2-Fc (2 µg/ml) for 30 min. After fixation and permeabilization, cells were stained with a primary phospho-specific anti-EphB antibody and a Cy3 secondary antibody and imaged. FL YFP shows total receptor protein, whereas FL anti-phospho Y594 labels the fraction of phosphorylated protein. Image acquisition and processing: 12x 0.2 µm z-stacked epiFL images; odc; adaptive-blind psf deconvolution; maximum-projection; equal scaling over all FL YFP and FL phospho images. Scale bar, 10 µm. **(B)** Quantification of EphB2 activation by immunostaining of individual transfected cells. Bar graph displays mean ratio ± SEM of phosphorylated versus total EphB2 protein (YFP-tag) over n= 25- 46 HeLa cells (FL intensity total protein <2000 [a.u.]) per condition tested as indicated. (* $p < 0.05$, ** $p < 0.01$, *** $p < 0.001$, n.s., not significant; one-way ANOVA with post-hoc Tukey-Kramer test; asterisks in red represent significance level to Fc/EtOH control stimulation of each individual data set).

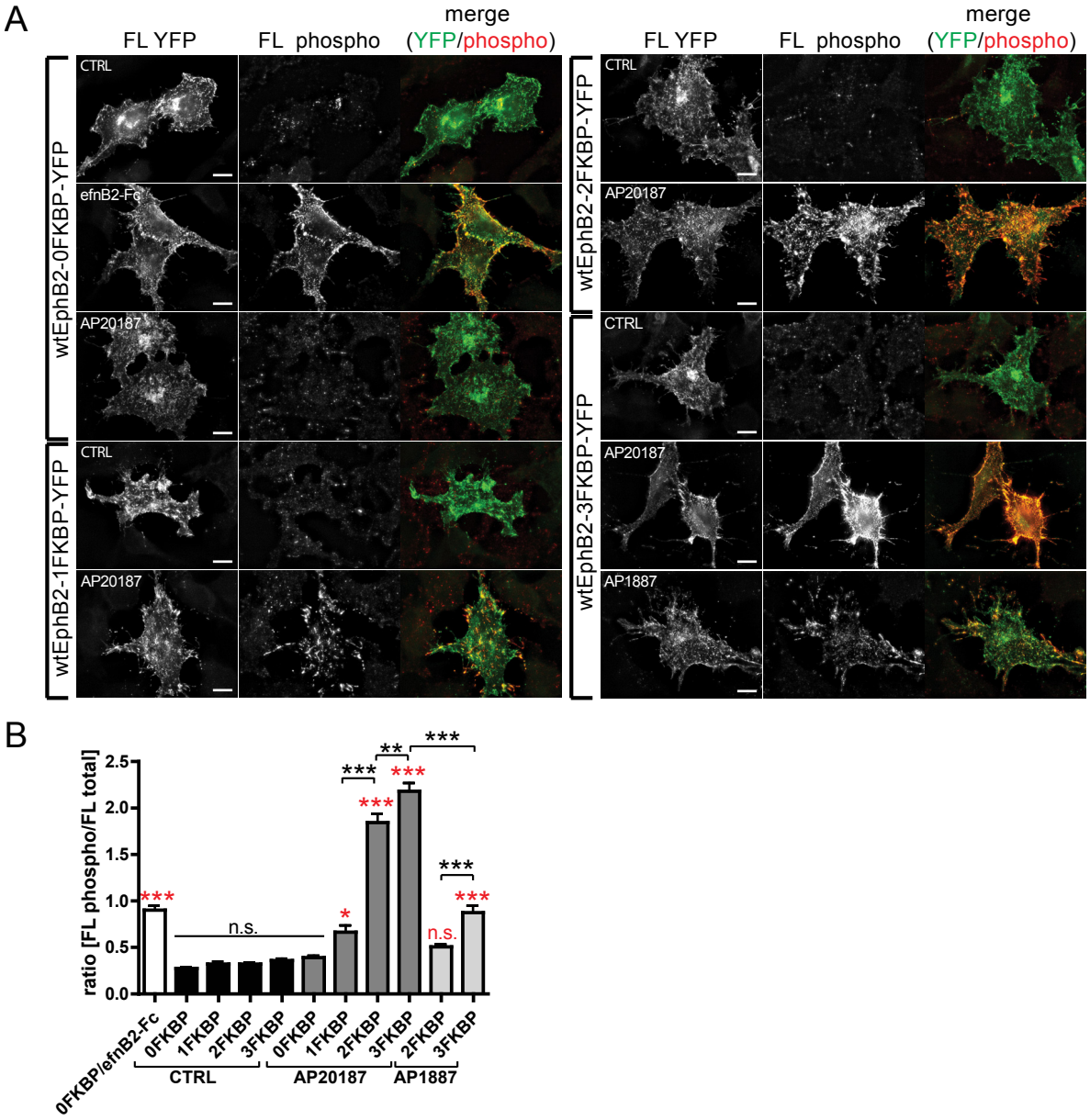

3.5.2 Eph clustering correlates with receptor activation and kinase activity

Remarkably, Eph clustering strictly correlates to cell collapse, which marks the ultimate functional cellular readout at the end of the Eph signaling cascade. It seemed therefore reasonable to also analyze the signaling vertices in between clustering and the cellular collapse response.

Starting with receptor activation at the single cell level, I stained for phosphotyrosine in Eph receptor isoform-expressing HeLa after conditioning the cells with the respective stimuli for 30 min (Fig. 3.20.A). Eph expression levels in single cells are accounted for by normalization

to total Eph receptor expressed (measured from FL signals) giving the relative Eph phosphorylation state per cell. Upon AP20187 stimulation, there was a positive correlation between the number of inserted FKBP domains and the EphB2 autophosphorylation state (Fig. 3.20A,B). AP1887 stimulation gave rise to low autophosphorylation levels for 3FKBP receptors, significantly differing from control but much weaker as compared to an AP20187 stimulation. Surprisingly, preclustered ephrinB2-Fc did not cause the same level of activation as compared to [2,3]FKBP receptor isoforms clustered with AP20187 in this assay. Interestingly, receptor activation did not significantly depend on Eph receptor densities, as measured by total FL intensities (data not shown).

Next, I determined EphB2 autophosphorylation of whole cell populations by immunoblotting. Stimulation with saturating doses of AP20187 (250 nM) modestly increased autophosphorylation of EphB2-1FKBP isoforms (Fig. 3.21A). Increasing numbers of FKBP domains also increased EphB2 autophosphorylation to levels equal or higher than those obtained with preclustered ephrinB2-Fc (Fig. 3.21A). A time course of EphB2 autophosphorylation carrying two or three FKBP domains revealed similar kinetics, but overall slightly higher and sustained autophosphorylation levels in 3FKBP compared to 2FKBP isoforms (Fig. 3.21B).

To determine the relative contribution of different Eph cluster sizes to the pool of activated receptors, I analyzed the phosphorylation levels of single oligomeric species using blue-native PAGE. The cluster size distribution pattern of wildtype EphB2 was similar to kd EphB2 (Fig. 3.21C cp. to Fig. 3.10A). EphB2 monomers across all isoforms displayed baseline autophosphorylation, whereas EphB2 dimers were markedly and similarly higher phosphorylated (Fig. 3.21C, bar graph). Surprisingly, trimers and tetramers saturated at levels ~2-fold over the autophosphorylation level displayed by EphB2 dimers. Hence, the higher and sustained autophosphorylation levels that I observed in the 3FKBP isoform are due to the shift from hypophosphorylated EphB2 dimers to fully phosphorylated oligomers.

Next, I tested if the reduced effectiveness of the low-affinity dimerizer AP1887 correlated with reduced EphB2 autophosphorylation. AP1887 stimulation caused the pool of activated receptors to increase slowly over time but eventually resulted in a similar abundance of activated receptors - as observed for AP20187 stimulation (Fig. 3.21D). Since activation of Ephs is autocatalytic, i.e. autophosphorylation results in Eph kinase activation, I conclude that AP1887 is less effective in this autocatalytic activation.

In blue-native PAGE, AP1887-induced higher-order clusters could not be detected most likely due to weak cohesiveness between receptor molecules (cp. Fig. 3.11B). However, in AP1887-stimulated cell lysates, autophosphorylation levels of EphB2 monomers were slightly elevated as compared to control (Fig 3.21E), indicating that AP1887-induced clustering forms at least transient interactions, which are sufficient to activate a small pool of receptor molecules. These results suggest that cluster quality or stability in addition to cluster size plays a role in receptor activation.

In analogy to the cell collapse assay using different external stimuli like ephrins and the anti-EphB2 antibody (cp. Fig. 3.19D), receptor activation was assessed through detection of autophosphorylation as done before (Fig 3.21F). Whereas preclustered ephrinB2-Fc and ephrinB3-Fc activated approximately the same pool of receptors, preclustered ephrinA5-Fc and anti-EphB2 antibody did not succeed in doing so.

To uncouple the intrinsic kinase/substrate bivalency of Ephs and to study kinase activity directly, I employed a substrate phosphorylation assay [113]. Since this assay is based on the related EphA4 receptor which also binds ephrinB ligands [321], I constructed EphA4-2FKBP and -3FKBP isoforms. I carried out a cell collapse assay for wtEphA4-3FKBP-YFP transfected HeLa stimulated with AP20187 to verify that these isoforms behave similarly to EphB2 in physiological activity (Fig. 3.22A). Receptor activation was tested by immunoblotting for autophosphorylation of the JM tyrosines (Fig. 3.22B). Since in eeEphA4-[2,3]FKBP-YFP Tyr604 and Tyr610 residues are mutated to glutamate, the JM tyrosine phospho-specific antibody failed to detect them. Substrate phosphorylation levels of cells transiently expressing 2 or 3FKBP wt isoforms, stimulated with ephrinB3-Fc were similarly increased (Fig. 3.22C). By contrast, dimerizer-induced clustering of the 3FKBP isoform caused stronger substrate phosphorylation than the 2FKBP isoform. For eeEphA4 receptor isoforms baseline substrate phosphorylation from control stimulated conditions was significantly increased as compared to wt constructs. This was due to the constitutive kinase activity of eeEphA4 receptors. Surprisingly, kinase activity can still be enhanced by clustering with either ephrinB3-Fc or AP20187. However, there is no difference in substrate phosphorylation between 2FKBP and 3FKBP isoforms stimulated with AP20187 dimerizer. Kinase activity, which may still be enhanced by induction of higher-order cluster size distributions through AP-induced clustering of 2 to 3 FKBP wt receptor isoforms, remained steady in the case of eeEphA4 isoforms.

This result indicates that eeEphA4 receptors are indifferent towards higher-order cluster sizes in respect to their kinase activity. In consequence, eeEphA4 receptors in contrast to wtEphA4 show a loss in signaling sensitivity towards surrounding clustering determinants.

Fig. 3.21 Eph clustering correlates with receptor activation in whole cell populations.
(A) Western blot of anti-FLAG immunoprecipitated EphB2-FKBP isoforms (with 0 to 3 FKBP domains as indicated) using anti-phosphoEphB2 antibodies; blots were stripped and reblotted for total EphB2 protein levels. Autophosphorylation analysis of cells stimulated with Fc/EtOH control or AP20187 (250 nM, t= 20 min) indicates a positive correlation between the fraction of autophosphorylated EphB2 (numbers below IP-blot) and the number of FKBP domains relative to a positive control stimulation with 2 µg/ml of preclustered ephrinB2-Fc. Scatter graph: quantification of phosphorylation (n= 3-4 experiments) relative to the positive control stimulation with 2 µg/ml of ephrinB2-Fc. Note, that AP20187 stimulation of the 1 FKBP isoform causes EphB2 autophosphorylation that is about 13-40 % of preclustered ephrinB2-Fc. **(B)** Representative time course of activation of EphB2 carrying 2 or 3 FKBP constructs. Experiment and quantifications were done as in (A). Note that phosphorylation levels of the 3FKBP construct are higher than the 2FKBP construct over all time points (graph and numbers below IP-blot). **(C)** Phosphorylation analysis of single EphB2 oligomeric species. Blue-native PAGE of lysates of COS-7 cells expressing different FKBP isoforms of wtEphB2 and stimulated with either vehicle (-) or AP20187 (250 nM for 20 min). Western blot was performed with anti-phospho-EphB2 antibodies (left blot); blots were stripped and reblotted for total EphB2 protein (right blot). EphB2 oligomers are indicated with numbers (1, monomers; 2, dimers; etc.). Bar graph: quantification of relative phosphorylation levels (± SEM, from n= 2 blots) of single oligomeric species sorted to different FKBP isoforms. All EphB2 monomers (irrespective of the number of FKBP domains present) exhibited only a small fraction of autophosphorylated receptors. EphB2 dimers were hypophosphorylated relative to trimers and tetramers. **(D)** Time course of EphB2 autophosphorylation induced by the low-affinity dimerizer AP1887. Experiment and quantifications (graph and number below blot) were done as in (A). EphB2-3FKBP-expressing cells were incubated with AP1887, AP20187 (at both 10 nM and 250 nM), or preclustered ephrinB2-Fc for 10 or 20 min. Note that the kinetics of EphB2 autophosphorylation is slower for AP1887 compared to AP20187 (in the case of both concentrations). After 20 min, 250 nM AP1887 is as effective as AP20187, and ephrinB2-Fc (2 µg/ml). **(E)** Phosphorylation analysis of the EphB2 monomeric species from stimulation with AP1887. Blue-native PAGE of lysates of COS-7 cells expressing the 3FKBP isoform of wtEphB2, stimulated with either vehicle (CTRL) or AP1887 (250 nM for 20 min). Western blot was performed as described in (C); AP1887-induced Eph complexes are not stable enough to be resolved in blue-native PAGE and appear as monomeric species hyperphosphorylated as compared to CTRL monomeric species. Graph: quantification of relative phosphorylation levels from 2 blots. Values are normalized to CTRL (= 1.0). **(F)** Western blot of total lysates from EphB2-YFP-expressing HeLa cells stimulated (t= 20 min) with preclustered ephrinX-Fc (2 µg/ml) and anti-EphB2 (11.1 µg/ml) antibody as indicated. Anti-phospho-EphB2 antibodies to detect receptor autophosphorylation and anti-Tubulin antibodies to ensure equal load per lane were used. Blots were stripped and reblotted for total EphB2 protein levels. Autophosphorylation analysis was done as described in (A) and indicates differences in the fraction of activated receptors upon different external stimuli (numbers below blot). For phosphorylation analysis of all blots, all levels were normalized to the ephrinB2-Fc stimulation condition (t= 20 min; 2 µg/ml) to give the arbitrary value of 1.0.

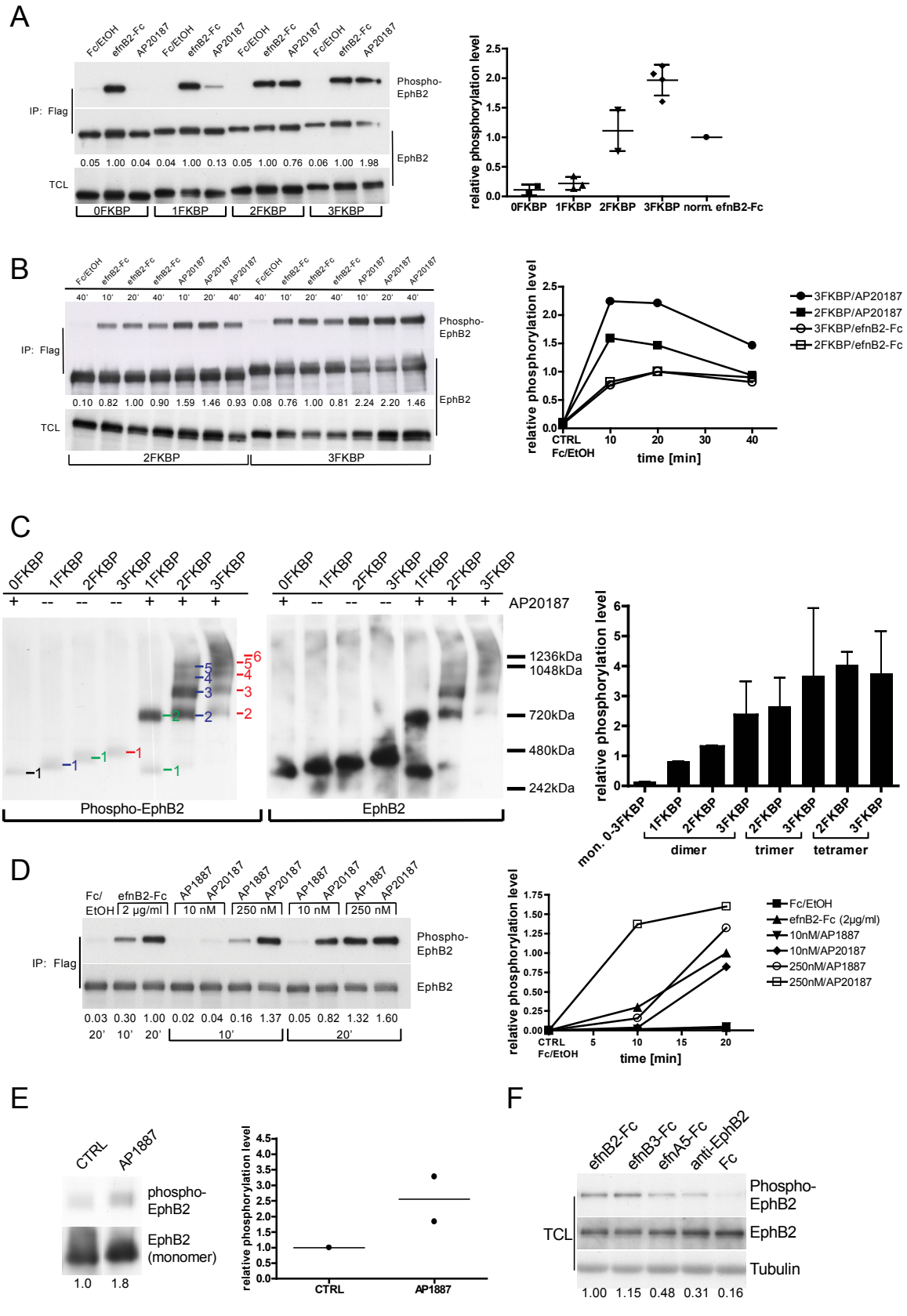
A
Fc/EtOH
efnB2-Fc
AP20187
Phospho-EphB2
IP: Flag
EphB2
TCL
0.05 1.00 0.04 0.04 1.00 0.13 0.05 1.00 0.76 0.06 1.00 1.98
0FKBP
1FKBP
2FKBP
3FKBP
relative phosphorylation level
0FKBP 1FKBP 2FKBP 3FKBP norm. efnB2-Fc
B
0.10 0.82 1.00 0.90 1.59 1.46 0.93 0.08 0.76 1.00 0.81 2.24 2.20 1.46
time [min]
CTRL Fc/EtOH
3FKBP/AP20187
2FKBP/AP20187
3FKBP/efnB2-Fc
2FKBP/efnB2-Fc
C
AP20187
1236kDa
1048kDa
720kDa
480kDa
242kDa
Phospho-EphB2
EphB2
mon. 0-3FKBP
dimer
trimer
tetramer
D
Fc/ EtOH
efnB2-Fc 2 µg/ml
AP1887
AP20187
10 nM
250 nM
0.03 0.30 1.00 0.02 0.04 0.16 1.37 0.05 0.82 1.32 1.60
20' 10' 20' 10' 20'
Fc/EtOH
efnB2-Fc (2µg/ml)
10nM/AP1887
10nM/AP20187
250nM/AP1887
250nM/AP20187
E
CTRL
AP1887
phospho-EphB2
EphB2 (monomer)
1.0 1.8
F
efnB2-Fc
efnB3-Fc
efnA5-Fc
anti-EphB2 Fc
Tubulin
1.00 1.15 0.48 0.31 0.16

Fig. 3.22 Eph clustering correlates with receptor kinase activity.
(A) Fluorescence time-lapse imaging of HeLa cells transiently expressing wtEphA4-3FKBP receptors (carrying YFP) in the presence of AP20187. Cells show the same response pattern as presented in Fig. 3.7. Images for start (immediately before stimulation), ~21 min and ~54 min are displayed in BF and FL channels. Co-expressed, myristoylated mCherry was used for better visualization of the cell during time-lapse imaging. Scale bars, 10 µm. **(B)** Western blot analysis of total lysates from [wt/ee]EphA4-[2,3]FKBP-YFP transfected HeLa to test for proper residue exchange from tyrosine to glutamate. Upon stimulation with control, ephrinB3-Fc (2 µg/ml) or AP20187 (250 nM) for 40 min constitutively kinase-active eeEphA4 was not autophosphorylated, as expected and shown by probing with a JM phosphotyrosine specific EphA4 antibody. AP20187 induced clustering was sufficient to activate wtEphA4 receptors as shown for EphB2. **(C)** Western blot of exogenous substrate phosphorylation by wildtype and constitutively active EphA4 (eeEphA4). The exogenous EphA4 substrate (JMA4-GST) consists of Glutathione S-transferase (GST) and the JM segment of EphA4 [113]. HeLa cells were transfected with JMA4-GST alone, or together with [wt/ee]EphA4-[2,3]FKBP. Cells were stimulated with either control stimuli (Fc/EtOH), preclustered ephrinB3-Fc or AP20187 for 40 min. JMA4-GST was immunoprecipitated from cell lysates and probed with anti-phosphotyrosine (clone 4G10) antibodies or anti-GST antibodies. Overall levels of EphA4 and Tubulin are shown as indicated. Numbers in blots and graph indicate relative substrate phosphorylation levels quantified from blots with unsaturated exposure normalized to ephrinB3-Fc stimulation. Lower band in JMA4-GST blot is likely to be endogenous GST (**), since it is also present in untransfected cells. Clustering by ephrinB3-Fc or AP20187 led to a further increase in substrate phosphorylation. Differences in kinase activity between eeEphA4-2/3FKBP are very small as compared to wtEphA4-2/3FKBP (for visualization see bar graph).

3.5.3 Dimerizer-induced Eph clusters cause growth cone collapse in neurons

Next, we asked if dimerizer-induced EphB2 clusters were able to trigger physiological cell responses such as growth cone collapse (GCC) in neurons (in collaboration with Irina Dudanova). Kinase-active EphB2 receptors carrying 3 FKBP domains were over-expressed in primary rat hippocampal neurons and dimerizer-induced GCC was measured. To do so, I constructed EphB2 isoforms lacking most of the ectodomain including the Eph receptor LBD (ΔNEphB2-3FKBP, Fig. 3.23A), because over-expression of full-length EphB2-3FKBP was not tolerated by primary neurons (cp. Fig. 3.5). ΔNEphB2 carrying 3 FKBP caused the same cell response pattern upon stimulation with AP20187 as compared to full-length EphB2-3FKBP (Fig. 3.23E) and also displayed normal activation and autophosphorylation (Fig. 3.23B). Neurons expressing ΔNEphB2-3FKBP in the absence of AP20187, or expressing ΔNEphB2 lacking FKBP domains, were indistinguishable from neurons transfected with a control YFP plasmid (Fig. 3.23C). AP20187 caused GCC of neurons expressing the 3FKBP, but not 0FKBP isoforms, to a similar extent as bath applied preclustered ephrinB2-Fc (Fig 3.23C,D). The low-affinity dimerizer AP1887 significantly increased the fraction of fully collapsed growth cones, but to a lesser extent than AP20187 (Fig. 3.23D). These results indicate that dimerizer-induced EphB2 clusters elicit physiological responses in neurons and further suggest that cluster stability or turnover determines the robustness of the response.

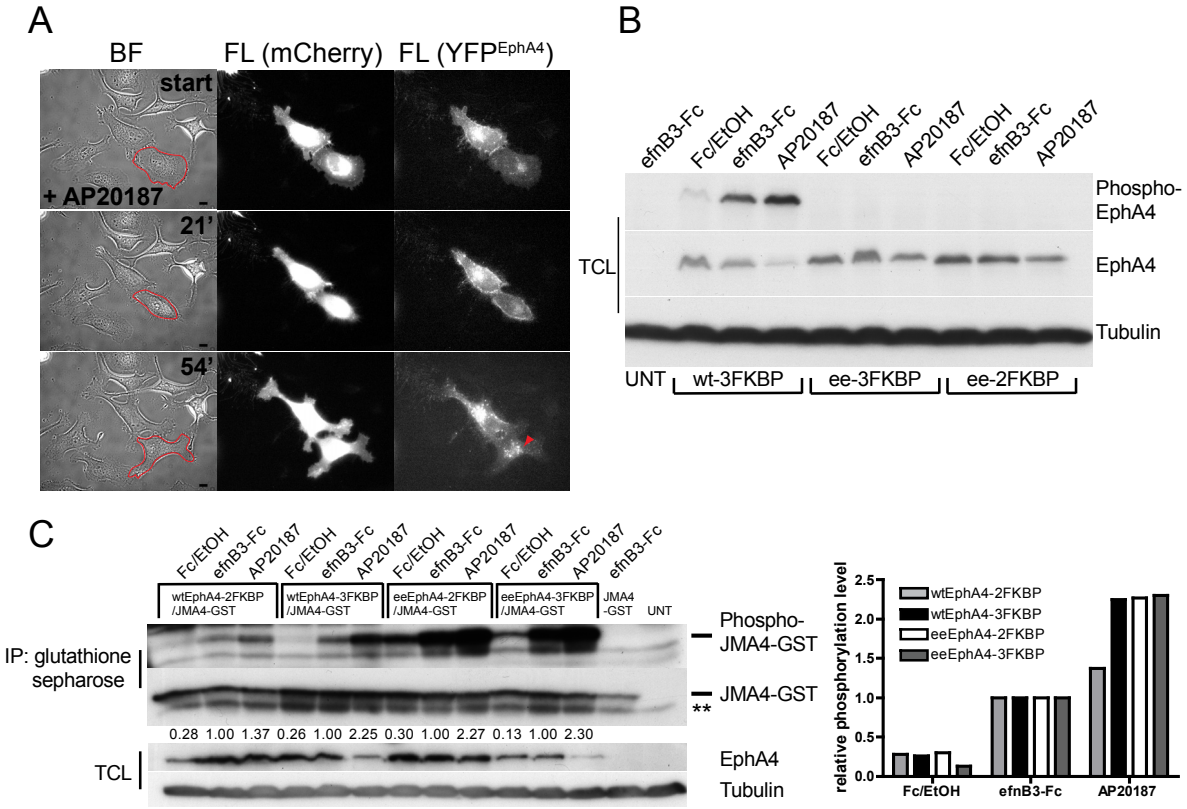

Altogether these findings about correlation of clustering to cellular responses suggest that the composition of higher-order clusters controls the Eph signaling cascade from autophosphorylation to substrate phosphorylation and that these biochemical differences underlie the observed graded physiological responses. Moreover, cluster quality or stability has a tremendous effect on the resulting cellular responses.

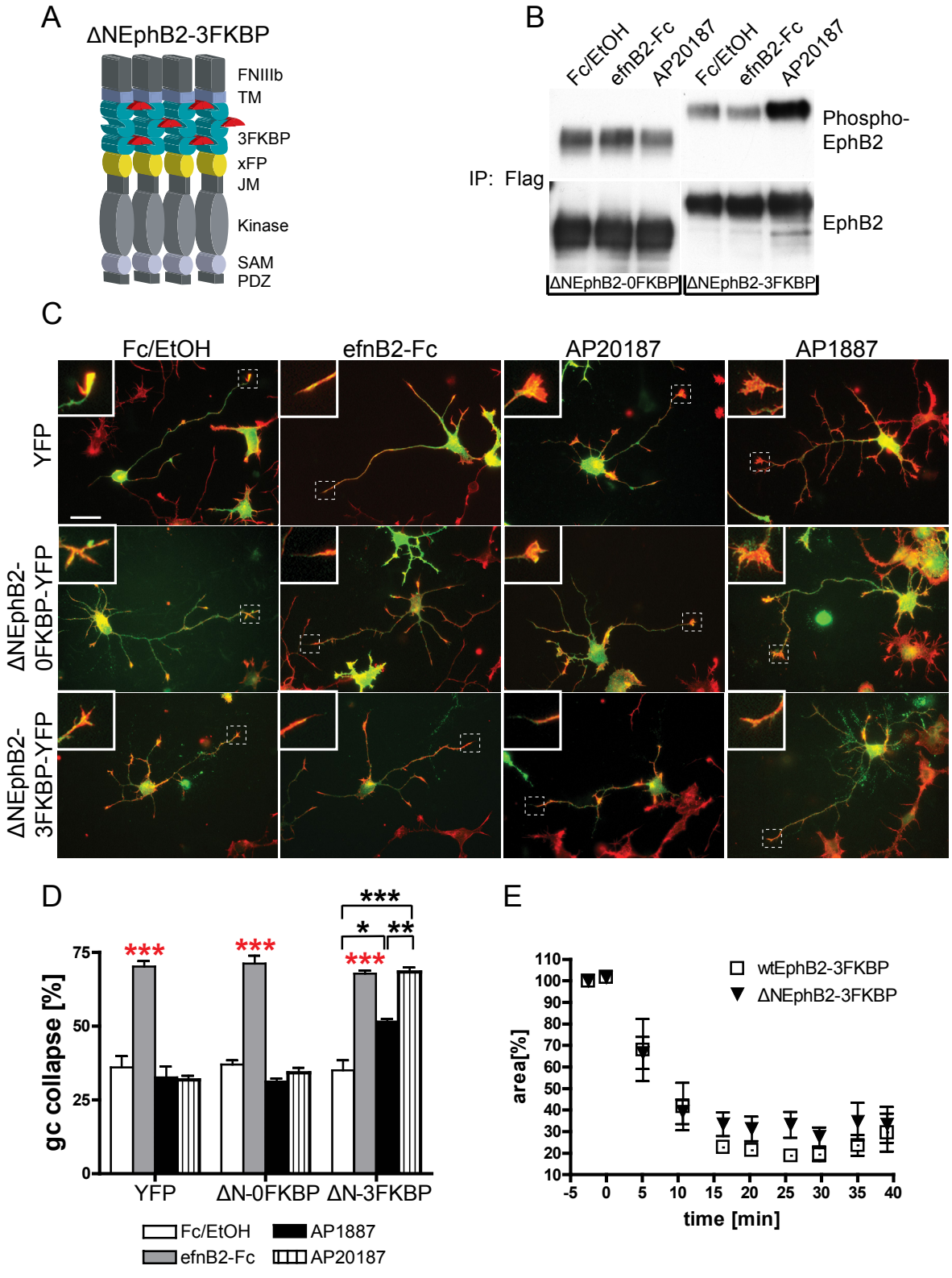
A
ΔNEphB2-3FKBP
FNIIIb
TM
3FKBP
xFP
JM
Kinase
SAM
PDZ
B
Fc/EtOH
efnB2-Fc
AP20187
Fc/EtOH
efnB2-Fc
AP20187
Phospho-EphB2
IP: Flag
EphB2
ΔNEphB2-0FKBP
ΔNEphB2-3FKBP
C
Fc/EtOH
efnB2-Fc
AP20187
AP1887
YFP
ΔNEphB2-0FKBP-YFP
ΔNEphB2-3FKBP-YFP
D
gc collapse [%]
75
50
25
0
***
***
***
***
**
YFP
ΔN-0FKBP
ΔN-3FKBP
Fc/EtOH
efnB2-Fc
AP1887
AP20187
E
area[%]
110
100
90
80
70
60
50
40
30
20
10
wtEphB2-3FKBP
ΔNEphB2-3FKBP
-5
0
5
10
15
20
25
30
35
40
time [min]

Fig. 3.23 Dimerizer-induced EphB2 clusters cause growth cone collapse in neurons.
(A) Domain structure of ΔNEphB2-3FKBP lacking the complete ectodomain except for the proximal FNIII domain (N-terminal signal peptide and FLAG epitope are not indicated). **(B)** Western blot of anti-FLAG-immunoprecipitated ΔNEphB2 with or without 3 FKBP domains probing against phospho-EphB2. Cells were previously stimulated either with control stimuli (Fc/EtOH), 2 µg/ml preclustered ephrinB2-Fc or 250 nM AP20187. An increase in EphB2 autophosphorylation over background is only seen after AP20187 stimulation of the 3FKBP isoform. EphrinB2-Fc is inactive due to the deletion of the Eph receptor LBD. Blot was stripped and reblotted with anti-EphB2 antibodies. **(C)** Dimerizer-induced growth cone collapse (GCC) of E18 rat hippocampal neurons (1 day in vitro). Neuronal cultures were either transfected with YFP, ΔNEphB2-0FKBP, or ΔNEphB2-3FKBP (all carrying a FLAG epitope tag), and stimulated with either control stimuli (Fc/EtOH), 2 µg/ml ephrinB2-Fc, or 250 nM AP20187 for 30 min, then fixed and stained with anti-GFP antibodies (green), and phalloidin (red) to visualize f-actin rich growth cones. Only the status of growth cones of the longest neurites (the axon) was quantified. Insets, indicated by stippled boxes, show growth cones. Scale bar, 30 µm. **(D)** Quantification of total GCC (mean ± SEM in percent of all growth cones counted). EphrinB2-Fc induced GCC in all cultures. AP20187 is as efficient as ephrinB2-Fc in inducing GCC in neurons expressing the 3FKBP isoform, whereas stimulation with AP1887 leads to an intermediate response (n= 3 experiments, *** p< 0.001, ** p< 0.01, * p< 0.05, Student's *t*-test; asterisks in red represent significance level to Fc/EtOH control stimulation of each data set). **(E)** Cell collapse assay comparing cells expressing 3FKBP isoforms of ΔNEphB2 or full-length EphB2. Cell responses do not significantly differ from each other (mean cell area ± SEM of n=5 and n=9 cells of full-length EphB2 and ΔNEphB2 cells respectively; p= 0.27, Mann-Whitney nonparametric *t*-test). **Data and analysis from panels (D) and (E) were contributed by Irina Dudanova.**

3.6 Eph receptor clustering is an integrator of signaling

3.6.1 Intracellular clustering determinants synergize with extracellular ephrins

Dimerizer-induced Eph clustering occurs intracellularly and may resemble intracellular mechanisms of Eph clustering, which can occur when scaffolding proteins interact via the PDZ-binding motif [151,251]. This prompted me to test whether extracellular ephrins would synergize with intracellular clustering mechanisms. I over-expressed EphB2 carrying a single FKBP domain in cells and stimulated with either AP20187 or sub-threshold doses of unclustered ephrinB2-Fc, or both (Fig. 3.24A). Mere dimerization by AP20187 caused on average a 2.3-fold higher fraction of activated receptor species (Figure 3.24.B). Sub-threshold doses of unclustered ephrinB2-Fc did not increase EphB2 autophosphorylation. However, co-stimulation with AP20187 and ephrinB2-Fc had a synergistic effect on EphB2 activation (Fig. 3.24B). This synergistic effect on receptor activation was also visible in cell collapse responses (Fig. 3.24C,D). Simultaneous application of both sub-threshold ephrinB2-Fc and AP20187 dimerizer led to a pronounced cell collapse response by about 40% of the initial cell surface area, whereas stimulation with sub-threshold ephrin was indistinguishable from control. AP20187 stimulation alone caused only a mild collapse response as already described earlier (cp. Fig. 3.19A).
Next, I tested if PDZ-adaptor proteins like GRIP1, GRIP2 and PICK1, which are known to bind EphB2 [151], would act in the same way as AP20187-induced dimerization, thereby

priming the cells for an external ephrin stimulus. In presence of PDZ-adaptor proteins, Eph receptor autophosphorylation increased despite the absence of an ephrin stimulus. As a control, co-transfected YFP kept EphB2 autophosphorylation levels at baseline. Autophosphorylation levels could not be significantly increased further by stimulation with ephrinB2-Fc in the case of co-expressed PDZ-adaptor proteins. Taken together, Eph kinase-dependent signaling, which was shown before to solely rely on receptor clustering, can serve as an integrative computational device for various clustering determinants - no matter if they provoke the clustered state of the receptor from the outside or the inside of the cell.

3.6.2 Inhibition of clustering by intracellular determinants antagonizes ephrin-induced responses

Next, I asked if the converse were true, i.e. if intracellular components or components *in cis* that prevent EphB2 from clustering would antagonize ephrinB2-Fc-induced effects. Hence, I co-expressed myr-FRB-mCherry together with wtEphB2-3FKBP-YFP and stimulated the cells with a high-affinity heterodimerizer AP21967, thereby coupling the EphB2-FKBP and FRB domains [312,322] (Fig. 3.25A). The presence of AP21967 prevented ephrinB2-Fc from inducing EphB2 clustering, autophosphorylation, and cell collapse (Fig. 3.25B,C,D).

Fig. 3.24 EphB2 dimerization sensitizes cells towards extracellular ephrinB2.
(A) Model showing possible synergistic response between extracellular (ephrinB2-Fc) and intracellular (dimerizer) clustering determinants. EphB2-1FKBP dimers form in the presence of AP20187. Both ephrin ligand and AP20187 together can form functional oligomers. **(B)** Western blots of anti-Flag immunoprecipitated EphB2-1FKBP over-expressed in HeLa cells probing against anti-phospho-EphB2 antibodies; blot was stripped and re-probed for total EphB2. Cells were previously stimulated with control (EtOH) or AP20187 (250 nM), in the absence or presence of 5 ng/ml (+) or 10 ng/ml (++) unclustered ephrinB2-Fc for 10 min. The fraction of activated Eph receptors was significantly higher, when both AP20187 and ephrinB2-Fc were added. Numbers below the blots indicate fold change in phosphorylation compared to Fc/ethanol control (1.0), normalized to total receptor protein levels (representative blot of 3 separate experiments). **(C)** Images of representative HeLa cells in BF and FL, expressing equal and low levels of wtEphB2 carrying 1 FKBP domain, before and after stimulation with the indicated combinations of stimuli. Cell collapse was scored from cell surface area measurements over time (red circles around cells). **(D)** Quantification of cell collapse responses from (C). (mean cell area ± SEM from n= 9 cells for condition efnB2/EtOH, Fc/EtOH, n= 10 cells for condition +efnb2/AP20187, ++efnB2/AP20187, n= 8, 11 for conditions ++efnB2/EtOH, Fc/AP20187; $p< 0.01$; Mann-Whitney nonparametric *t*-test). **(E)** Western blot of anti-FLAG-immunoprecipitated wtEphB2 probing against phospho-EphB2 and total EphB2 after stripping of the blot. Below, Western blot of total cell lysates (TCL) containing co-expressed proteins YFP, GRIP1, myc-tagged GRIP2 and PICK1 probed with antibodies anti-GFP, anti-GRIP1, anti-myc, anti-PICK1, respectively. Cells were previously stimulated either with control stimuli (Fc), 0.5 µg/ml unclustered ephrinB2-Fc for 10 min. An increase in EphB2 autophosphorylation is only seen when PDZ-adaptor proteins are co-transfected but not for YFP. Stimulation does not significantly enhance autophosphorylation levels of EphB2 when PDZ-adaptor proteins are co-transfected but for YFP. Asterisks in TCL blots indicate antibody-specific bands.

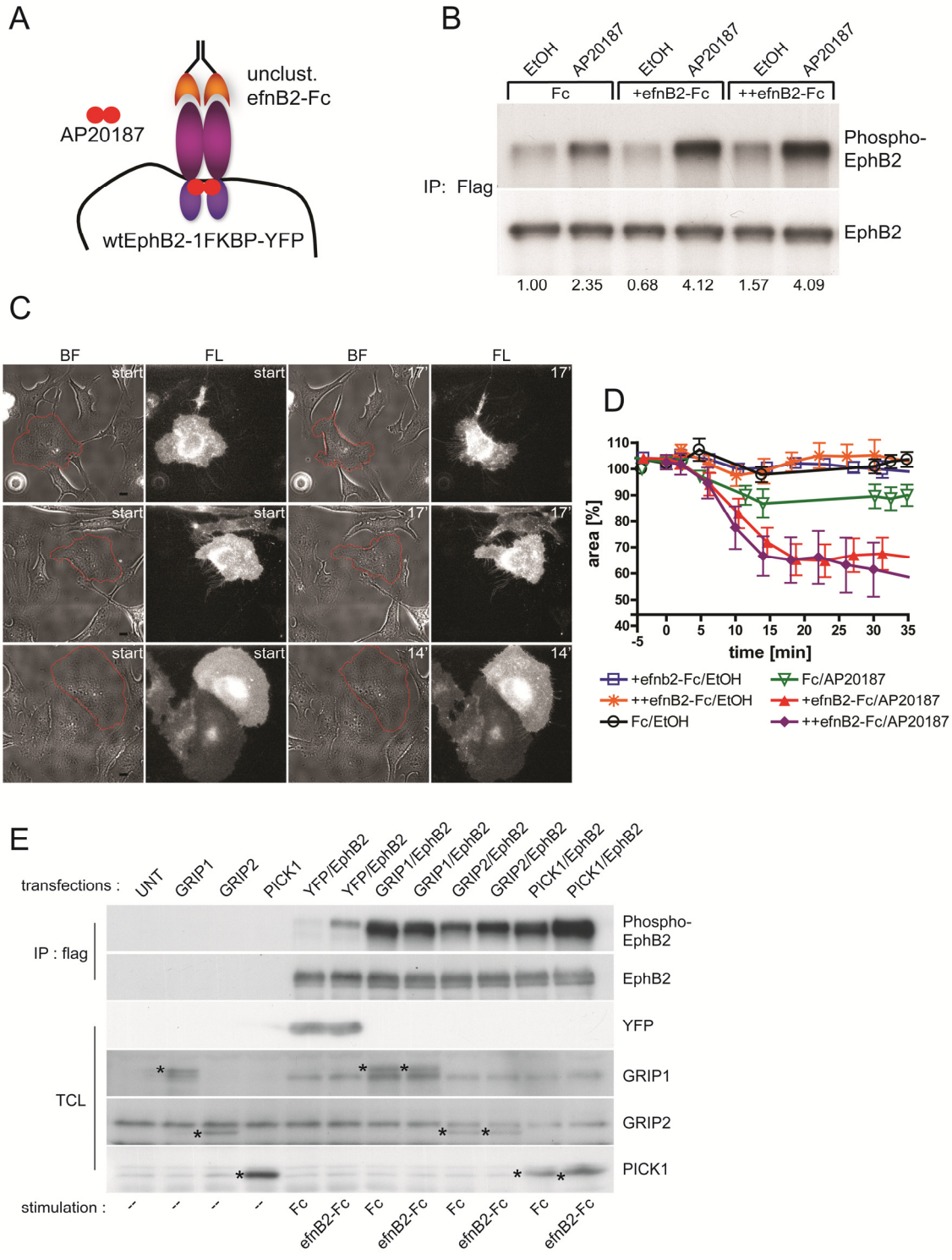
A
unclust.
efnB2-Fc
AP20187
wtEphB2-1FKBP-YFP
B
EtOH
AP20187
EtOH
AP20187
EtOH
AP20187
Fc
+efnB2-Fc
++efnB2-Fc
IP: Flag
Phospho-
EphB2
EphB2
1.00
2.35
0.68
4.12
1.57
4.09
C
BF
FL
BF
FL
+efnB2-Fc/AP20187
+efnB2-Fc/EtOH
Fc/AP20187
start
17'
14'
D
area [%]
time [min]
+efnb2-Fc/EtOH
++efnB2-Fc/EtOH
Fc/EtOH
Fc/AP20187
+efnB2-Fc/AP20187
++efnB2-Fc/AP20187
E
transfections :
UNT
GRIP1
GRIP2
PICK1
YFP/EphB2
YFP/EphB2
GRIP1/EphB2
GRIP1/EphB2
GRIP2/EphB2
GRIP2/EphB2
PICK1/EphB2
PICK1/EphB2
IP : flag
TCL
Phospho-
EphB2
EphB2
YFP
GRIP1
GRIP2
PICK1
stimulation :
Fc
efnB2-Fc

Interestingly, when AP21967 was added about 18 min after stimulation with ephrinB2-Fc, cell collapse came to an abrupt stop (Fig. 3.25E). The cell stopped responding immediately and the cell surface area remained constant over an extended period of time.

AP21967 also changed Eph-ephrin signaling in a cell-cell stimulation assay. In the absence of AP21967, EphB2 clusters, which emerge at the contact site between the two opposing cells, were internalized bi-directionally into both cells and trigger the typical repulsion response (Fig. 3.26A). In the presence of AP21967, however, EphB2 signaling entities remained static at cell edges without being internalized and cell repulsion was converted to an adhesive response (Fig. 3.26B).

Overall, the results from studying integration of clustering determinants indicate that the oligomerization state of EphB2, regulated by intracellular interactions, can affect the cell's sensitivity towards extracellular ephrinB2. Intracellular components that precluster EphB2 synergize, whereas those that keep EphB2 unclustered, antagonize with extracellular ephrinB2. In the context of a cell-cell stimulation assay intracellular inhibition of EphB2 clustering converts kinase-dependent repulsion to adhesion.

Fig. 3.25 Intracellular inhibition of EphB2 clustering negatively regulates kinase-dependent cell responses.
(A) Model showing intracellular steric hindrance (using myr-FRB-mCherry) of extracellular (ephrinB2-Fc-induced) clustering. In the presence of heterodimerizer AP21967 the co-expressed inhibitory construct myr-FRB-mCherry couples to the wtEphB2-3FKBP receptor keeping it as monomer. EphrinB2-Fc can still bind to the ectodomain of the receptor. **(B)** Representative images of HeLa cells transiently expressing kdEphB2-3FKBP-YFP and myr-FRB-mCherry, stimulated with ephrinB2-Fc alone or ephrinB2-Fc together with AP21967 (t= 10min). Stimulation with ephrinB2-Fc alone leads to accumulation of EphB2 in the plasma membrane of cell edges (lower left panel); the presence of AP21967 prevents this effect (lower right panel). Scale bar, 10 µm. Image processing: 9x 0.2 µm z-stacked epiFL images; odc; adaptive-blind psf deconvolution; sum-projection; equal scaling over all images. **(C)** Western blot of immunoprecipitated wtEphB2-3FKBP (carrying a Flag epitope-tag) using the anti-phospho-EphB2 antibody; blot was stripped and reblotted for total EphB2. Cells transfected with both wtEphB2-3FKBP and myr-FRB-mCherry were stimulated with ephrinB2-Fc in the presence or absence of AP21967. The presence of AP21967 prevents EphB2 autophosphorylation. **(D)** Quantification of cell collapse assays (images not shown). The presence of AP21967 prevents EphB2-3FKBP transfected cells to collapse in response to ephrinB2-Fc. (mean ± SEM cell area percentage of n= 9 imaged cells for each condition tested; p< 0.001, Mann-Whitney nonparametric *t*-test). **(E)** Representative images of HeLa cells transiently expressing wtEphB2-1FKBP-YFP and myr-FRB-mCherry stimulated with ephrinB2-Fc imaged using epiFL time-lapse. AP21967 or control (EtOH) was added 18 min after addition of ephrinB2-Fc and imaging was continued. In the presence of AP21967 cell collapse stops and adopts a steady state, whereas in control stimulated cells ephrin-induced collapse progresses normally. Graph: quantification of cell collapse assays as described previously from representative images above. (mean ± SEM cell area percentage of n= 8 imaged cells for each condition tested; p< 0.001, Mann-Whitney nonparametric *t*-test).

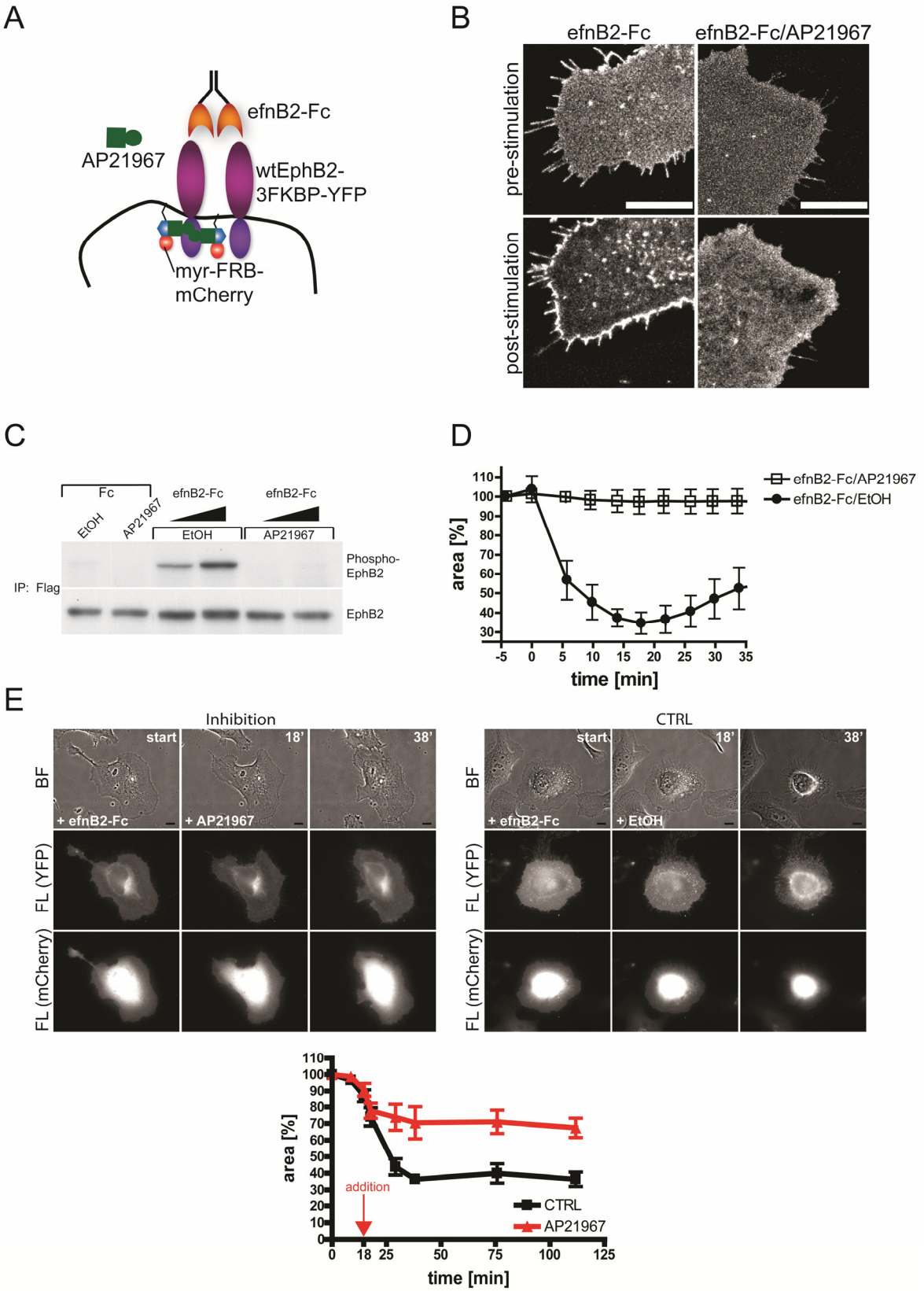
A
efnB2-Fc
AP21967
wtEphB2-
3FKBP-YFP
myr-FRB-
mCherry
B
efnB2-Fc
efnB2-Fc/AP21967
pre-stimulation
post-stimulation
C
Fc
efnB2-Fc
efnB2-Fc
EtOH
AP21967
EtOH
AP21967
IP: Flag
Phospho-
EphB2
EphB2
D
efnB2-Fc/AP21967
efnB2-Fc/EtOH
area [%]
time [min]
E
Inhibition
CTRL
BF
FL (YFP)
FL (mCherry)
start
18'
38'
+ efnB2-Fc
+ AP21967
+ EtOH
addition
CTRL
AP21967
area [%]
time [min]

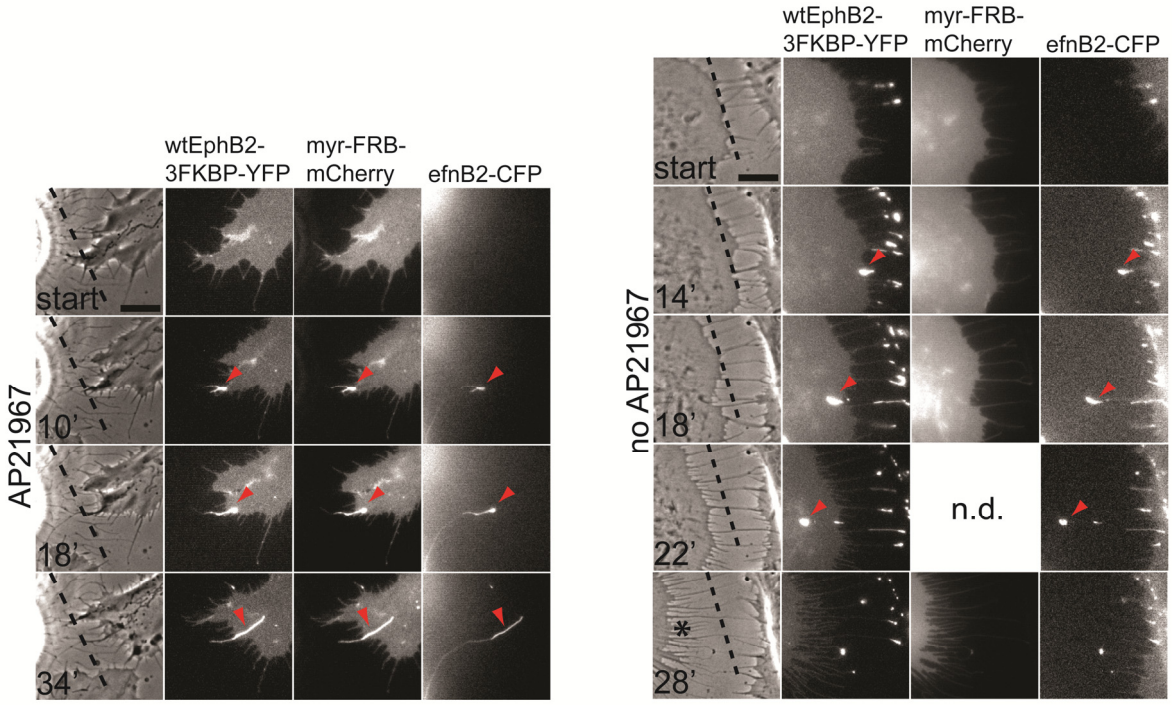

Fig. 3.26 Conversion of repulsive to adhesive Eph cellular responses.
Co-culture assay of HeLa cells co-expressing wtEphB2-3FKBP-YFP and myr-FRB-mCherry with HeLa cells expressing wildtype ephrinB2-CFP. EphB2 clusters (red arrows) can be seen in the contact region of the two cells. In the absence of AP21967, EphB2 clusters are internalized and the EphB2$^+$ cell (indicated by asterisk) retracts away from the ephrinB2$^+$ cell (the initial position of the EphB2$^+$ cell is marked by a stippled line); in the presence of 250 nM AP21967, EphB2 clusters stay near the contact-zone and cell repulsion is converted to an adhesive response. Scale bars, 10 µm. Abbreviations: n.d., not determined – imaging frame not acquired.

3.7 Ephrin clustering causes rapid reverse internalization

As outlined in Fig. 3.4, the dimerizer-inducible clustering system was also implemented for clustering the ligand with the same autonomous features as for Eph receptors. Primary focus was set on studying the role of cluster formation on the receptor side since cellular readouts are more accessible. However, I also performed initial experiments for ephrin ligand characterization of the AP-induced clustering response with promising results for a much more detailed further study.

3.7.1 Ephrin clustering causes fluorescence intensity rise in cell edges

Starting to study the mechanistic effects on the visual level using the dimerizer-induced system, it seemed reasonable to approach ephrin clustering by basic epiFL techniques.
HeLa cells, co-transfected with YFP-tagged ΔCephrinB2-3FKBP and control myr-mCherry constructs, were stimulated with dimerizer AP20187 while imaging in epiFL time-lapse (Fig. 3.27A). Approximately 8 to 13 min after addition of the compound, a significant FL intensity rise occurred at cell edges - in analogy to the phenotypic effect observed when clustering kdEphB2-3FKBP receptor isoforms (cp. Fig 3.8). By contrast, co-transfected myr-mCherry remained diffuse at cell edges, indicating the ephrin specificity of the readout. In analogy to Eph receptor clustering, I concluded that ligands also accumulate in the lateral part of the cell plasma membrane.
Inhibition of clustering could also be accomplished via co-transfection of the inhibitory construct myr-FRB-mCherry, which upon AP21967 addition couples with its FRB portion to the FKBP portion of the tagged ephrinB2 ligand isoform (Fig. 3.27B). This resulted in suppression of the phenotypic effect observed in Fig 3.27A for cells with medium to high expression levels of the inhibitory construct. In the control case under co-expression of myr-mCherry lacking the FRB domain or in cells with very low expression of myr-FRB-mCherry, ligand accumulation was still present (Fig. 3.27B,C). In total, measurements from multiple cells showed a negative correlation between myr-FRB-mCherry expression levels and the strength of the phenotypic effect (Fig. 3.27B). For cells expressing control construct myr-mCherry, a correlation to increasing myr-mCherry expression levels was not observed (Fig. 3.27B).
We see that the overall effects from ephrin clustering in FL imaging very much correspond to those monitored in Eph receptor clustering. Ligand accumulation at the lateral side of the cell was evident upon clustering. Ligand clustering can also be inhibited by application of the inhibitory construct myr-FRB-mCherry to keep ligands as monomers. Note that the AP21967 induced FRB-FKBP complex formation cannot be reversed, even not by the addition of AP20187 homodimerizer (data not shown).

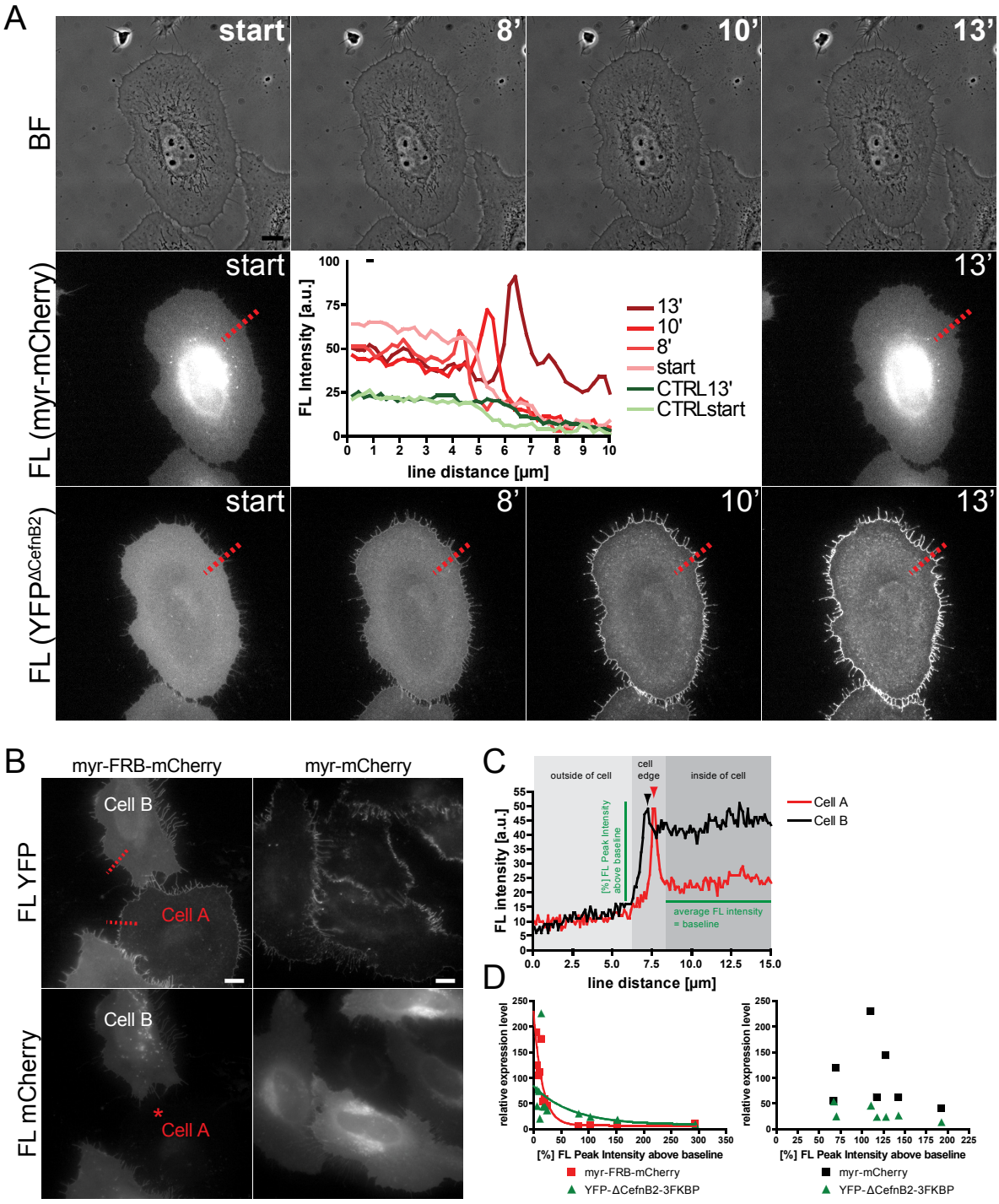

Fig. 3.27 Phenotypic effects of ephrin clustering in mammalian cells.
(A) HeLa cells were transfected with C-terminally truncated YFP-ΔCephrinB2-3FKBP and stimulated with AP20187 (100 nM) while imaging in single focal plane epiFL time-lapse. As a control and for better visualization of the cell, myr-mCherry was co-expressed. Upon stimulation, a strong FL intensity rise is observed for YFP FL at cell edges but not for mCherry FL. Images are background corrected. A linescan graph is shown to visualize time-dependent FL intensity. **(B)** HeLa cells expressing YFP-

ΔCephrinB2-3FKBP and myr-FRB-mCherry or control myr-mCherry were incubated with AP21967 (100 nM) for 1 hr, then stimulated with AP20187 (100 nM) for 1 hr and imaged for epiFL. Depending on low expression levels of myr-FRB-mCherry (Cell A, asterisk), which antagonizes ephrin clustering, ephrinB2 accumulation can be seen in the plasma membrane of cell edges (Cell A, FL YFP channel). Scale bars, 10 µm. **(C)** Linescans over cell edges (as indicated by red dotted lines in B) were performed from cells in both conditions to measure the strength of the phenotypic effect of FL intensity rise as displayed for cell A/B from panels in (B). The FL peak intensity in each linescan was normalized to the baseline average FL intensity beyond the cell edge on the inside of the cell. **(D)** FL peak intensity above baseline values, determined from linescans as described in (C), were plotted against the relative expression level, i.e. FL intensity signals from respective proteins. Note, that there is a negative correlation between myr-FRB-mCherry expression level and the strength of the phenotypic effect.

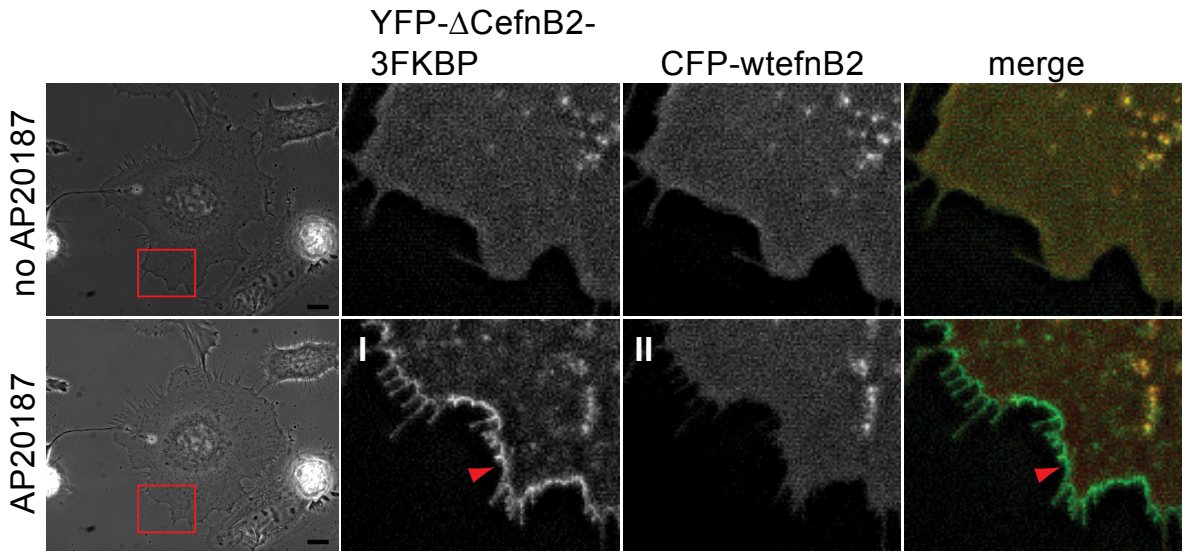

Fig. 3.28 Dimerizer-induced ephrin clustering is self-contained.
HeLa cells were co-transfected with YFP-ΔCephrinB2-3FKBP and CFP-tagged wtephrinB2 lacking FKBP (Cfp-wtephrinB2). Before stimulation with either AP20187 or ephrinB2-Fc, both ligand isoforms are evenly distributed in the cell (upper panels). Upon stimulation (t= 20 min) with 250 nM AP20187 YFP-ΔCephrinB2-3FKBP accumulates in the lateral edge of the cell (I- arrow), whereas EphB2 lacking FKBP remains evenly distributed (II). BF images on far left are low power magnifications. Red boxes indicate areas of higher magnifications. Scale bars, 10 µM. Image acquisition and processing: 3x 0.8 µm z-stacked epiFL images; odc; adaptive-blind psf deconvolution; sum-projection.

3.7.2 Dimerizer-induced ephrin clustering is self-contained

Again, in analogy to the characterization of the dimerizer-inducible system of cluster formation for Eph receptors, ephrin ligands were tested for the ability to recruit adjacent ligand monomers into dimerizer-induced clusters. HeLa cells, expressing both the YFP-tagged C-terminally truncated isoform containing 3FKBP domains and a CFP-tagged

wildtype ephrinB2 version were stimulated with AP20187. As described earlier, the addition of AP20187 caused the phenotypic effect of FL intensity rise at cell edges i.e. ligand accumulation for YFP-ΔCephrinB2-3FKBP (Fig. 3.28-I). The FL intensity distribution of co-transfected wtephrinB2 lacking FKBP domains, however, remained unaffected (Fig. 3.28-II), indicating that the two ligand variants did not interact under these conditions.
This result indicates that dimerizer-induced ephrinB2 clusters do not serve as nucleation points to which additional ephrin ligands are recruited by ephrin-ephrin interactions. The system of dimerizer-inducible clustering is therefore self-contained enabling the constitution of distinct ephrin cluster size distributions in living cells.

3.7.3 Dimerizer-induced clustering is sufficient to cause rapid ephrin internalization

In analogy to the investigation of dimerizer-induced Eph clustering, I asked how dimerizer-induced ephrin clustering would impact on cellular responses. Performing epiFL time-lapse of HeLa cells expressing YFP-ephrinB2-2FKBP isoforms stimulated with AP20187 led to transient ephrin ligand accumulation at cell edges and subsequent rapid processing of FL particles to the center of the cell (Fig. 3.29A). These particles pinched off from a bigger FL entity, which is located at the very cell edge (Fig. 3.29A, blowup image sequence). To further investigate this processing phenomenon, I also conducted immunocytochemistry experiments. HeLa cells expressing YFP-ephrinB2-2FKBP ligand isoforms were stimulated with either increasing concentrations of AP20187 dimerizer or positive control preclustered EphB2-Fc (Fig. 3.29B).

Fig. 3.29 Clustering correlates with the strength of ephrin internalization.
(A) Time-lapse epiFL image sequence (single focal plane) of HeLa cells expressing wildtype YFP-ephrinB2-2FKBP, stimulated with AP20187 (100 nM). A transient FL intensity rise was observed at cell edges indicating a temporary ligand accumulation (green arrows, blowup from green region outline). Subsequently, FL entities at cell edges (purple arrows, small panel blowups) are successively processed towards the center of the cell by pinching off from small particles (red arrows). Cells do not collapse upon clustering of ephrin ligand. **(B)** HeLa cells expressing the YFP-wtephrinB2-2FKBP ligand isoform were stimulated with either AP20187 (100 nM), preclustered EphB2-Fc (2 µg/ml) or control stimuli (EtOH or Fc) for 30 min, fixed and immunostained for surface ephrinB2 using the anti-GFP antibody (Invitrogen). Total ephrinB2 protein was visualized by the YFP-tag. Both for EphB2-Fc and AP20187 stimulation, internalized focal inclusions, not stained by the surface staining, become visible. Image acquisition and processing: 3x 0.8 µm z-stacked epiFL images; max-projection; bgcorr. **(C)** Quantification of internalized ligand ephrinB2 upon stimulation for 30 min with various concentrations of AP20187 and EphB2-Fc as indicated. The fraction of surface ligand to total ligand protein was determined by integrated FL intensity measurements over the whole cell surface area (mean ratio of FL surface/FL total ± SEM of n = 21-25 cells per condition; n.s., not significant, * $p< 0.05$, *** $p< 0.001$, student's *t*- test; asterisks in red indicate significance level to control EtOH). Note, that the strength of internalization correlates to the concentration of applied dimerizer. Scale bars, 10 µm.

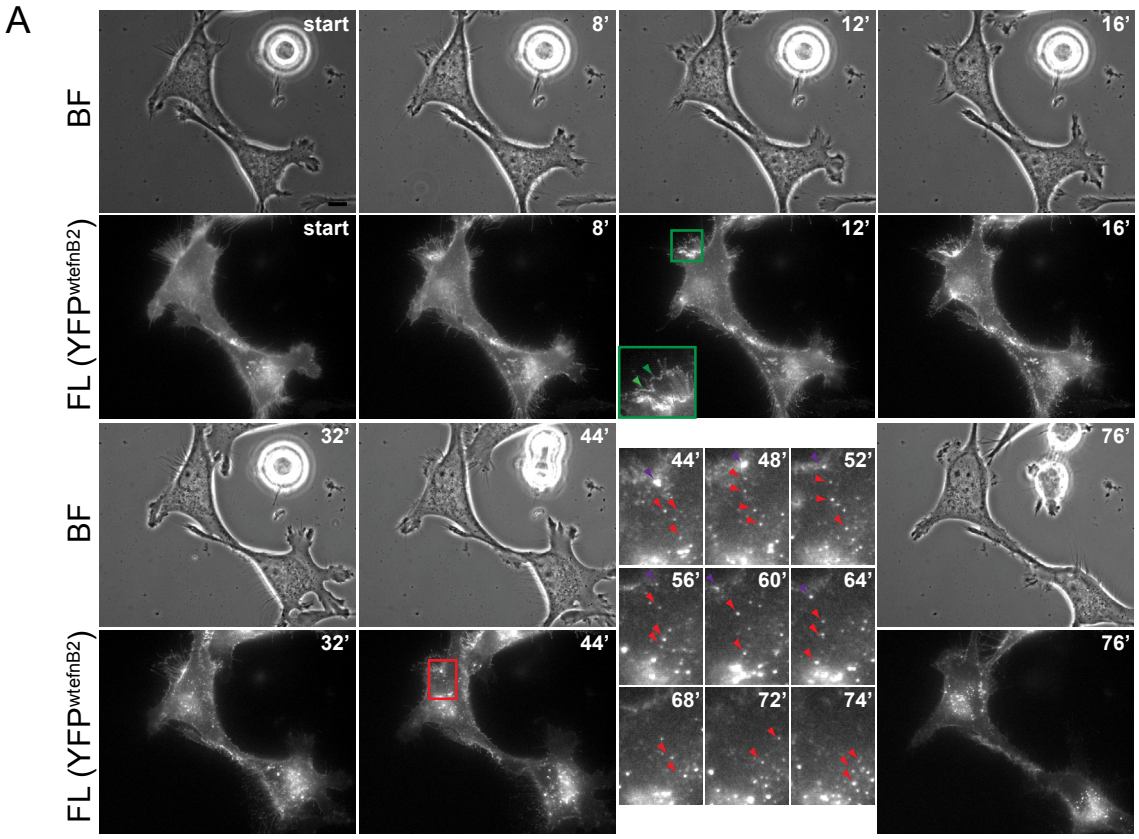
A
BF
FL (YFPwtefnB2)
start
8'
12'
16'
32'
44'
48'
52'
56'
60'
64'
68'
72'
74'
76'

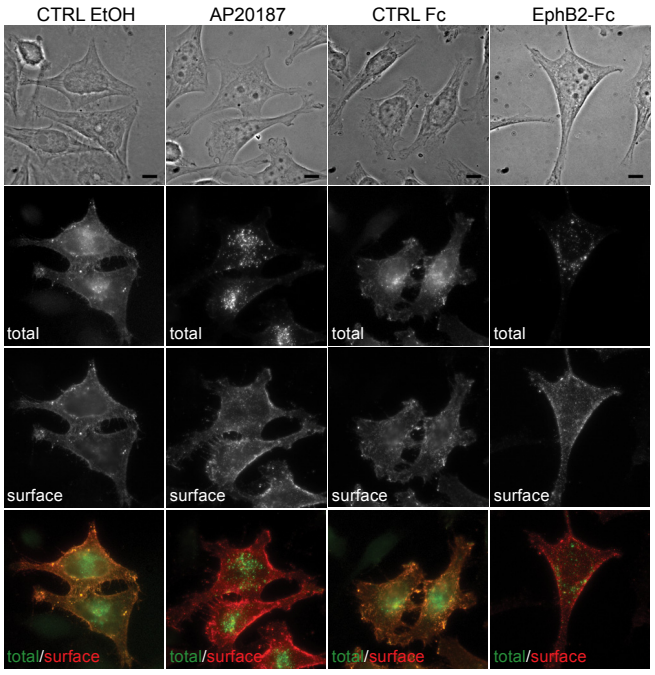
B
CTRL EtOH
AP20187
CTRL Fc
EphB2-Fc
total
surface
total/surface

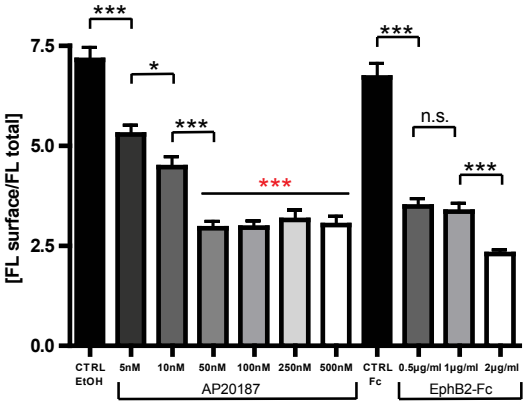
C
[FL surface/FL total]
7.5
5.0
2.5
0.0
***
*
n.s.
CTRL EtOH
5nM
10nM
50nM
100nM
250nM
500nM
CTRL Fc
0.5µg/ml
1µg/ml
2µg/ml
AP20187
EphB2-Fc

After fixation, staining and imaging, the fraction of internalized protein was visible as small FL dots devoid of surface staining, which could be seen upon stimulation with AP20187 or EphB2-Fc. Quantification for surface versus total protein corroborated the visual impression and showed a clear dose-response dependence for the strength of the internalization response (Fig 3.29C).

In contrast to Eph-mediated cell collapse, ephrin-expressing cells did not collapse in response to dimerizer-induced clustering (Fig 3.29A) complying with EphB2-Fc-induced cell responses (data not shown).

Overall, studying the obvious physiological ephrin-induced cellular responses, receptor-independent clustering with AP20187 dimerizer did not reveal significant differences as compared to receptor-dependent clustering. However, a closer look at clustering-dependent ephrin phosphorylation of C-terminal tyrosine residues by Src was not taken at that point of the study. For future investigations of ephrin clustering and its role for controlling signaling responses, the here established system of dimerizer-inducible ephrin clustering may serve the same aims in mimicking physiological responses as the system for Eph receptor clustering.

4. DISCUSSION

4.1 The system of dimerizer-induced clustering is a versatile tool to induce physiological Eph signaling responses.

A closer look at the constitution and processing of Eph/ephrin signaling entities in co-cultures of living cells immediately suggested, that unconventional strategies had to be implemented to meet the needs for a detailed mechanistic to functional study of the Eph/ephrin cluster formation process.
The intention to reduce and control parameters around the event of Eph/ephrin clustering led to the cell- and receptor/ligand-autonomous approach of dimerizer-induced cluster formation. Based on structural studies, it was clear to me, that multiple Eph-Eph domain interactions are necessary to produce extended signaling arrays [72,80,91,106], and that abrogation of interaction interfaces through site-directed mutagenesis might lead to dysfunctional receptor protein. A site-directed mutagenesis approach to impair clustering did therefore not seem reasonable.

Implementation of the FKBP/FRB system. Placing Eph clustering under the control of the FKBP homodimerization system in combination with the FRB heterodimerization system not only allows for a positive but also a negative control of clustering through steric hindrance by myr-FRB-mCherry. The FKBP-system has been used for other growth factor receptors, where the insertion of a single FKBP domain has previously been shown to be sufficient for dimerizer-induced activation of growth factor receptors, including FGFR1 (fibroblast growth factor receptor 1), ErbB receptors including EGFR, insulin receptor and PDGF receptors [323-328]. Insertion of up to 3 tandem copies of the FKBP domain was described for the transmembrane glycoprotein platelet endothelial cell adhesion molecule 1 (PECAM-1), FGFR1, ErB1/2 receptors, EGFR and serine/threonine kinase receptor transforming growth factor-β (TGF-β) leading to partially functional signaling [329-331]. While the focus in these studies was mainly set on the mere activation or dimerization of the target protein, later studies also employed the FKBP-system to specifically produce oligomer size distributions of EGFR-FKBP fusions for the testing of homo-FRET imaging approaches and to draw underlying functional conclusions [327,328]. To my knowledge, this study is the first to implement the FKBP/FRB-system for Ephs/ephrins, with special focus to produce different cluster size distributions, to alter cluster propensity by the use of the low-affinity homodimerizer AP1887 and to generate a range of functional readouts.

4.1.1 Features of the FKBP-system

Important features have emerged from the detailed investigation of the properties of the Eph dimerizer-inducible clustering system in comparison to ephrinB2-Fc induced clustering. An overview of different modes of clustering-induction is provided in Fig. 4.1A. Some specific aspects are elaborated in the following paragraphs and upcoming sections.

Specific Eph isoform receptor activation. Practically and in respect to the usability of the FKBP/dimerizer-induced system for Eph clustering, single Eph receptor isoforms can now be selectively clustered and activated *in vitro* but theoretically also *in vivo*. Ephrin stimulation on Eph receptors usually results in signal amplification of more than one Eph receptor, also of endogenously expressed Eph receptors, since most ephrins are cross-specific to several Eph isoforms. This fact points to the superiority of the dimerizer-inducible system in selectively studying one specific Eph isoform.

High controllability of clustering. AP-induced clustering is highly controllable. Fast diffusion rates and penetration of the whole cell ensure a high simultaneity of clustering induction on a small time scale, independent of recombinant protein quality as it is the case for ephrinB2-Fc. Dimerizer-induced clustering is, in contrast to ephrinB2-Fc clustering, reversible by the use of myr-FRB-mCherry co-expression and AP21967 application. Clustering may also be totally inhibited enabling the study of cellular responses over the whole range of cluster sizes from forced monomers to oligomers. Furthermore, the use of EphB2-FKBP isoforms lacking the LBD allows for a highly-controlled activation of Eph kinase-dependent signaling without unwanted signaling induction by endogenously expressed ephrin.

Available mechanistic readouts. Readouts for measuring absolute Eph cluster size distributions are difficult to produce. Whereas ephrinB2-Fc produces stoichiometrically undefined complexes together with Eph receptors, dimerizer-induced clusters are stoichiometrically well defined and may be visualized using blue-native PAGE.

Fig. 4.1 Dimerizer/ephrinB2-induced cluster configurations.
(A) Favorable assets of different modes of clustering-induction. (?) indicates a possible, experimentally not confirmed feature. **(B)** Model of ephrinB2-induced versus dimerizer-induced clusters. The Eph cluster platform is categorized into an extra- and intracellular cluster entity to mediate “cell-surface” and intracellular signaling, respectively. The way clustering is induced by either dimerizer or soluble ephrinB2-Fc may produce differential kinase-independent signaling responses based on the configuration of the extra-/intracellular cluster entities. **(C)** FKBP-induced cluster configurations. The number of FKBP domains is proposed to determine the complexity of the signaling arrays. Under certain assumptions (only in-register crosslinking of FKBP domains, no intra-receptor FKBP crosslinking, as indicated by red connectors in left cartoon) 2FKBP constructs may only form 1d-arrays and ring-like complexes whereas 3FKBP constructs may form 2d-platforms of denser packing.

DISCUSSION

A

Dimerizer-induced clustering

⊕ cluster size control
⊕ kinase-dependent signaling
? intracellular steric sign. platform
⊕ selective Eph isoform clustering
⊕ direct receptor-autonomous Eph clustering
⊕ better mechanistic readouts

EphrinB2-Fc-induced clustering

⊕ cell surface signalling
⊕ intracellular signaling
⊕ more physiological

Cell-cell contact-induced clustering

⊕ passive adhesion response
⊕ most physiological

B

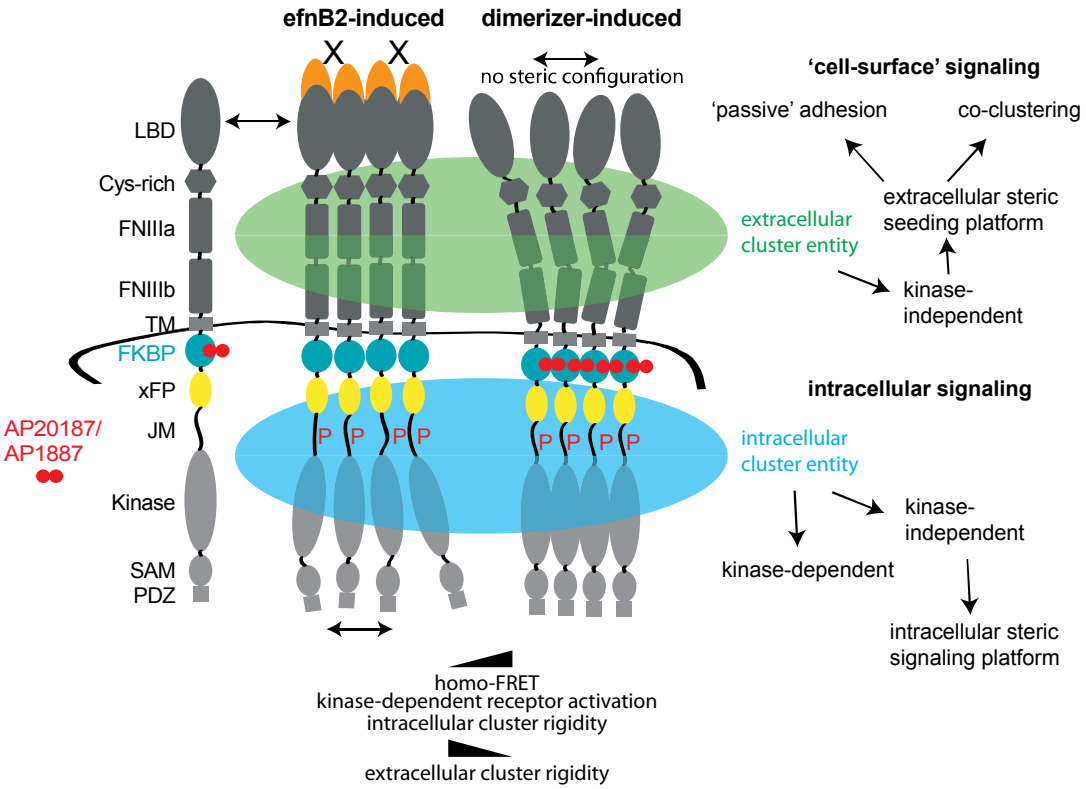

C

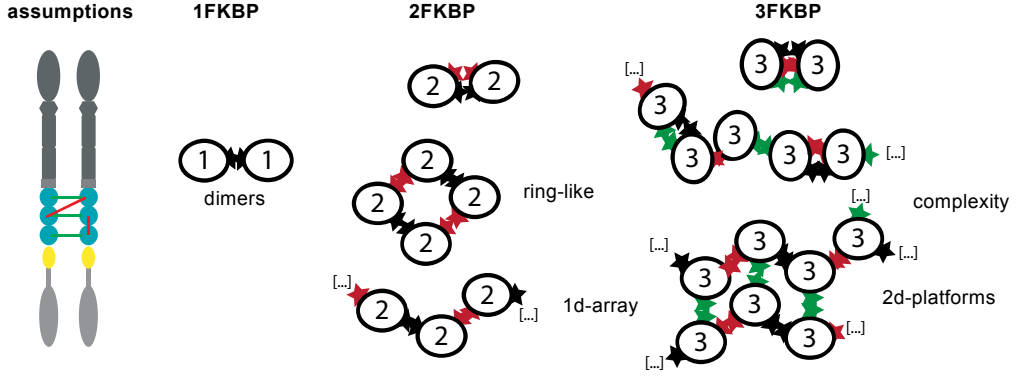

4.1.2 Ephrin-induced versus dimerizer-induced clusters

Eph receptor seeding mechanism. Detailed analysis of the mechanistic aspects of the dimerizer-inducible Eph receptor clustering system has revealed that in contrast to an ephrinB2 stimulation, a nucleation or seeding effect is absent (this study and [104]). Seeding of Eph receptors was shown to be mediated by the extracellular receptor part [72,91,104], by contrast, dimerizer-induced clustering is induced by non-covalent crosslinking at the intracellular receptor part. This fundamental difference in the way clustering is provoked for Eph receptors can explain the absence of a seeding mechanism for dimerizer-induced clustering. Structural biologists claim that ephrin binding does not cause structural rearrangements on the intracellular receptor part but that conformational changes remain strictly limited to extracellular domains (personal communication with Elena Seiradake and [106]). In consequence, intra- and extracellular parts of Eph receptors are structurally most likely mutually inert to conformational changes. A clustering seed, originating from the intracellular part of the receptor, would thereby not be mediated to the outside structural part of the receptor and vice versa. By contrast, ephrin engagement as extracellular clustering trigger causes Eph receptors to snap in register to produce extended 1-dimensional signaling arrays or 2-dimensional platform-like structures [72,79,89,332]. For dimerizer-induced clustering this trigger is obviously missing, signaling array-like structures are, however, produced by distinct dimerizer-induced clustering (Fig. 4.1C). This lack of uncontrolled seeding ensures the distinctness of cluster size distributions as observed for the FKBP-system and shown by homo-FRET imaging and blue-native PAGE.
Overall, this difference in the mode of ephrin-induced versus dimerizer-induced cluster formation raises the question if thereby induced spatial signaling entities may differ in their cluster architecture influencing downstream signaling events. Cluster architecture can be categorized into an extracellular steric seeding platform consisting of Eph/ephrin ectodomain complexes (Fig 4.1B extracellular cluster entity) and an intracellular steric platform (Fig. 4.1B, intracellular cluster entity).

Signaling via the intracellular signaling platform. Intracellular kinase activation is the major consequence of Eph clustering and most important for biological functions *in vivo* [28,31]. However, receptor clustering may also provide a kinase-independent, sensitive intracellular structural configuration, which is sufficient or in addition to receptor autophosphorylation necessary for docking of signaling adaptors. Interestingly, the well-studied adaptor protein ephexin1 binds to EphA4 receptors (intersectin in the case of EphB receptors) in a constitutive manner [122,127,129], and its activation through phosphorylation is controlled by Eph clustering [113]. This modification is also mediated by kinase-active eeEphA4, suggesting that this is a process that happens largely independent of the regulation of EphA4 kinase activity. It was suggested that ephexin1 is recruited into higher-order

clusters of EphA4 along with Src family kinases and possibly other adaptor proteins. This then leads to the activation of Src kinase and subsequent ephexin1 phosphorylation by Src.
My study reports, that dimerizer-induced clustering is sufficient to activate wtEph and N-terminally truncated Eph receptors and induce physiological signaling responses in heterologous cells and neurons. In light of the mechanistic aspects of the dimerizer-induced clustering system, it is highly unlikely that dimerizer-induced clustering forces the cytoplasmic domains by chance into an ordered signaling array that resembles the ephrin-induced physiological situation. Therefore a defined intracellular cluster configuration that might arrange specific interfaces for adaptor proteins is lacking and still, physiological Eph signaling responses are produced. Cell contraction responses are mainly mediated through the RhoA/ROCK/LIM kinase pathway through ephexin1 or intersectin to ultimately produce actin rearrangements [122,127,129]. Thus I conclude that dimerizer-induced clustering is sufficient to activate this pathway irrespective of producing a specific intracellular inter-receptor domain configuration [80]. Furthermore, recruitment of additional signaling components might either not be necessary to mediate kinase-dependent signaling responses or arbitrarily configured clusters are also sufficient for recruitment, e.g. through an unspecific co-clustering process.

Cell-surface signaling via the extracellular steric seeding platform. The extracellular cluster entity consists of multiple Eph/ephrin high-affinity interactions, which presumably potentiate along with growing cluster sizes to mediate strong adhesion to the opposing cell. This is, however, only the case in cell co-culture scenarios, where the cognate ligand is membrane-bound to the opposing cell. Dimer EphB2/ephrinB2 binding affinities are strong and dissociation constants (K_d) range in a sub-nanomolar order of magnitude [70,96]. The idea of extracellular strong and passive adhesive forces between cells can therefore be easily appreciated. This adhesive component of kinase-independent Eph function may be solely attributed to the extracellular steric seeding platform and reflects a pure passive mode of signaling mechanism. By contrast, kinase activity leading to *trans*-endocytosis of both receptor and ligand was shown to turn initial strong adhesion into contact-repulsion [237,238] involving an active kinase-dependent signaling process.
In this respect, both the FKBP-system and clustering with soluble ligand obviously fail to incorporate this kinase-independent mode of signaling through passive Eph/ephrin binding mediated adhesion. However, a secondary kinase-independent function may underlie the extracellular steric seeding platform. It may be able to evoke a signaling propensity, referred to as cell-surface signaling. The extracellular cluster entity may unspecifically co-cluster or specifically incorporate alien membrane proteins, i.e. produce cluster inclusions of alien (trans)membrane proteins, and thereby activate them.
Indeed, in this study, ephrinB2-Fc-induced clustering led to co-precipitation of an unidentified 50-55 kDa trans(membrane) protein. (Trans)membrane interacting partners *in cis* have been reported to be matrix metalloproteinases, γ-secretases, NMDA receptors [184,186,259], and

other, so far unknown, specific or unspecific Eph cluster inclusions of alien (trans)membrane proteins are suspected. ADAM10 recruitment was demonstrated to correlate with cluster sizes produced by mechanical restriction of EphA2 [294], highlighting a possible kinase-independent role of cell surface signaling. In this respect my focus was not set on identifying the co-precipitated protein nor the mode of interaction but to find differences in ephrinB2-Fc induced versus dimerizer-induced clustering and thereby learn more about the molecular basis of receptor functioning. Interestingly, dimerizer-induced clustering failed to co-precipitate the unidentified protein. This difference in producing a competent cluster configuration for co-clustering of the alien (trans)membrane protein between ephrinB2-Fc induced and dimerizer-induced clustering may rely on the fact, that dimerizer-induced clustering is initiated intracellularly. Hence, this mode of clustering then fails to produce an extracellular steric seeding platform competent for recruiting cell surface, trans(membrane) signaling partners or effectors and furthermore accentuates an important mechanistic difference between ephringB2-Fc and dimerizer-induced clustering. Dimerizer-induced clustering most likely does not produce an extracellular steric configuration.

4.1.3 Relevance of cluster size distributions and cluster quality

Quantitative assets of dimerizer-induced clustering based on theoretical and experimental considerations. The self-containment of the FKBP/dimerizer-induced Eph clustering system was shown to be a prerequisite for inducing discrete cluster size distributions in living cells. While correlation between the formation of higher-order oligomers and increasing numbers of FKBP domains is, based on theoretical mathematical combinatorics, rather intuitive, the situation in practice might differ considerably. Structural constraints exerted by the receptor environment may impair full rotational freedom of inserted FKBP domains due to FKBP-insertion within the polypeptide chain of the Eph receptor. Moreover, depending on the structural inter-domain flexibility, FKBP domains may also only interact with other FKBPs, which are situated in register in adjacent receptors determined for cross-linking. In the end, all these parameters not only contribute to controlling the actual cluster size distribution, but also the complexity of clusters, ranging from discrete dimers (1FKBP) over 1-dimensional arrays and ring-like cluster configurations (2FKBP) to 2-dimensional cluster platforms (3FKBP) (Fig 4.1C).

Blue-native PAGE represented a reliable method to resolve absolute cluster size distributions produced by the dimerizer-system. As predicted, dimers were the only higher-order species present when clustering 1FKBP isoforms with AP20187. For [2,3]FKBP isoforms, higher-order cluster size distributions became evident which were shifted to bigger oligomers in the case of 3FKBP isoforms. Surprisingly, however, the species of highest order distinguishable in blue-native PAGE are only of hexa-, potentially heptameric order. This indicates a rather early saturation in the cluster formation process using the FKBP/dimerizer system. Interestingly, the cluster size distribution for the 2FKBP variant was remarkably similar to the

one observed by Bader and colleagues despite the fact that a totally different system relationship was existent [328].
Similarly, homo-FRET imaging may be employed to relatively quantify cluster sizes as well as cluster size distributions [310]. Indeed, application of the high-affinity homodimerizer led to a strong decrease in FL anisotropy upon dimer formation and further subtle decreases for [2,3]FKBP cluster size distributions. Potentially, homo-FRET can be induced by nanoscale biochemical interactions or a high-FL concentration distribution due to over-expression. However, the drop in FL anisotropy must indeed rely on a nanometer-scale organization which can be conveniently discriminated from a FL concentration distribution by the lack of a positive correlation between intensity (fluorophore concentration) and the corresponding anisotropy (degree of homo-FRET) [333]. Thus, the observed drop in anisotropy is due to clustering of mGFP-tagged Eph receptors, as it is confirmed by cluster size distributions from blue-native PAGE. For the most part, the differences in anisotropy between the [1-3]FKBP dimerizer-induced clustering conditions rely on the number of proteins in a cluster but potentially also on the energy transfer efficiency between the fluorophores. The divergence in transfer efficiency may be due to variations of the reciprocal orientation of the fluorophores caused by differences in the complexity of clusters (this study and [309,310]).

Qualitative assets of dimerizer-induced clustering based on theoretical and experimental considerations. Complexity of clusters may be considered as a qualitative asset of dimerizer-induced clusters (Fig. 4.1C). As a thought-provoking impulse, cluster complexity can also be closely linked to cluster density and the geometry concept of the densest packing of spheres, if single receptor monomers in a lattice cluster are considered as spheres. This concept becomes immediately clear when comparing e.g. a cluster as a chain of 4 receptor monomers with a cluster as a ring-shaped 4 receptor entity. However, this qualitative parameter is inherent to the system of dimerizer-induced clustering and cannot be controlled by the experimenter.
Another qualitative aspect of cluster formation can be addressed by application of the low-affinity homodimerizer AP1887. AP1887-induced clustering presumably does not impact the complexity but rather the stability and cohesiveness of those oligomeric shapes. Moreover, it may attribute increased dynamics and a reduced half-time existence of clusters, which is owed to its increased off-rate in binding. Indeed, the use of the alternative low-affinity homodimerizer was a controllable means to vary the quality or stability of Eph clusters as could be experimentally proven. AP1887-induced clustering species were most likely not stable enough to overcome cell lysis and/or blue-native PAGE and AP1887-induced clustering also failed to generate a positive readout in homo-FRET imaging. Here the transience in the clustered state did most likely not allow the energy transfer efficiency to cause a decline in FL anisotropy. Note that the absence of a homo-FRET signal does not exclude the existence of clustering. Clusters that do not provide the stability fail to enable energy transfer between aligned mGFPs [310]. AP1887-dimerizer application must have

provoked the formation of low stability clusters, since on the functional side, it was sufficient to activate Eph receptors and induce signaling.
In summary, the FKBP-system is able to give control over quantitative and qualitative aspects of Eph clusters and thereby allows for the study of the respective functional outcomes.

Implications for physiological ephrin-induced Eph clustering. Cluster properties were also assessed by homo-FRET imaging upon stimulation with ephrinB2-Fc ligand. Interestingly, a drop of steady-state anisotropy upon clustering with increasing concentrations of ephrinB2-Fc saturated on a level higher than for dimerizer-induced clustering. This finding points to an increased intracellular structural flexibility in the vicinity of the mGFP. Since for ephrinB2-Fc clustering is induced externally, this mode of clustering might allow greater intracellular structural flexibility as compared to AP20187-induced clustering, where crosslinking takes place right next to the mGFP producing the FL anisotropy readout. Hence, one has to be careful with correlating absolute dimerizer-induced cluster properties with ephrinB2-induced clustering. However, relative conclusions and interpretations may be confidently assigned to ephrin-induced clustering.

Allosteric model for Eph clustering? An extracellular steric seeding mechanism has been implicated for Eph clustering which would allow ephrin-independent receptor recruitment upon ephrin binding [72,91,334]. This rather uncontrolled clustering mechanism, which is somehow reminiscent of the conformational spread mechanism, well characterized for bacterial chemotaxis receptors [274,297,298], is suited to recruit a proportion of receptors into a signaling cluster that would represent the overall receptor abundance of the cell. This concept was proposed to allow precisely adjusted cellular responses (heightened responsiveness) controlled by graded changes in ligand abundance and receptor/ligand occupancy, a characteristic feature of Eph-ephrin communication [104]. In light of the here presented results, I can neither confirm nor disprove the idea of an ephrin-independent extracellular steric seeding mechanism. However, I conclude from my results that a conformational spread mechanism may be strictly limited to sites of receptor contact. Homo-FRET imaging experiments using soluble ephrinB2-Fc or co-cultures reveal differential cluster size distributions for the overall stimulated cell or at sites of cell contact. This stands in slight contrast to the idea of a widespread Eph receptor seeding which would erase the fine differences in clustering upon ephrin stimulation. Revisiting the concept of conformational spread for Eph receptors, I suggest a limited recruitment of Eph receptors into existing clusters, which might not reflect the overall abundance of Eph receptors but the size or cluster perimeter. Eph receptor engagement into existing clusters might then saturate at the cluster edge and eventually come to a halt. Eph receptors, which line up at the edge of clusters, may not be conformationally competent to recruit further Eph receptors independent of ligand contact. I suggest the KNF model of allosteric ligand-receptor systems to come closest to the hereby elaborated concept of Eph cluster formation (cp. section 1.6.1 & [271,277]).

4.2 Eph receptor clustering serves as analog-to-digital converter to produce graded cellular signaling responses

4.2.1 Eph-Eph *cis*-interactions are sufficient to induce physiological signaling responses

Mechanisms that couple the event of ligand binding and dimerization to activation of the intracellular tyrosine kinase domains are surprisingly diverse for RTKs [9]. While ligand-binding for some RTKs like EGF receptor requires the precise positioning of receptors during dimer formation to activate the kinase, others are more tolerant in respect to inter-molecular orientation and positioning for kinase activation.
Until now, it was not clear if Eph receptors require the precise positioning of receptors in a dimer or cluster to activate the kinase. Binding of an ephrin ligand to the Eph LBD has been shown to provoke secondary-structure rearrangements, which are strictly localized to the interaction interface. Therefore it was proposed that downstream signaling is most likely triggered in the cytoplasmic sides, not through the conformational changes in the interacting ligands and receptors, but through their translocational rearrangements and repositioning relative to each other [70,80].
My present work shows that physiological Eph clusters can indeed be formed solely by Eph-Eph *cis*-interactions suggesting that ephrin *trans*-interactions may be necessary to trigger clustering, but not be required to form a highly-ordered array and elicit kinase-dependent cell responses. Dimerizer-induced clustering does most likely not allow specific translocational rearrangements and repositioning of receptors to each other supporting the hypothesis of packing density or crowding as being sufficient for kinase activation. Although it cannot be fully excluded, it seems unlikely that dimerizer-induced clustering may force the cytoplasmic domains into an ordered signaling array that resembles the ephrin-induced physiological situation. I consider dimerizer-induced EphB2 clusters to be disordered and to be simply crowded through non-covalent cross-linking by the homodimerizer.

4.2.2 Composition and quality of cluster size distributions determine the cellular response

Eph receptors form higher-order oligomers upon ephrin engagement leading to extended cell surface signaling arrays, which exert functional kinase-dependent signaling responses [31,34,72,91]. This unique feature immediately raises the question if clustering may govern these downstream signaling responses depending on the size and/or quality of clusters and the surrounding cellular context [32,290]. However, a direct and reliable correlation of Eph clustering to kinase-dependent Eph signaling has so far been missing. Moreover, a direct control over the Eph oligomerization state or quality of clusters was not possible to date. The

phenomenon of Eph clustering has so far only been indirectly addressed through application of distinct ephrin oligomeric species, produced by gel filtration or through application of an Eph antibody binding to the ectodomain [34,293]. Eph receptors were thereby reported to be able to discriminate these oligomeric species showing alternative signaling responses. However, an underlying mechanistic model, which explains these functional outcomes, remained elusive. The dimerizer-inducible system of Eph clustering made it now possible to bridge this gap by giving direct control over qualitative and quantitative properties of Eph clustering.

Functional effect of Eph cluster size distributions. AP20187-induced Eph cluster size distributions exerted respective kinase-dependent graded signaling responses with an overall enhancement of the phospho-activated cell state. Cluster size distributions positively correlated with every step in the Eph signaling cascade, from Eph receptor activation, indicated by phosphorylation of the JM tyrosines, to downstream cellular collapse responses, reflected by the degree in total collapse (collapse amplitude) and overall cell response pattern. By analyzing the fraction of activated Eph receptors engaged in single Eph cluster species using blue-native PAGE, I found that the composition of the EphB2 cluster sizes determined the strength of the cellular response. This is based on the fact that different oligomer sizes have distinct activation states. While EphB2 dimers were hypophosphorylated and largely inactive, EphB2 trimers were close to being fully activated, to an extent comparable with EphB2 tetramers. Hence, cluster populations significantly abundant in dimers (as generated by the 2 FKBP isoforms) would elicit a weaker cellular response than a cluster population consisting of predominantly higher-order oligomers.
The early saturation in receptor activation on the analytical level of cluster species was quite surprising to find and is reminiscent of an ON-OFF mechanism of receptor activation. However, the technical demands and low resolution of the single species analysis in blue-native PAGE must be taken into consideration. Furthermore, an ON-OFF mechanism of receptor activation might not exist for physiological ephrin-induced clustering since thereby induced clusters might be of different quality. This might convert an ON-OFF into a graded signaling output.

Functional effect of stability/quality of Eph clusters. My results with the low-affinity dimerizer indicated that stability of EphB2 oligomers also determined the strength of the response. AP1887-induced clustering caused a delay in Eph activation through the autocatalytic loop, supposedly due to the low stability of thereby induced clusters. Interestingly, stimulation with the low-affinity ephrinA5 led to the same result in receptor activation and cellular collapse response indicating that ligand-affinity and thereby caused receptor cohesiveness (stability) are closely linked and cause a difference in the collapse kinetics but not necessarily in the overall strength of the response. High-affinity interactions

like the ones with ephrinB1, ephrinB2 or an anti-Eph antibody resemble an AP20187-induced response reflecting high receptor cohesiveness *in cis*.
The modulatory effect of cluster stability also became evident in axon growth cone collapse assays using rat hippocampal neurons. The number of collapsed growth cones was reduced for AP1887-induced as compared to AP20187-induced clustering, which best reproduces an ephrinB2-Fc induced collapse. Upon AP1887 stimulation, Eph receptors engaged in clusters also displayed a slightly elevated activation level after separation in blue-native PAGE. However, stability of AP1887-induced clusters was fairly low resulting in absence of homo-FRET and monomeric receptor species in blue-native PAGE.
Initially, a study by Himanen and colleagues discovered the physiological ephrinA5-EphB2 interaction which also caused growth cone collapse in hippocampal neuronal cultures resembling the AP1887-induced collapse of my study [70]. Although genetic evidence is still missing, cross-subclass Eph/ephrin interactions, such as the one described between EphB2 and ephrinA5, are likely to be involved in important steps during development and are thereby of physiological relevance. AP1887-induced clustering of altered quality generating very similar cellular responses as ephrinA5-induced clustering may be likewise of biological significance. It may be speculated that low quality clustering is most likely not a general phenomenon of the Eph signaling system. Rather it is constrained to a relatively small but strategic subset of Eph/ephrin signaling scenarios *in vivo*.

4.2.3 Eph clustering is an analog-to-digital converter for signaling

The above discussed findings about quantitative and qualitative Eph clustering imply the introduction of an analog-to-digital converter concept for Eph signaling. Typically, an analog-to-digital converter (ADC) is an electronic device that converts a continuous analog quantity, i.e. voltage or current to a discrete time digital representation as number proportional to the magnitude of the input [335]. Thus, digitization is the process of approximating a continuous range of values using a finite set of discrete values or quanta.
Implementation of an ADC for Eph clustering requires certain characteristics of the signaling system, which are as follows. Firstly, Eph clustering *in cis* was proven to be sufficient for signaling, accentuating clustering as the solely critical and necessary step in inducing Eph signaling. Secondly, Eph signaling was shown to correlate to clustering in two ways - on the quantitative level depending on cluster size distributions and on the qualitative level depending on cluster stability. In clustering, considered as ADC device, the continuous analog input from various determinants, as for example ephrin ligand concentration, may be converted into a discrete digital representation, the respective clustered state, represented by cluster size and/or cluster quality, which will in the end solely determine an intracellular, kinase-dependent signaling response (Fig. 4.2).

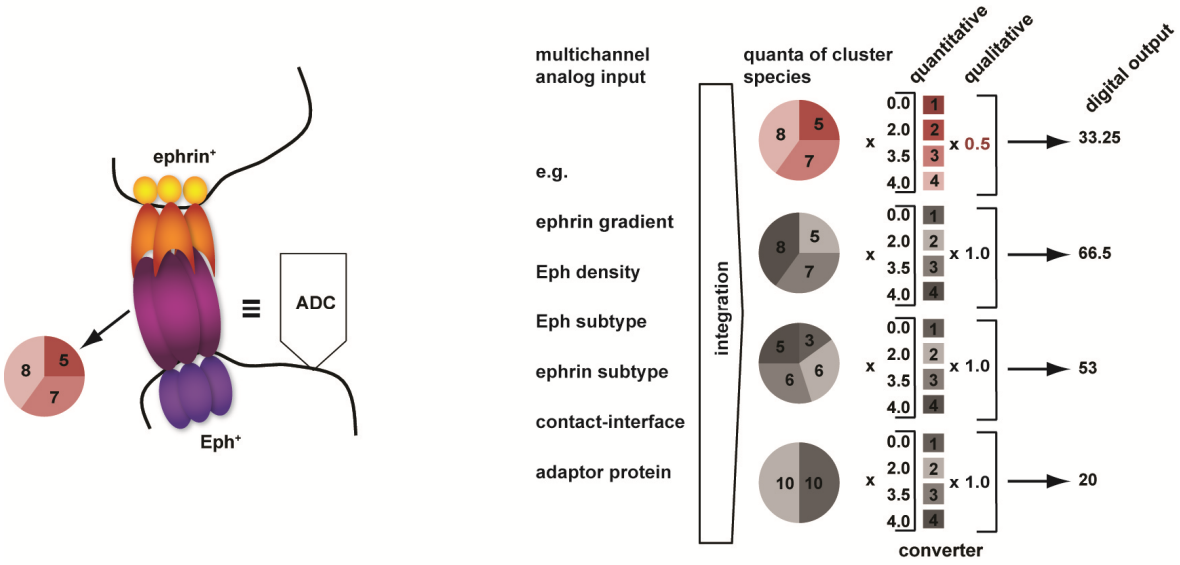

Fig. 4.2 Clustering as analog-to-digital converter of Eph signaling.
Ephrin engagement by Eph receptors produces discrete clustered states at sites of cell contact (left cartoon). These clustered states represent cluster size distributions of a certain cluster quality derived from multichannel analog inputs. Clustering may thereby be interpreted as an analog-to-digital converter to produce a uniform digital output. The conversion of analog signals into digits is computed as indicated by operators, however, only exemplary and vaguely based on experimental results.

Similarly, this concept was previously proposed for Ras-mediated EGF receptor signaling. Ras proteins are small GTPase molecular switches, which sit on membranes and, following activation by cell surface receptors, act as adaptors that recruit and facilitate activation of a wide variety of effectors [336]. Activated EGF receptors trigger the formation of Ras nanoswitches at the plasma membrane in direct proportion to the external EGF input through an unknown mechanism [337]. The plasma membrane thus digitizes analog EGF inputs using individual Ras nanoswitches as discrete quanta, functioning as a linear ADC. Ras nanoswitches are bistable, thereby functioning in a strictly switchlike ON-OFF mode. As already discussed above, a switchlike ON-OFF mode is also conceivable for Eph receptor activation. The immediate switchlike jump from low dimer activity, both on the level of receptor activation and cellular collapse response, to almost saturating signaling responses from [2,3]FKBP cluster size distributions comprising mainly trimers and tetramers is strikingly obvious. Similar to the Ras nanoswitches, the quanta of trimers or tetramers might then determine the overall signaling output. The digital pulses from individual Eph oligomers are then summed to give a final analog kinase-signaling output. However, a graded signaling output from single cluster species cannot be excluded due to weakness in resolution of the cluster species phosphorylation analysis. Moreover, physiological ephrin-induced cluster species might behave differently in terms of receptor activation mechanics. This graded

signaling output I accounted for by introducing distinct activation states for specific cluster species (Fig. 4.2 - quantitative converter) rather than only two ON-OFF switchlike low and high activation steady states.
Furthermore, I connected a second digitizing converter in series to the first one, which unlike the first digitizing converter does not reconsider the quantitative but qualitative aspects of clustering, also inherent to clusters as shown by experiments using the low-affinity AP1887 compound or low-affinity ephrinA5 ligand for EphB2 (Fig. 4.2 - quantitative converter). Both digitizing converters then synergize to generate one digital signaling output. Again, the ADC in Figure 4.2 is configured by a rather graded computation of both converters, which improves the resolution of the digital output. However, other more switch-like ON-OFF configurations might also be possible, since resolution of blue-native PAGE analysis did not allow an unbiased conclusion. Future *in silico* analysis of Eph clustering implemented as ADC device may generate more confidence in the configuration of the clustering ADC.

What is the benefit of a clustering ADC for Eph biological responses? Eph receptor signaling is very much limited to a sub-cellular scale of activation by membrane-bound ephrin ligand [33,238]. This stands in contrast to other RTK signaling systems, where receptor activation is less spatially restricted due to the soluble nature of ligand stimulators. Eph receptor signaling is also required to remain localized to sub-cellular regions and domains to mediate proper axon growth cone collapse or boundary formation processes. This situation requires a **high fidelity** of the signaling system to account for fine-tuned spatial cellular responses. Fidelity is defined as the similarity between the input (e.g. ephrin ligand) and output signals (e.g. kinase signaling). Indeed, an analog-digital-analog circuit relay generates a high-fidelity in signal transmission over a vast range of signaling inputs [287].
Another benefit of ADC signaling is the **robustness of the response**, which is a fundamental characteristic of all biological systems and is defined as “a property that allows a system to maintain its functions against internal and external perturbations” [338]. All biological systems are subject to a variety of random disturbances or variations, collectively referred to as noise. Eph receptor signaling suffers more than any other RTK signaling system from both extrinsic noise (generated external to the system), and intrinsic noise (noise inherent to the system itself). Purely analog systems are particularly vulnerable to distortion by noise when transmitting the growth factor signal across the membrane. Because of the small fraction of activated receptors upon ligand engagement as compared to the whole cell receptor population, a two-state signaling mode (cp. section 1.6.1), as observed for singular receptor signaling systems would be highly susceptible to intrinsic noise.
Lastly, one of the most striking features of a digitization step through clustering is the possibility to fuse various analog signals into one simple digital output, in a process of **integration**. Indeed, Eph/ephrins comprise the largest subgroup of all RTKs with high combinatory cross-specificity between subtype Ephs and ephrins. In terms of evolutionary aspects, it is therefore conceivable that the system had to invent a strategy to compute various

analog signals of different quality and strength into one single output, namely kinase activity. Other more cell-specific analog signals may also be integrated to finally produce the Eph/ephrin system's graded signaling nature.
In summary, the beauty of the ADC concept relies on its simplicity to integrate various analog signals in one robust digital output. Clustering ensures a high fidelity of response which enables graded, kinase-dependent signaling.

4.3 Clustering is a mechanistic relay for Eph receptor kinase activation

Clustering may be considered as an analog-digital converter to produce discrete digital outputs to cause graded kinase-dependent Eph signaling. However, the question, how this digital output is reconverted into an analog signal, which may be interpreted by the cell through downstream signaling pathways, remains unsolved so far. In the following paragraphs, I offer a model for a digital-to-analog converter, which is intrinsic to the mechanism of kinase activation of Eph receptors and allows for graded signaling responses.

Role of Eph oligomerization. The importance and possible role of Eph clustering for activation of signaling responses may be considered e.g. in direct comparison to kinase activation of other RTKs like EGFR to point out valuable functional features for Eph dimerization and oligomerization.
The current activation model of the EGFR predicts that binding of EGF results in dimerization of the EGFR, leading to the allosteric activation of the intracellular tyrosine kinase [17,339]. Although EGF binding and dimerization seem to be strictly connected, both microscopic and biochemical studies have demonstrated that in resting cells, the receptor is already found on the cell surface as non-active dimers, the so-called predimers [21,22,328,340-347]. Recent structural data also showed that the dimerization of the C-terminal part of the kinase prevents kinase activation and represents a mechanism through which the EGFR tyrosine kinase is inhibited in resting cells [18]. For Eph receptors, the pre-existence of such dimers might also be the case and has been suggested previously for rising Eph surface densities [80,106]. EGFR predimers must be inter-converted into functional dimers through EGF binding which re-orientates and re-positions the intracellular kinase domains of two EGFRs to enable full signal amplification in an ON-OFF mode. By contrast, full kinase signal amplification cannot be observed for Eph dimer formation, however, Eph receptors engaged in dimer species are activated to a small degree (this study).
Full Eph receptor activation is obtained upon higher-order clustering, which is permissive for full signal amplification and caused by ligand engagement. Recently a new study, which also used homo-FRET imaging to visualize oligomerization states, showed that EGFR also oligomerizes but that in contrast to Eph receptors, kinase activity is required to enable this process [327]. However, EGFR dimerization and oligomerization led to receptor internalization. This indicates a fundamental difference in the mechanistic and functional role

of oligomerization of both receptors. For Ephs, oligomerization may be seen as an overriding control, which acts as a mechanistic relay to cause kinase activity in a very sensitive manner, whereas for EGFR, oligomerization is not permissive but a secondary effect of receptor activation. In the latter, oligomerization may enhance catalytic substrate turnover through an enzymatic/substrate concentration effect [348]. For Ephs, this effect might also be true, but of subordinate role. More importantly, Eph receptors excel by their unique kinase activation mechanism, which was outlined in detail in section 1.3. Kinase activity is mainly controlled by JM tyrosine phosphorylation. However, this phosphorylation event does not result in an ON-OFF switch of kinase activation. Latest structural studies using NMR-technology also suggested that a further change in conformational dynamics underlies kinase activation. Kinase activity is therefore likely to be governed by a shift in the thermodynamic equilibrium between an open and closed kinase conformational state. This may serve as an analog signal which determines a graded kinase activity acting on downstream signaling effectors like Src or ephexin.

My work with the constitutively kinase-active eeEph receptor provides a more detailed insight into the kinase activation mechanism and its link to clustering. Although the opposite was published for neuronal cultures [113], eeEph receptor kinase activity could further be enhanced by clustering using the [2,3]FKBP-system in cell culture. Moreover, this increase in kinase activity came along with a remaining ability to induce cell collapse upon dimerizer application. These results suggest that eeEph receptors are only partially constitutively-active and are corroborated by findings of the Sicheri lab. A Tyr750Ala EphA4 mutant also showed an increased kinase activity again pointing to the fact that kinase activity may be further increased for eeEphA4 by abrogation of further structural constraints [107,112]. However, adaptiveness of eeEph receptor kinase activation was lost in response to differences between 2FKBP and 3FKBP cluster size distributions. This loss in adaptiveness was also observed in knock-in mice for eeEphA4, which only displayed a defect in thalamocortical mapping, where adaptive, gradual signaling was perhaps necessary to establish proper innervation [113].

In summary, the constitutively kinase-active eeEph receptor provides a deeper insight into kinase activation. Apparently, abrogation of JM structural constraints does not lead to a fully constitutively kinase-active Eph receptor. Additional structural constraints and an underlying thermodynamic equilibrium are additional regulators, representing Eph-intrinsic screws for a graded control of Eph kinase activity.

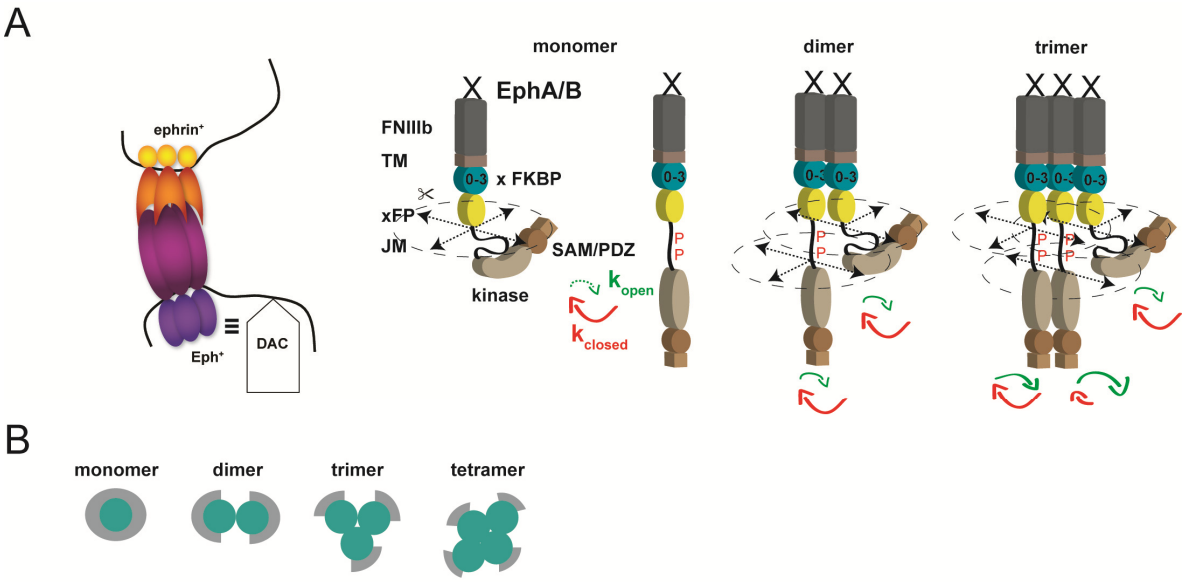

Fig. 4.3 Clustering serves as mechanistic relay for kinase activation by causing a macromolecular crowding effect.
(A) Eph kinase activation comprises phosphorylation of key residues in the JM segment and an underlying thermodynamic equilibrium between an open and closed kinase conformation. Clustering limits spatial freedom of receptors engaged in different cluster species of different quality. The thereby exerted molecular crowding effect may govern the conformational equilibrium to enhance kinase activity. This process may be interpreted as a digital-to-analog conversion to account for graded kinase signaling responses. **(B)** Receptors engaged in cluster species from monomers to tetramers experience different degrees of spatial freedom (indicated by grey areas).

Clustering produces a macromolecular crowding effect governing kinase activity (Fig. 4.3 & 4.4). In review of my results and present literature, I propose that clustering causes a shift in the thermodynamic equilibrium between an open, kinase-active and a closed, kinase-inactive conformational state, which is provoked by a macromolecular crowding effect caused by clustering (Fig 4.3A). In this sense, bigger or more stable clusters, digitized as discrete clustered states, simply cause the Eph intracellular domain to spend more time in the catalytically competent conformation.
For other RTKs, which display full signal amplification upon dimerization, the mechanistic component of action is more likely to function in an ON-OFF mode, e.g. through reorientation of inter-structural relationships between neighboring receptors snapping into a static conformation (e.g. EGFR). For Ephs, I propose a rather gradual transition to an active state governed by a thermodynamic equilibrium between an open and closed kinase conformation.
The underlying phenomenon of this shift of the thermodynamic equilibrium to the competent catalytic conformation may be a macromolecular crowding effect that limits the spatial freedom of each receptor molecule (Fig. 4.3B). Thermodynamic equilibria may be governed by crowding conditions in living systems, like the cell cytoplasm or membranes, which contain high concentrations of high-molecular-weight components that occupy a substantial

part of the volume of the medium [349]. Biochemical processes therefore proceed in a medium containing high concentrations of macromolecules (50-400 mg/ml) with concentrations of single macrosolute species being not so high. In fact, macromolecular crowding is more accurately termed “the excluded volume effect” because its most basic characteristic is the mutual impenetrability of all solute molecules. While macromolecular crowding is a well-established concept in enzyme kinetics changing the thermodynamic reaction equilibria and reaction rates, effects on conformational transitions have also been described lately [350,351]. Crowding affects the equilibria and transition rates between open and closed conformations of enzymes including kinases like adenylate kinase [350].

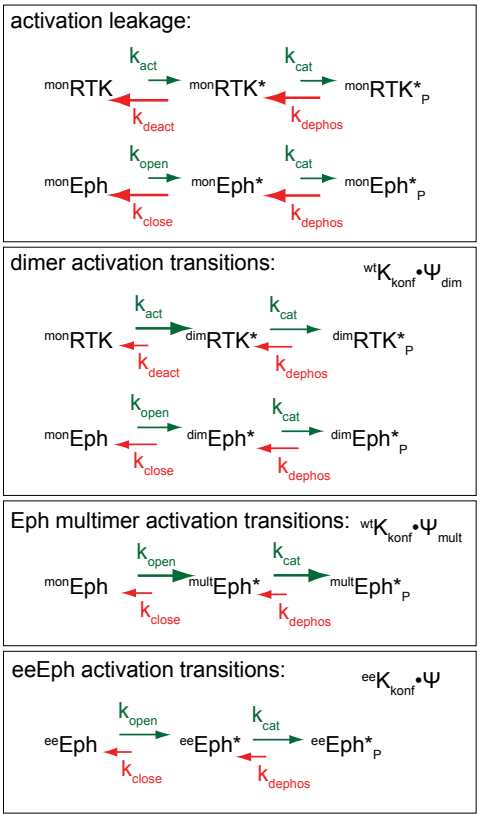

crowding:
non-ideality factor Ψ

$\Psi_{mon} < \Psi_{dim} < \Psi_{mult}$

$K_{konf} = \frac{k_{open}}{k_{close}}$

${}^{wt}K_{konf} < {}^{ee}K_{konf}$

Fig. 4.4 Eph/RTK enzyme kinetics. The activation process may be divided into two receptor transitions based on the known underlying mechanisms for Ephs, which undergo multimerization, and other RTKs, which undergo dimerization for full activation. The first transition represents a conformational change to a kinase-active conformation. For RTKs this transition is thought to occur in a rather ON-OFF switchlike mode, while for Ephs this transition may occur gradually. The change to an active kinase conformation may be governed by a rather ligand-independent thermodynamic equilibrium between two states (entirely receptor-mediated activation) or by a specific ligand-dependent conform-ational re-configuration (e.g. as for EGFR). While for RTKs dimerization or conformational re-configuration will already result in complete transition to the kinase-active state, Eph activation is initially only governed by the thermodynamic equilibrium, which may be affected by a macromolecular crowding effect. The crowding effect may be taken into account by the non-ideality factor ψ [351]. For eeEph receptors, the conformational equilibrium (K_{conf}) is shifted to a more open kinase conformation. The second transition typifies as autophosphorylation reaction of RTKs and Ephs. This reaction is determined by the intrinsic kinase activity of the receptor (k_{cat}) and the cell’s phosphatase activity (k_{dephos}) and results in the autocatalytic loop of RTK/Eph activation. For all RTKs a leakage in the activation mechanism is observed which is constantly opposed by phosphatase activity resulting in a low activation steady-state. k_{act} (forward) and k_{deact} (reverse) are conformational transition rates for dimerizing RTKs, k_{open} (forward) and k_{close} are conformational transition rates for multimerizing Eph receptors.

Results from eeEph constitutively kinase-active receptor studies also support the rationale for a molecular crowding effect governing a thermodynamic equilibrium between an open and closed kinase-active state. The residual ability of the eeEph receptor to adapt an increased kinase-active state upon clustering could in parts rely on the fact that the constitutive activity did not reach 100% prior clustering and that clustering, i.e. molecular crowding, provoked a further shift in the equilibrium to a more open conformation.

4.4 Eph clustering serves as the central integrator to elicit appropriate kinase-dependent signaling responses

This study reports that kinase-dependent cellular responses strictly correlate to Eph receptor clustering over several steps in the Eph signaling cascade, highlighting Eph clustering as higher-order control entity to elicit appropriate cellular responses. Clustering of Eph receptors is suggested to function as an ADC generating a uniform digital output, which after reconversion is "dumped" into the cell and produces a respective kinase-dependent signaling response. Interestingly, clustering, i.e. the ADC, may be able to integrate analog signals of different origin and quality, e.g. high-affinity extracellular ligand binding and low-affinity intracellular adaptor protein binding. The clustering ADC would then also serve as a central integrator of all receptor activation determining analog inputs. Thus, I reasoned that simultaneously to analog-to-digital conversion, clustering may serve as a central integrator to elicit appropriate kinase-dependent signaling responses through integration of various clustering determinants.

The FKBP/dimerizer system made it possible to test for this integrative feature of analog signals for Eph clustering. The Eph oligomerization state was manipulated from the intracellular side of the receptor and probed for integration with extracellularly applied clustering stimuli and subsequent cellular responses. Indeed, I provide direct evidence that manipulation of Eph oligomerization by intracellular forces alters the sensitivity of the cell towards extracellular ephrins. EphB2 dimerization and sub-threshold ephrinB2-Fc stimulation synergized to induce EphB2 autophosphorylation and cell collapse. Conversely, EphB2 monomerization (by steric hindrance) blocked ephrinB2-Fc-induced kinase signaling and cell collapse. Intrinsic and extrinsic clustering forces are thus interconnected, resulting in an overall clustered state, which represents the digitized output of a multichannel analog input (Fig. 4.5 & 4.6).

Fig. 4.5 Possible scenarios of analog signal integration based on the model approach using the FKBP/FRB-clustering system.
(A) Positive integration of clustering determinants. Extracellular and intracellular analog signals may act simultaneously on Eph receptors and synergize to produce a uniform output, i.e. in a respective phosphorylation (P) activation state of the receptor. **(B)** Negative integration of clustering determinants. Eph interaction partners may also negatively integrate to produce an alleviated

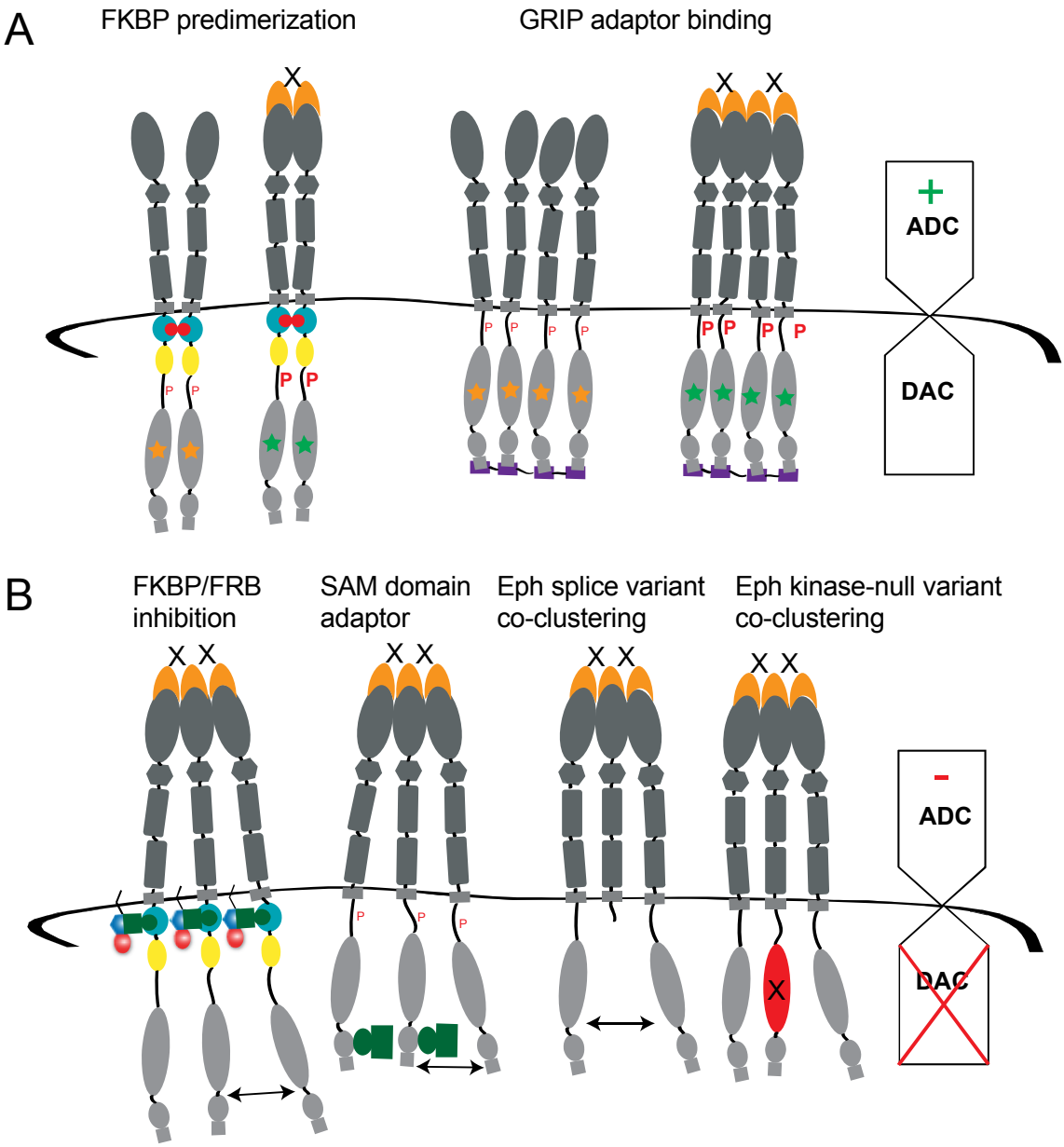

clustered state (arrows) with a lower phosphorylation activation state (as indicated by SAM domain adaptor protein binding). Moreover, steric interference may also result in total impairment of the kinase activation mechanism thereby silencing the digital-to-analog conversion (as e.g. in the case of Eph kinase-null variant co-clustering).

Can adaptor proteins represent an analog signaling component (Fig 4.5A)? Regulation of intrinsic Eph clustering may be carried out by multi-domain proteins that both bind the cytoplasmic region of the Eph and have the propensity to scaffold the receptors. Interaction of EphB2 with the multi-PDZ-domain adapter protein GRIP has previously been shown to regulate reverse signaling of ephrinB3 at specific hippocampal synapses [352]. Although the composition of EphB2 clusters was not analyzed in that study, it is conceivable that the

interaction with GRIP-preclustered EphB2 sensitizes the cells for the *trans*-interaction with ephrinB3. An earlier study identified other PDZ-adaptor proteins, among those are GRIP and PICK1, for direct interaction with EphB2 [151]. While PICK1 was clearly shown to be phosphorylated upon binding to EphB2, the activation status of EphB2 was not addressed. Here I was working to bridge this gap by testing GRIPs and PICK for their propensity to activate EphB2 when co-expressed. In fact, co-expression leads to autophosphorylation of EphB2 indicating receptor activation and possibly priming, i.e. preclustering of the EphB2 receptors similar to the experimental situation using the 1FKBP receptor isoform preclustered with AP20187. This re-examination of PDZ-adaptor protein binding with regard to the activation state of the EphB2 receptor accentuates the physiological relevance of such an integrative signaling mechanism computed into the clustered state. Cytosolic adaptor protein concentration may therefore, in addition to an external ephrin stimulus, represent an underlying analog input to the clustering ADC, which eventually alters the digital signaling output and downstream signaling responses.

Negative integration of clustering determinants (Fig. 4.5B). The clustering ADC may also serve as integrator in a negative sense meaning that adequate analog signals also deliver a negative component to the cumulative signaling response. More precisely, they might act through graded attenuation of clustering thereby reducing the crowding condition within the cluster they affect. Even more, physical Eph receptor interaction and steric interference through intimate co-clustering with e.g. Eph kinase-null receptors may totally impair the kinase activation mechanism and act in a rather ON-OFF kind of manner as dominant-negative effectors to shut down the DAC for kinase activation completely.
To also investigate these negative modes of regulation by surrounding determinants, I set up a model approach based on the inhibition by steric hindrance using an artificial intracellular inhibitor construct. Kinase activity and cellular collapse were abrogated in the presence of heterodimerizer AP21967. On the mechanistic level, ephrinB2 binding to the Eph LBD is not affected, presumably causing the constitution of an intact extracellular clustering platform irrespective of the intracellular steric interference (data not shown). Intracellularly, the inhibitory construct is assumed to keep Eph receptors at a distance from each other through FRB-FKBP domain coupling to the inhibitory construct. The intracellular cluster platform must therefore be impaired resembling an apparent “monomerized status” of Eph receptors. The model approach can only be validated as a proof of principle of the postulated concept. However, literature delivers various implications for validation of this model approach, elaborated as follows.
Adaptor proteins may indeed reduce signaling from Eph clusters by acting as spacers between single Eph monomers to produce the same mode of inhibition as for myr-FRB-mCherry. A hot candidate region, which might serve for interaction with adaptor proteins is the SAM domain. SAM domains of Eph receptors revealed a mechanism for modular dimerization [99,101]. This finding led to the speculation that Eph receptors may recruit signaling partners

through heteromeric SAM-SAM interactions. In fact, SHIP2 and ILK were shown to bind to Eph receptor and interestingly enough act on it in a rather inhibitory mode by opposing cluster internalization or promoting cell spreading rather than collapse [155,156]. Whereas active signaling links were established to pathways involving integrin- and Rac-signaling, now in reflection of the here presented results, passive Eph receptor silencing through steric interference might also play a significant role in inducing those specific signaling responses.
A more evident form of *cis*-inhibition based on steric hindrance or "apparent intracellular Eph monomerization" is the formation of mixed clusters of full-length EphA7 or EphA2 and the C-terminally truncated or soluble EphA7 splice form, respectively, which act as dominant-negative constructs on downstream signaling events [171,353]. A similar mode of interaction is seen for kinase-null EphB6 receptors which are proposed to heterodimerize with EphB4 or EphB1 and thereby become *trans*-phosphorylated [169,354,355]. Interestingly, this heterodimerization or formation of mixed clusters upon ephrin engagement is accompanied by a switch to rather adhesive signaling. It can thereby be speculated that the formation of mixed clusters incorporating kinase-dead receptors presumably produces a lower signaling potency of the paired EphB1 or EphB4 receptors. Again, steric interference or alleviation of the crowded clustered state could play a significant role and be an underlying mechanistic component for the functional consequences observed. Whereas these kinase-signaling deficient Eph receptors quite consistently antagonize their signaling potent interacting partner *in cis*, heterotypic and physical interactions between Eph receptors and other receptor families do not draw a clear antagonistic picture of signaling action [192]. However, for many other receptor cross-talk scenarios physical protein interactions are still unknown and signaling might only intersect on downstream mediators. Furthermore, the origin of signaling is often not assigned to either receptor species exclusively. The Eph receptor might function as a modulator for the other receptor and not be antagonized upon its own signaling potency.
Cis-interactions of Ephs and ephrins are also known to reduce Eph signaling [103,199-201]. However, how *cis*-interacting ephrins reduce Eph signaling was to date unknown and was only speculated upon to rely on steric interference [32]. This study now provides direct evidence for a possible steric interference mode of signaling inhibition for Eph receptors, thereby deactivating the analog-to-digital convering properties of Eph clustering.

Adhesive versus repulsive Eph signaling responses (Fig. 4.6). In retrospective of the discussed results, Eph kinase-dependent signaling responses seem to be strictly controlled by receptor clustering.
Furthermore, clustering serves as integrator for various analog signals, computed into one digital output, which is then reconverted into graded kinase-signaling. Kinase-dependent signaling responses almost always result in cell repulsion or contraction of the cell periphery. However, adhesive cellular responses have also been observed for Eph/ephrin signaling *in vivo* [30]. They are either mediated by specific kinase-dependent signaling through the integrin pathway or kinase-independent "cell surface" signaling through high binding

affinities between Ephs and their cognate ephrins [161,162,164-167,290]. Whereas kinase-dependent adhesion may only apply to a subset of Eph signaling scenarios, kinase-independent adhesion is intrinsically present in all Eph/ephrin signaling scenarios. I have addressed the mechanistic aspects underlying the switch from repulsive to kinase-independent adhesive signaling responses by the use of the inhibitory FKBP/FRB-system performing a co-culture assay with HeLa cells. In fact, steric interference disabled the digital-to-analog conversion to kinase activity resulting in a switch to adhesive signaling responses marked by e.g. filopodia sticking to the adjacent ephrin-expressing cell.
In consequence, adhesive versus repulsive cellular responses may be gradually balanced through the integrative computation of analog signals by the clustering ADC. In very severe cases, steric interference may also lead to total impairment of the DAC for kinase activity and result in a complete switch to cell adhesion.

4.5 Eph steady-state signaling network

Eph receptor signaling induced cellular responses are not the mere isolated response to receptor activation by clustering but the cumulative outcome of an *in vivo* network configuration, which underlies the Eph signaling system and is specific to the cellular background. In all cells, Eph kinase modules are tightly controlled by positive and negative feedback loops, in addition to an intrinsic self-enforcing autocatalytic feed-forward loop. Moreover, independent of Eph activation, a constant negative phospho-signaling regulation by phosphatases is a feature of inherent cell homeostasis, which might differ in activity levels in different cell types. For instance, PTP1B was shown to constitutively regulate EphA3 activity [176]. In my study, the autocatalytic feed-forward loop became visible in biochemical autophosphorylation assays using weak clustering stimuli like the low-affinity homodimerizer AP1887 or ligand ephrinA5 for EphB2. In contrast to the high-affinity homodimerizer AP20187, AP1887 produced a delay in the autocatalytic feed-forward loop of receptor activation (cp. Fig. 4.4). Absolute substrate phosphorylation levels were significantly higher for the constitutively kinase-active eeEph receptors as compared to wildtype receptors but eeEph-expressing cells were not affected by constitutive kinase-active signaling. This indicates a negative feedback loop on downstream kinase signaling targets, which desensitizes the cell to the constant higher level of kinase signaling. A clustering stimulus would then indeed cause a further enhancement of kinase activity but the cell would only be capable to respond towards the relative change in kinase activity - and not to the absolute state of receptor kinase activity. This effect may be seen in the reduced cell collapse response upon clustering of eeEph receptors.

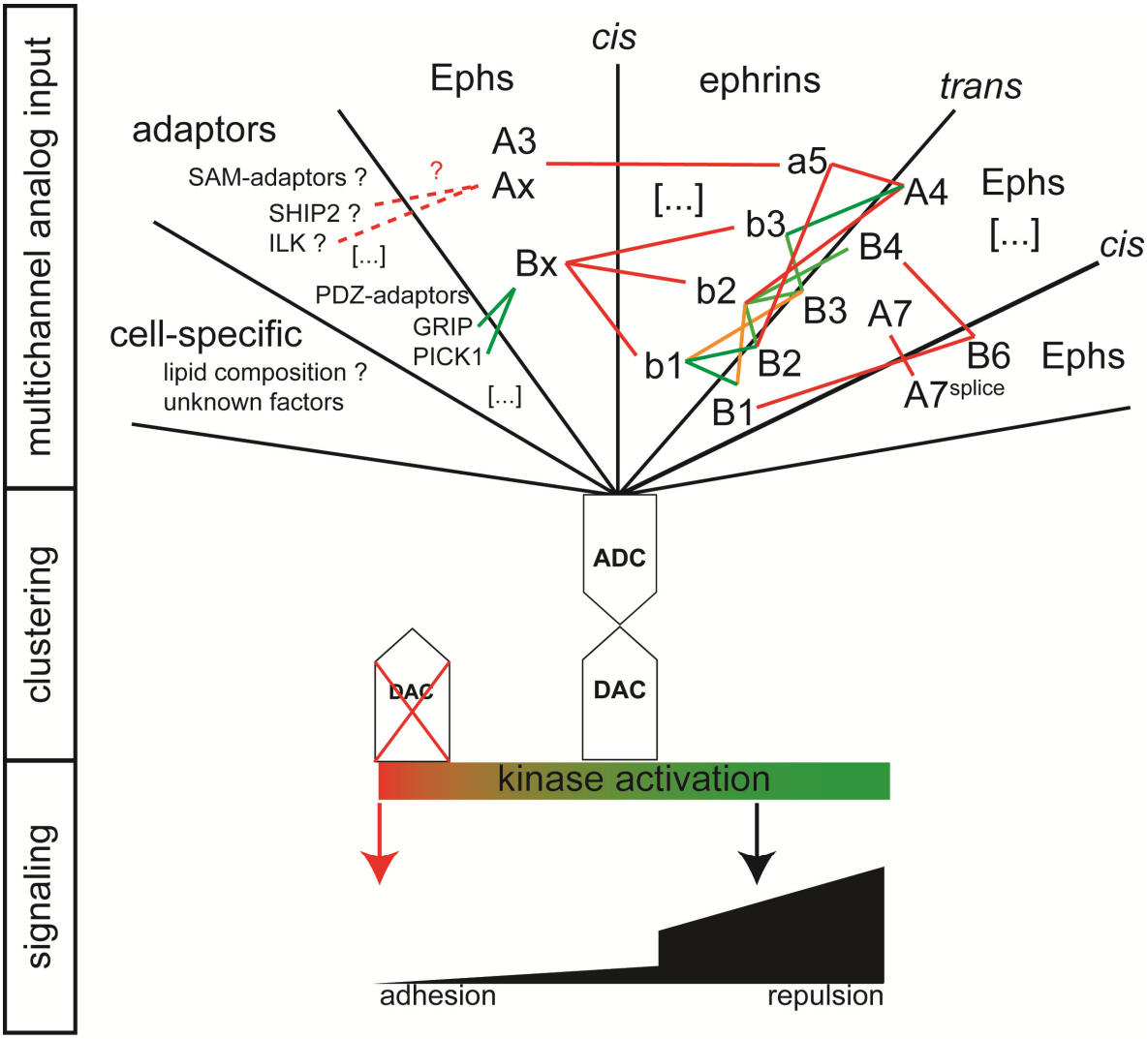

Fig. 4.6 Clustering as the central integrative device for Eph signaling.
Model depicting the computation of clustering determining multichannel analog signals which are transmitted into kinase activity by an analog-to-digital-to-analog conversion process through clustering. In the case of steric interference, which results in full impairment of the kinase activation mechanism, kinase-dependent repulsive signaling will convert into kinase-independent passive adhesion. A possible selection of analog signals is presented without claim to be complete. Eph-ephrin trans-interactions: color code of line indicates binding affinities (red: K_d > 5 nM; orange 1 nM < K_d < 5 nM ; green K_d < 1 nM according to [70,356]; Eph-ephrin *cis*-interactions: red lines indicate *cis*-inhibition of Eph receptors between ephrinAs and EphAs and ephrinBs and EphBs respectively; Eph-Eph *cis*-interactions: red lines indicated cis-inhibition between Eph receptors. A7splice = truncated splice form of EphA7 co-expressed with full-length EphA7. EphB6 is kinase-null. Adaptor proteins: heterotypic SAM-SAM domain interactions to adaptor proteins may be implicated in negatively regulating Eph receptor signaling. PDZ-adaptors are implicated in preclustering of Eph receptors and thereby priming them; cell-specific clustering determinants like lipid composition may also have an impact on clustering.

It is conceivable that integration of all negative and positive feedback loops together with receptor kinase activation upon clustering may result in a cumulative Eph signaling network response (Fig. 4.7). Prior to ephrin engagement, the Eph signaling network is kept on a low activation level in steady-state. This is accomplished through a permanent negative regulation of Eph receptor kinase activity leakiness by phosphatases. By contrast, the eeEph signaling network settles down on a much higher activity level in steady-state due to the constitutively kinase-active state of the receptor mutant. Clustering enhances Eph kinase activity instantaneously leading to a temporary distortion of the Eph signaling network steady-state of activation. Simultaneously, clustering may even have the ability to suppress a negative regulation of phosphatases by spatial exclusion from clusters. The Eph signaling network immediately tries to re-establish the initial pre-stimulation state and swings into a new steady-state of activity. This phase became obvious in cell collapse assays, when a cellular re-spreading process jumped in after reaching a maximal amplitude of collapse. Moreover, quenching of clustering in phase I of the cell response pattern (Fig. 4.7) resulted in a weaker collapse and faster adaption to a new steady-state. Negative feedback loops are most likely enhanced upon Eph receptor activation to accomplish this process.

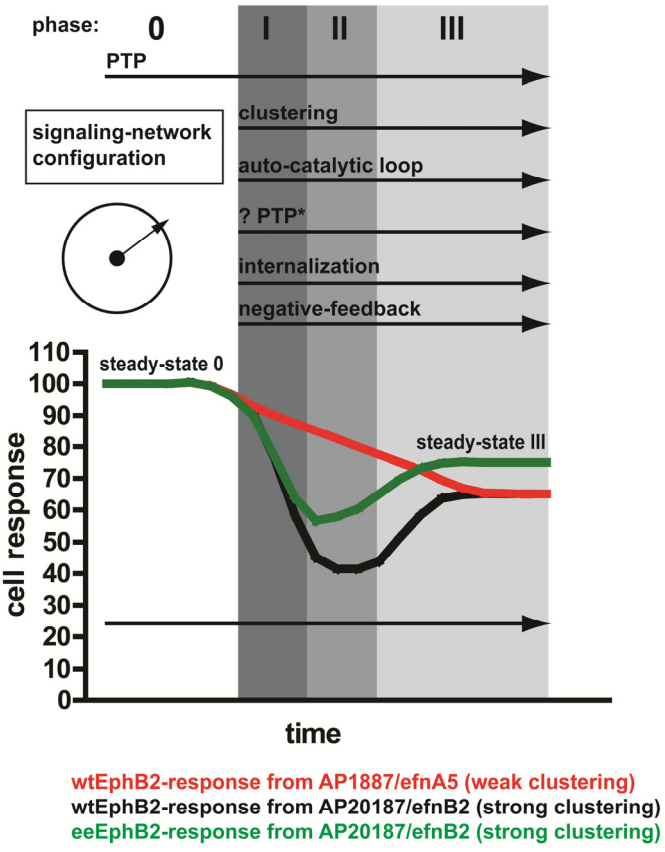

Fig. 4.7 Steady-state of activation of the Eph receptor signaling network. Curve graph delineates the cellular response pattern of Eph receptor-expressing cells over time. Arrows indicate underlying configurations of the signaling network (PTP-phosphatase activity; receptor internalization; negative feedback loops of downstream signaling cascade; Eph autocatalytic feed-forward loop; clustering; possibly more), which are constitutively active or are induced upon Eph clustering. The Eph receptor signaling network may be specifically configured (indicated by tachometer) according to cellular background and/or Eph intrinsic/extrinsic determinants such as constitutive kinase activity (eeEphB2) or a weak (AP1887/efnA5) or strong (AP20187/efnB2) clustering stimulus. (?) indicates a possible enhanced (*) PTP-activity upon receptor clustering.

Moreover, Eph receptor internalization, which is specific to receptor activation, likely represents an opposing force to receptor signaling and thereby supports negative feedback loops. Inhibition of Eph internalization was indeed shown to abrogate the re-spreading response [133]. Theoretically, additional phosphatases may also be activated upon Eph activation, which would also counteract Eph signaling and help in re-establishing the initial pre-stimulation state.

4.6 Eph clustering produces diffusion-limited spatial signaling entities redistributed to the lateral cell edge

RTK signaling in general, but also Eph signaling in particular is influenced by trafficking and processing prior and posterior to receptor activation [10,235]. Irrespective of its effect on Eph receptor signaling, I studied the effect of clustering on the distribution, movement and processing of Eph receptors. Prior to ligand engagement, Eph receptors are transported to the cell surface plasma membrane by guided vesicle transport, most likely along microtubules (this thesis and [251]). Indeed, the discovery that the microtubule motor protein KIF5 (also known as kinesin 1) interacts with a region of GRIP1, also established as scaffolding protein for Eph receptors, indicates an anterograde microtubule transport mechanism for Eph receptors [151,251,357]. Eph receptors, finely distributed in the membrane prior to ligand engagement, display surprisingly high density fluctuation rates as visualized by TIRF microscopic analysis. A more profound analysis using fluorescence correlation spectroscopy and/or FRAP (fluorescence recovery after photobleaching) may help to determine actual diffusion rates in future studies and confirm these preliminary implications. Immediately after clustering, spatially static Eph receptor accumulations emerged at sites where the stimulus could access the cell surface plasma membrane. Cluster accumulations were stable for an extended amount of time but then degraded in a process, which is most likely due to specific Eph receptor internalization. Interestingly, signaling entities also rapidly re-distributed to the lateral cell edge in a strict cluster size-dependent manner. Based on cell geometry concepts, the strong membrane curvature at the lateral cell edge may produce a membrane division of limited diffusion, which leads to Eph receptor cluster accumulations.

Strikingly, redistribution of Eph receptor signaling entities to the lateral side of the cell may serve an important role for Eph receptor spatial signaling properties. In contrast to many other signaling systems which have not implemented clustering mechanics for themselves, the Eph/ephrin signaling system requires a high sub-cellular spatial resolution for signaling in order to meet the needs for guided repulsive responses such as axon growth cone guidance or cell sorting into different domains. Triggers for contractions of cell protrusions, such as Eph signaling entities, must specifically act at the lateral cell side to be able to directly and locally affect actin cytoskeleton dynamics. In this respect, clustering may then indirectly serve as a means to re-distribute activated Eph receptor signaling entities to sub-cellular sites where local signaling is required to mediate contractive cell responses.

4.7 Outlook

Eph receptor clustering. This study has provided a deeper insight into the RTK-unique feature of Eph receptor clustering and its functional importance for signaling. Addressing oligomerization processes of proteins in living cells is by no means an easy and straightforward task. Thus, this work can only build the fundamental basis for further and more detailed studies - solidifying the here offered analog-to-digital converter model for clustering and bringing trafficking aspects of Eph receptor clustering into sharper focus. In ongoing, preliminary work I deal with a computational modeling approach to simulate the clustering ADC thereby corroborating experimental results.
Only little is also known about the intracellular vesicular pathways upon Eph internalization. Fractions of smaller clusters might be differentially trafficked and recycled in Rab11-positive compartments, whereas fractions of bigger clusters would follow the degradative sorting pathway to lysosomes.
Mechanistically, I propose clustering to be a relay for kinase activation by causing a macromolecular crowding effect, which may shift an underlying dynamic equilibrium between a closed and open kinase conformation. Based on the here presented results and implications from other studies, this model seems plausible. However, direct proof is missing. To obtain more definitive insights into the mechanism of Eph activation, structures of full-length Eph receptors or Eph kinase sensors would be necessary. The system of dimerizer-inducible cluster formation has proven to be a powerful tool. It is therefore conceivable to implement this system in further *ex vivo* and *in vivo* studies, in model organisms like zebrafish or mouse.

Role of Eph receptor clustering. Clustering of bacterial chemotaxis receptors has been studied over decades suggesting a whole list of advantages for the signaling system [267,286]. While some may be intuitively mapped onto the Eph signaling system, others remain questionable if they also apply for Eph receptor clustering. Furthermore, bi-directional signaling and co-clustering of the cognate ephrin ligand in the opposing cell complicates the signaling scenario and may prevent a one-to-one analogy to other signaling systems. It is therefore difficult to identify the specific, counter-intuitive advantages of the Eph signaling system. Three of them were proposed in this study: high fidelity, robustness and the possibility to integrate multiple analog signals. Others, like a heightened sensitivity of the signaling receiver are rather intuitive. Future studies will most likely contribute further pieces to the big puzzle about the role of Eph receptor clustering for signaling processes.

Therapeutic implications of receptor clustering. Mechanistic to functional studies of RTKs, involved in cancerogenesis, are generally of broad interest in pursuing new therapeutic strategies for signaling inhibition [358]. Therapeutic antibodies belong to the most promising new-age therapeutics of cancer biology. Their mechanisms of action range from induction of

apoptosis (e.g. Rituximab, Genentech/Roche) to competing for binding with ligand molecules (e.g. Trastuzumab, Genentech/Roche). It is therefore absolutely necessary to understand the target on a mechanistic to functional basis. This study delivers important insights into receptor mechanics and underlying signaling function. As an example of a way to suppress signaling, Eph receptors must be targeted in a way, which would keep them in their monomeric configuration, as it is the case for receptor inhibition via the myr-FRB-mCherry inhibitory construct used in this study.

Ephrin ligand clustering. Although the FKBP/FRB-system was also implemented for ephrins, Eph clustering has been the main focus of this study. Preliminary results point to the same benefits of the FKBP/FRB-system for studying ephrin clustering. Initial experiments demonstrated similar outputs for the dimerizer-induced and Eph-induced ephrin signaling responses and clustering seems to tightly correlate with internalization responses. The ephrin signaling pathway has not been studied in this context, which remains for further studies.

5. EXPERIMENTAL PROCEDURES

5.1 Molecular biology techniques

Expression constructs used in this thesis were either obtained from elsewhere as indicated in table 5.2, or cloned using standard molecular biology techniques [359].

Plasmid DNA Preparation. Plasmid DNA was purified from small-scale (4 ml, minipreparation), medium-scale (100 ml, midipreparation) or large-scale (250 ml, maxipreparation) bacterial cultures. Respective LB_0 medium (lysogeny broth medium, 10 g Bacto-Tryptone, 5 g Bacto-Yeast extract, 5 g NaCl, autoclaved) volumes were inoculated with single colonies picked from agarose plates (1 l LB media, 15 g Bacto-Agar, antibiotic, autoclaved) containing 100 µg/ml ampicillin or 50 µg/ml kanamycin and grown overnight at 37 °C shaking. After centrifugation of the cell suspensions, pellets were resuspended in buffer P1 (Qiagen, Hilden, Germany) and stored at -20 °C until DNA preparation. DNA preparations were carried out according to the Qiagen protocol using the respective scale-sized kits (27104, QIAprep Spin Miniprep Kit; 12163, QIAGEN Plasmid Maxi Kit; 12843, CompactPrep Plasmid Midi Kit).
After preparation, DNA pellets were re-dissolved in a suitable amount of TE buffer (10 mM Tris-HCL, 1 mM EDTA, pH 8.0) and plasmid DNA concentration (λ= 260nm) and quality of purity (260/280 nm ratio) was determined using the UV spectrometer NanoDrop 2000 (PeqLab, Erlangen, Germany).

Enzymatic treatment of DNA. Cleavage of plasmid DNA or DNA-fragments for insertion was done using digestion with restriction enzymes (NewEngland BioLabs, Ipswich, MA). Approximately 2-10 µg of DNA was cut in 20-100 µl of the appropriate restriction enzyme buffer and 2-10 units of restriction enzymes for 1 to 2 hrs, or overnight, at the enzyme-specific temperature. De-phosphorylation of cleaved plasmids with sticky ends was performed with calf intestine alkaline phosphatase (713023, Roche Diagnostics, Indianapolis, IN) according to the manufacturer's protocol. Ligations of plasmid backbones and target DNA-fragments were carried out in an incubation of a 1:1, 1:2 and 1:5 and molar ratio (total 400 ng DNA per 20 µl reaction volume) of plasmid and insert with 1 unit of T4 DNA Ligase (M0202L, NewEngland BioLabs) in ligase buffer at 4 °C overnight. The next morning, ligation samples were either frozen and stored for further use, or 2-5 µl of the mix was transformed via electroporation (settings: 25 µF, 2.5 kV, 200 Ω, GenePulser, BioRad, Hercules, CA) into 30 µl electrocompetent *E. Coli* cell suspension (OneShot Top10, C4040-52, Invitrogen) and plated on selective agarose plates.

Separation of DNA. For separation of DNA on agarose gels, 6x loading buffer (50 % glycerol v/v, 1x TAE buffer, 0.2 % w/v Laemmli buffer) was added to appropriate volumes of DNA and loaded on a 0.8-2 % agarose gel in TAE buffer (50x TAE: 242 g Tris base, 57.1 ml glacial acetic acid, 100 ml 0.5 M EDTA pH 8.0, add H_2O 1 l) containing ethidium bromide (2218.2, Roth, Karlsruhe, Germany, 6 µl per 100 ml agarose suspension), and run at 120-200 V for 30 min to 2 hrs. After electrophoresis, the gel was scanned in the transilluminator on a UV light box and printed. For preparative agarose gel, electrophoresis bands of interest were excised with a clean, sharp scalpel and purified using the QIAquick Gel Extraction Kit (28704, Qiagen) according to the manufacturer's protocol. The resulting extracted DNA was redissolved in sterile, distilled water.

DNA Purification. Small-scale DNA purification steps were carried out following restriction digests or de-phosphorylation using the QIAQuick PCR Purification Kit (28104, Qiagen) according to the manufacturer's protocol. For purifications followed by restriction digests, columns were rinsed with 70 % ethanol (v/v) in water, in addition to the washing steps, to remove any residual salt, which could interfere with restriction enzyme reaction conditions. DNA was eluted from columns in pure water.

Mutagenesis. For site-directed mutagenesis, the QuikChange II XL Site-Directed Mutagenesis Kit (200521, Stratagene, La Jolla, CA) was used. Mutagenesis primers were designed using an online tool (http://labtools.stratagene.com/QC) provided by the manufacturer. All steps were carried out exactly as outlined in the manufacturer's protocol.

Polymerase chain reactions. For production of inserts used for cloning, polymerase chain reactions (PCRs) were performed using respective templates and primers as indicated in tables 5.1 and 5.2. Template (100 ng), primers (0.2 µM each), nucleotides (1 mM of NTP mix), 1x polymerase reaction buffer, and sterile, distilled water to give a final volume of 50µl were mixed on ice in PCR tubes. PfuUltra High-Fidelity DNA Polymerase (2.5 units, 1 µl; 600385, Stratagene) was added last and the reaction mixture was kept on ice until the start of the cycle. PCR parameters comprised an initial hot start denaturing step of 95 °C for 2 min, followed by 30 cycles of double strand DNA denaturation, primer annealing and chain extension. Denaturation was performed for 1 min at 95 °C. Annealing temperatures were chosen to be between 3- 5 °C below calculated annealing temperatures for respective primer pairs (53- 68 °C) and kept for 30 s. Depending on the target-size of the amplified DNA-fragment, chain extension was performed for 1 min/kb DNA at 72 °C. After finishing the 30 cycles, the PCR-program entered a final 10 min chain extension period of 72 °C before cooling the reaction to 10 °C. For identification of possible positive clones from ligations, either restriction digests with subsequent analytical agarose gel electrophoresis from minipreparations were performed, or a bacterial colony-PCR was used. For colony-PCR, T4-Taq Polymerase (M0267L, NewEngland BioLabs) was added to a mix of the respective PCR

reaction buffer, primers and NTPs to give a master-mix without template DNA. Single colonies were then picked from agarose plates with a tip and replicated onto another agarose plate for later use. In parallel, the same tip was used to inoculate the aliquoted master-mix samples with template DNA. After PCR, possible positive clones were then identified by assessing correct band patterns using agarose gel electrophoresis. Finally, true positive clones were identified by sequencing [360].

***In vitro* RNA transcription** was carried out using the SP6 mMessage mMachine Transcription Kit (Ambion, Austin, TX) according to the manufacturer's protocol. Briefly, DNA (pSFVwtEphB2-xFKBP-YFP and pSFVhelper) was linearized using the restriction enzyme SpeI. The plasmids were then purified using a standard phenol/chloroform extraction [361,362] and 100-200 ng were then used as template for transcription under standard conditions. RNA was precipitated using the LiCl solution provided in the kit. It was then resuspended in nuclease-free water and analyzed for correct size and integrity by agarose gel electrophoresis.

5.2 Plasmids and cloning strategies

Table 5.1 List of oligonucleotides.
Key for use of oligonucleotides: C, Cloning; M, mutagenesis; S, sequencing; L= linker oligonucleotide; SG, synthetic gene. For PCR-primers, annealing temperatures were calculated using an online tool (http://www6.appliedbiosystems.com/support/techtools/calc/).

Name	Oligonucleotide Sequence (5' → 3')	Use
EphB2-1Fv-fwdG	TATAGCTAGCGTCTAGTGGAGTGCAGGTGGAGAC	C
EphB2-1Fv-revCG	TATAGGATCCCGACTAGTTTCCAGTTTTAGAAGCTCCAC	C
t3565g_t3567g	GACCCCAGGCATGAAGATCGAGATAGATCCTTTCACCTATG	M
t3565g_t3567g_antisense	CATAGGTGAAAGGATCTATCTCGATCTTCATGCCTGGGGTC	M
t3583g_t3585g	CGAGATAGATCCTTTCACCGAGGAAGATCCTAATGAGGCAG	M
t3583g_t3585g_antisense	CTGCCTCAATTAGGATCTTCCTCGGTGAAAGGATCATCTCG	M
a3566t	CCCCAGGCATGAAGATCTTTATAGATCCTTTCACCTA	M
a3566t_antisense	TAGGTGAAAGGATCTATAAAGATCTTCATGCCTGGGG	M
a3584t	GATCTTTATAGATCCTTTCACCTTTGAAGATCCTAATGAGGCAG	M
a3584t_antisense	CTGCCTCATTAGGATCTTCAAAGGTGAAAGATCTATAAAGATC	M
2-5-mchFRB	TATAACTAGTTCAGGCATGGTGAGCAAGGGCGAGGAG	C
2-3-mchFRB	TATAGGATCCTTAAAGCTTCTTGTACACCTCGTCCATGCCG	C
NT-MemFRB-fwd	AATTCATGCTGTGCTGTATGAGAAGAACCAAACAGGTTGAA AAGAATGATGAGGACCAAAAGATCGGCTCAAGTGGCATGGCTT	L
Nt-MemFRB-rev	GAATTCATGCTGTGCTGTATGAGAAGAACCAAACAGGTTGAAAA GAATGATGAGGACCAAAAGATCGGCTCAAGTGGCATGGCTTCT AGA	L
B2-1Fv-FWD	TATATCTAGAACTAGAGGAGTGCAGGTGGAGACTATC	C
B2-1FV-Rev	TATA GCGGCCGC CAGTGTGATGGATATC	C
linkSpeI/NotIfwd	CTAGTTGAGATATCGC	L
linkSpeI/NotIrev	GGCCGCGATATCTCAA	L
1-5-mcherry	TATAGGATCCACCGGTCGCCACCATGGTGAGCAAGGGCGAGGA G	C

1-3-mcherry	TATAAAGCTTGTACACCTCGTCCATGCCG	C
EphAfwdNheI	TATAGCTAGCGGCAGCGGCGTCCAAGTCGAAACCATTAG	C
EphArevNheI	GCTAGCGCCGCTGCTGCCCTTGTACAGCTCGTCCATGCCG	C
pSFVEphB2^{ecto}fwd	TATAGGATCC ATGAACTTTATCCCAGTCGACATTC	C
pSFVEphB2^{ecto}FKBPrev	TATAGGATCC*CG*ACTAGTTTCCAGTTTTAG	C
pSFVEphB2^{ecto}rev	TATAGGATCCCGGGCCCGCG	C
FLAG-FNIIIb-TM-Cyt	TATAGATATCGAGGTGTGGCAGGCTTGAGATCTGGCCATACACT TGAGTGACAATGACATCCACTTTGCCTTTCTCTCCACAGGTGTC CACTCCCAGGTCCAACTGCAGGCGAGCCTGAATTCTTTCGGGA CTGTCAGTGAATCCAGAGAAGCTAACATCTATGAACTCTGATTT GAATACAGGATTCAAGCGTGTACTGGCCTGTTTGGCAGAAAAAT ATCATTTCTGATCGACGATCATCATGAACTTTATCCCAGTCGACA TTCCACTCTTGATGATCTTCCTTGTGACAACTGGGGGCTCAGCG GACTACAAAGACGATGACGACAAGGGGCCCGGCTCAGGGGTG AACATCACCACCAACCAAGCAGCACCATCGGCCGTGTCCATCAT GCACCAGGTGAGCCGCACTGTGGACAGCATCACCCTGTCGTGG TCCCAGCCAGACCAGCCCAACGGTGTGATCCTGGACTACGAGC TGCAGTACTATGAGAAGGAGCTCAGTGAGTACAACGCCACGGC CATAAAAAGCCCCACCAACACAGTCACTGTGCAGGGCCTCAAA GCCGGCGCCATCTATGTCTTCCAGGTGCGGGCACGCACCGTTG CAGGCTATGGGCGCTACAGTGGCAAGATGTACTTCCAAACCAT GACAGAAGCCGAGTACCAGACCAGCATCAAGGAAAAGCTACCC CTCATCGTTGGCTCCTCCGCCGCCGGCTTAGTCTTCCTCATCGC TGTGGTCGTCATTGCCATCGTATGTAACAGACGGGGGTTTGAG CGTGCCGACTCAGAGCTAGCTATA	SG
CMVfor	CGCAAATGGGCGGTAGGCGTG	S
Seq-rev-ephrb2	TTTATGTTTCAGGTTCAGGG	S
Seq-fwd-ephrinb2TM	CTAGCACCGATGGCAACAG	S
Seq-fwd-EphB2TM	GGAAAAGCTACCCCTCATC	S
Seq-rev-pFRB	CCCTGAAAACTTTGCCCCCT	S
CT-ExFP-AS220 fwd	GAAGCGCGATCACATGGTCC	S
pSFV fwd	CTACGGCGGTCCTAGATTGG	S
pSFV rev	CCGTAAAACGTTTGCGTAGG	S
pSFVfwdup	GGCGAGGGACATTAAGGCG	S
pSFV revdown	CGGCGCTGATGAGTTGCTG	S
EphB2globrev	CGCTGGGAATGCTGCTGCAG	S
NTExFPrev	GTCCAGCTCGACCAGGATG	S
RevKinaseATP	GGTCGAACTGGCCCATGATG	S

Newly cloned plasmids were sequenced, at least over cloning sites, for sequence verification [360].

5.2.1 EphB2 mammalian expression constructs

All EphB2 mammalian expression constructs were under the control of the CMV-Promoter, with pcDNA3.1 as the backbone vector.

EphB2-xFP :

Expression constructs encoding either full-length wildtype (pJK10/12; pAS01), c-terminally truncated (pJK18; pAS02) and kinase-dead (K660R mutation) (pJK27; pAS03) murine

EphB2 with incorporated xFP variants were generated by Jenny Lauterbach [238,313] and used as wildtype controls and templates for cloning of FKBP constructs.

wt/ΔCEphB2-[1-3]FKBP-xFP (pAS04-08; pTM25,26; pTM40,41):
Wildtype and C-terminally truncated EphB2-EYFP (pJK12/pJK18) constructs served as templates for generating expression constructs encoding xFP-tagged murine EphB2 with the insertion of one to three FKBP clustering domains. For insertion of two and three FKBP domains at the 5' end of the JM domain, a NheISpeI-BamHI linker was introduced into the NheI/BamHI sites of pJK12 (5' of the EYFP in JM domain). For generation of the 3FKBP insert, one FKBP domain from pC_4-F_V1E was introduced into pC_4M-F_V2E, via the XbaI/SpeI restriction sites, to give the plasmid pC_4-F_V3E. Following these preparative steps, an EcoRV/NotI fragment of EphB2-EYFP (pJK12) containing the region of interest for insertion was subcloned into pBS plasmid. Then, ligated 2FKBP (from pC_4M-F_V2E) or 3FKBP domains (from pC_4M-F_V3E), respectively, were subcloned as XbaI/SpeI fragment into the SpeI site. Finally the new FKBP domain containing the EcoRV/NotI fragment in pBS was moved back via the same restriction sites into the original EphB2-EYFP (pJK12/pJK18) backbone to yield wt/ΔCEphB2-[2-3]FKBP-EYFP (pTM25 & pTM26). The wtEphB2-1FKBP-EYFP plasmid (pAS-1) was obtained with excision replacement of the 3FKBP domains by the 1FKBP domain insert via the NheI/BamHI restriction sites. The 1FKBP domain insert was amplified by PCR using the primer pair EphB2-1Fv-fwdG/ -revCG and template pC_4-F_V1E.
In wildtype constructs, the flanking amino acid sequence for insertions in the juxtamembrane region is …GFERADSE- LATRYTDKLQ-[1-3FKBP]-SRDPPVAT-[xFP]-YTDKLQHY….
For the C-terminally truncated EphB2-[2,3]FKBP constructs, the remaining EphB2 cytoplasmic domain is …GFERADSE, followed by three FKBP repeats and EYFP.

kdEphB2-[1-3]FKBP-xFP (pAS14-16) :
Kinase-dead variants of the clustering constructs pAS04/pTM25/pTM26 were produced via a subcloning strategy with excision exchange of the wildtype kinase-domain using enzymes BsrGI/XbaI. The kinase-dead fragment containing the K660R mutation was obtained from construct pJK27.

ee/eyEphB2-[2,3]FKBP-EYFP (pAS09-13):
Constitutively kinase-active eeEphB2-[2,3]FKBP-EYFP constructs were generated in two steps by site-directed mutagenesis using the Stratagene-QuikChange-II XL® Kit. Firstly, aa residue Y604 was mutated using primers t3565g_t3567g/-antisense and templates pTM25 & pTM26, to produce constructs eyEphB2-[0,2,3]FKBP-EYFP. Secondly, aa residue Y610 was mutated using primers t3583g_t3585g/-antisense to yield eeEphB2-[2,3]FKBP-EYFP.

ff/fyEphB2-[2,3]FKBP-EYFP (pAS17-20):
Plasmids ff/fyEphB2-[2,3]FKBP-EYFP were cloned in two steps by site-directed mutagenesis using the Stratagene-QuikChange-II XL® Kit. Firstly, aa residue Y604 was mutated using the primer pair a3566t/-antisense and templates pTM25 & pTM26, to produce constructs fyEphB2-[0,2,3]FKBP-EYFP. Secondly, aa residue Y610 was mutated using the primer pair a3584t/-antisense to yield ffEphB2-[2,3]FKBP-EYFP.

ΔNEphB2-[0,3]FKBP-EYFP (pAS21,22):
For cloning of the N-terminally truncated ΔNEphB2-[0,3]FKBP expression constructs, a synthetic gene segment was designed comprising the FNIII, TM and part of the JM domains. The gene was synthesized by MWG BIOTECH (Ebersberg, Germany) and provided in a backbone ready for excision via the EcoRV/NheI restriction sites. The DNA-fragment was then ligated into EcoRV/NheI-digested wtEphB2-[0,3]FKBP-EYFP to produce ΔNEphB2-[0,3]FKBP-EYFP.

xFP variants of EphB2 expression constructs. Simultaneous visualization of different combinations of isoforms required the cloning of various xFP-variants. In general, xFP was exchanged from the parent plasmid of interest via subcloning the AgeI/BsrGI excision product from xFP template plasmids pEYFP-N1, pECFP-C1, pmGFP-N1 or pmCitrine (Ola Sabet MPI Dortmund), pRSET-B-mcherry (from Tsien lab).

pSFVwtEphB2-[0,3]FKBP-YFP (plasmids for Semliki Forest Virus constitution; pAS23-26):
The JM-YFP-kinase-SAM-PDZ fragment was subcloned into pSFV using the BamHI/NotI restriction sites to give pSFVEphB2^{intra}. Subsequently, PCR-amplification of full-length wtEphB2-[0-3]FKBP-YFP using the primer pairs pSFVEphB2^{ecto}-fwd/ pSFVEphB2^{ecto}FKBP-rev (pSFVEphB2^{ecto}rev for 0FKBP) yielded the remaining EphB2^{ecto}-TM-xFKBP insert for subcloning into pSFVEphB2^{intra}.

5.2.2 EphA4 mammalian expression constructs

wtEphA4-EYFP-[2,3]FKBP (pAS27,28):
Wildtype EphA4-aa574-NheI with an in-frame NheI restriction site introduced at aa residue position 574 served as a template backbone for insertion of two and three FKBP domains with EYFP. The insert was PCR-amplified from wtEphB2-[2,3]FKBP-EYFP using the primer pair EphAfwdNheI/EphArevNheI and inserted at the NheI restriction site. The site of insertion was similar to that of the EphB2 expression constructs containing FKBP and xFP.

eeEphA4-EYFP-[2,3]FKBP pAS29,30):
Constitutively kinase-active eeEphA4-aa573-NheI served as a template and cloning was carried out as described for wtEphA4-EYFP-[2,3]FKBP.

5.2.3 EphrinB2 mammalian expression constructs

Expression constructs encoding for full-length wildtype murine EphB2 with incorporated xFP variants (pJK38; pAS33) were generated by Jenny Lauterbach [239,313] and used as wildtype controls and templates for cloning of FKBP constructs.

xFP-wtefnB2-[1-3]FKBP (pAS34-36; pTM13,14):
The wildtype xFP-wtefnB2 (pJK38) construct served as a template to generate expression constructs encoding for xFP-tagged murine ephrinB2, with the subsequent insertion of one to three FKBP clustering domains. For insertion of two and three FKBP domains downstream of the TM domain, the extracellular and transmembrane domains were PCR amplified and inserted into pBS using the EcoRI/SpeI restriction sites. After that, the intracellular domain, which was also PCR-amplified from pJK38, was cloned into the same pBS plasmid containing the EC and TM domains, using the restriction sites SpeI/NotI. Following these preparative steps, already ligated 2FKBP (from $pC_4M\text{-}F_V2E$) or 3FKBP domains (from $pC_4\text{-}F_V3E$) were subcloned as XbaI/SpeI fragments into the SpeI site. Finally, the new FKBP domain containing the cloned fragment in pBS was moved back to pJK38 using the XbaI/NotI restriction sites to yield xFP-wtefnB2-[2,3]FKBP.
For cloning the xFP-wtefnB2-1FKBP plasmid, xFP-wtefnB2-2FKBP (pTM13) was used as a template for PCR-amplification of a fragment comprising the 1FKBP domain and the efnB2 IC domain. For this, the b2-1FV-fwd/rev primer pair was used. The resulting fragment, with flanking XbaI/NotI restriction sites, was then ligated into the SpeI/NotI site of pTM30 to give xFP-wtefnB2-1FKBP.

xFP-ΔCefnB2-[2,3]FKBP (pAS37,38):
Full-length wildtype xFP-wtefnB2-[2,3]-FKBP served as a cloning template for the deletion of the cytoplasmic tail downstream of the FKBP domains. The cytoplasmic tail of ephrinB2 was excised using SpeI/NotI and vector was then re-ligated in the presence of annealed linker oligonucleotides linkSpeI/NotIfwd & linkSpeI/NotIrev (annealing conditions as outlined above), to give xFP-ΔCefnB2-[2,3]FKBP.

xFP variants of efnB2 expression constructs. Simultaneous visualization of different combinations of constructs required the cloning of various xFP-variants. For mCherry-wtefnB2-xFP constructs, EYFP was excised from EYFP-wtefnB2-xFKBP using the restriction enzymes BamHI/HindIII. mCherry PCR-amplified from pRSET-B-mCherry or ECFP from pECFP-C1, using the primer pair 1-5-mcherry/1-3-mcherry, was ligated into the remaining backbone.

5.2.4 Other expression constructs

myr-FRB-mCherry (pAS32):
pC_4-R_HE, containing the FRB fragment as an insert, was used as a backbone for generating myr-FRB-mCherry. The FP mCherry was PCR-amplified from vector pRSET-B-mCherry using the primer pair 2-5-mchFRB/2-3-mchFRB and inserted via the restriction sites SpeI/BamHI, to produce construct FRB-mCherry. For myristoylation of FRB-mCherry, myristoylation sequence encoding oligonucleotides NT-MemFRB-fwd/-rev were diluted in H_2O bidest. and annealed by heating to 95 °C and subsequent gradual cooling to 10 °C at a rate of 2 °C/min. Annealed oligonucleotides were then used for insertion into EcoRI/XbaI restriction sites to yield myr-FRB-mCherry.

An overview of all constructs cloned and used in this thesis is given in table 5.2. All constructs were sequence verified and tested for correct expression and ephrin-Fc induced signal induction, if applicable.

Table 5.2 List of expression constructs.

Plasmid	Description	Modification	Tags	Reference
Plasmids for cloning/co-expression				
pC_4-F_V1E	1FKBP	-	-	ARIAD Pharmaceuticals®
pC_4M-F_V2E	2FKBP	-	-	ARIAD Pharmaceuticals®
pC_4M-F_V3E	3FKBP	-	-	thesis; Taija Makinen
pC_4-R_HE	1FRB	-	-	ARIAD Pharmaceuticals®
pBS	cloning vehicle	-	-	Taija Makinen
pECFP-C1	ECFP	-	-	Clontech®
pEYFP-N1	EYFP	-	-	Clontech®
pRSET-B-mCherry	mCherry	-	-	Tsien lab [363]
pmyr-mCherry	mCherry	-	GPI	Tsien lab [363]
pmGFP-N1	based on pEGFP-N1	EGFP mutations + Ala206Lys	-	Ola Sabet, Clontech®
pSFV	viral target vector	-	-	[364]
pSFVhelper	viral structural genes	-	-	[364]
pcDNA3_EphA4wt_NheI	EphA4-aa574-NheI	aa574	-	Katrin Deininger
pcDNA3_EphA42E_NheI	eeEphA4-aa574-NheI	aa574 Tyr604Glu Tyr610Glu	-	Katrin Deininger
EphB2 expression plasmids				
pJK1	wtEphB2	-	FLAG	[313]

pJK2	kdEphB2	kinase-dead (Lys660Arg)	FLAG	[313]
pJK10/12 pAS01	wtEphB2-xFP	-	FLAG ECFP/EYFP mCherry/ mGFP	thesis; [313]
pJK18 pAS02	ΔCEphB2-xFP	cytoplasmic domain deletion	FLAG EYFP/ECFP	thesis; [313]
pJK27 pAS03	kdEphB2-xFP	kinase-dead	FLAG EYFP/ECFP mCherry/ mGFP	thesis; [313]
pAS04	wtEphB2-1FKBP-xFP	-	FLAG EYFP/ECFP mGFP	thesis
pTM25 pAS05	wtEphB2-2FKBP-xFP	-	FLAG EYFP/ECFP mGFP	thesis; Taija Makinen
pTM26 pAS06	wtEphB2-3FKBP-xFP	-	FLAG EYFP/ECFP mGFP	thesis; Taija Makinen
pTM40 pAS07	ΔCEphB2-2FKBP-xFP	cytoplasmic domain deletion	FLAG EYFP/ECFP mGFP	thesis; Taija Makinen
pTM41 pAS08	ΔCEphB2-3FKBP-xFP	cytoplasmic domain deletion	FLAG EYFP/ECFP	thesis; Taija Makinen
pAS09	eeEphB2-YFP	Tyr604Glu Tyr610Glu	FLAG EYFP	thesis
pAS10	eeEphB2-2FKBP-YFP	Tyr604Glu Tyr610Glu	FLAG EYFP	thesis
pAS11	eeEphB2-3FKBP-YFP	Tyr604Glu Tyr610Glu	FLAG EYFP	thesis
pAS12	eyEphB2-2FKBP-YFP	Tyr604Glu	FLAG EYFP	thesis
pAS13	eyEphB2-3FKBP-YFP	Tyr604Glu	FLAG EYFP	thesis
pAS14	kdEphB2-1FKBP-xFP	kinase-dead	FLAG EYFP/ECFP	thesis
pAS15	kdEphB2-2FKBP-xFP	kinase-dead	FLAG EYFP/ECFP	thesis
pAS16	kdEphB2-3FKBP-xFP	kinase-dead	FLAG EYFP/ECFP	thesis
pAS17	ffEphB2-2FKBP-YFP	Tyr604Phe Tyr610Phe	FLAG EYFP	thesis
pAS18	ffEphB2-3FKBP-YFP	Tyr604Glu Tyr610Glu	FLAG EYFP	thesis
pAS19	fyEphB2-2FKBP-YFP	Tyr604Phe	FLAG EYFP	thesis
pAS20	fyEphB2-3FKBP-YFP	Tyr604Phe	FLAG EYFP	thesis
pAS21	ΔNEphB2-0FKBP-YFP	-	FLAG EYFP	thesis
pAS22	ΔNEphB2-3FKBP-YFP	-	FLAG EYFP	thesis
pAS23	pSFVwtEphB2-0FKBP-YFP	-	FLAG EYFP	thesis

pAS24	pSFVwtEphB2-1FKBP-YFP	-	FLAG EYFP	thesis
pAS25	pSFVwtEphB2-2FKBP-YFP	-	FLAG EYFP	thesis
pAS26	pSFVwtEphB2-3FKBP-YFP	-	FLAG EYFP	thesis
EphA4 expression plasmids				
pID	EphA4	-	mCherry	Irina Dudanova
pAS27	wtEphA4-2FKBP-YFP		EYFP	thesis
pAS28	wtEphA4-3FKBP-YFP	-	EYFP	thesis
pAS29	eeEphA4-2FKBP-YFP	Tyr604Glu Tyr610Glu	EYFP	thesis
pAS30	eeEphA4-3FKBP-YFP	Tyr604Glu Tyr610Glu	EYFP	thesis
pAS31	FRB-mCherry	-	mCherry	thesis
pAS32	myr-FRB-mCherry	-	GPI mCherry	thesis
EphrinB2 expression plasmids				
pJK38 pAS33	xFP-wtefnB2	-	HA-tag EYFP ECFP mCherry	thesis [313]
pAS34	xFP-wtefnB2-1FKBP	-	HA-tag EYFP/ ECFP/ mCherry	thesis
pTM13 pAS35	xFP-wtefnB2-2FKBP	-	HA-tag EYFP/ECFP mCherry	thesis; Taija Makinen
pTM14 pAS36	xFP-wtefnB2-3FKBP	-	HA-tag EYFP/ECFP mCherry	thesis; Taija Makinen
pAS37	xFP-ΔCefnB2-2FKBP	cytoplasmic domain deletion	HA-tag EYFP/ECFP mcherry	thesis
pAS38	xFP-ΔCefnB2-3FKBP	cytoplasmic domain deletion	HA-tag EYFP/ECFP mcherry	thesis
Other expression plasmids				
pJEN121	JMA4- GST EphA4 substrate	-	GST	[113]
pSW12	GRIP1	-	-	[208,365]
pKB33	GRIP2	-	myc	Katja Brückner
pCMVSport6-PICK1 pAS39	murine PICK1	-	-	Imagenes cDNA clone MGC:54727

5.3 Cell culture techniques

5.3.1 Cell lines

Cell lines from table 5.3 were cultured and maintained according to standard protocols using appropriate culture growth media (Gibco, Invitrogen, Carlsbad, CA) and conditions [366].

Table 5.3 Cell lines.

Cell line	organism	ATCC number	origin	Reference
Human embryonic kidney (HEK)293T	*Homo sapiens* (human)	CRL-1573	ATCC	www.atcc.org
HeLa	*Homo sapiens* (human)	CCL-2	ATCC	www.atcc.org
COS-7 (kidney fibroblast-like cell line)	*Cercopithecus aethiops* (African green monkey)	CRL-1651	Bastiaens Lab, MPI Dortmund, Germany	www.atcc.org
BHK-21	*Mesocricetus auratus* (baby hamster Syrian kidney)	CCL-10	Stein Lab, MPI Neurobiology	www.atcc.org

5.3.2 Primary culture of hippocampal neurons

Hippocampal neurons were taken from the embryos of pregnant Wistar rats (MpiChbb:Thom, animal house, Max-Planck-Institute of Neurobiology) at embryonic day 18.5. The pregnant rat was deeply anesthetized using diethyl ether, and then sacrificed by decapitation. After decapitation, embryos were obtained and kept in ice-cold dissection medium (HBSS, #2402, Gibco, supplemented with sterile filtered 10% penicillin/streptomycin, 10 mM $MgSO_4$, 10 mM HEPES). Working under an open sterile hood, embryo heads were removed and the skull opened to take out the brain. Embryonic brains were placed in fresh dissection medium and dissected under a stereomicroscope. Brain cortices were removed from the midbrain and brainstem and the meniges were detached. The striatum was then removed, and the hippocampus was separated from the cortex and placed in fresh 15 ml dissection medium on ice. After removing the medium, up to 3 hippocampi were incubated in dissection medium supplemented with papain (1 mg/ml, Sigma Aldrich) for 20 min in a water bath, heated to 37 °C. The digestion reaction was stopped first by carefully removing the papain solution and then by washing hippocampi three times with 3 ml prewarmed Neurobasal-B27 (Neurobasal: #21103, Gibco; B27: #17504-049, Gibco) . The tissue was then triturated approximately 20 times with the help of fire polished Pasteur pipets, and the cell suspension was centrifuged for

5 min at 80 x g to remove the debris. The pellet was resuspended in an appropriate volume of Neurobasal-B27 medium. Cells were counted using a hemacytometer and plated on coated glass coverslips (1 mg/ml poly-D-lysine, Sigma-Aldrich; 5 µg/ml laminin, Invitrogen) in a 24-well plate at a density of 25,000 cells per well, or on coated glass botton live-cell dishes (LabTek, Nunc) for subsequent lipofectamine transfection the next day. AMAXA® transfection was immediately carried out after dissociation of neurons. Conditioned Neurobasal-B27 (~10 days) was added up to 50 % (v/v) to fresh Neurobasal-B27 and used for culturing of neurons after dissociation/transfection.

5.3.3 Preparation of Semliki Forest virus

For production of viral particles, two expression vectors were transfected simultaneously into BHK-21 cells using electroporation (twice, with interval 10-15 sec, settings: voltage 1.5 kV, capacity 25 µF, infinity resistance; time constant 0.7-0.8) (GenePulserII, BioRad). The first expression vector contained the cDNA of interest, as well as the nonstructural genes (nsP1-4) and the subgenomic 26S promoter. The second expression vector, pSFVhelper, contained coding regions for structural proteins. 36 hours after electroporation and seeding of BHK-21 cells, the medium containing released viral particles was collected (10 ml) and centrifuged to pellet cell debris at 2500 x g for 10 min at 4 °C. The supernatant was then collected and stored at 4 °C until concentration of viral particles via ultracentrifugation was performed the same day. The supernatant was spun for 2 hrs at 76800 x g and 4 °C using an SW41 rotor (Beckman, Brea, CA). The supernatant was aspirated and the viral pellet resuspended in ~250 µl of sterile filtered neurobasal medium overnight at 4 °C. It was then aliquoted and stored at -80 °C. For activation of the virus, structural proteins forming the spikes, necessary for infection of host cells but insensitive to endogenous proteases, had to be converted by an exogenous protease. 50 µl of viral solution was first digested with α-chymotrypsin at RT for 45 min (1:20 v/v), then inactivated at RT for 10 min with aprotinin (1:15 v/v). Activated virus was then aliquoted and stored at -80 °C until required further for infection of hippocampal cultures. For more details of SFV production please refer to [364].
After testing the virus in Hek293T cell culture, infection of hippocampal slices was performed overnight by adding ~5-10 % (v/v) of the virus suspension to neurons cultured in neurobasal growth medium for 1 day *in vitro*. Cultures were imaged the morning following infection.

5.3.4 Mammalian cell transfection

Cell culture transfections. COS-7 cells used for homo-FRET experiments, immunostainings and blue-native PAGE were grown to 70 % confluency and transfected overnight with various EphB2-xFKBP constructs using FUGENE6 reagent (Roche Diagnostics, Mannheim, Germany). HeLa cells were grown to 70 % confluency and transfected in growth medium overnight with 0.5 to 5 µg of DNA using a Calcium-Phosphate transfection kit (Invitrogen,

Carlsbad, CA). The next morning, COS-7 cells were washed with D-PBS (Sigma Aldrich), and HeLa cells were washed with wash buffer (135 mM NaCl, 4 mM KCl, 1 mM Na_2HPO_4, 2 mM $CaCl_2$, 1 mM $MgCl_2$, 20mM HEPES, 20mM d-Glucose, pH 7.3), before the addition of fresh growth medium. 12-16 hrs before stimulation, cells were starved in growth medium containing dialyzed 0.5 % fetal bovine serum (HyClone, Logan, Utah). For FKBP domain containing constructs, FK506 (300 nM) was added to the growth medium after transfection to reduce Eph clustering.

Transfection of primary hippocampal neuron cultures. Depending on the assay performed, but usually the next day (DIV 1), cultures plated on coverslips or in live-cell chambers were transfected with lipofectamine ltx® or lipofectamine 2000® (Invitrogen) according to the manufacturer's protocol. Prior transfection, growth medium was exchanged for Neurobasal without B27 serum and kept in incubator. For transfection of 1.8 cm² wells in a volume of 0.5 ml, 0.7-1 µg of DNA was diluted in 50 µl of Opti-Mem (GlutaMAX, #51985,Gibco). In parallel, 2 µl of lipofectamine was added to 50 µl of Opti-Mem and incubated for 5 min at RT. Subsequently, the DNA mix was added to the lipofectamine mix to yield a final volume of ~100 µl, which was further incubated for 20 min at RT before adding to the well. Transfection was stopped after 1.5-2.5 hrs by washing twice with 7 mM HEPES in HBSS. Culturing of transfected neurons on cover slips or in live-cell chambers was continued on in growth medium from prior transfection supplemented with up to 1/3 (v/v) fresh Neurobasal-B27. Cultures were maintained in a humidified incubator with an atmosphere of 5 % CO_2 at all times.
For transfection of N-terminally truncated ΔNEphB2-0FKBP or ΔNEphB2-3FKBP constructs (1 µg/transfection), AMAXA® nucleofection for rat neurons (Lonza, Basel, Switzerland) was used according to the manufacturer's protocol. After dissociation of the neurons, 600-800,000 cells were electroporated in AMAXA transfection buffer with 1 µg DNA using program O-003 for rat hippocampal neurons and seeded at a density of ~60,000 cells/cm². To reduce receptor clustering, 300 nM FK506 was added to the cultures 1 hr after plating.

5.4 Clustering reagents and stimulations

FKBP/FRB-system of non-covalent crosslinking. For non-covalent, homotypic crosslinking of EphB2/A4 receptors or ephrinB2 ligands the ARGENT® Regulated Homo(Hetero)dimerization kit from ARIAD Pharmaceuticals (ver. 2.0 - for reference see www.ariad.com) was implemented. The kit allows complex cellular events to be brought together under small molecule control via a homo/heterodimerizer. The reagents of the homodimerizer kit are based on the abundant cytoplasmic human FKBP12 (FK506 Binding Protein 12) and its small molecule ligands FK506 and rapamycin. The first generation homodimerizer system was invented by the Schreiber and Crabtree laboratories [367]. They chemically linked two FK506 molecules together, which produced two binding entities for

FKBP12 on one small molecule ligand, thereby creating a non-covalent crosslinker. Affinity and specificity was subsequently improved by Clackson and colleagues [368,369], resulting in the newest generation homodimerizer AP20187 with a high sub-nanomolar affinity to a Phe36Val mutated FKBP12 (FKBP-F_V) and a weaker homodimerizer AP1887 with lower binding affinity to FKBP [369,370].
AP21967, included in the heterodimerizer kit, is a chemical derivate of rapamycin (rapalog) that circumvents the cell cycle inhibitory effects of rapamycin. It functions by binding with high-affinity to FKBP and to FRB, a 93 amino acid portion of the large PI3K homolog FRAP (FK506-rapamycin complex associated protein; RAFT, mTOR), thereby joining the two proteins together [312,322].
Homo and hetero-dimerizing agents AP20187 (same EC_{50} as AP1903, personal communication with Tim Clackson, ARIAD Pharmaceuticals) [369], AP1887 [316], and AP21967 were obtained from ARIAD Pharmaceuticals, dissolved in ethanol and stored at -20 °C. The affinities of the homodimerizers AP20187 (IC_{50}= 1.8 nM) and AP1887 (IC_{50}= 40 nM) to a single FKBP-F_V domain were determined using FL polarization competition assays [316]. Prior to stimulation, dimerizers were diluted in starving medium used for stimulation to the concentration indicated in figures.

Soluble ligand stimulation. Human IgG Fc fragment (Jackson ImmunoResearch, West Grove, PA), mouse ephrinB2-Fc (AF496-EB), human ephrinB3-Fc (AF395) and human ephrinA5-Fc (AF374) fusion proteins (R&D Systems, Minneapolis, MN) were used for stimulations. Pre-clustered Fc fragment and ephrin-Fc fusion proteins were incubated with goat anti-human Fc at a ratio of 5:1 for 30 min at room temperature. Stimulations were carried out in a CO_2-controlled incubator at 37 °C for the indicated time. Following stimulation, the cells were placed on ice.
For stimulation with FL labeled ephrinB2-Fc, recombinant protein (AF496-EB, R&D Systems) was treated with Alexa-dye 594 according to the kit protocol (Alexa Fluor 594 Microscale protein labeling kit, A30008, Invitrogen). The conjugate was cleared of excess dye by subjecting it to a purification resin and eluting in PBS. Concentration of Alexa-conjugated ephrinB2-Fc was estimated by absorbance spectroscopy before and after conjugation at 280 nm and 590 nm wavelength.

Inhibitor compounds. For inhibition of acto-myosin-dependent cell contraction, the myosin-II inhibitor (S)-(-)-blebbistatin (#1852, Tocris Bioscience, Bristol, UK) was added to the culture medium at least 10 min before manipulation of the cells.
Dynasore (D7693, Sigma Aldrich) was used as dynamin-1/2 specific GTPase inhibitor to block dynamin-dependent endocytosis [371]. It was prepared in DMSO (dimethyl-sulfoxide) and added to the growth medium 15 min prior start of the experiment at a final concentration of 80 µm.

For inhibition of receptor clustering of FKBP-domain containing Eph/ephrin isoforms, 300 nM FK506 (F4679; Sigma Aldrich) was added after transfection. FK506 powder was reconstituted in ethanol.

5.5 Protein chemistry techniques

5.5.1 Antibodies

Primary antibodies used in experiments are as follows: rabbit anti-phospho EphB1/2 Y594/Y604 (ab61791, Abcam, Cambridge, UK); mouse anti-phospho tyrosine (clone 4G10, homemade), mouse anti-FLAG M2 (F-3165, Sigma Aldrich, St. Louis, MO); rabbit SAM-domain specific anti-EphB2 [172]; rabbit anti-GST (sc-33613, Santa Cruz Biotechnologies, Santa Cruz, CA); rabbit anti-FKBP12 (PA1-026A, Affinity BioReagents, Golden, CO); mouse monoclonal anti-α-Tubulin (Sigma Aldrich); mouse monoclonal anti-GRIP (#611318, BD Biosciences, Franklin Lakes, NJ); rabbit anti-PICK1 (ab3420, Abcam); ectodomains-specific goat anti-EphB2^{Ecto} (AF467, R&D Systems); rabbit anti-phospho-EphA2/3/4 Y588/Y596 (ab62256, Abcam); mouse monoclonal anti-c-myc (MA1-980, Sigma Aldrich); mouse monoclonal anti-EphA4/Sek (610471, BD Biosciences); mouse monoclonal anti-GFP JL-8 (632380, Clontech, Mountain View, CA); rabbit anti-GFP (Invitrogen, Carlsbad, CA), 1:2000; rabbit anti-mouse monoclonal anti-Tau1 (Chemicon, Temecula, CA), 1:500, and goat anti-human IgG Fc_γ fragment specific for clustering of Fc-fusion proteins (Jackson ImmunoResearch).

Secondary antibodies used were: donkey anti-mouse Cy3- or Cy5-conjugated, anti-rabbit Cy2-conjugated, and anti-rabbit/anti-mouse horse radish peroxidase (hrp) conjugated (Jackson ImmunoResearch). Streptavidin-hrp (GE Healthcare, Chalfont St. Giles, UK) was used to probe for biotinylated protein.

5.5.2 Immunoprecipitations and Western blotting

HeLa cells were harvested in lysis buffer (50 mM Tris pH 7.5, 120 mM NaCl, 1 mM EDTA, 1 % TritonX-100, 10 % glycerol) supplemented with protease and phosphatase inhibitor cocktail tablets (Roche, Mannheim, Germany). For phosphorylation blotting, lysates were cleared by centrifugation and equal amounts were then incubated with 40 µl of anti-FLAG M2-agarose resin (A2220, Sigma Aldrich) overnight at 4 °C rotating, then washed 4 times with lysis buffer. Proteins were eluted by the addition of loading buffer and analyzed by Western blot. After SDS-PAGE separation of immunoprecipitations, semi-dry transfer of proteins to PVDF membranes and blocking with 5 % BSA (Sigma Aldrich) in PBS with 0.1

% Tween-20 (Bio-RAD, Hercules, CA), membranes were incubated overnight with the respective primary antibody. They were then incubated with the species-specific secondary hrp-coupled antibody, and proteins were detected with an enhanced chemiluminescence kit (GE Healthcare, Uppsala, Sweden). For re-blotting, membranes were stripped for 15 min with stripping buffer (Thermo Scientific, Rockford, IL) at room temperature, blocked again with BSA and re-probed using a primary antibody for total protein detection.
In the biochemical kinase activity assay, co-expressed kinase substrate GST-JMA4 was pulled down with a 50 % slurry of glutathione sepharose 4B (GE Healthcare, Uppsala, Sweden), then eluted with loading buffer and subjected to SDS-PAGE for Western blotting as described above. Quantifications of unsaturated Western blots were done using Gel-Pro Analyzer software (Media Cybernetics, Bethesda, MN), normalizing to positive ephrinB2-Fc stimulation controls.

5.5.3 Blue-native PAGE

COS-7 cells were lysed in NativePAGE sample buffer (Invitrogen, Carlsbad, CA) supplemented with 1 % n-dodecyl-b-D-maltoside and complete protease and phosphatase inhibitor cocktail (Roche, Mannheim, Germany). After centrifugation for 30 min at 13,000 x g, equal amounts of cell lysates and a NativeMark unstained protein standard (Invitrogen) were separated on a 3-12 % NativePAGE gradient gel (Invitrogen) in NativePAGE G-250 sample buffer (Invitrogen) (final concentration 0.25 %). Proteins were then transferred to PVDF membrane and autophosphorylation was detected. For re-blotting, membranes were stripped, blocked again with BSA and re-probed using a primary antibody for total protein detection. For analysis of cluster sizes and phosphorylation states using kd/wtEphB2-xFKBP-mGFP isoforms, developed blots were scanned lane by lane using an average optical density line scan with equal scan width (software MetaMorph, Molecular Devices). Values were normalized to each total lane input resulting from the sum of incremented optical densities and plotted against line-increments from lane scans.

5.5.4 Surface biotinylation

For surface biotinylation of plasma membrane proteins, HeLa cells were washed once with ice cold D-PBS (pH 8.0) after stimulation of the cells using ephrinB2-Fc/dimerizer. Cells were then incubated for 30 min with 1 mg/ml EZ-Link Sulfo-NHS-SS-Biotin (Thermo Fisher Scientific, Waltham, MA) diluted in ice-cold D-PBS (pH 8.0). To quench the biotinylation reaction, cells were then rinsed for 5 min with ice cold D-PBS supplemented with 1 % BSA (w/v). Before cell lysis, cell were washed once more with ice cold D-PBS.

5.5.5 Immunocytochemistry

Cells were fixed with pre-warmed 2 % paraformaldehyde, 4 % sucrose in D-PBS for 5 min at RT, rinsed twice with ice cold D-PBS, incubated with ice cold 50 mM ammonium chloride in D-PBS for 10 min, and then rinsed again. For phosphorylation labeling of Eph receptors, cells were permeabilized for 5 min with ice cold 0.1 % Triton X-100 in D-PBS at 4 °C. For surface labeling of Eph receptors, cells were not permeabilized. Blocking was performed for 30 min at RT, or overnight at 4 °C, with 5 % donkey serum (Jackson ImmunoResearch), 3 % BSA in PBS. Cells were then incubated with primary antibodies for 60 min at RT. After washing, cover slips were mounted using the ProLong antifade kit (Molecular Probes, Eugene, OR) or Aqua-Poly/Mount (Polysciences, Warrington, PA).
Neuronal cultures were fixed using warm (37 °C) 4 % paraformaldehyde/ 8 % sucrose, permeabilized with 0.1 % Triton X-100 for 5 min and incubated with blocking solution (4 % goat serum, 4 % donkey serum, 2 % BSA in PBS) for 1 hr at room temperature, followed by incubation with primary antibody in blocking solution for 2 hrs at RT. After washing with PBS, secondary antibodies diluted 1:250 in blocking solution were added for 1 hr at RT. Texas-Red-conjugated phalloidin (1:100) was applied together with the secondary antibodies. Coverslips were mounted with fluorescent mounting medium (Dako, Hamburg, Germany) and imaged for epiFL using the Axioplan epifluorescent microscope (Zeiss, Göttingen, Germany). Images were acquired with MetaMorph software (Molecular Devices). Only axonal growth cones were quantified (an axon being defined as the longest neurite positive for Tau1).

5.6 Cell microscopy assays and image analysis

5.6.1 Cell collapse and co-culture assays

For cell collapse assays, 12-16 hrs prior to the start of the assay, transfected HeLa were detached from the flask using D-PBS lacking Ca^{2+} and Mg^{2+} (Sigma Aldrich) supplemented with 3 mM EDTA. After washing twice in D-PBS containing Ca^{2+} and Mg^{2+}, cells were seeded in Lab-Tek glass bottom live-cell chambers (Nunc, Rochester, NY) or MatTek glass bottom dishes (MatTek, Ashland, MA) coated with 1 mg/ml poly-D-lysine (Sigma Aldrich) and 5 µg/ml mouse laminin (Invitrogen, Carlsbad, CA). For cells expressing FKBP receptor isoforms, DMEM starving medium was supplemented with FK506 (300 nM, Sigma Aldrich). One hour before the start of the experiment, cells on dishes were washed with D-PBS, and imaging medium DMEM without phenol red, supplemented with 25 mM HEPES (Invitrogen), was added. Time-lapse imaging was performed as described in section 5.6.2. Before stimulation, reference images were acquired. Sequential images were acquired every 3 to 4 min following addition of the stimulus. Cell edges of montaged stacks were drawn using

a graphpad pen (Intous 4, Wacom, Otone, Saitama, Japan) and MetaMorph software (Molecular Devices, Silicon Valley, CA). Area of cell growth surfaces at all time points were normalized to the pre-stimulation image cell growth surface (set to 100 %).
For cell co-culture assays, the donor cell population was seeded ~30 min prior to the start of the assay on top of the recipient cell population, after the detachment procedure using D-PBS/EDTA as described above.

5.6.2 Epifluorescent and confocal imaging

Time-lapse epiFL imaging. EpiFL time-lapse imaging was performed using a Zeiss Axiovert 200M or a Zeiss Axioobserver Z1 microscope equipped with a temperature-controlled carbon dioxide-incubation chamber set to 37 °C, 65 % humidity, and 5 % CO_2. Single focal planes, intermittently refocused manually, were acquired every 2 to 5 min in brightfield and FL illumination over a time period of 2 hrs with a 40x phase contrast objective (Zeiss, Göttingen, Germany). Illumination was provided by a X-Cite lamp (series 120, Lumen Dynamics Group, Mississauga, Canada) and images recorded with a Coolsnap HQ camera (Photometrics, Tucson, AZ).

High-resolution imaging and processing. For high-resolution epifluorescent live-cell recordings, a 100x phase contrast objective (Zeiss) was used with z-stack resolution of 0.267 µm in fast acquisition mode. Z-stacks of images were corrected for optical density and subjected to adaptive-blind psf deconvolution (AutoQuantX, Media Cybernetics, Bethesda, MN), followed by sum or maximum intensity projection as indicated in figures. For confocal time-lapse recordings (supplementary video 1), an Olympus Fluoview® FV1000 confocal microscope (Olympus Life Science Europe, Hamburg, Germany) equipped with an Argon ion laser (Melles Griot, Albuquerque, NM) and a temperature controlled CO_2 incubation chamber (EMBL, Heidelberg, Germany) at 37 °C was employed. For all live cell experiments, either a 60x/1.2 W UPlanSApo or 60x/1.35 Oil UPlasSApo objective (Olympus) was used. Fixed samples were imaged with either a Leica Confocal SP2 (Leica Microsystems, Wetzlar, Germany), an Axioobserver Z1 (Zeiss) equipped with a CSU-X1 spinning-disc confocal unit (Yokogawa, Tokyo, Japan) or the epifluorescent microscopes Axiovert 200M or Axioobserver Z1 (Zeiss), with subsequent deconvolution processing of acquired z-stacks as described above. For FL background correction, the average FL signal from an area with no cells was linearly subtracted from the whole image.

Standard image processing. During image acquisition with constant exposure times using MetaMorph software, or the acquisition software provided by the microscope manufacturer, 12 or 16-bit TIFF images were obtained with non-saturating pixel intensities. Post acquisition, images were processed using MetaMorph (Molecular Devices) or ImageJ software [372], as indicated in figure legends. For FL background correction, the low-level background average

intensity was measured and subtracted from the whole image (Gaussian background distribution was assumed). For image display, images were dynamically scaled to 0.1% of lowest and 0.01% of the highest FL pixel intensity and subsequently converted into 8-bit images. Fixed image scaling was also used for image sequences, when appropriate. The same scaling mode was always applied for both sample and control.

FL quantification. Quantification of FL signals was done after image processing comprising deconvolution, background correction and maximum projection, if performed. Integrated FL intensities from surface or phosphorylation staining were measured from regions or whole cell bodies and normalized to the total protein FL signals. Very high or very low expressing cells were excluded from the analysis as indicated in figure legends. Average intensity linescans over areas of cells were performed for better visualization, or quantification of peak intensities of FL signals in the cell edge as indicated in figures. FL thresholds were set for quantifications, if applicable.

5.6.3 Homo-FRET imaging

Theoretical background. Homo-FRET (Förster resonance energy transfer) between identical fluorophores can be conveniently measured by observing its effect on fluorescence anisotropy [373]. This can be implemented in fluorescence microscopes by the addition of polarizing optics. Homo-FRET can be observed by exploiting the difference in polarization of the emission of the fluorophores. Such differences are quantified by the fluorescence anisotropy r:

$$r = \frac{I_{par} - I_{per}}{I_{par} + 2I_{per}}$$

with the emission intensities (I) parallel (par) and perpendicular (per) to the excitation polarization direction (Fig. 5.1) [310].
Excitation with polarized light results in photoselection of fluorophores, with their absorption transition dipole moments oriented parallel to the polarization direction of the excitation light. When the emission transition dipole moment is parallel to the absorption transition dipole moment, the anisotropy of this directly excited fluorophore is at its maximum. However, the observed anisotropy is often lower. Rotation leads to a broadening of the orientation distribution of the fluorophores, and consequently, a lower anisotropy. Importantly, energy transfer to neighbouring identical fluorophores will also decrease the anisotropy of the emission. The measured anisotropy is the average of the individual anisotropies of “directly excited fluorophores” and “fluorophores indirectly excited after energy transfer”. The latter fluorophores have not been photoselected by the excitation light, and therefore exhibit a lower anisotropy. This reduced anisotropy depends on the fraction of the emission that originates from these indirectly excited fluorophores. Thus, homo-FRET imaging has the ability to determine distances between fluorophores. It can be used to quantify cluster sizes, as well as cluster size distributions. The interpretation of homo-FRET signals is complicated by the fact

that both the mutual orientations of the fluorophores and the number of fluorophores per cluster affect the fluorescence anisotropy in a similar way [310].

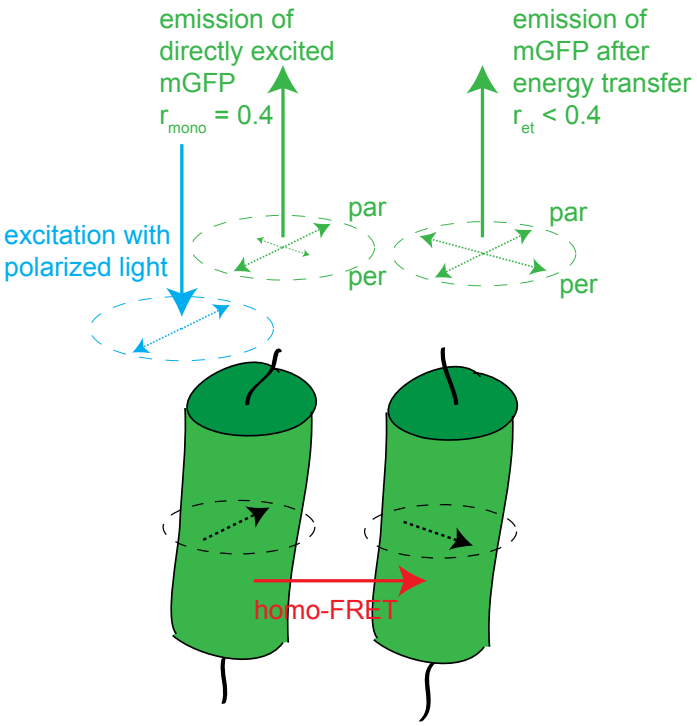

Fig. 5.1 Cartoon depicting homo-FRET in a mGFP-dimer.
Adapted from [310].

Experimental procedure. Homo-FRET imaging was carried out at room temperature in imaging medium as described by Squire et *al.* [309] in transiently transfected COS-7 cells. Images were acquired 15-24 hrs post-transfection, using an Olympus IX81 inverted microscope (Olympus, Hamburg, Germany) equipped with an MT20 illumination system. A linear dichroic polarizer (Meadowlark optics, Frederick, CO) was placed in the illumination path of the microscope, and two identical polarizers were placed in an external filter wheel at orientations parallel and perpendicular to the polarization of the excitation light. The fluorescence was collected using a 20x 0.7 NA air objective, and parallel and polarized emission images were acquired sequentially on an Orca CCD camera (Hamamatsu Photonics, Hamamatsu City, Japan). Data acquisition was controlled by the CellR software supplied by the microscope manufacturer. AP20187/AP1887 or soluble ephrinB2-Fc was added 1 min after the start of time-lapse imaging. In addition to the recording of single cells, images of the same cells were taken prior to the addition of the stimulant and after 20 min - at the end of the time-lapse recording. Image and anisotropy analysis was done by Ola Sabet (MPI Dortmund, Germany) with image and anisotropy analysis programs as described by Squire et *al.* [309]. Steady-state anisotropy was calculated in each pixel of the image. For displaying calculated anisotropy images, ImageJ was used to set the threshold between 0.17 and 0.30 with an appropriate color coded look-up table for visualization.

5.6.4 Total Internal Reflection Fluorescence (TIRF) microscopy

Theoretical background. TIRF (total internal reflection fluorescence) microscopy makes use of the evanescent wave to selectively illuminate and excite fluorophores in a restricted region of the specimen immediately adjacent to the glass-water interface. The evanescent electromagnetic field decays exponentially from the interface and thus penetrates to a depth of only approximately 100 nm into the specimen. This allows the visualization of the basal plasma membrane (~7.5 nm thick) of cells and the adjacent cytoplasmic zone beneath [374].

Experimental procedure. TIRF microscopy was performed on an Olympus IX81 microscope equipped with an 60x NA= 1.8 TIRFM APOCHROMAT oil objective at room temperature in HEPES buffered (25 mM) imaging medium. The microscope is coupled to Argon lasers, which pass through condensers allowing manipulation of the incident angle of light onto the specimen. For FL background correction, the average FL signal from an area with no cells was linearly subtracted from the whole image. TIRF images were analyzed and/or quantified as described in figure legends.
In order to determine if Eph receptors are differentially distributed upon induction of clustering, the ratio of TIRF intensity maps of the Eph receptor isoforms with that of a myristoylated mCherry was calculated. The contrast or disparity in the resulting ratio map provided an estimate of differences arising from Eph distribution upon clustering.

5.7 Statistical analysis

Results are expressed as the means ± SEM. To analyze statistical significance, either the Mann-Whitney nonparametric *t*-test, one-way ANOVA with posthoc Bonferroni/Tukey-Kramer test or Student's *t*-test was used appropriately, as indicated in figure legends. All datasets passed the Kolmogorov and Smirnov test for Gaussian distribution. Significance level of $p = 0.05$ was used to evaluate significance of differences of means (* $p < 0.05$; ** $p < 0.01$; *** $p < 0.001$). For biochemical experiments, representative blots are shown.

6. BIBLIOGRAPHY

1 Waters, C. M. and Bassler, B. L. (2005) Quorum sensing: cell-to-cell communication in bacteria. *Annual review of cell and developmental biology*. 21, 319-46

2 Alberts, B. *et al.* (2008) *Molecular Biology of The Cell*, Garland Science.

3 Bear, M. F. *et al.* (2006) *Neuroscience: Exploring the Brain*, Lippincott Williams & Wilkins.

4 Honoré, T. *et al.* (1982) The Binding of [3 H]AMPA, a Structural Analogue of Glutamic Acid, to Rat Brain Membranes. *Journal of Neurochemistry*. 38, 173-178

5 Song, I. and Huganir, R. L. (2002) Regulation of AMPA receptors during synaptic plasticity. *Trends in Neurosciences*. 25, 578-588

6 Mayer, M. L. (2005) Glutamate receptor ion channels. *Current opinion in neurobiology*. 15, 282-8

7 Janetopoulos, C. *et al.* (2001) Receptor-mediated activation of heterotrimeric G-proteins in living cells. *Science (New York, N.Y.)*. 291, 2408-11

8 Wettschureck, N. and Offermanns, S. (2005) Mammalian G proteins and their cell type specific functions. *Physiological reviews*. 85, 1159-204

9 Lemmon, M. a and Schlessinger, J. (2010) Cell signaling by receptor tyrosine kinases. *Cell*. 141, 1117-34

10 Schlessinger, J. (2000) Cell Signaling by Receptor Tyrosine Kinases A large group of genes in all eukaryotes encode for. *October*. 103, 211-225

11 Blume-Jensen, P. and Hunter, T. (2001) Oncogenic kinase signalling. *Nature*. 411, 355-65

12 Hubbard, S. R. and Miller, W. T. (2007) Receptor tyrosine kinases: mechanisms of activation and signaling. *Current opinion in cell biology*. 19, 117-23

13 Chao, M. V. (2003) Neurotrophins and their receptors: a convergence point for many signalling pathways. *Nature reviews. Neuroscience*. 4, 299-309

14 Wehrman, T. *et al.* (2007) Structural and mechanistic insights into nerve growth factor interactions with the TrkA and p75 receptors. *Neuron*. 53, 25-38

15 Huse, M. and Kuriyan, J. (2002) The conformational plasticity of protein kinases. *Cell*. 109, 275-82

16 Shewchuk, L. M. *et al.* (2000) Structure of the Tie2 RTK domain: self-inhibition by the nucleotide binding loop, activation loop, and C-terminal tail. *Structure (London, England : 1993)*. 8, 1105-13

17 Zhang, X. *et al.* (2006) An allosteric mechanism for activation of the kinase domain of epidermal growth factor receptor. *Cell*. 125, 1137-49

18 Jura, N. *et al.* (2009) Mechanism for activation of the EGF receptor catalytic domain by the juxtamembrane segment. *Cell*. 137, 1293-307

19 Red Brewer, M. *et al.* (2009) The juxtamembrane region of the EGF receptor functions as an activation domain. *Molecular cell*. 34, 641-51

20 Ullrich, A. and Schlessinger, J. (1990) Signal transduction by receptors with tyrosine kinase activity. *Cell*. 61, 203-12

21 Clayton, A. H. A. *et al.* (2005) Ligand-induced dimer-tetramer transition during the activation of the cell surface epidermal growth factor receptor-A multidimensional microscopy analysis. *The Journal of biological chemistry*. 280, 30392-9

22 Gadella, T. W. and Jovin, T. M. (1995) Oligomerization of epidermal growth factor receptors on A431 cells studied by time-resolved fluorescence imaging microscopy. A stereochemical model for tyrosine kinase receptor activation. *The Journal of cell biology*. 129, 1543-58

23 Ward, C. W. *et al.* (2007) The insulin and EGF receptor structures: new insights into ligand-induced receptor activation. *Trends in biochemical sciences*. 32, 129-37

24 Weiss, A. and Schlessinger, J. (1998) Switching Signals On or Off by Receptor Dimerization. *Cell*. 94, 277-280

25 Wiesmann, C. and de Vos, A. M. (2001) Nerve growth factor: structure and function. *Cellular and molecular life sciences : CMLS*. 58, 748-59

26 Nolen, B. *et al.* (2004) Regulation of protein kinases; controlling activity through activation segment conformation. *Molecular cell*. 15, 661-75

27 Gale, N. W. *et al.* (1996) Eph Receptors and Ligands Comprise Two Major Specificity Subclasses and Are Reciprocally Compartmentalized during Embryogenesis. *Neuron*. 17, 9-19

28 Pasquale, E. B. (2008) Eph-ephrin bidirectional signaling in physiology and disease. *Cell*. 133, 38-52

29 Palmer, A. and Klein, R. (2003) Multiple roles of ephrins in morphogenesis, neuronal networking, and brain function. *Genes & development*. 17, 1429-50

30 Pasquale, E. B. (2005) Eph receptor signalling casts a wide net on cell behaviour. *Nature reviews. Molecular cell biology*. 6, 462-75

31 Davis, S. *et al.* (1994) Ligands for EPH-related receptor tyrosine kinases that require membrane attachment or clustering for activity. *Science (New York, N.Y.)*. 266, 816-9

32 Egea, J. and Klein, R. (2007) Bidirectional Eph-ephrin signaling during axon guidance. *Trends in cell biology*. 17, 230-8

33 Kullander, K. and Klein, R. (2002) Mechanisms and functions of Eph and ephrin signalling. *Nature reviews. Molecular cell biology*. 3, 475-86

34 Stein, E. *et al.* (1998) Eph receptors discriminate specific ligand oligomers to determine alternative signaling complexes, attachment, and assembly responses. *Genes & Development*. 12, 667-678

35 Luo, L. and Flanagan, J. G. (2007) Development of continuous and discrete neural maps. *Neuron*. 56, 284-300

36 Poliakov, A. *et al.* (2004) Diverse roles of eph receptors and ephrins in the regulation of cell migration and tissue assembly. *Developmental cell*. 7, 465-80

37 Adams, R. H. and Eichmann, A. (2010) Axon guidance molecules in vascular patterning. *Cold Spring Harbor perspectives in biology*. 2, a001875

38 Kuijper, S. *et al.* (2007) Regulation of angiogenesis by Eph-ephrin interactions. *Trends in cardiovascular medicine*. 17, 145-51

39 Adams, R. H. and Klein, R. (2000) Eph receptors and ephrin ligands. essential mediators of vascular development. *Trends in cardiovascular medicine*. 10, 183-8

40 Hiratsuka, S. (2011) Vasculogenensis, angiogenesis and special features of tumor blood vessels. *Frontiers in bioscience : a journal and virtual library*. 16, 1413-27

41 Dalva, M. B. *et al.* (2007) Cell adhesion molecules: signalling functions at the synapse. *Nature reviews. Neuroscience*. 8, 206-20

42 Yamaguchi, Y. and Pasquale, E. B. (2004) Eph receptors in the adult brain. *Current opinion in neurobiology*. 14, 288-96

43 Klein, R. (2009) Bidirectional modulation of synaptic functions by Eph/ephrin signaling. *Nature neuroscience*. 12, 15-20

44 Filosa, A. *et al.* (2009) Neuron-glia communication via EphA4/ephrin-A3 modulates LTP through glial glutamate transport. *Nature neuroscience*. 12, 1285-92

45 Wu, J. and Luo, H. (2005) Recent advances on T-cell regulation by receptor tyrosine kinases. *Current opinion in hematology*. 12, 292-7

46 Muñoz, J. J. *et al.* (2009) Organizing the thymus gland. *Annals of the New York Academy of Sciences*. 1153, 14-9

47 Holen, H. L. *et al.* (2011) Ephrin-B3 binds specifically to B lymphocytes in blood and induces migration. *Scandinavian journal of immunology*. 74, 144-54

48 Konstantinova, I. *et al.* (2007) EphA-Ephrin-A-mediated beta cell communication regulates insulin secretion from pancreatic islets. *Cell*. 129, 359-70

49 Edwards, C. M. and Mundy, G. R. (2008) Eph receptors and ephrin signaling pathways: a role in bone homeostasis. *International journal of medical sciences*. 5, 263-72

50 Zhao, C. *et al.* (2006) Bidirectional ephrinB2-EphB4 signaling controls bone homeostasis. *Cell metabolism*. 4, 111-21

51 Barker, N. *et al.* (2007) Identification of stem cells in small intestine and colon by marker gene Lgr5. *Nature*. 449, 1003-7

52 Clevers, H. and Batlle, E. (2006) EphB/EphrinB receptors and Wnt signaling in colorectal cancer. *Cancer research*. 66, 2-5

53 de Lau, W. *et al.* (2007) WNT signaling in the normal intestine and colorectal cancer. *Frontiers in bioscience : a journal and virtual library*. 12, 471-91

54 Du, J. *et al.* (2007) Eph/ephrin signaling as a potential therapeutic target after central nervous system injury. *Current pharmaceutical design*. 13, 2507-18

55 Goldshmit, Y. *et al.* (2011) EphA4 Blockers Promote Axonal Regeneration and Functional Recovery Following Spinal Cord Injury in Mice. *PloS one*. 6, e24636

56 Goldshmit, Y. *et al.* (2006) Roles of Eph receptors and ephrins in the normal and damaged adult CNS. *Brain research reviews*. 52, 327-45

57 Wu, Z. *et al.* (2007) Caenorhabditis elegans neuronal regeneration is influenced by life stage, ephrin signaling, and synaptic branching. *Proceedings of the National Academy of Sciences of the United States of America*. 104, 15132-7

58 Simón, A. M. *et al.* (2009) Early changes in hippocampal Eph receptors precede the onset of memory decline in mouse models of Alzheimer's disease. *Journal of Alzheimer's disease : JAD*. 17, 773-86

59 Cissé, M. *et al.* (2011) Reversing EphB2 depletion rescues cognitive functions in Alzheimer model. *Nature*. 469, 47-52

60 Ireton, R. C. and Chen, J. (2005) EphA2 receptor tyrosine kinase as a promising target for cancer therapeutics. *Current cancer drug targets*. 5, 149-57

61 Noren, N. K. and Pasquale, E. B. (2004) Eph receptor-ephrin bidirectional signals that target Ras and Rho proteins. *Cellular signalling*. 16, 655-66

62 Genander, M. and Frisén, J. (2010) Ephrins and Eph receptors in stem cells and cancer. *Current opinion in cell biology*. 22, 611-6

63 Pasquale, E. B. (2010) Eph receptors and ephrins in cancer: bidirectional signalling and beyond. *Nature reviews. Cancer*. 10, 165-80

64 Bonaparte, M. I. *et al.* (2005) Ephrin-B2 ligand is a functional receptor for Hendra virus and Nipah virus. *Proceedings of the National Academy of Sciences of the United States of America*. 102, 10652-7

65 Negrete, O. A. *et al.* (2005) EphrinB2 is the entry receptor for Nipah virus, an emergent deadly paramyxovirus. *Nature*. 436, 401-5

66 Negrete, O. A. *et al.* (2006) Two key residues in ephrinB3 are critical for its use as an alternative receptor for Nipah virus. *PLoS pathogens*. 2, e7

67 Bowden, T. A. *et al.* (2008) Structural basis of Nipah and Hendra virus attachment to their cell-surface receptor ephrin-B2. *Nature structural & molecular biology*. 15, 567-72

68 Wilkinson, D. G. (2001) Multiple roles of EPH receptors and ephrins in neural development. *Nature reviews. Neuroscience*. 2, 155-64

69 Committee for Eph nomenclature (1997) Unified nomenclature for Eph family receptors and their ligands, the ephrins. Eph Nomenclature Committee. *Cell*. 90, 403-4

70 Himanen, J.-P. *et al.* (2004) Repelling class discrimination: ephrin-A5 binds to and activates EphB2 receptor signaling. *Nature neuroscience*. 7, 501-9

71 Qin, H. *et al.* (2010) Structural characterization of the EphA4-Ephrin-B2 complex reveals new features enabling Eph-ephrin binding promiscuity. *The Journal of biological chemistry*. 285, 644-54

72 Seiradake, E. *et al.* (2010) An extracellular steric seeding mechanism for Eph-ephrin signaling platform assembly. *Nature structural & molecular biology*. 17, 398-402

73 Koolpe, M. *et al.* (2005) EphB receptor-binding peptides identified by phage display enable design of an antagonist with ephrin-like affinity. *The Journal of biological chemistry*. 280, 17301-11

74 Fry, D. C. and Vassilev, L. T. (2005) Targeting protein-protein interactions for cancer therapy. *Journal of molecular medicine (Berlin, Germany)*. 83, 955-63

75 Noberini, R. *et al.* (2008) Small molecules can selectively inhibit ephrin binding to the EphA4 and EphA2 receptors. *The Journal of biological chemistry*. 283, 29461-72

76 Noberini, R. *et al.* (2011) A Disalicylic Acid-Furanyl Derivative Inhibits Ephrin Binding to a Subset of Eph Receptors. *Chemical biology & drug design*. DOI: 10.1111/j.1747-0285.2011.01199.x

77 Qin, H. *et al.* (2008) Crystal structure and NMR binding reveal that two small molecule antagonists target the high affinity ephrin-binding channel of the EphA4 receptor. *The Journal of biological chemistry*. 283, 29473-84

78 Himanen, J. P. *et al.* (1998) Crystal structure of the ligand-binding domain of the receptor tyrosine kinase EphB2. *Nature*. 396, 486-91

79 Himanen, J. P. *et al.* (2001) Crystal structure of an Eph receptor-ephrin complex. *Nature*. 414, 933-8

80 Himanen, J.-P. and Nikolov, D. B. (2003) Eph signaling: a structural view. *Trends in neurosciences*. 26, 46-51

81 Toth, J. *et al.* (2001) Crystal structure of an ephrin ectodomain. *Developmental cell*. 1, 83-92

82 Song, J. *et al.* (2002) Solution structure and backbone dynamics of the functional cytoplasmic subdomain of human ephrin B2, a cell-surface ligand with bidirectional signaling properties. *Biochemistry*. 41, 10942-9

83 Chrencik, J. E. *et al.* (2006) Structural and biophysical characterization of the EphB4*ephrinB2 protein-protein interaction and receptor specificity. *The Journal of biological chemistry*. 281, 28185-92

84 Nikolov, D. B. *et al.* (2005) Crystal structure of the ephrin-B1 ectodomain: implications for receptor recognition and signaling. *Biochemistry*. 44, 10947-53

85 Nikolov, D. *et al.* (2007) Crystal structure of the human ephrin-A5 ectodomain. *Protein science : a publication of the Protein Society*. 16, 996-1000

86 Goldgur, Y. *et al.* (2009) Structure of the ligand-binding domain of the EphB2 receptor at 2 A resolution. *Acta crystallographica. Section F, Structural biology and crystallization communications*. 65, 71-4

87 Himanen, J. P. *et al.* (2009) Ligand recognition by A-class Eph receptors: crystal structures of the EphA2 ligand-binding domain and the EphA2/ephrin-A1 complex. *EMBO reports*. 10, 722-8

88 Chrencik, J. E. *et al.* (2006) Structure and thermodynamic characterization of the EphB4/Ephrin-B2 antagonist peptide complex reveals the determinants for receptor specificity. *Structure (London, England : 1993)*. 14, 321-30

89 Smith, F. M. *et al.* (2004) Dissecting the EphA3/Ephrin-A5 interactions using a novel functional mutagenesis screen. *The Journal of biological chemistry*. 279, 9522-31

90 Lackmann, M. *et al.* (1998) Distinct subdomains of the EphA3 receptor mediate ligand binding and receptor dimerization. *The Journal of biological chemistry*. 273, 20228-37

91 Himanen, J. P. *et al.* (2010) Architecture of Eph receptor clusters. *Proceedings of the National Academy of Sciences of the United States of America*. DOI: 10.1073/pnas.1004148107

92 Bowden, T. A. *et al.* (2009) Structural plasticity of eph receptor A4 facilitates cross-class ephrin signaling. *Structure (London, England : 1993)*. 17, 1386-97

93 Singla, N. *et al.* (2010) Crystal structure of the ligand-binding domain of the promiscuous EphA4 receptor reveals two distinct conformations. *Biochemical and biophysical research communications*. 399, 555-9

94 Lackmann, M. *et al.* (1997) Ligand for EPH-related kinase (LERK) 7 is the preferred high affinity ligand for the HEK receptor. *The Journal of biological chemistry*. 272, 16521-30

95 Himanen, J. P. and Nikolov, D. B. (2002) Purification, crystallization and preliminary characterization of an Eph-B2/ephrin-B2 complex. *Acta crystallographica. Section D, Biological crystallography*. 58, 533-5

96 Pabbisetty, K. B. *et al.* (2007) Kinetic analysis of the binding of monomeric and dimeric ephrins to Eph receptors: correlation to function in a growth cone collapse assay. *Protein science : a publication of the Protein Society*. 16, 355-61

97 Day, B. *et al.* (2005) Three distinct molecular surfaces in ephrin-A5 are essential for a functional interaction with EphA3. *The Journal of biological chemistry*. 280, 26526-32

BIBLIOGRAPHY

98 Bocharov, E. V. *et al.* (2008) Spatial structure and pH-dependent conformational diversity of dimeric transmembrane domain of the receptor tyrosine kinase EphA1. *The Journal of biological chemistry*. 283, 29385-95

99 Stapleton, D. *et al.* (1999) The crystal structure of an Eph receptor SAM domain reveals a mechanism for modular dimerization. *Nature structural biology*. 6, 44-9

100 Thanos, C. D. *et al.* (1999) Oligomeric structure of the human EphB2 receptor SAM domain. *Science (New York, N.Y.)*. 283, 833-6

101 Behlke, J. *et al.* (2001) Self-association studies on the EphB2 receptor SAM domain using analytical ultracentrifugation. *European biophysics journal : EBJ*. 30, 411-5

102 Smalla, M. *et al.* (1999) Solution structure of the receptor tyrosine kinase EphB2 SAM domain and identification of two distinct homotypic interaction sites. *Protein science : a publication of the Protein Society*. 8, 1954-61

103 Carvalho, R. F. *et al.* (2006) Silencing of EphA3 through a cis interaction with ephrinA5. *Nature neuroscience*. 9, 322-30

104 Wimmer-Kleikamp, S. H. *et al.* (2004) Recruitment of Eph receptors into signaling clusters does not require ephrin contact. *The Journal of cell biology*. 164, 661-6

105 Hubbard, S. R. and Till, J. H. (2000) Protein tyrosine kinase structure and function. *Annual review of biochemistry*. 69, 373-98

106 Himanen, J.-P. *et al.* (2007) Cell-cell signaling via Eph receptors and ephrins. *Current opinion in cell biology*. 19, 534-42

107 Wybenga-Groot, L. E. *et al.* (2001) Structural basis for autoinhibition of the Ephb2 receptor tyrosine kinase by the unphosphorylated juxtamembrane region. *Cell*. 106, 745-57

108 Ellis, C. *et al.* (1996) A juxtamembrane autophosphorylation site in the Eph family receptor tyrosine kinase, Sek, mediates high affinity interaction with p59fyn. *Oncogene*. 12, 1727-36

109 Zisch, A. H. *et al.* (1998) Complex formation between EphB2 and Src requires phosphorylation of tyrosine 611 in the EphB2 juxtamembrane region. *Oncogene*. 16, 2657-70

110 Binns, K. L. *et al.* (2000) Phosphorylation of tyrosine residues in the kinase domain and juxtamembrane region regulates the biological and catalytic activities of Eph receptors. *Molecular and cellular biology*. 20, 4791-805

111 Kalo, M. S. and Pasquale, E. B. (1999) Multiple in vivo tyrosine phosphorylation sites in EphB receptors. *Biochemistry*. 38, 14396-408

112 Wiesner, S. *et al.* (2006) A change in conformational dynamics underlies the activation of Eph receptor tyrosine kinases. *The EMBO journal*. 25, 4686-96

113 Egea, J. *et al.* (2005) Regulation of EphA 4 kinase activity is required for a subset of axon guidance decisions suggesting a key role for receptor clustering in Eph function. *Neuron*. 47, 515-28

114 Hubbard, S. R. (2001) Theme and variations: juxtamembrane regulation of receptor protein kinases. *Molecular cell*. 8, 481-2

115 Van Aelst, L. and D'Souza-Schorey, C. (1997) Rho GTPases and signaling networks. *Genes & development*. 11, 2295-322

116 Tapon, N. and Hall, A. (1997) Rho, Rac and Cdc42 GTPases regulate the organization of the actin cytoskeleton. *Current opinion in cell biology*. 9, 86-92

117 Ridley, A. J. (2001) Rho family proteins: coordinating cell responses. *Trends in cell biology*. 11, 471-7

118 Kozma, R. *et al.* (1997) Rho family GTPases and neuronal growth cone remodelling: relationship between increased complexity induced by Cdc42Hs, Rac1, and acetylcholine and collapse induced by RhoA and lysophosphatidic acid. *Molecular and cellular biology*. 17, 1201-11

119 Riento, K. and Ridley, A. J. (2003) Rocks: multifunctional kinases in cell behaviour. *Nature reviews. Molecular cell biology*. 4, 446-56

120 Wu, K. Y. *et al.* (2005) Local translation of RhoA regulates growth cone collapse. *Nature*. 436, 1020-4

121 Kozma, R. *et al.* (1997) Rho family GTPases and neuronal growth cone remodelling: relationship between increased complexity induced by Cdc42Hs, Rac1, and acetylcholine and collapse induced by RhoA and lysophosphatidic acid. *Mol. Cell. Biol.* 17, 1201-1211

122 Shamah, S. M. *et al.* (2001) EphA receptors regulate growth cone dynamics through the novel guanine nucleotide exchange factor ephexin. *Cell*. 105, 233-44

123 Beg, A. A. *et al.* (2007) alpha2-Chimaerin is an essential EphA4 effector in the assembly of neuronal locomotor circuits. *Neuron*. 55, 768-78

124 Shi, L. *et al.* (2007) Alpha2-chimaerin interacts with EphA4 and regulates EphA4-dependent growth cone collapse. *Proceedings of the National Academy of Sciences of the United States of America*. 104, 16347-52

125 Wegmeyer, H. *et al.* (2007) EphA4-dependent axon guidance is mediated by the RacGAP alpha2-chimaerin. *Neuron*. 55, 756-67

126 Iwasato, T. *et al.* (2007) Rac-GAP alpha-chimerin regulates motor-circuit formation as a key mediator of EphrinB3/EphA4 forward signaling. *Cell*. 130, 742-53

127 Sahin, M. *et al.* (2005) Eph-dependent tyrosine phosphorylation of ephexin1 modulates growth cone collapse. *Neuron*. 46, 191-204

128 Knöll, B. and Drescher, U. (2004) Src family kinases are involved in EphA receptor-mediated retinal axon guidance. *The Journal of neuroscience : the official journal of the Society for Neuroscience*. 24, 6248-57

129 Irie, F. and Yamaguchi, Y. (2002) EphB receptors regulate dendritic spine development via intersectin, Cdc42 and N-WASP. *Nature neuroscience*. 5, 1117-8

130 Penzes, P. *et al.* (2003) Rapid induction of dendritic spine morphogenesis by trans-synaptic ephrinB-EphB receptor activation of the Rho-GEF kalirin. *Neuron*. 37, 263-74

131 Wahl, S. *et al.* (2000) Ephrin-A5 induces collapse of growth cones by activating Rho and Rho kinase. *The Journal of cell biology*. 149, 263-70

132 Cheng, Q. *et al.* (2003) Cdk5/p35 and Rho-kinase mediate ephrin-A5-induced signaling in retinal ganglion cells. *Molecular and cellular neurosciences*. 24, 632-45

133 Groeger, G. and Nobes, C. D. (2007) Co-operative Cdc42 and Rho signalling mediates ephrinB-triggered endothelial cell retraction. *The Biochemical journal*. 404, 23-9

134 Yu, H. H. *et al.* (2001) Multiple signaling interactions of Abl and Arg kinases with the EphB2 receptor. *Oncogene*. 20, 3995-4006

135 Harbott, L. K. and Nobes, C. D. (2005) A key role for Abl family kinases in EphA receptor-mediated growth cone collapse. *Molecular and cellular neurosciences*. 30, 1-11

136 Campbell, S. L. *et al.* (1998) Increasing complexity of Ras signaling. *Oncogene*. 17, 1395-413

137 Johnson, G. L. and Lapadat, R. (2002) Mitogen-activated protein kinase pathways mediated by ERK, JNK, and p38 protein kinases. *Science (New York, N.Y.)*. 298, 1911-2

138 Forcet, C. *et al.* (2002) Netrin-1-mediated axon outgrowth requires deleted in colorectal cancer-dependent MAPK activation. *Nature*. 417, 443-7

139 Hughes, P. E. *et al.* (1997) Suppression of integrin activation: a novel function of a Ras/Raf-initiated MAP kinase pathway. *Cell*. 88, 521-30

140 Marshall, C. J. (1995) Specificity of receptor tyrosine kinase signaling: transient versus sustained extracellular signal-regulated kinase activation. *Cell*. 80, 179-85

141 Miao, H. *et al.* (2001) Activation of EphA receptor tyrosine kinase inhibits the Ras/MAPK pathway. *Nature cell biology*. 3, 527-30

142 Elowe, S. *et al.* (2001) Downregulation of the Ras-mitogen-activated protein kinase pathway by the EphB2 receptor tyrosine kinase is required for ephrin-induced neurite retraction. *Molecular and cellular biology*. 21, 7429-41

143 Kim, I. *et al.* (2002) EphB ligand, ephrinB2, suppresses the VEGF- and angiopoietin 1-induced Ras/mitogen-activated protein kinase pathway in venous endothelial cells. *The FASEB journal : official publication of the Federation of American Societies for Experimental Biology*. 16, 1126-8

144 Miller, M. A. *et al.* (2003) An Eph receptor sperm-sensing control mechanism for oocyte meiotic maturation in Caenorhabditis elegans. *Genes & development*. 17, 187-200

145 Picco, V. *et al.* (2007) Ephrin-Eph signalling drives the asymmetric division of notochord/neural precursors in Ciona embryos. *Development (Cambridge, England)*. 134, 1491-7

146 Tong, J. *et al.* (2003) Manipulation of EphB2 regulatory motifs and SH2 binding sites switches MAPK signaling and biological activity. *The Journal of biological chemistry*. 278, 6111-9

147 Pratt, R. L. and Kinch, M. S. (2002) Activation of the EphA2 tyrosine kinase stimulates the MAP/ERK kinase signaling cascade. *Oncogene*. 21, 7690-9

148 Vindis, C. *et al.* (2003) EphB1 recruits c-Src and p52Shc to activate MAPK/ERK and promote chemotaxis. *The Journal of cell biology*. 162, 661-71

149 Klemke, R. L. *et al.* (1997) Regulation of cell motility by mitogen-activated protein kinase. *The Journal of cell biology*. 137, 481-92

150 Hsueh, Y. P. and Sheng, M. (1998) Eph receptors, ephrins, and PDZs gather in neuronal synapses. *Neuron*. 21, 1227-9

151 Torres, R. *et al.* (1998) PDZ proteins bind, cluster, and synaptically colocalize with Eph receptors and their ephrin ligands. *Neuron*. 21, 1453-63

152 Buchert, M. *et al.* (1999) The junction-associated protein AF-6 interacts and clusters with specific Eph receptor tyrosine kinases at specialized sites of cell-cell contact in the brain. *The Journal of cell biology*. 144, 361-71

153 Kullander, K. *et al.* (2001) Kinase-dependent and kinase-independent functions of EphA4 receptors in major axon tract formation in vivo. *Neuron*. 29, 73-84

154 Park, E. K. *et al.* (2004) Ectopic EphA4 receptor induces posterior protrusions via FGF signaling in Xenopus embryos. *Molecular biology of the cell*. 15, 1647-55

155 Yamazaki, T. *et al.* (2009) EphA1 interacts with integrin-linked kinase and regulates cell morphology and motility. *Journal of cell science*. 122, 243-55

156 Zhuang, G. *et al.* (2007) Regulation of EphA2 receptor endocytosis by SHIP2 lipid phosphatase via phosphatidylinositol 3-Kinase-dependent Rac1 activation. *The Journal of biological chemistry*. 282, 2683-94

157 Hock, B. *et al.* (1998) PDZ-domain-mediated interaction of the Eph-related receptor tyrosine kinase EphB3 and the ras-binding protein AF6 depends on the kinase activity of the receptor. *Proceedings of the National Academy of Sciences of the United States of America*. 95, 9779-84

158 Richter, M. *et al.* (2007) The EphA4 receptor regulates neuronal morphology through SPAR-mediated inactivation of Rap GTPases. *The Journal of neuroscience : the official journal of the Society for Neuroscience*. 27, 14205-15

159 Aoto, J. *et al.* (2007) Postsynaptic ephrinB3 promotes shaft glutamatergic synapse formation. *The Journal of neuroscience : the official journal of the Society for Neuroscience*. 27, 7508-19

160 Hung, A. Y. and Sheng, M. (2002) PDZ domains: structural modules for protein complex assembly. *The Journal of biological chemistry*. 277, 5699-702

161 Zou, J. X. *et al.* (1999) An Eph receptor regulates integrin activity through R-Ras. *Proceedings of the National Academy of Sciences of the United States of America*. 96, 13813-8

162 Prevost, N. *et al.* (2002) Interactions between Eph kinases and ephrins provide a mechanism to support platelet aggregation once cell-to-cell contact has occurred. *Proceedings of the National Academy of Sciences of the United States of America*. 99, 9219-24

163 Nagashima, K.-I. *et al.* (2002) Adaptor protein Crk is required for ephrin-B1-induced membrane ruffling and focal complex assembly of human aortic endothelial cells. *Molecular biology of the cell*. 13, 4231-42

164 Miao, H. *et al.* (2000) Activation of EphA2 kinase suppresses integrin function and causes focal-adhesion-kinase dephosphorylation. *Nature cell biology*. 2, 62-9

165 Carter, N. *et al.* (2002) EphrinA1-induced cytoskeletal re-organization requires FAK and p130(cas). *Nature cell biology*. 4, 565-73

166 Huynh-Do, U. *et al.* (1999) Surface densities of ephrin-B1 determine EphB1-coupled activation of cell attachment through alphavbeta3 and alpha5beta1 integrins. *The EMBO journal*. 18, 2165-73

167 Becker, E. *et al.* (2000) Nck-interacting Ste20 kinase couples Eph receptors to c-Jun N-terminal kinase and integrin activation. *Molecular and cellular biology*. 20, 1537-45

168 Gu, C. and Park, S. (2001) The EphA8 receptor regulates integrin activity through p110gamma phosphatidylinositol-3 kinase in a tyrosine kinase activity-independent manner. *Molecular and cellular biology*. 21, 4579-97

169 Truitt, L. and Freywald, A. (2011) Dancing with the dead: Eph receptors and their kinase-null partners. *Biochemistry and cell biology = Biochimie et biologie cellulaire*. 89, 115-29

170 Matsuoka, H. *et al.* (2005) Biphasic functions of the kinase-defective Ephb6 receptor in cell adhesion and migration. *The Journal of biological chemistry*. 280, 29355-63

171 Holmberg, J. *et al.* (2000) Regulation of repulsion versus adhesion by different splice forms of an Eph receptor. *Nature*. 408, 203-6

172 Grunwald, I. C. *et al.* (2004) Hippocampal plasticity requires postsynaptic ephrinBs. *Nature neuroscience*. 7, 33-40

173 Henkemeyer, M. *et al.* (1996) Nuk controls pathfinding of commissural axons in the mammalian central nervous system. *Cell*. 86, 35-46

174 Pitulescu, M. E. and Adams, R. H. (2010) Eph/ephrin molecules--a hub for signaling and endocytosis. *Genes & development*. 24, 2480-92

175 Huynh-do, U. *et al.* (1999) Surface densities of ephrin-B1 determine EphB1-coupled activation of cell attachment through α v β 3 and α 5 β 1 integrins. 18, 2165-2173

176 Nievergall, E. *et al.* (2010) PTP1B regulates Eph receptor function and trafficking. *The Journal of cell biology*. DOI: 10.1083/jcb.201005035

177 Shintani, T. *et al.* (2006) Eph receptors are negatively controlled by protein tyrosine phosphatase receptor type O. *Nature neuroscience*. 9, 761-9

178 Parri, M. *et al.* (2005) EphrinA1 repulsive response is regulated by an EphA2 tyrosine phosphatase. *The Journal of biological chemistry*. 280, 34008-18

179 Poliakov, A. *et al.* (2008) Regulation of EphB2 activation and cell repulsion by feedback control of the MAPK pathway. *The Journal of cell biology*. 183, 933-47

180 Chong, S.-W. and Jiang, Y.-J. (2005) Off limits--integrins holding boundaries in somitogenesis. *Trends in cell biology*. 15, 453-7

181 Nakamoto, T. *et al.* (2004) Neurobiology: New connections between integrins and axon guidance. *Current biology : CB*. 14, R121-3

182 Wimmer-Kleikamp, S. H. and Lackmann, M. (2005) Eph-modulated cell morphology, adhesion and motility in carcinogenesis. *IUBMB life*. 57, 421-31

183 Bourgin, C. *et al.* (2007) The EphA4 receptor regulates dendritic spine remodeling by affecting beta1-integrin signaling pathways. *The Journal of cell biology*. 178, 1295-307

184 Dalva, M. B. *et al.* (2000) EphB Receptors Interact with NMDA Receptors and Regulate Excitatory Synapse Formation. *Cell*. 103, 945-956

185 Takasu, M. A. *et al.* (2002) Modulation of NMDA receptor-dependent calcium influx and gene expression through EphB receptors. *Science (New York, N.Y.)*. 295, 491-5

186 Litterst, C. *et al.* (2007) Ligand binding and calcium influx induce distinct ectodomain/gamma-secretase-processing pathways of EphB2 receptor. *The Journal of biological chemistry*. 282, 16155-63

187 Bordji, K. *et al.* (2011) Synapses, NMDA receptor activity and neuronal Aβ production in Alzheimer's disease. *Reviews in the neurosciences*. 22, 285-94

188 Schmitt, A. M. *et al.* (2006) Wnt-Ryk signalling mediates medial-lateral retinotectal topographic mapping. *Nature*. 439, 31-7

189 Halford, M. M. *et al.* (2000) Ryk-deficient mice exhibit craniofacial defects associated with perturbed Eph receptor crosstalk. *Nature genetics*. 25, 414-8

190 Trivier, E. and Ganesan, T. S. (2002) RYK, a catalytically inactive receptor tyrosine kinase, associates with EphB2 and EphB3 but does not interact with AF-6. *The Journal of biological chemistry*. 277, 23037-43

191 Kamitori, K. *et al.* (2005) Receptor related to tyrosine kinase RYK regulates cell migration during cortical development. *Biochemical and biophysical research communications*. 330, 446-53

192 Arvanitis, D. and Davy, A. (2008) Eph/ephrin signaling: networks. *Genes & development*. 22, 416-29

193 Hindges, R. *et al.* (2002) EphB forward signaling controls directional branch extension and arborization required for dorsal-ventral retinotopic mapping. *Neuron*. 35, 475-87

194 Mann, F. *et al.* (2002) Topographic mapping in dorsoventral axis of the Xenopus retinotectal system depends on signaling through ephrin-B ligands. *Neuron*. 35, 461-73

195 Kramer, E. R. *et al.* (2006) Cooperation between GDNF/Ret and ephrinA/EphA4 signals for motor-axon pathway selection in the limb. *Neuron*. 50, 35-47

196 Dudanova, I. *et al.* (2010) GDNF acts as a chemoattractant to support ephrinA-induced repulsion of limb motor axons. *Current biology : CB*. 20, 2150-6

197 Dudanova, I. *et al.* (2010) GDNF acts as a chemoattractant to support ephrinA-induced repulsion of limb motor axons. *Current biology : CB*. 20, 2150-6

198 Gauthier, L. R. and Robbins, S. M. (2003) Ephrin signaling: One raft to rule them all? One raft to sort them? One raft to spread their call and in signaling bind them? *Life sciences*. 74, 207-16

199 Hornberger, M. R. *et al.* (1999) Modulation of EphA receptor function by coexpressed ephrinA ligands on retinal ganglion cell axons. *Neuron*. 22, 731-42

200 Yin, Y. *et al.* (2004) EphA receptor tyrosine kinases interact with co-expressed ephrin-A ligands in cis. *Neuroscience research*. 48, 285-96

201 Kao, T.-J. and Kania, A. (2011) Ephrin-Mediated cis-Attenuation of Eph Receptor Signaling Is Essential for Spinal Motor Axon Guidance. *Neuron*. 71, 76-91

202 Marquardt, T. *et al.* (2005) Coexpressed EphA Receptors and Ephrin-A Ligands Mediate Opposing Actions on Growth Cone Navigation from Distinct Membrane Domains. *Cell*. 121, 127-139

203 Kalo, M. S. *et al.* (2001) In vivo tyrosine phosphorylation sites of activated ephrin-B1 and ephB2 from neural tissue. *The Journal of biological chemistry*. 276, 38940-8

204 Palmer, A. *et al.* (2002) EphrinB phosphorylation and reverse signaling: regulation by Src kinases and PTP-BL phosphatase. *Molecular cell*. 9, 725-37

205 Cowan, C. A. and Henkemeyer, M. (2001) The SH2/SH3 adaptor Grb4 transduces B-ephrin reverse signals. *Nature*. 413, 174-9

206 Essmann, C. L. *et al.* (2008) Serine phosphorylation of ephrinB2 regulates trafficking of synaptic AMPA receptors. *Nature neuroscience*. 11, 1035-1043

207 Zhang, H. *et al.* (2005) A GIT1/PIX/Rac/PAK signaling module regulates spine morphogenesis and synapse formation through MLC. *The Journal of neuroscience : the official journal of the Society for Neuroscience*. 25, 3379-88

208 Segura, I. *et al.* (2007) Grb4 and GIT1 transduce ephrinB reverse signals modulating spine morphogenesis and synapse formation. *Nature neuroscience*. 10, 301-10

209 Xu, N.-J. and Henkemeyer, M. (2009) Ephrin-B3 reverse signaling through Grb4 and cytoskeletal regulators mediates axon pruning. *Nature neuroscience*. 12, 268-76

210 Georgakopoulos, A. *et al.* (2006) Metalloproteinase/Presenilin1 processing of ephrinB regulates EphB-induced Src phosphorylation and signaling. *The EMBO journal*. 25, 1242-52

211 Foo, S. S. *et al.* (2006) Ephrin-B2 controls cell motility and adhesion during blood-vessel-wall assembly. *Cell*. 124, 161-73

212 Tanaka, M. *et al.* (2003) Association of Dishevelled with Eph tyrosine kinase receptor and ephrin mediates cell repulsion. *The EMBO journal*. 22, 847-58

213 Lee, H.-S. *et al.* (2006) Dishevelled mediates ephrinB1 signalling in the eye field through the planar cell polarity pathway. *Nature cell biology*. 8, 55-63

214 Boutros, M. and Mlodzik, M. (1999) Dishevelled: at the crossroads of divergent intracellular signaling pathways. *Mechanisms of development*. 83, 27-37

215 Mäkinen, T. *et al.* (2005) PDZ interaction site in ephrinB2 is required for the remodeling of lymphatic vasculature. *Genes & development*. 19, 397-410

216 Brückner, K. *et al.* (1999) EphrinB ligands recruit GRIP family PDZ adaptor proteins into raft membrane microdomains. *Neuron*. 22, 511-24

217 Grootjans, J. J. *et al.* (2000) Syntenin-syndecan binding requires syndecan-synteny and the co-operation of both PDZ domains of syntenin. *The Journal of biological chemistry*. 275, 19933-41

218 Lu, Q. *et al.* (2001) Ephrin-B reverse signaling is mediated by a novel PDZ-RGS protein and selectively inhibits G protein-coupled chemoattraction. *Cell*. 105, 69-79

219 Knöll, B. and Drescher, U. (2002) Ephrin-As as receptors in topographic projections. *Trends in neurosciences*. 25, 145-9

220 Knöll, B. *et al.* (2001) A role for the EphA family in the topographic targeting of vomeronasal axons. *Development (Cambridge, England)*. 128, 895-906

221 Lim, Y.-S. *et al.* (2008) p75(NTR) mediates ephrin-A reverse signaling required for axon repulsion and mapping. *Neuron*. 59, 746-58

222 Marquardt, T. *et al.* (2005) Coexpressed EphA receptors and ephrin-A ligands mediate opposing actions on growth cone navigation from distinct membrane domains. *Cell*. 121, 127-39

223 Coate, T. M. *et al.* (2009) Reverse signaling by glycosylphosphatidylinositol-linked Manduca ephrin requires a SRC family kinase to restrict neuronal migration in vivo. *The Journal of neuroscience : the official journal of the Society for Neuroscience*. 29, 3404-18

224 Holmberg, J. *et al.* (2005) Ephrin-A2 reverse signaling negatively regulates neural progenitor proliferation and neurogenesis. *Genes & development*. 19, 462-71

225 Davy, A. *et al.* (1999) Compartmentalized signaling by GPI-anchored ephrin-A5 requires the Fyn tyrosine kinase to regulate cellular adhesion. *Genes & development*. 13, 3125-35

226 Davy, A. and Robbins, S. M. (2000) Ephrin-A5 modulates cell adhesion and morphology in an integrin-dependent manner. *The EMBO journal*. 19, 5396-405

227 Huai, J. and Drescher, U. (2001) An ephrin-A-dependent signaling pathway controls integrin function and is linked to the tyrosine phosphorylation of a 120-kDa protein. *The Journal of biological chemistry*. 276, 6689-94

228 Brown, D. A. and London, E. (1998) Functions of lipid rafts in biological membranes. *Annual review of cell and developmental biology*. 14, 111-36

229 Tsui-Pierchala, B. A. *et al.* (2002) Lipid rafts in neuronal signaling and function. *Trends in neurosciences*. 25, 412-7

230 Munro, S. (2003) Lipid rafts: elusive or illusive? *Cell*. 115, 377-88

231 Marler, K. J. M. *et al.* (2008) A TrkB/EphrinA interaction controls retinal axon branching and synaptogenesis. *The Journal of neuroscience : the official journal of the Society for Neuroscience*. 28, 12700-12

232 Poopalasundaram, S. *et al.* (2011) EphrinA6 on chick retinal axons is a key component for p75(NTR)-dependent axon repulsion and TrkB-dependent axon branching. *Molecular and cellular neurosciences*. 47, 131-6

233 Airaksinen, M. S. and Saarma, M. (2002) The GDNF family: signalling, biological functions and therapeutic value. *Nature reviews. Neuroscience*. 3, 383-94

234 Ibáñez, C. F. (2010) Beyond the cell surface: new mechanisms of receptor function. *Biochemical and biophysical research communications*. 396, 24-7

235 Gur, G. *et al.* (2004) *Endocytosis of Receptor Tyrosine Kinases: Implications for Signal Transduction by Growth Factors*, Landes Bioscience.

236 Mann, F. *et al.* (2003) B-type Eph receptors and ephrins induce growth cone collapse through distinct intracellular pathways. *Journal of neurobiology*. 57, 323-36

237 Marston, D. J. *et al.* (2003) Rac-dependent trans-endocytosis of ephrinBs regulates Eph-ephrin contact repulsion. *Nature cell biology*. 5, 879-88

238 Zimmer, M. *et al.* (2003) EphB – ephrinB bi-directional endocytosis terminates adhesion allowing contact mediated repulsion. *Group*. 5,

239 Lauterbach, J. and Klein, R. (2006) Release of full-length EphB2 receptors from hippocampal neurons to cocultured glial cells. *The Journal of neuroscience : the official journal of the Society for Neuroscience*. 26, 11575-81

240 Spacek, J. and Harris, K. M. (2004) Trans-endocytosis via spinules in adult rat hippocampus. *The Journal of neuroscience : the official journal of the Society for Neuroscience*. 24, 4233-41

241 Cowan, C. W. *et al.* (2005) Vav family GEFs link activated Ephs to endocytosis and axon guidance. *Neuron*. 46, 205-17

242 Yoo, S. *et al.* (2010) EphA8-ephrinA5 signaling and clathrin-mediated endocytosis is regulated by Tiam-1, a Rac-specific guanine nucleotide exchange factor. *Molecules and cells*. 29, 603-9

243 Brantley-Sieders, D. M. *et al.* (2004) EphA2 receptor tyrosine kinase regulates endothelial cell migration and vascular assembly through phosphoinositide 3-kinase-mediated Rac1 GTPase activation. *Journal of cell science*. 117, 2037-49

244 Irie, F. *et al.* (2005) EphrinB-EphB signalling regulates clathrin-mediated endocytosis through tyrosine phosphorylation of synaptojanin 1. *Nature cell biology*. 7, 501-9

245 Jørgensen, C. *et al.* (2009) Cell-specific information processing in segregating populations of Eph receptor ephrin-expressing cells. *Science (New York, N.Y.)*. 326, 1502-9

246 Vihanto, M. M. *et al.* (2006) Caveolin-1 is required for signaling and membrane targeting of EphB1 receptor tyrosine kinase. *Journal of cell science*. 119, 2299-309

247 Zerial, M. and McBride, H. (2001) Rab proteins as membrane organizers. *Nature reviews. Molecular cell biology*. 2, 107-17

248 Deininger, K. *et al.* (2008) The Rab5 guanylate exchange factor Rin1 regulates endocytosis of the EphA4 receptor in mature excitatory neurons. *Proceedings of the National Academy of Sciences of the United States of America*. 105, 12539-44

249 Fasen, K. *et al.* (2008) Ligand binding induces Cbl-dependent EphB1 receptor degradation through the lysosomal pathway. *Traffic (Copenhagen, Denmark)*. 9, 251-66

250 Zhang, G. *et al.* (2006) Quantitative phosphotyrosine proteomics of EphB2 signaling by stable isotope labeling with amino acids in cell culture (SILAC). *Journal of proteome research*. 5, 581-8

251 Hoogenraad, C. C. *et al.* (2005) GRIP1 controls dendrite morphogenesis by regulating EphB receptor trafficking. *Nature neuroscience*. 8, 906-15

252 Parker, M. *et al.* (2004) Reverse endocytosis of transmembrane ephrin-B ligands via a clathrin-mediated pathway. *Biochemical and biophysical research communications*. 323, 17-23

253 Nakada, M. *et al.* (2006) Ephrin-B3 ligand promotes glioma invasion through activation of Rac1. *Cancer research*. 66, 8492-500

254 Bochenek, M. L. *et al.* (2010) Ephrin-B2 regulates endothelial cell morphology and motility independently of Eph-receptor binding. *Journal of cell science*. 123, 1235-46

255 Hattori, M. *et al.* (2000) Regulated cleavage of a contact-mediated axon repellent. *Science (New York, N.Y.)*. 289, 1360-5

256 Janes, P. W. *et al.* (2005) Adam meets Eph: an ADAM substrate recognition module acts as a molecular switch for ephrin cleavage in trans. *Cell*. 123, 291-304

257 Janes, P. W. *et al.* (2009) Cytoplasmic relaxation of active Eph controls ephrin shedding by ADAM10. *PLoS biology*. 7, e1000215

258 Tomita, T. *et al.* (2006) Presenilin-dependent intramembrane cleavage of ephrin-B1. *Molecular neurodegeneration*. 1, 2

259 Lin, K.-T. *et al.* (2008) Ephrin-B2-induced cleavage of EphB2 receptor is mediated by matrix metalloproteinases to trigger cell repulsion. *The Journal of biological chemistry*. 283, 28969-79

260 Xu, J. *et al.* (2009) Peptide EphB2/CTF2 generated by the gamma-secretase processing of EphB2 receptor promotes tyrosine phosphorylation and cell surface localization of N-methyl-D-aspartate receptors. *The Journal of biological chemistry*. 284, 27220-8

261 Inoue, E. *et al.* (2009) Synaptic activity prompts gamma-secretase-mediated cleavage of EphA4 and dendritic spine formation. *The Journal of cell biology*. 185, 551-64

262 Yang, T. and Zaman, M. H. (2009) Equilibrium and Non-Equilibrium Thermodynamic Processes in Cell–Matrix Interactions. *Journal of Non-Equilibrium Thermodynamics*. 34, 195-217

263 Grakoui, A. *et al.* (1999) The immunological synapse: a molecular machine controlling T cell activation. *Science (New York, N.Y.)*. 285, 221-7

264 Cairo, C. W. (2007) Signaling by committee: receptor clusters determine pathways of cellular activation. *ACS chemical biology*. 2, 652-5

265 Thompson, C. J. (1979) *Mathematical Statistical Mechanics*, Princeton University Press.

266 Ising, E. (1925) Beitrag zur Theorie des Ferromagnetismus. *Zeitschrift für Physik*. 31, 253-258

267 Duke, T. and Graham, I. (2009) Equilibrium mechanisms of receptor clustering. *Progress in biophysics and molecular biology*. 100, 18-24

268 Baxter, R. J. (1982) *Exactly Solved Models in Statistical Mechanics*, Academic Press, London.

269 Bragg, W. and Williams, E. (1934) The effect of thermal agitation on atomic arrangement in alloys. *Proc. Roy. Soc. London*. 145, 699-730

270 Nix, F. and Shockley, W. (1938) Order-disorder transformations in alloys. *Reviews of Modern Physics*. 10, 1-71

271 Bray, D. and Duke, T. (2004) Conformational spread: the propagation of allosteric states in large multiprotein complexes. *Annual review of biophysics and biomolecular structure*. 33, 53-73

272 Monod, J. *et al.* (1965) On the Nature of Allosteric Transitions: a Plausible Model. *Journal of molecular biology*. 12, 88-118

273 Koshland, D. E. *et al.* (1966) Comparison of experimental binding data and theoretical models in proteins containing subunits. *Biochemistry*. 5, 365-85

274 Bray, D. and Duke, T. (2004) Conformational spread: the propagation of allosteric states in large multiprotein complexes. *Annual review of biophysics and biomolecular structure*. 33, 53-73

275 Mello, B. A. and Tu, Y. (2003) Quantitative modeling of sensitivity in bacterial chemotaxis: the role of coupling among different chemoreceptor species. *Proceedings of the National Academy of Sciences of the United States of America*. 100, 8223-8

276 Lenarcic, R. *et al.* (2009) Localisation of DivIVA by targeting to negatively curved membranes. *The EMBO journal*. 28, 2272-82

277 Sourjik, V. (2004) Receptor clustering and signal processing in E. coli chemotaxis. *Trends in microbiology*. 12, 569-76

278 Changeux, J. P. *et al.* (1967) On the cooperativity of biological membranes. *Proceedings of the National Academy of Sciences of the United States of America*. 57, 335-41

279 Bray, D. *et al.* (1998) Receptor clustering as a cellular mechanism to control sensitivity. *Nature*. 393, 85-8

280 Duke, T. a and Bray, D. (1999) Heightened sensitivity of a lattice of membrane receptors. *Proceedings of the National Academy of Sciences of the United States of America*. 96, 10104-8

281 Chan, C. *et al.* (2001) Cooperative enhancement of specificity in a lattice of T cell receptors. *Proceedings of the National Academy of Sciences of the United States of America*. 98, 5758-63

282 Groff, J. R. and Smith, G. D. (2008) Ryanodine receptor allosteric coupling and the dynamics of calcium sparks. *Biophysical journal*. 95, 135-54

283 Graham, I. and Duke, T. (2005) The logical repertoire of ligand-binding proteins. *Physical biology*. 2, 159-65

284 Wadhams, G. H. *et al.* (2005) Requirements for chemotaxis protein localization in Rhodobacter sphaeroides. *Molecular microbiology*. 58, 895-902

285 Shimizu, T. S. *et al.* (2000) Molecular model of a lattice of signalling proteins involved in bacterial chemotaxis. *Nature cell biology*. 2, 792-6

286 Bray, D. (2002) Bacterial chemotaxis and the question of gain. *Proceedings of the National Academy of Sciences of the United States of America*. 99, 7-9

287 Harding, A. and Hancock, J. F. (2008) Ras nanoclusters: combining digital and analog signaling. *Cell cycle (Georgetown, Tex.)*. 7, 127-34

288 Santiago, A. and Erickson, C. A. (2002) Ephrin-B ligands play a dual role in the control of neural crest cell migration. *Development (Cambridge, England)*. 129, 3621-32

289 Hansen, M. J. *et al.* (2004) Retinal axon response to ephrin-as shows a graded, concentration-dependent transition from growth promotion to inhibition. *Neuron*. 42, 717-30

290 Vearing, C. J. and Lackmann, M. (2005) "Eph receptor signalling; dimerisation just isn't enough". *Growth factors (Chur, Switzerland)*. 23, 67-76

291 Gerlai, R. *et al.* (1999) Regulation of learning by EphA receptors: a protein targeting study. *The Journal of neuroscience : the official journal of the Society for Neuroscience*. 19, 9538-49

292 Martin, M. *et al.* (1997) Identification of a subpopulation of human renal microvascular endothelial cells with capacity to form capillary-like cord and tube structures. *In vitro cellular & developmental biology. Animal*. 33, 261-9

293 Vearing, C. *et al.* (2005) Concurrent binding of anti-EphA3 antibody and ephrin-A5 amplifies EphA3 signaling and downstream responses: potential as EphA3-specific tumor-targeting reagents. *Cancer research*. 65, 6745-54

294 Salaita, K. *et al.* (2010) Restriction of receptor movement alters cellular response: physical force sensing by EphA2. *Science (New York, N.Y.)*. 327, 1380-5

295 Castellana, E. T. *et al.* (2006) Direct writing of metal nanoparticle films inside sealed microfluidic channels. *Analytical chemistry*. 78, 107-12

296 Groves, J. T. *et al.* (1997) Micropatterning fluid lipid bilayers on solid supports. *Science (New York, N.Y.)*. 275, 651-3

297 Gestwicki, J. E. *et al.* (2000) Tuning chemotactic responses with synthetic multivalent ligands. *Chemistry & biology*. 7, 583-91

298 Kim, S.-H. *et al.* (2002) Dynamic and clustering model of bacterial chemotaxis receptors: structural basis for signaling and high sensitivity. *Proceedings of the National Academy of Sciences of the United States of America*. 99, 11611-5

299 Dufour, A. *et al.* (2006) Genetic analysis of EphA-dependent signaling mechanisms controlling topographic mapping in vivo. *Development (Cambridge, England)*. 133, 4415-20

300 Mey, J. and Thanos, S. (2000) Development of the visual system of the chick. I. Cell differentiation and histogenesis. *Brain research. Brain research reviews*. 32, 343-79

301 Thanos, S. and Mey, J. (2001) Development of the visual system of the chick. II. Mechanisms of axonal guidance. *Brain research. Brain research reviews*. 35, 205-45

302 Feldheim, D. A. and O'Leary, D. D. M. (2010) Visual map development: bidirectional signaling, bifunctional guidance molecules, and competition. *Cold Spring Harbor perspectives in biology*. 2, a001768

303 Monschau, B. *et al.* (1997) Shared and distinct functions of RAGS and ELF-1 in guiding retinal axons. *The EMBO journal*. 16, 1258-67

304 Brown, A. *et al.* (2000) Topographic mapping from the retina to the midbrain is controlled by relative but not absolute levels of EphA receptor signaling. *Cell*. 102, 77-88

305 Feldheim, D. A. *et al.* (2000) Genetic analysis of ephrin-A2 and ephrin-A5 shows their requirement in multiple aspects of retinocollicular mapping. *Neuron*. 25, 563-74

306 Murai, K. K. and Pasquale, E. B. (2002) Can Eph receptors stimulate the mind? *Neuron*. 33, 159-62

307 Kayser, M. S. *et al.* (2006) Intracellular and trans-synaptic regulation of glutamatergic synaptogenesis by EphB receptors. *The Journal of neuroscience : the official journal of the Society for Neuroscience*. 26, 12152-64

308 GAUTIER, I. (2001) Homo-FRET Microscopy in Living Cells to Measure Monomer-Dimer Transition of GFP-Tagged Proteins. *Biophysical Journal*. 80, 3000-3008

309 Squire, A. *et al.* (2004) Red-edge anisotropy microscopy enables dynamic imaging of homo-FRET between green fluorescent proteins in cells. *Journal of structural biology*. 147, 62-9

310 Bader, A. N. *et al.* (2010) Homo-FRET Imaging as a Tool to Quantify Protein and Lipid Clustering. *Chemphyschem : a European journal of chemical physics and physical chemistry*. DOI: 10.1002/cphc.201000801

311 Zacharias, D. A. *et al.* (2002) Partitioning of lipid-modified monomeric GFPs into membrane microdomains of live cells. *Science (New York, N.Y.)*. 296, 913-6

312 Chen, J. *et al.* (1995) Identification of an 11-kDa FKBP12-rapamycin-binding domain within the 289-kDa FKBP12-rapamycin-associated protein and characterization of a critical serine residue. *Proceedings of the National Academy of Sciences of the United States of America*. 92, 4947-51

313 Köhler, J. (2005) , Imaging of the dynamics of Eph receptors and their ephrin ligands in mature hippocampal neurons. , Max Planck Institut of Neurobiology

314 Jordan, M. *et al.* (1996) Transfecting mammalian cells: optimization of critical parameters affecting calcium-phosphate precipitate formation. *Nucleic acids research*. 24, 596-601

315 Wittig, I. *et al.* (2006) Blue native PAGE. *Nature protocols*. 1, 418-28

316 Yang, W. *et al.* (2003) Regulation of gene expression by synthetic dimerizers with novel specificity. *Bioorganic & medicinal chemistry letters*. 13, 3181-4

317 Chung, I. *et al.* (2010) Spatial control of EGF receptor activation by reversible dimerization on living cells. *Nature*. 464, 783-7

318 Clague, M. J. and Urbé, S. (2001) The interface of receptor trafficking and signalling. *Journal of cell science*. 114, 3075-81

319 Deribe, Y. L. *et al.* (2009) Regulation of epidermal growth factor receptor trafficking by lysine deacetylase HDAC6. *Science signaling*. 2, ra84

320 Fix, M. *et al.* (2004) Imaging single membrane fusion events mediated by SNARE proteins. *Proceedings of the National Academy of Sciences of the United States of America*. 101, 7311-6

321 Gale, N. W. *et al.* (1996) Elk-L3, a novel transmembrane ligand for the Eph family of receptor tyrosine kinases, expressed in embryonic floor plate, roof plate and hindbrain segments. *Oncogene*. 13, 1343-52

322 Choi, J. *et al.* (1996) Structure of the FKBP12-rapamycin complex interacting with the binding domain of human FRAP. *Science (New York, N.Y.)*. 273, 239-42

323 Muthuswamy, S. K. *et al.* (1999) Controlled dimerization of ErbB receptors provides evidence for differential signaling by homo- and heterodimers. *Molecular and cellular biology*. 19, 6845-57

324 Whitney, M. L. *et al.* (2001) Control of myoblast proliferation with a synthetic ligand. *The Journal of biological chemistry*. 276, 41191-6

325 Wang, Q. *et al.* (2005) Control of epidermal growth factor receptor endocytosis by receptor dimerization, rather than receptor kinase activation. *EMBO reports*. 6, 942-8

326 Yang, J.-xin *et al.* (1998) Small-molecule control of insulin and PDGF receptor signaling and the role of membrane attachment. *Current Biology*. 8, 11-18

327 Hofman, E. G. *et al.* (2010) Ligand-induced EGF receptor oligomerization is kinase-dependent and enhances internalization. *The Journal of biological chemistry*. 285, 39481-9

328 Bader, A. N. *et al.* (2009) Homo-FRET imaging enables quantification of protein cluster sizes with subcellular resolution. *Biophysical journal*. 97, 2613-22

329 Stockwell, B. R. and Schreiber, S. L. (1998) Probing the role of homomeric and heteromeric receptor interactions in TGF-beta signaling using small molecule dimerizers. *Current biology : CB*. 8, 761-70

330 Zhao, T. and Newman, P. J. (2001) Integrin activation by regulated dimerization and oligomerization of platelet endothelial cell adhesion molecule (PECAM)-1 from within the cell. *The Journal of cell biology*. 152, 65-73

331 Zhan, L. *et al.* (2006) Controlled activation of ErbB1/ErbB2 heterodimers promote invasion of three-dimensional organized epithelia in an ErbB1-dependent manner: implications for progression of ErbB2-overexpressing tumors. *Cancer research*. 66, 5201-8

332 Himanen, J. P. (2011) Ectodomain structures of Eph receptors. *Seminars in cell & developmental biology*. DOI: 10.1016/j.semcdb.2011.10.025

333 Varma, R. and Mayor, S. (1998) GPI-anchored proteins are organized in submicron domains at the cell surface. *Nature*. 394, 798-801

334 Wimmer-Kleikamp, S. H. *et al.* (2004) Recruitment of Eph receptors into signaling clusters does not require ephrin contact. *The Journal of cell biology*. 164, 661-6

335 Lerch, R. (2004) *Elektrische Meßtechnik. Analoge, digitale und computergestützte Verfahren*, Springer-Verlag GmbH; Auflage: 2., neu bearb. und erw. A.

336 Henis, Y. I. *et al.* (2009) Ras acylation, compartmentalization and signaling nanoclusters (Review). *Molecular membrane biology*. 26, 80-92

337 Tian, T. *et al.* (2007) Plasma membrane nanoswitches generate high-fidelity Ras signal transduction. *Nature cell biology*. 9, 905-14

338 Kitano, H. (2007) Towards a theory of biological robustness. *Molecular systems biology*. 3, 137

339 Garrett, T. P. J. *et al.* (2002) Crystal structure of a truncated epidermal growth factor receptor extracellular domain bound to transforming growth factor alpha. *Cell*. 110, 763-73

340 van Belzen, N. *et al.* (1988) Direct visualization and quantitative analysis of epidermal growth factor-induced receptor clustering. *Journal of cellular physiology*. 134, 413-20

341 Moriki, T. *et al.* (2001) Activation of preformed EGF receptor dimers by ligand-induced rotation of the transmembrane domain. *Journal of molecular biology*. 311, 1011-26

342 Yu, X. *et al.* (2002) Ligand-independent dimer formation of epidermal growth factor receptor (EGFR) is a step separable from ligand-induced EGFR signaling. *Molecular biology of the cell*. 13, 2547-57

343 Zhu, H.-J. *et al.* (2003) Epidermal growth factor receptor: association of extracellular domain negatively regulates intracellular kinase activation in the absence of ligand. *Growth factors (Chur, Switzerland)*. 21, 15-30

344 Saffarian, S. *et al.* (2007) Oligomerization of the EGF receptor investigated by live cell fluorescence intensity distribution analysis. *Biophysical journal*. 93, 1021-31

345 Sako, Y. *et al.* (2000) Single-molecule imaging of EGFR signalling on the surface of living cells. *Nature cell biology*. 2, 168-72

346 Teramura, Y. *et al.* (2006) Single-molecule analysis of epidermal growth factor binding on the surface of living cells. *The EMBO journal*. 25, 4215-22

347 Martin-Fernandez, M. *et al.* (2002) Preformed oligomeric epidermal growth factor receptors undergo an ectodomain structure change during signaling. *Biophysical journal*. 82, 2415-27

348 Adam, G. *et al.* (2007) *Physikalische Chemie und Biophysik (Springer-Lehrbuch) (German Edition)*, Springer.

349 Zhou, H.-X. *et al.* (2008) Macromolecular crowding and confinement: biochemical, biophysical, and potential physiological consequences. *Annual review of biophysics*. 37, 375-97

350 Dong, H. *et al.* (2010) Effects of macromolecular crowding on protein conformational changes. *PLoS computational biology*. 6, e1000833

351 Chebotareva, N. a *et al.* (2004) Biochemical effects of molecular crowding. *Biochemistry. Biokhimiia*. 69, 1239-51

352 Contractor, A. *et al.* (2002) Trans-synaptic Eph receptor-ephrin signaling in hippocampal mossy fiber LTP. *Science (New York, N.Y.)*. 296, 1864-9

353 Oricchio, E. *et al.* (2011) The eph-receptor a7 is a soluble tumor suppressor for follicular lymphoma. *Cell*. 147, 554-64

354 Truitt, L. *et al.* (2010) The EphB6 receptor cooperates with c-Cbl to regulate the behavior of breast cancer cells. *Cancer research*. 70, 1141-53

355 Freywald, A. *et al.* (2002) The kinase-null EphB6 receptor undergoes transphosphorylation in a complex with EphB1. *The Journal of biological chemistry*. 277, 3823-8

356 Blits-Huizinga, C. T. *et al.* (2004) Ephrins and their receptors: binding versus biology. *IUBMB life*. 56, 257-65

357 Setou, M. *et al.* (2002) Glutamate-receptor-interacting protein GRIP1 directly steers kinesin to dendrites. *Nature*. 417, 83-7

358 Gschwind, A. *et al.* (2004) The discovery of receptor tyrosine kinases: targets for cancer therapy. *Nature reviews. Cancer*. 4, 361-70

359 Sambrook, J. (2000) *Molecular Cloning: A Laboratory Manual, Third Edition (Volume 1)*, Cold Spring Harbor Laboratory Press.

360 Sanger, F. *et al.* (1977) DNA sequencing with chain-terminating inhibitors. *Proceedings of the National Academy of Sciences of the United States of America*. 74, 5463-7

361 Hassler, C. (2007) , Characterization of developmental role and mechanistic function of Kremen proteins.

362 Chomczynski, P. and Sacchi, N. (1987) Single-step method of RNA isolation by acid guanidinium thiocyanate-phenol-chloroform extraction. *Analytical Biochemistry*. 162, 156-159

363 Shaner, N. C. *et al.* (2004) Improved monomeric red, orange and yellow fluorescent proteins derived from Discosoma sp. red fluorescent protein. *Nature biotechnology*. 22, 1567-72

364 Cokic, B. (2009) , Regulation of AMPA receptor function and synaptic localization by stargazin and PSD-95. , Max-Planck Institute for Neurobiology

365 Weinges, S. (2006) , Molecular dissection of ephrinB reverse signaling.

366 Freshney, R. I. (2005) *Culture of Animal Cells: A Manual of Basic Technique*, Wiley-Liss.

367 Spencer, D. M. *et al.* (1993) Controlling signal transduction with synthetic ligands. *Science (New York, N.Y.)*. 262, 1019-24

BIBLIOGRAPHY

368 Amara, J. F. *et al.* (1997) A versatile synthetic dimerizer for the regulation of protein-protein interactions. *Proceedings of the National Academy of Sciences of the United States of America*. 94, 10618-23

369 Clackson, T. (1998) Redesigning an FKBP-ligand interface to generate chemical dimerizers with novel specificity. *Proceedings of the National Academy of Sciences*. 95, 10437-10442

370 Yang, W. (2003) Regulation of gene expression by synthetic dimerizers with novel specificity. *Bioorganic & Medicinal Chemistry Letters*. 13, 3181-3184

371 Macia, E. *et al.* (2006) Dynasore, a cell-permeable inhibitor of dynamin. *Developmental cell*. 10, 839-50

372 Abramoff, M. D. *et al.* (2004) Image processing with ImageJ. *Biophotonics international*. 11, 36-42

373 Jares-Erijman, E. A. and Jovin, T. M. (2003) FRET imaging. *Nature biotechnology*. 21, 1387-95

374 Fish, K. N. (2009) Total internal reflection fluorescence (TIRF) microscopy. *Current protocols in cytometry / editorial board, J. Paul Robinson, managing editor ... [et al.]*. 12, Unit12.18

ACKNOWLEDGEMENTS

Zu allererst und am meisten möchte ich denjenigen lieben Menschen danken, die immer ein Teil meines Lebens gewesen sind und sein werden, denn ohne sie wäre ich nicht die Person, die ich heute bin. Ich danke meinen Eltern und meiner Schwester, denn sie waren in all meinen bisherigen Lebenslagen nicht nur der Fels in der Brandung sondern ermöglichten erst meine lange Ausbildung zum Wissenschaftler. Ihr Verständnis und ihre Unterstützung waren und sind von enormer Bedeutung für mich. Mein besonderer Dank gilt auch meiner großen Liebe Judith für all ihre Unterstützung, Liebe und Verständnis während der letzten Jahre. Lange Telefonate am Abend und schöne Wochenenden ließen alltägliche Sorgen vergessen und halfen über die Ferne hinweg. Einen riesen Dank auch an die ganze Großfamilie Rech, allen voran Pia, bei denen ich mich von Beginn an als Familienmitglied aufgenommen fühlen durfte. Ohne Hata, meine gute Fee, hätte ich an Wochenenden keine Zeit für wichtigere Dinge gehabt... auch hierfür den größten Dank. Großer Dank und Verbundenheit möchte ich auch meiner Oma entgegenbringen, welche mir immer wie eine zweite Mama ist. Nicht zuletzt möchte ich auch meinen Freunden danken, die in guten und schlechten Tagen fest an meiner Seite standen, allen voran meinem Studienfreund Josef und meinem langjährigen Schulfreund Rainer.

I thank my supervisor, Rüdiger Klein, who has given me the opportunity to carry out my PhD in an international scientific environment. I am grateful for critical discussions and support. I appreciate the freedom he has given me to develop my own ideas and interests.
I wish to acknowledge Philippe Bastiaens at the MPI for Molecular Physiology in Dortmund, who has invited me to perform my homo-FRET imaging and TIRF imaging experiments in the great scientific environment of his department. In this regard I am very grateful to Ola Sabet, who has not only been an immensely supportive and a valuable collaborator but has also grown a friend during the long-lasting and strenuous nightshifts in front of the microscopes. I thank Irina Dudanova for performing the neuronal growth cone collapse assays and Taija Makinen for first clonings in the early stages of the project.
I acknowledge past and present members of the Klein lab for providing a nice working atmosphere, technical help, discussions and criticism. My special thanks go out to Christine Hassler, my “lunch buddy”, an excellent scientist and talented mind, who has enriched my life in the lab by discussions about everything under the sun. I would also like to express my gratitude to Maria Sakkou, Tom Gaitanos, Irina Dudanova, Bernadette Antoni, Joaquim Egea, Marsilius Mues, Daniel del Torro Ruiz for intimate discussions about my project, sharing of reagents and experimental help, nice conversations and colleagueship. I thank my students Katharina Wenz and Franziska Tippel for experimental help in the lab. Special thanks to people working in the service units, especially Helena Tultschin, the whole IT-group of the MPI of Neurobiology and our lab technicians Gonül, Jana, Louise, Parvin and Pilar for making life easier for all of us in the lab. I would like to thank my thesis advisory committee

members Rüdiger Klein, Ilona Grunwald-Kadow and Bastian Hengerer most sincerely for their interest, critical discussion, suggestions and encouragement. I would also like to acknowledge the people working in the IMPRS coordination office, especially Hans-Joerg Schaeffer, for managing a fantastic graduate school.
I sincerely appreciate the scientific suggestions and discussions of my Ph.D. fellows, especially Bernadette Antoni, Falko Hampel, Pontus Klein, Graziana Gatto, Christian Erlacher, Daniel Stephan, Marsilius Mues, Matthias Traut and Clara Essmann. I would also like to thank people from Visitron GmbH, Jürgen Kraus and Roland Guckler, for support on microscopes. Finally, special thanks to Christine Hassler, Louise and Tom Gaitanos, Graziana Gatto, Irina Dudanova, Daniela Rech and Janina Erl for critically reading the thesis.

CURRICULUM VITAE

01.2007 – 02.2012	**International Max Planck Research School (IMPRS) for Molecular and Cellular Life Sciences,** Munich **Max-Planck-Institute for Neurobiology,** Department Molecular Neurobiology, Prof. Dr. Rüdiger Klein **Max-Planck-Institute for Molecular Physiology,** Department Systemic Cell Biology, Prof. Dr. Philippe Bastiaens doctoral thesis
10.2004 – 10.2006	**Technische Universität München,** (TUM), Garching/Munich Master of Science in Biochemistry
10.2001 – 09.2004	**Technische Universität München,** (TUM), Garching/Munich Bachelor of Science in Biochemistry
08.2000 – 06.2001	**Deutsches Rotes Kreuz e.V., Kreisverband Ulm,** civil service
09.1990 – 06.2000	**Johann-Vanotti-Gymnasium, Ehingen (Donau),** Abitur